THE SCATTERING OF ELECTRONS POSITRONS AND PROTONS IN NUCLEAR PHOTOGRAPHIC EMULSIONS.

A Thesis

Submitted to the University of Glasgow

in candidature for the degree of Doctor of Philosophy

by

William Bosley

Department of Physics,

University College of North Staffordshire,

July, 1954.

CONTENTS.

The Scattering of electrons, positrons and protons in nuclear photographic plates.

Section I. Preface and Introductory Summary of other work on single and multiple scattering.

1.1 Preface.

The work described in this thesis was carried out at the Natural Philosophy Department of the University of Glasgow. The work began in January, 1951 and the author's part in it ended in December, 1952, though data obtained since that date have been included in one section of the thesis (that describing the single scattering measurements) by permission of those at present working on the problem.

The course of the work may be summarised as follows. Various types of photographic emulsion were exposed to electrons and positrons of energies up to 20 MeV and to protons of up to 140 MeV. The multiple scattering of the tracks of these particles was examined and it was found that for these types of emulsion which had previously been studied by other authors the results agreed with the earlier work as well as with modern theory. For other (diluted) emulsions, the scattering constants were determined for the first time and found to agree with those predicted by theory.

On the conclusion of the multiple scattering measurements the single scattering process was studied for electrons and positrons of about 10 MeV, it being found necessary to use a new set of emulsions,with greater track densities, in order to obtain satisfactory results. The variation of the scattering cross section with the angle of scattering was determined and compared with the results of other workers with particles of comparable energies, where these were available and with theory.

It was found that in the case of electrons a considerable effect was produced by the finite size of the scattering nuclei, in agreement with the findings of other authors, but in the case of positrons, where there appears to be no previous experimental work, even less evidence of this effect than is predicted by theory was found.

The thesis begins with an account of previous work on both single and multiple scattering (sections 1.2 and 1.3). The remainder of the thesis is concerned with the present work. This work began with the construction and calibration of a spectrometer in which positrons or electrons of known energies between 5 and 20 MeV could be directed into photographic emulsions after having been produced in a lead plate by the X-radiation from the Natural Philosophy Department's 30 MeV synchrotron. This part of the work, which is described in section 2.1, was carried out by the author in collaboration, so far as the actual exposures were concerned, with the operators of the 30 MeV synchrotron. After exposure these emulsions were processed by the author as described in section 2.2. The proton tracks were obtained in emulsions exposed, for another purpose, to the beam of the synchro-cyclotron at the Atomic Energy Research Establishment, Harwell. These plates were exposed and processed by Miss C. F. Lees.

The multiple scattering measurements are described in section 2.3.1. They were all made either by the author or by Dr. Muirhead. The various corrections which it was necessary to apply to the experimental results were calculated, as also were the theoretical values of the scattering constants, for an account of this part of the work published in the Philosophical Magazine (Bosley and Muirhead, P. M., 43, 63 (1952)), by the author and by Dr. Muirhead. For this thesis more detailed results than had previously been published were felt to be necessary and the results given here were all re-calculated by the author, as described in section 2.3.2.

A paper describing the use of the above measurements in determining the energy of particles emitted in an unusual, high energy disintegration produced in a diluted emulsion by a cosmic ray particle was published in the Philosophical Magazine (Bosley and Muirhead, P.M., 43, 783 (1952)).

The single scattering measurements described in section 2.4.1 were originally made in the emulsions previously exposed to the 30 MeV synchrotron radiation, but it was soon found desirable to use a greater density of tracks in order to speed up the collection of data and new exposures were made by the author and Mr. I. S. Hughes in collaboration with the operators of the Natural Philosophy Department's 1 MeV H. T. set. These emulsions were processed by the author and Mr. Hughes.

Initially the single scattering measurements were made by the author, but later the work was transferred to specially trained microscopists working under his supervision and since the author left the Natural Philosophy Department this supervision has been taken over by Mr. Hughes working under Dr. Muirhead.

The experimental results were corrected in the manner described in section 2.4.2 by the author and Mr. Hughes. The distribution of angles of scattering was then compared with other published results and with the theoretical predictions, taking into account the finite size of the scattering nuclei and other factors, by the author (section 2.4.3).

The author is indebted to Professor P. I. Dee, F.R.S., in whose laboratory, and under whose supervision, the work herein described was carried out; to Dr. H. Muirhead, the author's immediate instructor; and to Mr. I. S. Hughes, his collaborator. He also wishes to acknowledge the help of Mr. J. M. Reid, in charge of the 30 MeV synchrotron; to Dr. J. G. Rutherglen and his associates operating the H. T. set; to Miss C. F. Lees who exposed and processed the emulsions in which proton tracks were examined; to Mrs. H. Muirhead, Mrs. P. Friedlander and Miss E. Rose, microscopists in the Natural Philosophy Department; and to Mr. F. Rowerth of the University College of North Staffordshire who helped greatly in the preparation of the figures for this thesis.

Finally, the author is indebted to the Nuffield Foundation for the award of a grant for part of the period during which the work herein described was carried out.

1.2. Previous work on single scattering.

1.2.1. Theory.

The purpose of this section is to summarise the results of (a) those authors who have attempted to derive a useable and reasonably accurate formula for the cross sections for scattering of electrons and positrons by nuclei, assuming that the nuclei act as infinitely small points, and (b) those who have applied modifications to these cross sections necessitated, for example, when the size of the scattering nuclei is comparable with the wavelength of the particles being scattered. Thus we shall obtain an expression for the theoretical scattering cross sections with which our experimental values may be compared.

(a) Scattering of electrons by a point nucleus

The problem of the scattering of electrons by nuclei was first attempted by means of wave mechanical methods, by Mott (1) in 1929. Mott obtained an exact formula for the cross section for scattering, but unfortunately this formula is so complex that its complete general evaluation has never been carried out. Numerical values of the cross sections have, therefore, had to be obtained in one of two ways; either an approximation to the full Mott formula, valid for certain experimental conditions, has been obtained, or (in fact only in the case of mercury) the exact equation has been evaluated numerically for a specific nucleus.

Mott's full equation for the differential cross section , which will be required in discussing some of the approximate formulae, has the form:

$$\sigma = q^2(1-\beta^2)F^*F \operatorname{Csc}^2\theta/2 + G^*G \operatorname{Sec}^2\theta/2 \qquad (1)$$

where $q = \alpha/\beta$, $\alpha = ze^2/\hbar c$, $\beta = v/c$ and θ = angle of scattering.

The functions F and G may be expressed as

$F = F_o + F_1$, $G = G_o + G_1$, where F_o and G_o are the values of F and G when $\alpha = 0$.

$$F_o = 1/2 \exp(iq \, l_n \, \sin^2 \theta/2) \frac{\Gamma(1 - iq)}{\Gamma(1 + iq)}, \quad G_o = -iqF_o \mathrm{Cot}^2 \theta/2.$$

$$F_1 = 1/2 \sum_{k=0}^{\infty} \left[kD_k + (k+1)D_{k+1} \right] (-)^k P_k(\cos\theta),$$

$$G_1 = 1/2 \sum_{k=0}^{\infty} \left[k^2 D_k - (k+1)^2 D_{k+1} \right] (-)^k P_k(\cos\theta),$$

where Γ is the gamma-function, P_k the Legendre polynomial, and

$$D_k = \frac{e^{-\pi i k}}{(k + iq)} \frac{\Gamma(k - iq)}{\Gamma(k + iq)} - \frac{e^{-\pi i \rho_k}}{(\rho_k + iq)} \frac{\Gamma(\rho_k - iq)}{\Gamma(\rho_k + iq)}, \quad \rho_k = (k^2 - \ ^2)^{\frac{1}{2}}.$$

Mott himself carried out a partial evaluation of this formula, giving two approximations for the cross section:-

$$\sigma_{M_1} = \left(\frac{ze^2}{2m_oc^2}\right)^2 \frac{(1-\beta^2)}{\beta^4} \left\{ \mathrm{Csc}^4 \theta/2 - \beta^2 \mathrm{Csc}^2 \theta/2 \right\} \qquad (2)$$

valid only for very small z or very small θ, and

$$\sigma_{M_2} = \left(\frac{ze^2}{2m_oC^2}\right)^2 \frac{(1-\beta^2)}{\beta^4} \left\{ \mathrm{Csc}^4 \frac{\theta}{2} - \beta^2 \mathrm{Csc}^2 \theta/2 + \pi\alpha\beta \mathrm{Cos}^2 \theta/2 \, \mathrm{Csc}^3 \theta/2 \right\} \qquad (3)$$

valid for a wider range of Z and θ. The limitations of these two formulae will be discussed below (Fig. 3 and 4).

In most theoretical treatments of electron scattering, the cross sections are given as ratios, R, to the classical Rutherford cross section:-

$$\sigma_R = \left(\frac{Ze^2}{2m_oc^2}\right)^2 \frac{(1-\beta^2)}{\beta^4} \mathrm{Csc}^4 \theta/2 \qquad (4)$$

so that in the case of the two approximations given above we have

$$R_{M_1} = 1 - \beta^2 \sin^2 \theta/2 \qquad (5)$$

Table I.

TABLE I

θ	A (θ)		B (θ)		C (θ)		D (θ)	
	Real	Imag^y	Real	Imag^y	Real	Imag^y	Real	Imag^y
30°	-.326	.064	-.086	.491	.580	-.010	-.107	-.129
45°	-.510	.114	-.201	.375	.404	-.069	-.217	-.221
60°	-.637	.167	-.339	.209	.313	-.167	-.344	-.310
80°	-.780	.235	-.537	-.033	.289	-.351	-.525	-.417
90°	-.846	.266	-.636	-.150	.305	-.448	-.614	-.464
100°	-.893	.295	-.729	-.263	.332	-.553	-.699	-.505
120°	-.980	.344	-.897	-.455	.408	-.750	-.847	-.574
135°	-1.028	.373	-.995	-.568	.464	-.876	-.940	-.612
150°	-1.062	.394	-1.072	-.650	.511	-.971	-1.007	-.638
180°	-1.089	.411	-1.133	-.720	.551	-1.052	-1.062	-.657

θ	E (θ)		H (θ)		I (θ)		J (θ)	
	Real	Imag^y	Real	Imag^y	Real	Imag^y	Real	Imag^y
30°	2.249	-.676	1.483	1.044	3.105	.471	0	1.711
45°	1.267	-.480	1.221	1.371	1.261	.733	0	1.199
60°	0.785	-.347	.953	1.174	.354	.781	0	.851
80°	0.437	-.221	.643	0.817	-.110	.678	0	.532
90°	0.325	-.173	.514	.658	-.200	.591	0	.413
100°	0.240	-.133	.401	.514	-.206	.495	0	.315
120°	0.122	-.072	.219	.281	-.174	.305	0	.167
135°	0.065	-.040	.123	.158	-.085	.173	0	.091
150°	0.028	-.017	.051	.065	-.071	.085	0	.040
180°	0	0	0	0	0	0	0	0

$$R_{M_2} = 1 - \beta^2 \sin^2\theta/2 + \pi\alpha\beta \sin\theta/2 \cos\theta/2 \qquad (6)$$

Other small Z or small θ approximations to the full Mott formula have been fiven by Urban[2]:-

$$R_U = 1 - \beta^2 \sin^2\theta/2 + \pi\alpha\beta \sin\theta/2 \qquad (7)$$

and by McKinley and Feshbach[3]:-

$$R_{Mck} = 1 - \beta^2 \sin\theta/2 + \pi\alpha\beta \sin\theta/2(1 - \sin\theta/2) \qquad (8)$$

The validity of these approximations also is discussed below (fig. 3 and 4).

A more complex approximation, but one valid up to the middle Z region of the periodic table is the "α^4" approximation given, together with equation (8), by McKinley and Feshbach, who expanded the functions F_1 and G_1 of Mott's full equation as a power series in α and α/β, the coefficients depending on the angle of scattering. They evaluated the coefficients up to those of the fourth power of α, obtaining the expressions:-

$$F_1 = A(\theta)\alpha^2 + B(\theta)\alpha^3/\beta + C(\theta)\alpha^4/\beta^2 + D(\theta)\alpha^4 + \ldots \qquad (9)$$

$$G_1 = E(\theta)\alpha^2 + H(\theta)\alpha^3/\beta + I(\theta)\alpha^4/\beta^2 + J(\theta)\alpha^4 + \ldots \qquad (10)$$

where A - J are given, for the range $\theta = 30^\circ$ to $\theta = 180^\circ$, in Table I.

Before comparing these cross section formulae, mention should be made of the exact evaluation of Mott's full equation, for mercury nuclei, by Bartlett and Watson[4] for electrons of various energies up to approximately 2 MeV. This exact cross section is shown, in terms of the ratio to the Rutherford cross section, as a function of θ in fig. 1 for an energy of 2 MeV. The corresponding values of the cross section obtained from the "α^4" approximation and from the two Mott approximations are shown for comparison. Since the cross sections obtained by the "α^4" approximation extrapolate smoothly to the Bartlett and Watson value, this value can be combined with the "α^4" approximation to give reasonably accurate scattering cross section values valid for all Z, the required correction to the α^4 approximation being proportional to Z^4. These values of R are plotted for 1, 2 and 4 M eV, as functions of Z, in fig. 2. McKinley and Feshbach state that above 4 MeV. the ratio R obtained in this way is independent of energy within the accuracy of their calculations.

From these curves (fig. 2) the present writer has prepared those shown in fig. 3, in which the value of R is plotted against θ for Z = 6, 15 and 25. These give us the only criteria against which the various light element approximations may be compared, since in this region of the periodic table no exact evaluations have been made. All the light element approximations mentioned above are plotted in this figure for comparison, and one can see that for very light elements (Z = 6) all the approximate formulae give values in reasonable agreement with one another and with the "improved "α^4" values up to about $\theta = 90^\circ$. For greater values of Z, as is to be expected, the range of θ over which the curves approximate to the improved "α^4" curve is reduced, but the second Mott approximation gives values within 10% of the improved "α^4" ones for all values of Z up to 47 (see fig. 4) and for all values of θ up to 90°, the discrepancy being greatest in the region of Z = 15.

Since in the present work the nuclei most concerned in the scattering process are those of bromine and of silver, all the above values of the cross sections have been determined for these nuclei. They are plotted in fig. 4. For comparison with experiment the McKinley and Feshbach "α^4" values corrected by means of Bartlett and Watson's evaluation will be used, although the agreement between these values and those given by the second Mott approximation is very good. McKinley and Feshbach state that their values should lie within 2% of the true cross sections for point nuclei.

(b) Scattering of positrons by point nuclei.

With positrons as with electrons, two methods of obtaining a useful theoretical value of the scattering cross section are available. Approximate formulae, valid under certain conditions, have been obtained by Yadav and by Feshbach, while Massey has evaluated the exact cross section for mercury nuclei.

Feshbach[5] has extended the earlier calculations of McKinley and Feshbach, in which the "α^4" approximation referred to above was obtained, and combined with Bartlett and Watson's exact cross section values for mercury to give reasonably accurate values for all Z. Feshbach uses the same method to evaluate the functions F and G of Mott's full formula for $\beta = 1$, $Z = 13, 29, 47, 62$, and 80 and for $\theta = 30^\circ, 60^\circ, 80^\circ, 90^\circ, 100^\circ, 135^\circ$, and 150°. He does this for both electron and positron scattering, the latter being obtained merely by replacing +Z by −Z in the functions F and G. In the original paper the results of the calculations are given as the ratio positron cross section / electron cross section plotted against Z for various values of θ. These are shown in fig. 5 and the values of positron cross section / Rutherford cross section obtained by the present author by combining Feshbach's results with those of McKinley and Feshbach given above (in fig. 3 and 4) are shown in fig. 6.

Independently, Yadav[6] has performed similar calculations in which F and G are obtained for positrons by replacing +Z by −Z in the "α^4" expressions. Whereas Feshbach assumed for his calculations a value of $\beta = 1$, Yadav determines the scattering cross section for each value of Z for four

TABLE 2

$R = \sigma_L(\theta) \,/\, \sigma_R(\theta)$

z	E	30°	45°	60°	80°	90°	100°	120°	135°	150°
10	1	0.903	0.825	0.731	0.591	0.519	0.448	0.314	0.232	0.16[illegible]
	2	0.897	0.812	0.711	0.558	0.480	0.403	0.258	0.159	0.0[illegible]
	5	0.894	0.807	0.702	0.544	0.463	0.383	0.233	0.140	0.0[illegible]
	10	0.893	0.806	0.700	0.541	0.460	0.379	0.229	0.134	0.09[illegible]
20	1	0.875	0.791	0.687	0.560	0.492	0.425	0.300	0.224	0.16[illegible]
	2	0.867	0.777	0.675	0.526	0.452	0.379	0.243	0.139	0.09[illegible]
	5	0.865	0.770	0.665	0.511	0.434	0.358	0.217	0.130	0.08[illegible]
	10	0.862	0.769	0.663	0.507	0.430	0.354	0.212	0.124	0.05[illegible]
30	1	0.854	0.769	0.678	0.543	0.478	0.414	0.298	0.22[illegible]	0.1[illegible]
	2	0.845	0.752	0.651	0.507	0.436	0.365	0.226	0.136	0.096
	5	0.840	0.745	0.640	0.491	0.417	0.343	0.209	0.125	0.0[illegible]
	10	0.839	0.744	0.638	0.487	0.413	0.339	0.204	0.119	0.056
40	1	0.836	0.751	0.659	0.529	0.465	0.403	0.289	0.220	0.170
	2	0.826	0.733	0.633	0.480	0.420	0.352	0.227	0.136	0.09[illegible]
	5	0.821	0.724	0.621	0.472	0.399	0.329	0.199	0.119	0.061
	10	0.820	0.723	0.168	0.469	0.396	0.325	0.193	0.113	0.053
50	1	0.823	0.741	0.651	0.522	0.460	0.400	0.291	0.224	0.175
	2	0.812	0.721	0.621	0.483	0.413	0.346	0.224	0.131	0.098
	5	0.806	0.711	0.610	0.463	0.392	0.321	0.194	0.119	0.063
	10	0.805	0.709	0.607	0.460	0.388	0.316	0.188	0.113	0.058
60	1	0.813	0.732	0.646	0.517	0.456	0.398	0.294	0.229	0.172
	2	0.800	0.710	0.610	0.476	0.407	0.341	0.228	0.136	0.102
	5	0.793	0.700	0.601	0.455	0.385	0.314	0.190	0.120	0.067
	10	0.791	0.698	0.597	0.450	0.379	0.309	0.184	0.113	0.060
70	1	0.803	0.722	0.635	0.508	0.446	0.394	0.297	0.237	0.191
	2	0.790	0.697	0.598	0.466	0.396	0.335	0.219	0.162	0.111
	5	0.781	0.686	0.586	0.443	0.373	0.306	0.186	0.124	0.076
	10	0.780	0.683	0.583	0.436	0.367	0.298	0.179	0.116	0.067
80	1	0.795	0.703	0.612	0.487	0.427	0.385	0.300	0.245	0.201
	2	0.780	0.677	0.577	0.445	0.376	0.322	0.215	0.167	0.123
	5	0.770	0.663	0.560	0.420	0.353	0.290	0.181	0.131	0.096
	10	0.768	0.660	0.556	0.413	0.345	0.280	0.173	0.123	0.080

Table II.

TABLE 2

$R = \sigma(\theta) / \sigma_R(\theta)$

θ		30°	45°	60°	80°	90°	100°	120°	135°	150°	18
Z	E										
10	1	0.903	0.825	0.731	0.591	0.519	0.448	0.314	0.232	0.168	0.1
	2	0.897	0.812	0.711	0.558	0.480	0.403	0.258	0.169	0.099	0.0
	5	0.894	0.807	0.702	0.544	0.463	0.383	0.233	0.140	0.068	0.0
	10	0.893	0.806	0.700	0.541	0.460	0.379	0.229	0.134	0.063	0.0
20	1	0.875	0.791	0.697	0.560	0.492	0.425	0.300	0.224	0.166	0.1
	2	0.867	0.777	0.675	0.526	0.452	0.379	0.243	0.159	0.096	0.0
	5	0.863	0.770	0.665	0.511	0.434	0.358	0.217	0.130	0.068	0.0
	10	0.862	0.769	0.663	0.507	0.430	0.354	0.212	0.124	0.058	0.0
30	1	0.854	0.769	0.676	0.543	0.478	0.414	0.296	0.222	0.167	0.1
	2	0.845	0.752	0.651	0.507	0.436	0.365	0.236	0.155	0.096	0.0
	5	0.840	0.745	0.640	0.491	0.417	0.343	0.209	0.125	0.062	0.0
	10	0.839	0.744	0.638	0.487	0.413	0.339	0.204	0.119	0.056	0.0
40	1	0.836	0.751	0.659	0.529	0.465	0.403	0.289	0.220	0.170	0.1
	2	0.826	0.733	0.633	0.490	0.420	0.352	0.227	0.156	0.095	0.0
	5	0.821	0.724	0.621	0.472	0.399	0.329	0.199	0.119	0.061	0.0
	10	0.820	0.723	0.168	0.469	0.396	0.325	0.193	0.113	0.055	0.0
50	1	0.823	0.741	0.651	0.522	0.460	0.400	0.291	0.224	0.175	0.1
	2	0.812	0.721	0.621	0.483	0.413	0.346	0.224	0.151	0.098	0.0
	5	0.806	0.711	0.610	0.463	0.392	0.321	0.194	0.119	0.063	0.0
	10	0.805	0.709	0.607	0.460	0.388	0.316	0.188	0.113	0.056	0.0
60	1	0.813	0.732	0.646	0.517	0.456	0.398	0.294	0.229	0.172	0.1
	2	0.800	0.710	0.610	0.476	0.407	0.341	0.222	0.156	0.102	0.0
	5	0.793	0.700	0.601	0.455	0.385	0.314	0.190	0.120	0.067	0.0
	10	0.791	0.698	0.597	0.450	0.379	0.309	0.184	0.113	0.060	0.0
70	1	0.803	0.722	0.635	0.508	0.446	0.394	0.297	0.237	0.191	0.1
	2	0.790	0.697	0.598	0.466	0.396	0.335	0.219	0.162	0.111	0.06
	5	0.781	0.686	0.586	0.443	0.373	0.306	0.186	0.124	0.076	0.02
	10	0.780	0.683	0.583	0.436	0.367	0.298	0.179	0.116	0.067	0.02
80	1	0.795	0.703	0.612	0.487	0.427	0.385	0.300	0.245	0.201	0.1
	2	0.780	0.677	0.577	0.445	0.376	0.322	0.215	0.167	0.123	0.07
	5	0.770	0.663	0.560	0.420	0.353	0.290	0.181	0.131	0.090	0.03
	10	0.768	0.660	0.556	0.413	0.345	0.280	0.173	0.123	0.080	0.03

energies:- 1, 2, 5, and 10 MeV. As may be seen from Table II, where Yadav's results are given, above 2 MeV the energy dependence of R is very small. The result for 10 MeV is plotted in fig. 7, and comparison with the corresponding curve taken from Feshbach's work (fig. 6) shows good agreement.

The exact scattering cross section for mercury, which both the above authors used in checking their approximations, was calculated by Massey who[7], on the assumption that the positron was a Dirac particle with positive charge, made the necessary changes of sign in Bartlett and Watson's electron calculations. His result, together with the original result for electrons, is shown in fig. 8. Also in this figure are shown the positron versions of the two Mott approximations mentioned above. It may be seen that of these the simpler one, R_{M_1}, is the more accurate and gives fair agreement with the exact cross section at all angles.

Again, as in the case of electron scattering, the values used for comparison with experiment will be the improved "α^4" ones given by Feshbach and estimated by him to lie within 2% of the true point nucleus cross section for all values of θ.

(c) Modification of cross sections due to finite size of nucleus.

Having obtained a reasonably accurate evaluation of the cross section for scattering by a point nucleus, we must now consider the modifications to this cross section made necessary by the fact that at the energies with which we are concerned the nucleus may no longer be considered as a point, since the wave-length of the incident electrons is of the same order of magnitude as the dimensions of the scattering nuclei. In this case, as Acheson[8] has pointed out, a reduction of the cross section is to be expected in some directions owing to interference between the scattered waves originating from different parts of the nucleus.

The effects of finite nuclear size were first considered by Rose[9] who took two cases - the scattering of electrons by (a) deuterium and (b) heavy nuclei. The first case will not be considered here. For the second case Rose calculated the deviation from "point nucleus" scattering for a scattering angle of 90° and an energy of 50 MeV, assuming a uniform charge density. The validity of these results was questioned by Acheson[8] on the grounds that Rose had employed the Born approximation in his calculations so that they could not be expected to apply to heavy nuclei.

Without using this approximation Acheson made a calculation of the phase shift produced in the scattered electron wave for two nuclear models (a) a uniform distribution of charge throughout the nucleus, and (b) a shell distribution (uniform distribution of charge over the surface of the nucleus). He assumed that the nuclear radius could be represented by $r = 1.45 \times 10^{-13} A^{1/3}$ cm. and obtained the ratio of the scattering cross section to that for a point nucleus for Z = 13, 29, 50, and 79 and for electron energies of 15 - 35 MeV. These results, including extrapolated values for 10 MeV obtained by the present writer, are shown in fig. 9.

Acheson points out in his paper that different charge distributions will produce different phase changes - raising the possibility that accurate measurements of scattering cross sections might yield information on the distribution of charge in the nucleus. Feshbach[10] however, has shown that provided that the quantity $ER/\hbar c \ll 1$ (E = electron energy, R = nuclear radius), that is up to energies of 20 - 30 MeV, the effects of different distributions (if spherically symmetrical) are the same as those of changes of nuclear size. In particular, a shell distribution, in which the charge is uniformly distributed over the surface of a sphere of radius R_s, produces the same scattering as a uniform distribution throughout a sphere of radius R_v if $R_s = 0.56 R_v$.

Rosen[11] has pointed out in a recent paper that the expression which Feshbach assumes in his paper to be much less than unity is in fact in many cases (for example, for heavy nuclei and energies of about 20 MeV) of the same order, or bigger than, unity. Rosen verifies Feshbach's conclusions [illegible] that the conclusions given above apply up to energies of about 20 MeV.

Recently Elton[12] has extended these calculations to higher energies and has shown that, at least up to about 40 MeV., there is no hope of distinguishing experimentally between different charge distributions. Elton has used the Born approximation to estimate at what energies effects due to nuclear size become appreciable and has then carried out an accurate numerical calculation at one energy and for one type of nucleus. These calculations were made for (A) a point nucleus, (B) a uniform spherical charge distribution and (C) a uniform shell distribution. B and C were both for a nuclear radius of $(e^2/mc^2) A^{1/3} = 1.41 \times 10^{-13} A^{1/3}$ cm. In Table III Elton's values of $\sigma(B)/\sigma(A)$ obtained with the Born approximation are given for aluminium for $\theta = 30°$ and $150°$ and for electron energies from 2.5 to 40 MeV. In Table IV the same quantities are given for gold. From these tables it may be seen that noticeable deviations from "point nucleus" scattering may be expected for energies > 40 MeV. for light elements and > 20 MeV for heavy ones.

Elton's exact calculation was carried out for gold nuclei and an energy of 20 MeV. The ratio $\sigma_{(B,C)}(\theta)/\sigma_{(A)}(\theta)$ so obtained is shown,

Tables III & IV

TABLE 3

ALUMINIUM

θ	30°		150°	
E_e/mc^2	B	C	B	C
5	1.00	1.00	1.00	1.00
10	1.00	1.00	1.00	0.99
20	1.00	1.00	0.96	0.94
40	1.00	0.98	0.86	0.78
80	0.96	0.94	0.55	0.35

TABLE 4

GOLD

θ	30°		150°	
E_e/mc^2	B	C	B	C
5	1.00	1.00	1.00	0.99
10	1.00	1.00	0.97	0.95
20	1.00	0.98	0.87	0.79
40	0.97	0.94	0.57	0.37
80	--	--	--	--

uniformly distributed over the surface of a sphere of radius R_s, produces the same scattering as a uniform distribution throughout a sphere of radius R_u if $R_s = 0.36\ R_u$.

Bodmer[11] has pointed out in a recent paper that the expression which Feshbach assumes in his proof to be much less than unity is in fact in many cases (for example for heavy nuclei and energies of about 20 MeV) of the same order, or bigger than, unity. Bodmer verifies Feshbach's conclusions without this limitation, and estimates that the conclusions given above apply up to energies of about 30 MeV.

Recently Elton[12] has extended these calculations to higher energies and has shown that, at least up to about 40 MeV., there is no hope of distinguishing experimentally between different charge distributions. Elton has used the Born approximation to estimate at what energies effects due to nuclear size become noticeable and has then carried out an accurate numerical calculation at one energy and for one type of nucleus. These calculations were made for (A) a point nucleus, (B) a uniform spherical charge distribution and (C) a uniform shell distribution. B and C were both for a nuclear radius of $(e^2/2mc^2)A^{1/3} = 1.41 \times 10^{-13} A^{1/3}$ cm. In Table III Elton's values of $\sigma_{(B,C)}(\theta)/\sigma_{(A)}(\theta)$ obtained with the Born approximation are given for aluminium, for $\theta = 30^\circ$ and 150° and for electron energies from 2.5 to 40 MeV. In Table IV the same quantities are given for gold. From these tables it may be seen that noticeable deviations from "point nucleus" scattering may be expected for energies > 40 MeV. for light elements and > 20 MeV for heavy ones.

Elton's exact calculation was carried out for gold nuclei and an energy of 20 MeV. The ratio $\sigma_{(B,C)}(\theta)/\sigma_{(A)}(\theta)$ so obtained is shown, as a function of θ, in fig. 10.

Parzen[13] has carried out similar calculations for scattering by mercury nuclei of 100 MeV electrons, using (a) a nuclear radius of 8.09×10^{-13} cm. and a uniform charge distribution, (b) the same radius with the charge density increasing by 43% from the centre to the outer edge (the type of distribution suggested by Feenberg[14]) and (c) a uniform distribution with the radius decreased by 5% - to indicate the sensitivity of the scattering to nuclear size. The results are shown in fig. 11 where the similarity to an optical diffraction pattern may be seen at once. Unfortunately, as has since been pointed out,[15] a numerical error was made in the calculation of these results and the actual values given in fig. 11 cannot be regarded as reliable. The general shape of the curve is, however, that to be expected for a sharply bounded nucleus of the type used in the calculation.

For positrons Elton and Parker[16] have recently calculated the effect by a method similar to that used by Elton for electrons and described above. The calculation was made for gold nuclei and an energy of 20 MeV. As can be seen from fig. 12 the effect is considerably smaller than for electrons, which is to be expected since the positrons will not, in general, approach as close to the nucleus as will electrons of the same energy. Also, as fig. 13 shows, the ratio $\sigma^-(\theta)/\sigma^+(\theta)$ is very considerably altered when this effect is taken into account.

(d) Other effects.

In a general consideration of electron and positron scattering several other factors, besides the finite size of the scattering nucleus, must be taken into consideration. For example, scattering by atomic electrons and the action of these electrons in screening the nuclear charge and the effect of nuclear multipole moments and of radiation by the electrons when scattered may all, under certain circumstances, modify the scattering cross section.

In the work to be described in Section 2 cases of electron-electron or positron-electron scattering can, provided that the atomic electron acquires a significant energy, be easily distinguished from nuclear scattering events by the presence of a second track at the scattering point. In other work, such as the measurement of scattering in foils with ionisation chambers or Geiger counters as detectors, it is not so easy to separate the two types of scattering, though in this case allowance may be made by reducing the measured cross sections by an amount calculated from the theory of electron-electron scattering. In the work of Lyman, Hanson and Scott, to be described later[17], the use of an analysing magnet enabled electron-electron events to be separated out because of the considerable energy loss which the scattered particle undergoes in this process. This is shown later (in fig. 18). These authors made a study of electron-electron scattering at the same time as their nuclear scattering work was done, and found that their results agreed well with Møller's theory[18]. Because of the above considerations this process will not be considered further here.

The effects of nuclear screening by atomic electrons have been considered by Mohr[19] for gold atoms and electron energies of up to 1 MeV. The calculations indicate that, in this case, screening is important only for large angles of scattering ($\theta > 90^{\circ}$) and that for relativistic velocities the effect is independent of energy. Mohr's accurate equations are complicated, but for angles of scattering less than 90° it is shown that

Table V.

TABLE 5

$\Delta\sigma$ (%)									
E_e (Mev)		2.5			4.0			9.5	
θ	45°	90°	135°	45°	90°	135°	45°	90°	135°
ΔE (Kev.)									
10	4.8	7.4	8.7	6.9	9.9	11.3	12.4	15.9	17.5
25	3.9	6.0	7.1	5.7	8.1	9.3	10.5	13.5	14.8
50	3.2	5.0	5.9	4.7	6.8	7.9	9.0	11.7	12.8
100	2.5	3.9	4.7	3.8	5.5	6.4	7.6	9.9	10.8

the ratio of the scattering cross section to the Rutherford cross section is given by

$$R = \left(1 + \frac{\pi}{2} \cdot \frac{z}{137.2} \cdot \frac{v}{c} \cdot \sin \frac{\theta}{2}\right)^2 \qquad (11)$$

From this formula the dependence upon θ and independence of energy mentioned above can be seen and it is also clear that the effect is less important for smaller values of Z, so that in the present work ($\theta < 90^\circ$, Z = 35 or 47) the effect will be small. This is shown in fig. 14, where Mohr's results are plotted for an energy of about 1 MeV. and it can be seen that up to $\theta = 90^\circ$ the unmodified Bartlett and Watson formula (or its equivalent for lighter nuclei, the corrected "α^4" formula) is adequate.

The effects of nuclear multipole moments have recently been considered by Parker[20] who showed that the nuclear magnetic and electric quadripole moments (and so very probably also higher order multipoles) could be ignored in scattering experiments because the alteration to the cross section caused by these moments is much less than the experimental error. (Even if the nuclei were aligned so as to give the maximum effect it would amount only to about 0.1% of the normal cross section.)

The last effect which we shall consider, that due to radiation of energy by scattered particles, has been the subject of calculations by Schwinger[21], and by Elton and Robertson[22], who pointed out errors in Schwinger's work. Since in a consideration of this effect the Born approximation is used, the results hold only for low Z elements (up to about Z = 15 according to McKinley and Feshbach[3]). Calculations valid for values of Z corresponding to silver and bromine have not yet been made. Table V, taken from Elton and Robertson's paper, shows the percentage

Table VI.

TABLE 6

Scat-terer.	Energy (MeV)	Angle of Scatter (θ)	(Metres) Track Length	No. of Deflections	σ Exptl. / σ Theo.
N	0.4 - 1.1	20 - 180°	875	201	0.85
N	1.5 - 3.0	20 - 180°	180	212	10 - 100
N	0.2 - 1.1	20 - 180°	82	113	1.7
N	1.5 - 3.0	20 - 180°	116	92	12
N	0.3 - 2.5	20 - 180°	294	47	0.7
N	0.2 - 3.0	15 - 180°	515	42	1.3
N	0.2 - 3.1	15 - 180°	367	41	1.5
F	0.2 - 3.0	15 - 180°	910	113	1.2
A	1.7 - 2.4	30 - 100°	350	48	0.75
A	0.2 - 1.1	20 - 150°	103	308	1.0
A	1.5 - 3.0	20 - 150°	130	84	2.5
A	0.2 - 3.0	20 - 180°	708	135	1.5
Kr	0.2 - 3.0	40 - 180°	140	10	0.16
I	0.7 - 1.2	20 - 180°	-	-	0.4
I	0.8 - 3.2	15 - 180°	459	249	1.0
Xe	0.5 - 2.6	40 - 180°	240	51	0.2
Xe	2.1	20 - 180°	64	161	0.85
Xe	2.1	40 - 180°	172	101	0.85
Hg	0.5 - 1.1	20 - 180°	350	152	0.15

Table VI

change in the scattering cross section caused by the radiation of an amount of energy up to ΔE during the scattering process. It can be seen from this Table that for values of ΔE detectable in the present work, provided that the effect for silver and bromine nuclei is not much greater than that for $Z < 15$, the correction will be small.

To summarise the effects of the various processes and factors considered in this section we may say that it appears fairly certain that the effects of electron-electron scattering, of multipole nuclear moments and of nuclear screening will, in the work to be described in Section 2, be negligible and that although accurate calculations of the effect have not been made, the indications are that the effect of radiation during scattering will be small. Only the effects of finite nuclear size are likely to be appreciable and for these the expected variation of cross-section for electrons can readily be calculated, and, as will be shown in the following section, this variation has been verified by other experiments. For positrons the effect will be smaller but it has not been verified experimentally.

1.2.2. Experimental work on the single scattering of electrons and positrons.

(a) Electrons.

Although measurements of the scattering of electrons have been made continually over the past thirty years, until about six years ago considerable divergence existed between different authors' experimental results. Table VI, taken from a paper by Randels, Chao and Crane[(23)], summarizes some of the early results and their wide divergence can be seen at once. Most of the disagreement has now been shown to be due to

Table VII

Table VII

TABLE 7

Gas.	Energy Range (Mev).	Eff. Energy (Mev).		No. of Scatters						
				15-25°	25-30°	35-45°	45-55°	55-65°	65-75°	75-85°
Air	0.9-1.3	1.1	Th.	63	14.1	5.1	2.3	1.3	0.7	0.4
			Ex.	43	16.0	6.5	2.0	2.0	2.0	0
Air	1.3-1.6	1.4	Th.	66	14.7	5.3	2.4	1.4	0.8	0.5
			Ex.	45.5	22.0	6.0	2.5	2.0	0	0
A	0.8-3.3	2.4	Th.	30.3	7.2	2.7	1.3	0.7	0.4	0.2
			Ex.	30.0	10.5	5.0	2.5	1.0	0	1.0
A	3.3-9.3	4.6	Th.	32.2	7.6	2.8	1.4	0.7	0.4	0.2
			Ex.	52.0	10.5	4.5	5.0	1.0	0	0
Kr	1.9-9.3	4.5	Th.	33.0	7.5	2.8	1.4	0.7	0.4	0.3
			Ex.	43.0	7.0	1.0	1.0	0	0	1.0
Xe	1.5-2.9	2.0	Th.	80.0	17.0	6.0	2.8	1.5	0.9	0.5
			Ex.	73.5	17.0	7.5	3.0	1.0	2.0	1.0
Xe	2.9-5.8	4.7	Th.	47.0	21.0	7.4	3.5	1.8	1.0	0.6
			Ex.	62.5	23.5	3.5	2.5	3.0	2.0	0
Xe	5.8-2.0	7.5	Th.	90.0	20.0	6.9	3.3	1.8	1.0	0.6
			Ex.	86.5	27.5	18.0	3.5	3.0	0	0
Total			Th.	569.5	126.7	45.3	21.0	11.5	6.5	3.9
			Ex.	529.5	152.5	64.0	27.0	13.5	9.0	3.0

experimental short-comings, such as, in the case of scattering by foils, insufficient correction for multiple scattering effects and for geometrical effects of the apparatus. About six years ago careful experiments were performed which established reasonably well the agreement between experiment and theory up to electron energies of at least 3 MeV, and more recently agreement has been found at higher energies. Some of these experiments will be described before an account is given of the more recent work.

A typical example of the expansion chamber experiments is that of Randels, Chao and Crane, described in the paper mentioned above. The apparatus is shown in fig. 15. Electrons from a radio-active source (P^{32} for energies up to 1.5 MeV., Ra for 1.5 to 2.5 MeV. and Li^{8} for 2.5 to 12 MeV.) passed through a crude slit system before entering an expansion chamber through a thin window. A magnetic field was applied across the chamber and the radii of curvature of those tracks exhibiting a scatter were measured both before and after the scatter. The chamber was operated automatically and about 800 scatters were found with $15^{\circ} < \theta < 90^{\circ}$ in a total track length of 2173 metres with, in turn, air, argon, krypton and xenon fillings and for electron energies of from 0.9 to 12 MeV. θ was determined in this experiment by fitting specially drawn cards to the tracks. The results, after correction for multiple scattering effects, were compared with the simpler Mott formula (σ_{M_1}), given in Section 1.2.1. They are shown in Table VII from which it can be seen that generally the experimental cross sections tend to be greater than the value of σ_{M_1} and reference to fig. 3, of Section 1.2.1 confirms that σ_{M_1} is rather smaller than the true cross section. In view of the poor statistics probably no more quantitive

TABLE 8

Angular Interval	Observed no. of Scatters	Corrected no.	Theo.
85 - 100°	74	88	[illegible]
100 - 120°	34	34	[illegible]
120 - 180°	23	23	[illegible]
Total 85-180°	131	145	11[illegible]

Table VIII.

<u>TABLE 8</u>

Angular Interval	Observed No. of Scatters	Corrected No.	Theo. No.[1]
85 - 100°	74	88	55
100 - 120°	34	34	37
120 - 180°	23	23	26
Total 85-180°	131	145	118

conclusion can be drawn from the results. Loss of energy in scattering was found to be very small (only two cases of loss of more than 50% of the incident energy were found.)

An improved technique was used by Champion and Roy(24) for the study of large angle scattering events. The labour of searching for such scatters was reduced by using Geiger counters to detect events in which θ was greater than 90°. On the occurrence of such events during the sensitive time of the expansion chamber the counters, shown by C_1, C_2, and C_3 in fig. 16, caused the chamber illumination to flash. In this way about 1500 expansions were made for each photograph which was taken and only 130 photographs were taken for an effective total track length of nearly 100 Km. with electrons of about 1 MeV. scattered by nitrogen. The observed number of scatters for a given angular interval was corrected for the selectivity of the apparatus (for example, a scatter of less than 120° at Q in fig. 16 would not be recorded) and this effect was kept small by accepting only those tracks whose scatter occurred within the dotted circle shown in the figure.

The results of this experiment are shown in Table VIII, and it can be seen that, with the exception of the angular interval from 85° to 100°, the agreement with Mott's formula (again σ_{M_1} was used) is good. The discrepancy for the 85° - 100° interval is attributed by the authors to the tendency of an observer to include some tracks with scatters of less than 85° in this group rather than to reject them altogether. Again statistical considerations prevent more detailed conclusions being made from the results.

With the development of the Van de Graaff generator intense beams

Table IX

TABLE 9

Element	E_e (MeV)	θ						
		30°	35°	40°	45°	50°	55°	60°
		σ Exptl. / σ Theo.						
Be	2.1	-	1.02	0.98	0.93	1.00	0.97	0.93
	2.2	-	0.97	0.98	0.96	0.99	0.99	1.11
	2.3	-	0.98	1.00	1.01	1.00	0.99	1.02
Ae	2.1	-	0.94	0.94	0.94	0.93	0.95	0.91
	2.2	-	1.00	1.02	1.03	1.06	1.02	1.03
	2.3	-	1.02	1.00	1.05	0.99	1.04	1.00
Cu	1.49	0.97	-	0.88	-	1.12	-	-
	1.81	0.96	-	1.09	-	1.07	-	-
	2.00	1.05	-	0.96	-	0.96	-	-
	2.27	1.15	-	1.06	-	-	-	-
Ag	1.27	-	-	0.93	-	-	-	-
	1.49	0.97	-	1.03	-	1.02	-	-
	1.81	0.97	-	1.02	-	1.03	-	-
	2.00	1.01	-	1.06	-	1.07	-	-
Au & Pt	1.49	-	-	-	-	1.08	-	-
	1.81	-	-	-	-	1.09	-	-
	2.00	-	-	1.10	-	1.10	-	-

of effectively mono-energetic electrons became available and the possibility of using ionisation chambers in scattering measurements ~~were~~ increased. Van de Graaff and his associates(25) in fact disposed of most of the disagreement between the earlier experimental results by making precise measurements with an electrostatic generator and an ionisation chamber. Their apparatus is shown diagramatically in fig. 17. A differential ionisation chamber, which recorded only those particles penetrating the front window but not penetrating the centre electrode, was used to reduce the background current and θ was measured, to 1 min. of arc, over a range from 30° to 60°. The energy of the electrons was known to 1% and they were scattered by thin foils at the centre of the scattering chamber.

The ratio of observed scattering cross section to that given by the second Mott formula (σ_{M_2} of section 1.2.1) for Be, Al, Cu, and Ag and that given by Bartlett and Watson for Au and Pt are shown in Table IX for electron energies of 1.27 to 2.30 MeV. It is seen at once that in this case, where statistical uncertainties are small, good agreement with theory is obtained - the experimental error being estimated to be about $\pm 4\%$. Reference to fig. 3 of Section 1.2.1 shows that the agreement between σ_{M_2} and the true cross section is good even up to 10 MeV. for all those elements for which it was used in this work.

Recently Paul and Reich(26) have published the results of an experiment in which 2.2 MeV. electrons from a betatron were scattered by foils of Al, Sn, and Pt, the scattered beam being detected by two Geiger counters in coincidence. The variations of σ with Z was found to be different from that predicted by McKinley and Feshbach (the " α^4 " formula of section 1.2.1). The results are shown in fig. 18, from which it can be seen that for high Z elements the divergence from the "α^4" curve amounts to about 20%. On the other hand, this divergence arises entirely from the measurements with Pt foils, the other results being in agreement with McKinley and Feshbach's calculations and it appears possible that some experimental condition may have been responsible for the disagreement in the case of Pt.

For energies greater than those available from the Van de Graaff type of accelerator and for large scattering angles accurate experimental results have until recently been very rare. When it became possible to extract the beam from accelerators such as the betatron, however, the possibility of further accurate work arose.

In 1951 Lyman, Hanson and Scott(17) reported the results of one of the most thorough and complete measurements of electron scattering so far carried out. The 15.7 MeV. electron beam of a betatron was extracted, focussed magnetically and allowed to pass, entirely in vacuo, to a thin scattering foil of polystyrene, Al, Cu, Ag or Au. Scattered electrons were detected at angles of from 30° to 150° by means of a coincidence arrangement of Geiger counters and the undeflected beam was measured with a Faraday chamber. Before reaching the detector the scattered electrons were analysed by a magnetic field so that the energy distribution after scattering could be determined and during the measurement of elastic scattering all electrons which had lost more than 3% of their initial energy were excluded from the detector.

The apparatus, which is shown in fig. 19, was carefully aligned and the observed scattered intensities were corrected for multiple scattering, electron-electron scattering, loss of electrons due to radiation of more than

3% of initial energy and the effects of the detecting aperture size. None of these corrections amounted to more than 10%. The energy spectrum of the scattered electrons is shown, for the case of scattering through 30° by carbon nuclei (polystyrene scatterer), in fig. 20, in which electron-electron and electron-nucleus events can be seen to be clearly separated. Results were collected in this work over the period of a year, during which time the errors of measurement were gradually reduced - the results shown in fig. 21 are the last and most accurate. In this figure the experimental cross section is expressed as a ratio to the simpler Mott formula (σ_{M_1}) and plotted against θ for various scattering elements (the lines merely connect together the experimental points and have no theoretical significance). Accurate theoretical cross sections (σ_c) were calculated for scattering by point nuclei from the α^4 formula and the ratio $\sigma_{expt.}/\sigma_c$ was plotted against θ as shown in fig. 22. The variation of this ratio from unity was attributed to the effects of the finite size of the scattering nuclei and the curves of fig. 22 are those calculated by the method of Acheson (mentioned in Section 1.2.1) for a nucleus of radius $r = 1.37 \times A^{1/3} \times 10^{-13}$ cm. Only in the case of scattering by gold nuclei was it possible to distinguish between different charge distributions in the nucleus and as can be seen from fig. 22 the experimental results favoured a uniform rather than a shell distribution and might be taken to indicate a distribution in which the charge density was greater at the centre of the nucleus than at the surface.

Recently Fidd et al.[27] have published an account of their experiments on electron scattering at energies up to 50 MeV. The electrons were scattered, while still inside the vacuum chamber of a "race-track", by a thin foil and the scattered particles emerged through an aluminium window to a detecting system consisting of a magnetic analyser and a Geiger counter telescope, all of which could be set at any angle from 45° to 135° with respect to the incident beam. A similar detector was set permanently at 90° on the opposite side of the target from the rotatable detector and was used to normalise readings. Because the incident beam intensity and effective target thickness could not be determined accurately, absolute cross sections could not be obtained. The ratio $\sigma(\theta)/\sigma(90^\circ)$, when plotted against θ as shown, for a 0.007 inch tungsten foil, in fig. 23, agreed reasonably well with a uniform charge distribution model. The agreement was not so good, however, when, as in fig. 24, the ratio $\sigma(60^\circ)/\sigma(90^\circ)$ was plotted against (mass number)$^{1/3}$. A uniform charge distribution with $r = 1.45 \times A^{1/3} \times 10^{-13}$ cm. (which corresponds to that used by Lyman et al.[17]) predicts a constant value of about eleven for all elements. It is stated in this paper that the nuclear model proposed by Wilson[28], which consists of a saturated core of charge surrounded by an exponentially decreasing distribution, may give the best agreement with the experimental results. Further measurements of this kind at higher energies would be of great value in establishing the nature of the distribution.

Recently an experiment of this type, similar in its experimental arrangement and its accuracy, to that of Lyman, Hanson and Scott but using electrons of 125 to 150 MeV. energy has been described by Hofstadter et al.[15]. The source of electrons was a "racetrack" from which the beam was removed by a deflecting magnet. After removal the beam was focused onto a scattering foil by a second magnet and the electrons scattered at a given angle in the foil were analysed by a third magnet and detected by a Cerenkov counter.

The unscattered beam was monitored by an ionisation chamber.

When measurements were made with this apparatus it was found that the scattered beam suffered energy losses depending upon the angle of scattering and the type of scattering nucleus. These losses were interpreted as resulting from the recoil of the scattering nucleus. The amount by which the peak of the scattered beam was shifted could be used to identify the scattering nucleus, as is shown by fig. 25 where the beam is scattered at 45° by a polyethylene target. The two peaks due to scattering by hydrogen and by carbon are seen to be clearly resolved.

After results had been obtained at a low energy (25 MeV) to check that they agreed with those of Lyman, Hanson and Scott, measurements were made at 125 and 150 MeV with foils of beryllium, gold, lead and tantalum. The results are shown in fig. 26. Fig. 26(a) shows that a marked deviation from "point nucleus" scattering occurs and that Parzen's prediction of sharp maxima and minima in the scattered intensity is not verified, indicating that the nuclear boundary is not sharp. Several types of charge distributions were used in efforts to fit these results and the best fit was found for a distribution decreasing exponentially with increasing radius. It is pointed out in Hofstadter et al.'s paper and in one by Schiff[29] on the interpretation of the experimental results, that accurate values of the theoretical cross sections, not involving the Born approximation, have not been made for these energies and that the main conclusions which can be made from the results are that the charge density falls with increasing distance from the centre of the nucleus and that the nuclear boundary is, at any rate for electrons scattering forces, not sharp.

(b) Positrons.

The experimental data on positron scattering are much less complete than those on electron scattering and here again considerable divergence is to be found between the early results of different experimenters. Disagreement was particularly marked between different early measurements of the ratio of elastic to inelastic scattering - Barker and Champion[30], Le Prince Ringuet[31], Sen Gupta[32] and others using cloud chambers reported much more inelastic scattering than theory predicted, whereas Bothe[33] using a magnetic β-ray spectrograph to analyse the scattered particles did not find any anomalous inelastic scattering. All the above experimenters used radio-active sources to provide their incident particles and much of the disagreement is undoubtedly due to uncertainties over the particle energy, to poor statistics and to experimental difficulties such as poor cloud chamber illumination.

The most recent positron scattering results are those of Cusack[34], of Howatson and Atkinson[35], and of Roy and Groven[36], all using expansion chambers, and that of Lipkin[37] in which a Geiger counter and a magnetic spectrograph were used to detect the scattered beam. The experiments of Cusack and of Howatson and Atkinson were very similar, differing mainly in the gas filling of the expansion chamber which was nitrogen in the former case and argon in the latter. In both cases an automatic chamber was used with gas discharge illumination and about 150 metres of track were examined. Howatson and Atkinson selected tracks of about 0.7 MeV. energy from Cu^{62} whereas Cusack used a mean energy of about 0.3 MeV. from Cu^{64}, thereby almost doubling the number of scattering events observed. Roy and Groven used Rh^{102} to provide positrons of 0.53 - 0.98 MeV. energy, which were scattered in nitrogen. 8000 photographs yielded 85 scatters in 712 metres of track.

Tables X & XI

TABLE 10

Author	Energy (MeV)	Scatterer	No. of Scatters	Concl
Fowler and Oppenheimer (1938)	10.5	Pb	9 (>14.5°)	e^-/e^+ =
Lasich (1948)	0.45	Au	30 (>17°)	e^-/e^+ =
	0.68	Au	30 (>17°)	e^-/e^+ =
	0.95	Au	30 (>17°)	e^-/e^+ =
Howatson and Atkinson (1951)	0.7	A	65.5(>20°)	N_{Exp}/N_{The}
Cusack (1952)	0.3	N	114 (>20°)	N_{Exp}/N_{The}
Roy and Groven (1952)	0.53-0.98	N	85 (>15°)	N_{Exp}/N_{The}

TABLE 11

Foil	Energy (MeV)	$(e^-/e^+)_{Meas^d.}$	$(e^-/e^+)_{Corr^d.}$	Statistical Error (%)
0.00068" Cu	0.68	1.73	1.73	4
	0.98	1.93	1.93	5
	1.29	2.07	2.06	11
0.0002" Pt	0.68	2.27	3.17	4
	0.98	2.88	3.30	5
	1.29	3.00	3.68	11
0.0001" Pt	0.68	3.13	3.14	5
	0.98	3.13	3.22	4
	1.29	3.60	3.70	10

The results of these experiments are shown, together with those of earlier work by Lasich[38] and by Fowler and Oppenheimer[39], in Table X, which is considered to represent all the reliable experimental evidence on positron scattering available from expansion chamber work. It can be seen that the results are very meagre and do not offer any marked support for theory. Neither of the recent experiments described above yielded any evidence of excessive inelastic scattering.

Undoubtedly the most valuable experiment on positron scattering which has so far been performed is that of Lipkin in which the scattering of 1 MeV. positrons and electrons was compared using Al, Cu, Pt, and Pb foils. The apparatus is shown in fig. 27. Electrons from Ce^{144} or positrons from Ga^{66} were focused by the solenoid onto the scattering foil and those which were scattered through 57.9° passed out along the axis of the solenoid to an analysing magnet after which they reached a Geiger counter where they were detected. One disadvantage of this apparatus is that only one scattering angle could be used, but against this must be counted the fact that electron and positron scattering could be compared under almost identical conditions and the ratio σ^{-}/σ^{+} found accurately. McKinley and Feshbach's value for the ratio of electron to positron scattering cross sections for carbon was accepted in this experiment and used to normalise the source strengths before comparisons of the scattering by other elements were made. Corrections were applied to the observed numbers of scattered electrons and positrons to allow for multiple scattering in the foils, the effects of which were checked in the case of scattering by platinum by using two foils of different thicknesses.

The results of this work are shown in Table XI. Again no evidence of excessive inelastic scattering was found - in fact only in the case of aluminium was any evidence found of this type of scattering.

To summarise the present position concerning the single scattering of electrons and positrons, the experimental results for electrons appear at all energies to agree reasonably with the predictions of theory when allowance is made for finite nuclear size etc. In the case of positron scattering, however, much less experimental evidence has been obtained and at the energies available in the present work ($\sim$ 10 MeV.) the information is very meagre.

1.3. Previous work on multiple scattering.

1.3.1. Theory.

In this section the theoretical treatment of multiple scattering by various authors will be summarised, first the original theory of E. J. Williams and then the later theories which have been developed by various writers in order to improve the range of application and the accuracy of the theoretical predictions.

(a) Williams' theory of multiple scattering.

The first comprehensive theory of multiple scattering of charged particles by atoms was given by E. J. Williams in 1938[40]. This theory will be outlined below so that the later modifications may be made clear. Williams considered a beam of electrons of velocity v passing through a medium with N atoms per cc. and with atomic number Z. The probability that in travelling a distance t in this medium an electron will suffer a single deflection through an angle θ to $\theta + d\theta$ is given by

$$P(\theta)d\theta = 2\pi Nt\sigma(\theta)\sin\theta\, d\theta \,.$$

Assuming that conditions are such that the Rutherford theory of single scattering applies (i.e. for small angles, low Z nuclei and negligible effects due to finite nuclear size etc.), we have

$$P(\theta)d\theta = \left[8\pi NtZ^2e^4(1-\beta^2)/m^2v^4\theta^3\right] d\theta \quad (\text{putting } \sin\theta/2 = \theta/2 \text{ and } \cos\theta/2 = 1)$$

If we now take some angle θ_1, such that the probability of scattering through an angle greater than θ_1 in the distance t is unity, we have

$$\int_{\theta_1}^{\pi} P(\theta)d\theta = 1$$

so that

$$\theta_1^2 = 4\pi NtZ^2e^4(1-\beta^2)/m^2v^4.$$

Since the Rutherford cross section increases rapidly with decreasing angle the occurrence of scattering through angles smaller than θ_1 will be frequent and these scatters will give an approximately Gaussian distribution of the resultant angle, α, i.e.

$$P_1(\alpha)d\alpha = (2/\pi\bar{\alpha})\exp.(-\alpha^2/\pi(\bar{\alpha})^2)d\alpha = (2/\pi\bar{\alpha})\exp.(-\alpha^2/2\overline{\alpha^2})\, d\alpha$$

where $\bar{\alpha}$ is the mean and $\overline{\alpha^2}$ the mean square, of the individual deflections making up α. Hence

$$\overline{\alpha^2} = \int_0^{\theta_1}\theta^2P(\theta)d\theta = \left[8\pi NtZ^2e^4(1-\beta^2)/m^2v^4\right]\left[\log\theta\right]_0^{\theta_1} \qquad (12)$$

In order to obtain a finite value for $\overline{\alpha^2}$ we must set a lower limit to the permissible values of θ and this is justified by the effects of electron screening, which we have hitherto neglected. If an electron passes outside the outermost shell of an atom we may take its deflection to be zero, whilst if it passes inside this shell it will suffer a deflection not less than a certain value, θ_{MIN}. The value of θ_{MIN} depends upon whether the experimental conditions favour the classical or the Born approximation cases, i.e. upon whether $Ze^2/137\beta \gg 1$ (classical) or $\ll 1$ (Born approximation). In the latter case, which usually applies in electron scattering, Williams found, on the assumption of a Fermi-Thomas atomic field, that

$\theta_{MIN} = 2.1\, Z^{\frac{1}{2}}\hbar\,(1-\beta^2)^{\frac{1}{2}}/mva_o$ where a_o is the radius of the first Bohr orbit of hydrogen, giving

$$\overline{\alpha^2} = 2\,\theta_1^2 \log\left[65.3\,\beta\,\theta_1/(1-\beta^2)^{\frac{1}{2}}Z^{\frac{1}{3}}\right] \qquad (13)$$

The corresponding result for the classical case was $\theta_{MIN} = 3.8\, Z^{1/3}e^2/pva_o$.

Considering only the projections, ϕ, of the true scattering angles in the plane perpendicular to the line of view - the quantities usually measured in expansion chamber and photographic plate determinations of scattering, one finds $\phi_{MIN} = 1.75\, Z^{\frac{1}{3}}\,\hbar/p\,a_o$. The mean absolute deviation of ϕ is

$$\langle\phi\rangle = \left[2e^2(N\,Z^2)^{\frac{1}{2}}t^{\frac{1}{2}}/pv\right]\left[\log \phi_1^2/\phi^2_{MIN}\right]^{\frac{1}{2}}$$

and

$$\overline{\alpha_1} = \left[2(NZ^2)^{\frac{1}{2}}e^2t^{\frac{1}{2}}/pv\right]\left[\ln(2\pi Z^{1/3}Nt\,\hbar^2/3.1\, m^2v^2\phi\right]^{\frac{1}{2}} = \delta\, xL_N \qquad (14)$$

Finally, if the contribution of projected scatters $> \phi_1$ is taken into account, one finds $\overline{\alpha_T} = (1.45\,\delta + 0.80\,\overline{\alpha_1})$ (15)

(b) Improvements on Williams' theory.

Since this study of multiple scattering was published in 1938, several authors have described modifications and improvements to it. All the modified theories are however closely related, and all lead to formulae similar to equation (14) above, with the same value of δ in all cases but different expressions for L.

Goudsmit and Saunderson[41] have developed a more rigorous theory than that outlined above, in which they denote by $P(\theta)d\omega$ the probability that, in a collision, an electron will be scattered into the solid angle $d\omega$ around θ, i.e. $P(\theta) = \sigma(\theta)/Q$ where Q is the total cross section. $P(\theta)$ is then expanded in the form $P(\theta) = \sum(2n + 1)f_n P_n(\cos\theta)$ and the chance of the scattered electron being in the solid angle $d\omega$ around θ after two collisions, and then, generally, after s collisions, is calculated. Combining with this the probability W(s) that an electron will suffer s collisions, Goudsmit and Saunderson find for a Fermi-Thomas field

$$\overline{\alpha}^2 = \left[8\pi Nt\ Z^2 e^4(1 - \beta^2)/m^2v^4\right] \log(0.64\ \theta_1/\theta_{MIN})$$

that is

$$\overline{\alpha} = \delta \times \ln(0.64\ \theta_1/\theta_{MIN})^{\frac{1}{2}} = \delta \times L_{G.S.} \qquad (16)$$

in agreement with Williams' equation (equation (14) above) from the simpler treatment. The difficulties of the two approximations (Born approximation and classical) for different experimental conditions still remain, however.

In 1947 Molière[42] derived a multiple scattering equation in which the disadvantage of two different solutions for the extreme conditions ($Ze^2/137\beta \gg 1$ or $\ll 1$) and none for the intermediate state ($Z e^2/137\beta \simeq 1$) was removed by means of an exact quantum-mechanical study of single scattering, yielding an expression for ϕ_{MIN} which holds with reasonable accuracy for all values of $Ze^2/137\beta$. This expression is:-

$$\phi_{MIN} = \left[Z^{\frac{1}{3}} \hbar (1 - \beta^2)^{\frac{1}{2}} / 0.4865 \times 10^{-8} mv \right] (1.13 + 3.76\, Ze^2/(137\beta)^{\frac{1}{2}} \tag{17}$$

Molière's expression for the combination of single scattering events is of the form:

$$P(\phi)d\phi = \left[(2/\pi^{\frac{1}{2}})e^{-\phi^2} + f^{(1)}(\phi)/B + f^{(2)}(\phi)/B^2 \right] d\phi \tag{18}$$

where $P(\phi)d\phi$ refers to the projected angle of scattering, $f^{(1)}(\phi)$ and $f^{(2)}(\phi)$ are functions given in Molière's paper, and B is given by $B - \ln B = \ln \Omega_b - 0.115$ (19) where $\Omega_b = \pi \delta^2 / \Phi_{MIN}$ and is a measure of the average number of collisions suffered by an electron in traversing a distance t of the medium.

In order that the approximations made in deriving this formula should be valid it is necessary that $1/B^n$ should be small for values of n greater than 2 and it can be shown that this condition is satisfied for most media for $t > 10^{-3}$ cm.

The mean deviation of ϕ is given by

$$\langle\phi\rangle = \delta B^{\frac{1}{2}}(1 + 0.982/B - 0.117/B^2) = \delta \times L_M \tag{20}$$

which corresponds to Williams' expression (Eqn. (14)), but has the advantage that it applies for all values of $Ze^2/137\beta$. Values of L_M have been given, as a function of the kinetic energy of the scattered particles (in units of their rest energy), and for various values of t, by Goldschmidt-Clermont [43]. These values are shown in fig. 28.

Recently Bethe[44] has shown that Molière's theory may be derived on a simpler mathematical basis than that originally used and has shown that the theories of Molière, Snyder and Scott, Goudsmit and Saunderson and of Lewis[45] (not dealt with in this account) are all closely related and in the same circumstances lead to very similar results. In an abstract Spencer and Blanchard[46] mention further modifications to the Molière theory intended to avoid this theory's limitation to small angle components of multiple scattering by using Feshbach's distribution of single scattering angles instead of the simpler one used by Molière. It is stated that the agreement with experiment is improved (see Hanson, Lanzl, Lyman and Scott, section 1.3.2) as a result of this modification.

Snyder and Scott's study of the problem[47] is based on the solution of Fermi's fundamental diffusion equation[48] with the assumption that the Born approximation holds good (i.e. the theory applies for only one of Williams' two cases). These authors express their results in terms of η_o, an angular unit depending upon the radius at which atomic electron screening is effective:- $\eta_o = \hbar Z^{\frac{1}{3}}(1 - \beta^2)^{\frac{1}{2}}/a_o mv$ (analogous to Williams' ϕ_{MIN}) and λ, a unit path length in the absorber:- $1/\lambda = \pi \int^2/t\eta_o^2$.

It can be shown[49] that, for normal Ilford G5 emulsions,

$$\eta_o = 1.39(m/m_e)\left[(E_k/E_T)^2 - 1\right]^{-\frac{1}{2}} \qquad (21)$$

and

$$\lambda = 0.160\left[(E_k/E_T)^2 - 1\right]\left[E_T/E_k\right]^2 \qquad (22)$$

where m and m_e are the rest masses of the scattered particle and of the electron, and E_k and E_T are the kinetic and total energies of the scattered particle. We calculate the mean angle of scattering in degrees from

$$\langle\theta\rangle = \langle\eta\rangle_{av.} \times \eta_0 \qquad = \eta_0 \int \eta \, W(\eta)\, d\eta \qquad (23)$$

where $W(\eta)$ is the probability of scattering through an angle η in a distance t and can be evaluated from functions given in tables in Snyder and Scott's paper. As stated above the results of this theory are very similar to those of Moliere's work.

Comparisons of the different theories for particular experimental conditions are given in the following section, for example, in fig. 33.

It has been shown above that all the theories lead to the equation

It has been shown above that all the theories lead to the equation

$\langle\phi$

$$\langle\phi\rangle = \left[2e^2(NZ^2)^{\frac{1}{2}} t^{\frac{1}{2}}/pv\right] \times L$$ (for singly charged particles). This may be

exp[illegible] (24)

where $K = 2e^2(NZ^2)^{\frac{1}{2}}L$ (25)

and is called the "scattering constant" of the medium. Because L is not quite independent of the particle velocity and the value of t, K is not a true constant of the medium. The determination of K for a particular medium under particular conditions is necessary in order that the medium may be used for multiple scattering determinations of particle energies; and measurements of the variation of K with particle velocity and with t are of interest in checking the theories.

1.3.2. Experiment.

Experiments in which measurements of multiple scattering have been made and compared with theoretical predictions fall into two groups. The first group, of which the best example is probably the work of Hanson, Lanzl, Lyman and Scott[50], consists of experiments in which the spatial distribution of a beam of electrons after passing through a thin foil is determined by a detector (probably an ionisation chamber) and compared with the distribution predicted by theory. In the second group of experiments measurements are made on individual tracks and the scattering constant of the medium determined and compared with the theoretical value.

An experiment of the first type has been described by Kulchitsky and Latychev[51]. In this work the multiple scattering of 2.25 MeV. electrons (from a 200 mC. Rd. source) in aluminium, copper, iron, molybdenum, silver, tin, gold and lead was studied. The electrons were analysed, before being scattered, by an electromagnet, and after scattering they were detected by a coincidence pair of Geiger counters which could be set at various angles to the incident beam. In each case the thickness of the scattering foil was chosen so that the half-width of the scattered beam was about 10°. The results of this experiment are shown by the solid dots in fig. 29, where the width of the scattered beam (in units of $(4\pi N(Z^2 + Z)e^4/p^2v^2)^{\frac{1}{2}}$) is plotted against the number of collisions Ω_b. The solid line represents the prediction of the Molière theory. This figure is taken from Hanson, Lanzl, Lyman and Scott's paper and is referred to again below.

Hanson, Lanzl, Lyman and Scott's experiment was performed, with only a few modifications, with the apparatus with which single scattering measurements were made and which has been described earlier and is shown in fig. 19 of section 1.2.2. In the multiple scattering experiments 15.7 MeV. electrons were extracted from a betatron and passed in vacuo to a scattering foil and thence to an analyser and detector. The Geiger counter detector used in the single scattering measurements was replaced by an ionisation chamber arranged to collect at a given angle all the scattered electrons whose energy was within 6% of the incident energy. In order to reach the analyser and ionisation chamber it was necessary for the scattered electrons to pass through an aperture of width 0.18°, and before being scattered the electrons converged onto the foil with a full angular width of 1°. Corrections for beam width were therefore felt to be unnecessary.

It can be seen from fig. 30, where the experimental results for two gold foils of different thicknesses are compared with the predictions of the unmodified Molière theory, that over the angular range plotted (0 to 6°) the agreement is good - within 3% for all points. The dotted lines represent a simple Gaussian distribution of the scattering. Using a slightly larger aperture to define the scattering angle measurements were extended to angles of 30° and the complete results for this range are shown in fig. 31 (0^{0} to 6° small aperture, 6° to 30° large aperture). It may be seen that the agreement between theory and experiment is still very close, though in the region 6° to 15° all the experimental points lie above the theoretical curve. This discrepancy is shown up more clearly when the results are displayed by plotting the ratio of scattering by thick and thin foils. In Bethe's paper, mentioned above, this is done, incorporating Bethe's modifications to the Molière theory, and as can be seen from fig. 32, the agreement between theory and experiment is then excellent.

Measurements were also made in this work of scattering by beryllium foils. Curves corresponding to those of figs. 30, 31 and 32 for gold are not given by the authors for beryllium, but comparisons of the widths of the scattered beam with the theoretical beam widths are given, together with Kulchitsky and Latychev's earlier results, in fig. 29, referred to above. The results of Hanson et al. are indicated in this figure by the crosses.

An example of an experiment falling between the two groups mentioned at the beginning of this section has been described by Groetzinger et al.[52]. These authors initially made individual measurements on 132 electron tracks photographed in an expansion chamber with a P^{32} source, but expressed their results in the same form as in the above experiment. The electrons were in the energy range 50 to 1,700 kev. and the measured root mean square angle of scattering is shown as a function of electron momentum ($H\rho$) by the dotted curve in fig. 33. The solid curves represent the results of the various theories referred to earlier. It can be seen that except at the lowest energies the agreement between experiment and Molière's theory is very good.

Following this experiment the investigation was extended to higher energies and to include the multiple scattering of positrons[53]. In this later work the scattering of electrons from Rh^{106} and positrons from Mn^{52} were compared, the results being shown in fig. 34.

In the second type of experiment the method of measuring the multiple scattering of a single track devised by Fowler[54] is most often used. This method will be described more fully later, but, briefly, it consists of measuring the displacement of the track from a reference line (set approximately parallel to the track at the point where the measurements begin) at fixed intervals along this line. The difference between adjacent readings of the displacement (say y_n and y_{n+1}) gives a measure of the angle between the reference line and a chord drawn across the track between the points at which the readings are taken. Second differences $(y_n - y_{n+1})$ -

Tables XII & XIII

TABLE 12.

Particles	β^2	t (μ)	Ω b/s	Ω b	K	
105 MeV e^+	1	200	310	620	26.7 ± 0.6	26.2
185 MeV e^+	1	400	310	1240	24.9 ± 0.8	24.0
336 MeV Protons	0.46	600	515	3150	30.7 ± 1.0	29.2
5 - 50 MeV Protons	0.07	80	900	710	-	26.1
9 - 35 MeV Protons	0.02 (aver.)	72	1320	850	-	27.5

TABLE 13.

Particles	β^2	t (μ)	Expt[1]. K	Expt[1]. Kc	Theo Kc
105 MeV e^+	1	200	26.7 ± 0.6	26.2 ± 0.6	25.3
185 MeV e^+	1	400	24.9 ± 0.8	24.0 ± 0.8	26.4
336 MeV P	0.46	600	30.7 ± 1.0	29.2 ± 1.0	27.7
5-50 MeV P and M	0.14	80	-	26.1 ± 0.7	25.6
10-20 MeV P	0.02	72	-	27.5 ± 0.5	25.9
40-280 MeV e^-	1	-	-	26 ± 1	-
		250	-	24.4 ± 0.8	26.5
337 MeV P	0.46	500	-	24.5 ± 0.8	27.4
		750	-	24.6 ± 0.9	28.0
167 MeV (Av.) e^-, e^+	1	-	-	21.2 ± 0.7	22.1

$(y_{n+1} - y_{n+2}) = y_n - 2y_{n+1} + y_{n+2}$ then give the change of this angle over one interval along the reference line, which, under suitable conditions, is the resultant angle α, of the multiple scattering over this interval.

The angle of scattering derived from theory is the mean of those between tangents to the track, and the relation between this and the mean of the angles between chords is given[54], for a Gaussian distribution, by

$$\overline{|\alpha|} = (2/3)^{\frac{1}{2}} \overline{|\phi|} \qquad (26)$$

where $\overline{|\alpha|}$ is the mean angle between chords, and $\overline{|\phi|}$ is that between tangents. As mentioned above (Eqn. 24 of section 1.3.1) the scattering constant of the emulsion is found from an experimental value of $\overline{|\phi|}$ by $K = \overline{|\phi|} \times pv/t^{\frac{1}{2}}$.

Experimental determinations of the scattering constants of emulsions have been given by Corson[49], McDiarmid[55], and Voyvodic and Pickup[56] but the most comprehensive set of experiments are probably those carried out by the Bristol group. In a series of papers (57, 58, 59, 60 and 61) members of this group describe very fully measurements of the scattering constants of G5 emulsions for positrons, protons and mesons in the energy range 5 to 336 MeV. and compare their results with the values predicted by Molière's theory. Their results are summarised in Table XII and compared with the values predicted by Molière in fig. 35 (a) and (b). In this figure K is plotted against the quantity Ω_b which was defined in the discussion of Molière's results earlier and is a measure of the number of collisions which a particle undergoes in traversing one cell length.

Ω_b/t, the number of collisions per unit length of path is a function only of β. The points given in fig. 35(b) refer to the scattering constant determined when all individual values of α greater than four times the mean value have been removed. These values of the scattering constant are termed the "cut-off" values. The authors remark that the energy of the positrons was not known as accurately as that of the other particles, so that points 1 and 2 are less accurate than the others but that the agreement between theory and experiment (all points are within about 10% of the theoretical curves) is reasonable so far as the "uncut" values of scattering constant are concerned. The difference between "cut" and "uncut" values is however, for each pair of points, less than that predicted by theory. This is attributed to the use of a thin emulsion (100 μ) since in this case, especially for large cell-sizes, tracks which stay in the emulsion for a sufficient distance to make them acceptable for measurement will tend to be those without large scatters.

Table XIII shows values of the scattering constant of Ilford G5 emulsions determined by various authors for different experimental conditions.

To summarise the present position concerning multiple scattering of electrons and positrons we may say that the previous experimental results are in reasonable agreement with theory. Results at the energies involved in the present work are, however, meagre, and for diluted emulsions none have been published.

Section 2. Account of present work.

2.1. Exposure of the Plates.

For this investigation electrons and positrons of approximately 10, 15, and 20 MeV energy were observed in Ilford G5 photographic emulsions. In the early part of the experiment these particles were obtained by pair production in a lead plate from the X-ray beam of a 30 MeV synchrotron. Later a 1 MeV H.T. set was used to provide electrons from the reaction $Li^7(d,p)Li^8$, $Li^8 \rightarrow Be^8 + e^-$ (τ = 0.95 sec., E_{Max} = 16 MeV) and positrons from pair production in lead by the 14 and 17 MeV γ-rays from $Li^7(p,\gamma)Be^8$. The multiple scattering measurements made to determine the scattering constants of normal and diluted emulsions, utilised only those plates exposed with the synchrotron, but single scattering measurements were made on both sets of plates.

2.1.1. Exposure of plates to electrons and positrons using 30 MeV synchrotron

The experimental arrangement for the synchrotron exposures is shown in fig. 36. Rough collimation of the X-ray beam was provided by the lead blocks 1 and 2, and a pencil beam was selected by means of the circular lead block 3, which had a tapered hole along its axis. The alignment of these lead blocks was checked by means of a light beam shining along the direction of the peak of the synchrotron X-ray intensity which was found by measurements of the activity induced into a number of identical copper rods set in line across the X-ray beam. The beam emerging from the tapered hole was incident upon a lead converter, 0.5 cm. thick, fixed into a vacuum chamber sitting between the poles of an electromagnet. After deflection through 180°, electrons of the required energy passed out of the magnetic field and, still in vacuo, entered the photographic plate, (3" x 3" x 400μ). As much lead shielding as possible was placed between the X-ray source and the plates in order to reduce the stray electron background and so increase the visibility of the required tracks (the chances of confusion between stray tracks and those of the required particles were very much reduced by the acceptance conditions to be described later).

The design of the apparatus was, to a large extent, determined by the shape of the electro-magnet used to analyse the electrons from the converter. This piece of apparatus was borrowed from another section of the department and adapted for use in the present experiment. The magnet poles were rectangular in shape, 24 cm. x 12 cm., and the gap was 0.7 cm. wide. As the magnet was later to be used for its original purpose, it was not possible to increase the gap and so a slim vacuum chamber was made to fit between the magnet poles and lead blocks were fixed inside it to assist in the selection of the electrons. This is shown in fig. 38. A removable case held the plates so that the electrons from the converter struck their centre regions with an angle of incidence which could be varied from 0° to 15°. A shutter, operated externally by means of a small magnet, was provided to enable the box to be transported between being loaded in a dark-room and being fixed to the vacuum chamber. During an exposure the pressure in this system was maintained at not more than 0.1 mm. Hg by means of a small rotary pump. Because of the small magnet gap the walls of the chamber could not be made sufficiently thick to withstand atmospheric pressure and so the gap was itself sealed off as well as possible and pumped to prevent the walls of the chamber from collapsing. A pressure of about 5 to 10 mm. Hg was maintained in the outer enclosure and was found to be satisfactory.

The magnet was operated, with a large ($560\mu F$) smoothing condenser connected across it, from the laboratory 250 v D.C. mains and controlled by a series resistance chain. The magnetic field was calibrated by means of a search-coil (five turns of 26 S.W.G. copper wire on a 3 cm. x 3 cm. square former) and a flux-meter. A check point was established by the deflection of an α-particle beam in the field in the manner described by Rutherford, Chadwick and Ellis (62).

The apparatus with which this calibration point was established is shown in fig. 38. The photographic plate was exposed in vacuo to the α-particles from a fine copper wire on which had been deposited Thoron. The magnet current was reversed during the exposure and for part of the time was switched off. After exposure the plate was developed and scanned and a distribution of the long range (8.776 MeV) ThC" α- particles plotted. In order to be accepted these particles had to lie within about $\pm 10^{\circ}$ of the incident direction from the source and to be dipping into the emulsion at not more than 15°. The distribution is shown in fig. 39. The radius of curvature of the particles was then calculated from the relation

$\rho^2 = (1/4d^2)(d^2 + b^2)\left[(a + b)^2 + d^2\right]$ where a and b are as shown in fig. 38 and d is one half of the distance between the centres of the two α-particle peaks. From the $H\rho$ value of the particles (4.267×10^5 Oersted cm.) the mean field strength over the region traversed by the beam was found to be 5,367 Oersteds for the particular current used (3.50 amp.) The magnetisation curve together with the α-particle calibration point is shown in fig. 40.

The radius of curvature of the selected electrons in the vacuum chamber was 10 cm. and their kinetic energy was determined from the relationship $E_k = 300\ H\rho - 0.51 \times 10^6$ electron-volts (which applies for $v \simeq c$). This gives H = 3,500, 5,170 and 6,840 Oersteds for E_k = 10, 15, and 20 MeV respectively. The width of the accepted beam leaving the magnet (acceptance angle = 10°) was 0.3 cm. and the X-ray beam width at the converter was about 1 cm., so that the resolution was about ± 4%. The sign of the selected particles was chosen by means of a reversing switch connected across the magnet.

With the aid of a number of rather crude simplifying assumptions about the shape of the synchrotron X-ray spectrum, the variation of the pair-production cross section with X-ray energy and the geometry of the apparatus, the number of electrons reaching the plate per roentgen of X-rays could be calculated for any electron energy interval. This was found to be about 30 per square cm. per roentgen for any energy setting between 5 and 15 MeV and about 10 per square cm. per roentgen for a setting of 20 MeV (assuming a peak X-ray energy of 25 MeV). These figures were not expected to be more than a rough guide to the actual numbers of electrons, but they gave an indication of the order of magnitude of the required exposure times and of the relative exposures for particles of different energies.

A preliminary exposure was made in order to determine the actual number of tracks reaching the plate for a given irradiation and to examine the visibility of these tracks against the general background. It was found that roughly twice as many tracks of selected particles as indicated by the calculation actually reached the plate and that these could quite easily be seen above the background of stray tracks.

Following this test a series of ten plates was exposed with a

Tables XIV, XVI + XVII

TABLE 14

Plate Identification Letter	A_1	B_1	C_1	D_1	E_1	F_1	G_1	H_1	I_1
Type of Particle	e	p	e	p	e	p	e	p	e
Expos. Time (Min.)	15	15	5	5	5	5	10	10	5
Mag. Car. (Amp)	1.35	1.35	0.55	0.55	2.05	2.05	4.60	4.60	3.:
Momentum $\left(\frac{\text{MeV}}{c}\right)$	7	7	3	3	10	10	20	20	15
Estimated No. of Particles/Sq.cm.	1,000	1,000	400	400	1,000	1,000	500	500	1,0(

TABLE 15

Plate Identification Letter	A_2	B_2	C_2	D_2	E_2	F_2	G_2	H_2	I_2
Type of Emulsion	N	N	N	N	X2	X2	X2	X4	X4
Type of Particle	e	p	e	p	e	p	e	e	p
Expos. Time (Min.)	45	45	30	30	30	30	20	30	30
Magnet Current (Amp)	o.55	0.55	4.60	4.60	4.60	4.60	3.25	4.60	4.60
Momentum $\left(\frac{\text{MeV}}{c}\right)$	3	3	20	20	20	20	15	20	20
Estimated No. of Particles /Sq. cm.	2,000	2,000	800	800	800	800	2,000	800	80 0

TABLE 16

Plate Identification Letter	A_3	B_3	C_3	D_3	E_3	
Type of Particle	e	e	e	e	p	
Energy (MeV)	10.1	10.1	10.1	10.1	10.1	1
No. of Particles/Sq.cm.	3×10^5	8×10^4	1.8×10^5	3×10^5	6.6×10^4	6.6

synchrotron output of about 2 roentgens per minute at one metre from the synchrotron target (the converter was at this distance from the target). The exposures are detailed in Table XIV.

Some time after this set of exposures a further set of ten plates was irradiated; this set was made up of four normal G5 plates, three "X2 diluted "G5's, containing twice the normal gelatin content and three "X4 diluted "G5's. Details of this set are given in Table XV (the output of the synchrotron was in this case about 1 roentgen per minute at one metre).

2.1.2. Exposure of plates to electrons and positrons using H.T. set.

A considerable time after the above exposures had been made, the analysing magnet having been returned to its owners, it was found necessary to expose a further series of plates in order to increase the rate of collection of data for the single scattering measurements. In this series the 1 MeV high tension set was used and the exposure was greatly assisted by the fact that a large, calibrated, double-focusing spectrometer was available with the set. Further, the "camera" box in which the previous sets of plates had been exposed could easily be fitted to the exit port of this spectrometer and a β-particle counter was available with which to measure directly the flux of particles issuing from this port.

The apparatus is shown in fig. 41; for the exposure to electrons a deuteron beam was incident on the lithium hydroxide target and electrons from this target passed direct to the spectrometer and round to the camera box which in this case, to facilitate its removal without any disturbance of the vacuum inside the spectrometer, was left at atmospheric pressure. Before entering the camera the electrons passed out of the spectrometer through a .002" aluminium window. For the positron exposures a proton beam was used and a block of lead, 0.7 cm. thick was placed immediately in front of the target to act as a converter for the γ-rays emitted in the $Li^7(p,\gamma)Be^8$ reaction. Four inches of lead were used to screen the camera box from the γ-radiation from the lithium. A door was provided in the spectrometer to enable the beam to be cut off so that, when the counter was being used to monitor the focused beam, a background measurement could be made. By means of this counter the number of electrons entering the plate was found to be about 170 per square cm. (perpendicular to the beam) per unit charge of the H.T. set current integrator and the plate exposures were then measured by means of this integrator.

The magnetic field of the spectrometer was measured by means of a built-in search-coil and a flux-meter which had previously been calibrated. Table XVI gives details of the exposures.

2.1.3. Exposure of plates to protons.

The exposure of a set of plates to protons of approximately 50, 70 and 140 MeV energy, obtained from the Harwell synchro-cyclotron, was made for a separate project by Miss C. F. Lees. The plates were exposed at nearly grazing incidence in a box of the type shown in fig. 42. Aluminium windows, 0.001" thick, were fitted to the front and rear of the box which was maintained at atmospheric pressure during the exposure.

For the two lower energy values thick aluminium absorbers were placed between the proton source and the plates, the required thickness being calculated from the range-energy relation for protons[63]. After the exposure the energy of the protons was calculated accurately in each case. Details of this calculation will be given later (Section 2.3.2)

A large batch of plates, including G5 normal, X2 diluted and X4 diluted, were exposed in this way, and of these one of each type for each proton energy was used in the present work in a determination of multiple scattering.

2.2. Development of Plates.

The general method of processing all the above plates after exposure was the same. The temperature cycle method devised by the Bristol group(64.) was used, the procedure being outlined below.

The plates were first immersed horizontally in distilled water at room temperature in shallow photographic dishes which were then placed in a refrigerator and coolled to 5°C. The plates remained at this temperature for three hours by which time they had absorbed practically their full amount of water. They were then transferred to a developing solution consisting of 6.7 gm. of anhydrous sodium sulphite and 3.0 gm. of Amidol per 930 cc. of distilled water. The developer had been pre-cooled to 5°C and after transfer to it the plates were left for a further period of three hours in order that the developer might completely permeate the plates. During this period practically no development took place because of the low temperature and at the end of it the plates were removed, the excess developer was absorbed by filter paper and they were placed on a horizontal brass plate whose temperature was maintained, by means of a thermostat controlled water-bath, at 27 ± 0.5°C. During the time that the plates were on the hot-plate and development was taking place their surfaces were covered with glycerine to prevent excessive oxidation. After thirty minutes the plates were removed and placed in a "stop-bath" consisting of a 0.5% aqueous solution of acetic acid at room temperature, and again cooled down to 5°C. in the refrigerator. After one and a half hours, during the last fifteen minutes of which the temperature was gradually raised to room temperature, the plates were placed in a fixing bath consisting of 400 gm. of sodium thiosulphate and 30 gm. of sodium bisulphite per 1000 cc. of tap water, at room temperature. The time taken for the plates to become transparent was noted and fixation was continued for half as long again. At the end of this period (about 2 - 2½ days) tap water was allowed to flow very slowly into the fixing solution. Very gradual dilution was necessary to ensure that distortion of the emulsion was minimised. When all traces of the fixing solution had been removed from the plates (as shown by the potassium permanganate test) they were allowed to dry in the damp atmosphere of the dark room.

The entire processing operation occupied about six to eight days, varying from one batch of plates to another and when it was completed the edges of the plates were bound with "Cellotape" to prevent them from peeling away from the glass backing plates. Their surfaces were then cleaned with alcohol to remove the slight silver deposit which had accumulated there during development.

2.3. Multiple Scattering.

After the plates had been processed their centre regions were searched and tracks found there and satisfying the conditions described below were accepted for measurement of multiple scattering. The microscope used in this work was a Cooke, Troughton and Sims M4000 type with a "nuclear research" stage on which both x- and y-shifts were operated by micrometers reading to 5 microns. The plates were fixed onto the stage by means of "Cellotape" strips and were aligned so that the edge of the plates which, during exposure, had been parallel to the incident beam lay along the x-direction. Scanning for tracks was then carried out in that direction.

The conditions of acceptance of a track for measurement were as follows:-

(a) Its direction of travel in the plane of the emulsion and just below the surface must lie within 15° of the x-direction.

(b) Its angle of dip into the emulsion must lie between 0° and 15°, corresponding, for a shrinkage factor of 2.3, to 0° to 30° before processing (the angle between the plate and the median plane of the analysing magnet had been set to 15° for the exposures.)

(c) It must stay in the emulsion for at least 1500μ, measured along the x-direction of the stage.

2.3.1. Measurement of angles of multiple scattering.

In measuring the multiple scattering the Fowler second difference method was used[54]. A pair of X15 Kellner eye-pieces, one fitted with a graticule of the type shown in fig. 43, and a X45 oil immersion objective were employed, giving an overall magnification of approximately 1,000 times (including the magnification of the microscope stand.) The length of the scale shown in fig. 43 corresponded to a length in the emulsion of 100μ under these conditions and it was set parallel to the y-direction of the stage. Starting in each case about 100μ from the point at which the track entered the emulsion, readings were taken, at fixed intervals in the x-direction, of the position on the eye-piece scale of an imaginary line drawn through the grains making up the track for about 10μ on either side of the scale. In the case of the 10 MeV particles the interval between readings, called the "primary cell-size", was 25μ, for the 15 and 20 MeV particles it was 50μ.

Tables of these "y" readings were made and from them the first differences $(y_n - y_{n+1})$ and second differences $(y_n - 2y_{n+1} + y_{n+1})$ were obtained for cell-sizes (i.e. x-direction displacements) of 25 (10 MeV only), 50, 100, 200 and 400μ. As has been mentioned in section 1.3.2, and can be seen from fig. 44, the second difference values give a measure of the changes of direction of chords drawn across the track over the intervals chosen. The relationship is

$$\alpha \simeq (\delta/s)x(360/2\pi)x(100/60) \qquad (27)$$

where δ is the second difference value in scale divisions (of which 60 equal 100μ) and α is the change of direction in degrees.

At the beginning of this work the two observers by whom almost all the multiple scattering measurements were made (H.M. and W.B.) carried out a series of checks in which both observers made measurements on the same tracks, in order to check the accuracy of observation. It was found that after a short period of practice the two sets of measurements would correspond to within 0.2 scale divisions for each reading.

After the measurements had been made the decision whether or not to include a particular track in the determination of scattering constant was made in the following way. For each track, using a cell-size of 100μ, the mean value of the second differences (taken without regard to their signs) was found, excluding any individual second difference value greater than four times the mean value for that track (this limitation was imposed to exclude comparatively large single scatters and will be referred to later). For a given type of track and of emulsion the distribution of mean second difference values for all the measured tracks was then plotted and the median found. A typical distribution of mean second difference values ($\overline{|\delta|}$) is given in fig. 45 for 10 MeV electrons in normal emulsions ($t = 50\mu$). Any track whose value of $\overline{|\delta|}$ did not lie within 40% of the median was excluded from the calculations of scattering constants. In this way it was hoped to remove (a) tracks of fast cosmic ray particles which had by chance happened to satisfy the acceptance conditions and (b) tracks of stray electrons from the synchrotron X-ray source which after being scattered had been similarly accepted. Between 20 and 25 tracks were measured for each type of incident particle (10, 15, 20 MeV electrons and 10 MeV positrons) and of emulsion (normal, X2 and X4) and of these usually about 10% were rejected by the above selection.

As will be described in detail below, the measured values of second difference consist of the true values combined with various errors, such as those due to the random distribution of the silver grains over the true paths of the incident particles and those due to the non-linearity of the microscope stage movement. These errors give rise to what is termed - by analogy with the measurement of radio signals - "noise"; here as in telephony the aim is to obtain as high a value of the signal to noise ratio as is possible.

A determination of the "noise level" of a particular microscope may be made, assuming it to be independent of cell-size, by performing scattering measurements on the tracks of very fast particles, whose true scattering will be small, or by measuring the scattering of tracks of the type being investigated, with a very small cell-size since the dependence on cell-size of the true scattering is known ($\bar{\alpha}$ is proportional to $t^{1/2}$). Such measurements were made in the present case using both fast particle tracks and small cell-sizes with 10 to 20 MeV electron tracks. There is some evidence that the noise level is not independent of cell-size[58]; this will be referred to again later.

As a check of the coordinate method of determination of $\overline{|\alpha|}$, direct angle measurements were made on some of the tracks by means of the goniometer fitted to one of the microscope eye-pieces. In these measurements the central line drawn perpendicular to the scale on the eye-piece graticule (fig. 43) was set to be tangential to the track at 50μ intervals and the changes of angle were determined for this cell-size. Values of $\overline{|\phi|}$ obtained in this way were compared with the corresponding values determined by the Fowler method; the relationship between the chord angles and the tangent angles is, as mentioned in section 1.3.2 equation (26) , $\overline{|\alpha|} = (2/3)^{\frac{1}{2}} \overline{|\phi|}$

The method of measurement of the proton tracks and the acceptance conditions applied to them were the same as for the electron and positron tracks except that greater lengths of track were used (up to 8,000 μ) and no direct angular measurements were made, the cell-sizes being much greater than those used for the electrons and positrons.

Table XVII

TABLE 17

Type of Particle and Normal Mmtum. (MeV/c)	Emulsion	Cell-Size (μ)	No. of Indiv. δ Values UNCUT	No. of Indiv. δ Values CUT	$\overline{\vert\delta\vert}$ Meas. (di… UNCUT	$\overline{\vert\delta\vert}$ Meas. (di… CUT
10 $\frac{\text{MeV}}{c}$ e's	Normal	25	866	810	.440	.35
		50	530	492	1.115	.91
		100	273	262	3.035	2.67
		200	111	108	8.34	7.89
		400	44	44	23.1	23.1
10 $\frac{\text{MeV}}{c}$ p's	Normal	25	701	671	.421	.36
		50	687	667	1.025	.92
		100	336	326	2.68	2.45
		200	159	152	7.63	6.86
		400	69	68	20.6	19.8
15 $\frac{\text{MeV}}{c}$ e's	Normal	50	530	504	.770	.65
		100	258	249	2.08	1.89
		200	120	115	5.90	5.01
		400	52	52	16.1	16.1
20 $\frac{\text{MeV}}{c}$ e's	Normal	50	640	612	.629	.52
		100	312	306	1.595	1.48
		200	148	140	4.41	3.79
		400	66	66	11.89	11.89
20 $\frac{\text{MeV}}{c}$ e's	X2	50	549	509	.470	.36
		100	248	266	1.16	.93
		200	122	119	3.36	3.10
		400	50	50	9.84	9.84
20 $\frac{\text{MeV}}{c}$ e's	X4	50	402	377	.448	.348
		100	193	187	1.12	.956
		200	87	85	3.36	3.14
		400	35	35	9.95	9.95

2.3.2. Determination of scattering constants.

The above measurements having been made it was necessary to apply certain corrections to the measured values of mean angle of scattering, and also to determine the effective momentum of the particles producing the tracks in order that the corresponding values of scattering constant might be determined.

(a) Electrons and positrons.

After the preliminary analysis described above had been made to decide which of the measured tracks should be used in the scattering constant determination, the $|\delta|$ values of all those tracks which were accepted were combined, for each cell-size, emulsion and particle type, in one distribution of the type shown, for 10 MeV electrons and a cell-size of 50μ, in normal emulsion, in fig. 46. In plotting this curve all the individual values of $|\delta|$ of the tracks were included (i.e. no cutting was applied to the individual tracks). This having been done, the median position was determined and a 'cutting point' was established, for all the tracks combined, at a value of $|\delta|$ equal to four times the median value. Two values of $\overline{|\delta|}$ were then obtained from each distribution, an 'uncut' and a 'cut' value. These are given for all the particles investigated and for each type of emulsion, in Table XVII.

It was then necessary to apply corrections to these values before calculating the values of $\overline{|\alpha|}$ from which the scattering constants could be determined.

The first correction was for 'microscope noise' and the method of correction used was based on that described in the second of the Bristol

Table XVIII

group's multiple scattering papers[58]. The true mean second difference is given (by equation (24) of section 1.3.1) by $\overline{|\delta|_t} = \langle\alpha\rangle \cdot t = Kt^{3/2}/pv$. If the noise is independent of the cell-size and has a mean value $\bar{\epsilon}$, we may write

$$\left(\overline{|\delta|_m}\right)^2 = \left(\overline{|\delta|_t}\right)^2 + \left(\bar{\epsilon}\right)^2 = At^3 + \left(\bar{\epsilon}\right)^2 \qquad (28)$$

where A, provided that K can be regarded as independent of cell-size, is a constant. We may therefore, as was mentioned above, determine $\bar{\epsilon}$ by making scattering measurements with very small cell-sizes. This was done and the values obtained are shown in Table XVIII. The mean value of $\bar{\epsilon}$ so obtained is 0.149 ± .008 for normal emulsion, 0.175 ± .014 for X2 diluted, and 0.211 ± .015 for X4 diluted. It is to be expected that the noise will be greater for X2 and X4 than for normal emulsion, because of the smaller number of grains in the tracks.

The experimental values of $\overline{|\delta|_t}$ may be obtained without measurements of $\bar{\epsilon}$ being made, assuming that $\bar{\epsilon}$ is independent of t, since we have, from equation (28) above, $\left(\overline{|\delta|_{m_2}}\right)^2 - \left(\overline{|\delta|_{m_1}}\right)^2 = At_2^3 - At_1^3$, therefore

$$\left[\frac{\left(\overline{|\delta|_{m_2}}\right)^2 - \left(\overline{|\delta|_{m_1}}\right)^2}{t_2^3 - t_1^3}\right]^{1/2} = A^{1/2} = K/pv = \overline{|\delta|_{t_1}}/t_1^{3/2} \qquad (29)$$

Using the values of $\overline{|\delta|_m}$ given in Table XVII we find the $\overline{|\delta|_t}$ values given in columns 4 (uncut) and 7 (cut) of Table XIX. For each determination adjacent cell-sizes were used, i.e. the '25 μ' value of $\overline{|\delta|_t}$ is derived from $\overline{|\delta|_{m_{25}}}$ and $\overline{|\delta|_{m_{50}}}$, and so on. The values of $\overline{|\delta|_t}$ obtained by simple correction with the measured value of $\bar{\epsilon}$ are shown in columns 3 (uncut) and 6 (cut), and in columns 5 and 8 are given the corresponding values of $\overline{|\delta|_t}$ reduced to a

Table XVIII.

TABLE 18

Emulsion	Particles	Cell-Size (μ)	No. of Obser^{ns}.	$\bar{\epsilon}$	Mean
Normal	Fast, Min. Ion^{n}.	10	138	0.138	0.137 ±
	"	"	55	0.136	
	"	"	53	0.127	
	"	"	58	0.143	
X2	20 $\frac{Mev}{c}$ e's	10	80	0.178	0.175 ±
	"	"	40	0.172	
X4	Fast, Min. Ion^{n}.	10	118	0.211	0.211 ±

group's multiple scattering papers[58]. The true mean second difference is given (by equation (24) of section 1.3.1) by $\overline{|\delta|}_T = \langle\alpha\rangle \cdot t = Kt^{3/2}/pv$. If the noise is independent of the cell-size and has a mean value $\bar{\epsilon}$, we may write

$$\left(\overline{|\delta|}_{M}\right)^2 = \left(\overline{|\delta|}_{T}\right)^2 + \left(\bar{\epsilon}\right)^2 = At^3 + \left(\bar{\epsilon}\right)^2 \qquad (28)$$

where A, provided that K can be regarded as independent of cell-size, is a constant. We may therefore, as was mentioned above, determine $\bar{\epsilon}$ by making scattering measurements with very small cell-sizes. This was done and the values obtained are shown in Table XVIII. The mean value of $\bar{\epsilon}$ so obtained is 0.137 ± .008 for normal emulsion, 0.175 ± .014 for X2 diluted, and 0.211 ± .016 for X4 diluted. It is to be expected that the noise will be greater for X2 and X4 than for normal emulsion, because of the smaller number of grains in the tracks.

The experimental values of $\overline{|\delta|}$ may be corrected without measurements of $\bar{\epsilon}$ being made, assuming that $\bar{\epsilon}$ is independent of t, since we have, from equation (28) above, $\left(\overline{|\delta|}_{M_2}\right)^2 - \left(\overline{|\delta|}_{M_1}\right)^2 = At_2^3 - At_1^3$, therefore

$$\left[\frac{\left(\overline{|\delta|}_{M_2}\right)^2 - \left(\overline{|\delta|}_{M_1}\right)^2}{t_2^3 - t_1^3}\right]^{1/2} = A^{1/2} = K/pv = \overline{|\delta|}_{T_1}/t_1^{3/2} \qquad (29)$$

Using the values of $\overline{|\delta|}_M$ given in Table XVII we find the $\overline{|\delta|}_T$ values given in columns 4 (uncut) and 7 (cut) of Table XIX. For each determination adjacent cell-sizes were used, i.e. the '25 μ' value of $\overline{|\delta|}_T$ is derived from $\overline{|\delta|}_{M_{25}}$ and $\overline{|\delta|}_{M_{50}}$, and so on. The values of $\overline{|\delta|}_T$ obtained by simple correction with the measured value of $\bar{\epsilon}$ are shown in columns 3 (uncut) and 6 (cut), and in columns 5 and 8 are given the corresponding values of $\overline{|\delta|}_T$ reduced to a

Table XIX

cell size of 100 μ; these should be the same for all measurements with the given emulsion and type of particle. They have been calculated for all cell-sizes although for the larger ones (greater than 100 μ) the noise correction is very small.

Since the agreement between the values of [illegible] obtained this way was satisfactory the more complicated corrections, allowing for variations of $\bar{\varepsilon}$ with cell-size and discussed by [illegible] et al. (30), were not used.

The second correction applied to the observed [illegible] values was one to compensate for the distortion of the emulsion during processing. When the emulsion is soaked in water it expands considerably and on transfer to the different processing solutions stresses are set up in the softened gelatine as the solutions diffuse through the emulsion. Finally, on fixing and drying large quantities, first of silver bromide and then of water, are removed from the emulsion and a great reduction of volume occurs. Ideally these changes in volume should result only in the movement of a given point in the emulsion in a direction perpendicular to the surface and no effects should be produced in the projections of tracks onto planes parallel to the surface. In practice, however, particularly near the edges of the plates, some distortion of the projected tracks may occur. Such distortion may be minimised by careful processing and by using only those tracks found in the central regions of the plates.

In the present work correction for distortion was found to be necessary only in the case of electron tracks in [illegible] emulsions for which, because of the reduced amount of silver bromide which they contain, the expansion on soaking is much greater than for normal emulsions.

Table XIX

TABLE 19

Particle and Emulsion	Cell-Size, t. (μ)	UNCUT			CUT		
		$(\overline{\lvert\delta_1\rvert}^2-\epsilon^2)^{1/2}$	$t^{3/2}\left(\frac{\overline{\lvert\delta_2\rvert}^2-\overline{\lvert\delta_1\rvert}^2}{t_2^3-t_1^3}\right)^{1/2}$	$100^{3/2}\left(\frac{\overline{\lvert\delta_2\rvert}^2-\overline{\lvert\delta_1\rvert}^2}{t_2^3-t_1^3}\right)^{1/2}$	$(\overline{\lvert\delta_1\rvert}^2-\epsilon^2)^{1/2}$	$t^{3/2}\left(\frac{\overline{\lvert\delta_2\rvert}^2-\overline{\lvert\delta_1\rvert}^2}{t_2^3-t_1^3}\right)^{1/2}$	$100^{3/2}\left(\frac{\overline{\lvert\delta_2\rvert}^2-\overline{\lvert\delta_1\rvert}^2}{t_2^3-t_1^3}\right)^{1/2}$
10 $\frac{MeV}{c}$ e's Normal	25	.404	.389	3.10	.305	.318	2.54
	50	1.10	1.06	3.00	.894	.948	2.68
	100	3.03	2.98	2.98	2.67	2.82	2.82
	200	8.34	9.00	3.17	7.89	8.20	2.90
	400	23.1	-	-	23.1	-	-
10 $\frac{MeV}{c}$ p's Normal	25	.396	.353	2.82	.339	.322	2.58
	50	1.02	.934	2.64	.918	.860	2.43
	100	2.68	2.76	2.67	2.45	2.42	2.42
	200	7.63	7.55	2.66	7.63	8.44	2.48
	400	20.6	-	-	20.6	-	-
15 $\frac{MeV}{c}$ e's Normal	50	.750	.733	2.07	.630	.664	1.88
	100	2.08	2.09	2.09	1.87	1.76	1.76
	200	5.90	5.80	2.06	5.01	5.80	2.05
	400	16.1	-	-	16.1	-	-
20 $\frac{MeV}{c}$ e's Normal	50	.604	.555	1.57	.493	.523	1.48
	100	1.59	1.56	1.56	1.44	1.32	1.32
	200	4.41	4.46	1.47	3.79	4.28	1.51
	400	11.9	-	-	11.9	-	-
20 $\frac{MeV}{c}$ e's X2	50	.437	.423	1.18	.321	.327	0.92
	100	1.15	1.19	1.19	.916	1.12	1.12
	200	3.30	3.52	1.24	3.10	3.53	1.25
	400	9.84	-	-	9.84	-	-
20 $\frac{MeV}{c}$ e's X4	50	.395	.389	1.10	.275	.326	0.95
	100	1.10	1.20	1.20	.932	1.13	1.13
	200	3.36	3.53	1.25	3.13	3.07	1.06
	400	9.95	-	-	9.95	-	-

Table XIX

cell size of 100μ; these should be the same for all measurements with a given emulsion and type of particle. Values have been calculated for all cell-sizes although for the larger ones (greater than 100μ) the noise correction is very small.

Since the agreement between the values of $\overline{|\delta|}_{100}$ obtained in this way was satisfactory the more complicated corrections, allowing for variations of $\bar{\epsilon}$ with cell-size and discussed by Menon et al.[58] were not used.

The second correction applied to the observed $\overline{|\delta|}$ values was that to compensate for the distortion of the emulsion during processing. When the emulsion is soaked in water it expands considerably and on transfer to the different processing solutions stresses are set up in the softened gelatine as the solutions diffuse through the emulsion. Finally, on fixing and drying large quantities, first of silver bromide and then of water, are removed from the emulsion and a great reduction of volume occurs. Ideally these changes in volume should result only in the movement of a given point in the emulsion in a direction perpendicular to the surface and no effects should be produced in the projections of tracks onto planes parallel to the surface. In practice, however, particularly near the edges of the plates, some distortion of the projected tracks may occur. Such distortion may be minimised by careful processing and by using only those tracks found in the central regions of the plates.

In the present work correction for distortion was found to be necessary only in the case of electron tracks in X4 diluted emulsions for which, because of the reduced amount of silver bromide which they contain, the expansion on soaking is much greater than for normal emulsions.

Distortion has been considered by Fowler[54] who has pointed out that the deviation produced by distortion in an otherwise straight track can be written $\Delta = F\,\delta z$ where Δ is the change in direction of the track in passing from a depth z to one $z + \delta z$ and F is a constant for a particular direction of the projected track and a particular region of the emulsion. For a given track, therefore (or for all parallel tracks in a given region of the plate), distortion will result in a change, always in the same direction, of all the individual δ values. If the tracks all dip into the emulsion at the same rate the changes in the δ values caused by the distortion will all be the same. Distortion effects may therefore be investigated by plotting the δ values of a track or of all tracks from a given region, taking account of their signs. The median of this distribution will, in the absence of distortion, be zero, and its displacement from zero gives the correction to be applied to the individual δ values. This correction having been applied $\overline{|\delta|}$ may be determined as before.

In the present work plots of the δ values were made for the 20 MeV electron tracks in normal, X2 and X4 emulsions, since the effects of distortion would, of course, be most important and most easily detected for those particles with the smallest value of $\overline{|\delta|}$. Such plots are shown in fig. 47(a) -(d) for 50 and 100μ cell-sizes. The lower plots are for individual tracks, with the medians indicated and the upper ones are the compounded results for each group of particles. For the larger cell-sizes (200 and 400μ) the statistics were not sufficiently good to make plots for individual tracks of any value. Plots for each group of tracks are shown for these cell-sizes in fig. 47(e).

Tables XX + XXI

Tables XX & XXI

TABLE 20

Particle	Emul-sion	Cell-Size (μ)	UNCUT No. of Obs.	UNCUT $\overline{\lvert\delta\rvert}_{meas.}$	UNCUT $(\overline{\lvert\delta\rvert}_n^2 - \bar{\epsilon}^2)^{1/2}$	CUT No. of Obs.	CUT $\overline{\lvert\delta\rvert}_{meas.}$	CUT $(\overline{\lvert\delta\rvert}_n^2 - \bar{\epsilon}^2)^{1/2}$
20 MeV/c e's	X 4	50	402	0.448	0.395	377	0.347	0.275
		100	193	1.08	1.06	187	0.790	0.761
		200	87	2.69	2.68	85	2.06	2.04
		400	35	8.8	8.8	35	8.8	8.8

TABLE 21

Particle and Emulsion	Av. Incline^n θ	Correction, $(\cos\theta)^{1/2}$
10 MeV/c e's Normal	7.5°	0.987
10 MeV/c p's Normal	2.7°	0.998
15 MeV/c e's Normal	2.8°	0.998
20 MeV/c e's Normal	7.6°	0.987
20 MeV/c e's X 2	3.0°	0.998
20 MeV/c e's X 4	2.5°	0.999

From fig. 47 it can be seen that no correction is required in the case of the normal and X2 diluted emulsions. Since the normal and X2 emulsions used for the exposures to 10 and 15 MeV particles were from the same batch as those used for the 20 MeV ones and since they were processed together, it was to be expected that no correction would be required in these cases and checks indicated that this was so.

The electrons in the X4 emulsions could not be treated as one group since, to facilitate scanning in the region in which there was a good density of tracks, the plate had been turned through 180° on the microscope stage after measurement of the fourteenth track. As was to be expected, the corrections to the two groups were in opposite directions and of about the same magnitude (-0.3 divisions for tracks 1 - 14, and +0.5 divisions for tracks 15 - 22 for $t = 100\mu$). The distributions of δ are shown in fig. 48 together with the size of the correction required to restore the median to zero. Fowler has shown that the value of $\overline{|\delta|}$ obtained from a corrected distribution of δ values is not sensitive to changes in the size of the correction applied, provided that this correction is not too large. The values of $\overline{|\delta|}$ obtained from the corrected δ values are shown in Table XX.

The third correction which was applied was made necessary because the projected electron tracks were not quite parallel to the x-direction of the microscope stage. This meant that the cell-sizes measured along the track were slightly greater than the displacement along the x-direction, so that a slightly larger value of $\overline{|\delta|}$ was obtained than that corresponding to t. The correction was applied by obtaining from the original measurements of y the average inclination of each set of tracks to the x-direction. The cell-

Table XXII

Table XXII

TABLE 22

Emulsion & Particles	Cell-Size (μ)	UNCUT			CUT		
		$\overline{\|D\|}_T$ (div.)	$\overline{\|\alpha\|}$ (deg.)	$\overline{\|\alpha\|}_{100}$ (deg.)	$\overline{\|D\|}_T$ (div.)	$\overline{\|\alpha\|}$ (deg.)	$\overline{\|\alpha\|}_{100}$ (deg.)
	25	.398	1.52	3.04	.301	1.15	2.30
10 MeV/c e's Normal	50	1.09	2.08	2.94	.881	1.68	2.38
	100	2.99	2.86	2.86	2.58	2.46	2.46
	200	8.23	3.94	2.78	7.79	3.72	2.63
	400	22.8	5.55	2.78	22.8	5.55	2.78
10 MeV/c p's Normal	25	.396	1.42	2.84	.339	1.30	2.60
	50	1.02	1.91	2.70	.918	1.75	2.48
	100	2.68	2.56	2.56	2.45	2.34	2.34
	200	7.63	3.64	2.57	7.63	3.64	2.57
	400	20.6	4.92	2.46	20.6	4.92	2.46
15 MeV/c e's Normal	50	.750	1.43	2.02	.630	1.20	1.70
	100	2.08	1.99	1.99	1.87	1.79	1.79
	200	5.90	2.82	1.99	5.01	2.39	1.69
	400	16.1	3.84	1.92	16.1	3.84	1.92
15 MeV/c e's Normal	50	Direct Angle Meas^t.	1.36 ± .06	1.92	Direct Angle Meas^t.	1.22 ± .06	1.73
20 MeV/c e's Normal	50	.595	1.13	1.60	.486	.930	1.32
	100	1.57	1.50	1.50	1.42	1.35	1.30
	200	4.36	2.07	1.46	3.25	1.79	1.27
	400	11.7	2.80	1.40	11.7	2.80	1.40
20 MeV/c e's M2	50	.437	.834	1.18	.321	.613	.868
	100	1.15	1.08	1.08	.916	.893	.893
	200	3.36	1.60	1.13	3.10	1.48	1.05
	400	9.84	2.35	1.18	9.84	2.35	1.18
20 MeV/c e's X4	50	.395	.754	1.06	.275	.525	.744
	100	1.06	1.01	1.01	.761	.726	.726
	200	2.68	1.28	0.91	2.04	1.00	.707
	400	8.8	2.10	1.05	8.8	2.10	1.05

size corresponding to the measured value of $|\overline{\delta_1}|$ was $t/\cos\theta$ where θ is the average angle of inclination of the tracks and since $|\overline{\delta_1}| \propto t^{3/2}$ the values of mean second difference corresponding to a cell-size t is $|\overline{\delta_1}|(\cos\theta)^{3/2}$. The values of θ and the corresponding correction factors are given in Table XXI. This method of correction is obviously an approximate one, but in view of the small size of the correction it was felt to be adequate.

The values of $|\overline{\alpha}|$ obtained from the corrected $|\overline{\delta}|$ values are shown in Table XXI. In the case of the 15 MeV electrons, these values were compared with those obtained by the direct measurement of scattering angles. As mentioned in section 2.3.1, the direct measurements were made only for a cell-size of 50 μ and they were limited in accuracy by the error in reading the goniometer. A vernier allowed the angle of scattering to be read to 0.25°. The results are included in Table XXII. In view of the limited accuracy and poor statistics of the direct measurement method, the agreement between the two methods is felt to be satisfactory.

Before the scattering constants could be calculated it was necessary to determine the appropriate value of momentum for the particles producing each set of tracks, allowing for their loss of energy after leaving the analysing magnet. This loss of energy was allowed for by determining the average of the lengths of track used for each group of electrons or positrons and then calculating the amount of energy lost (a) by ionisation and (b) by radiation, in travelling a distance equal to half this average (i.e. in travelling to the centre of the 'average track').

The rate of energy loss by an electron due to radiation is given by Fermi[65] as

Table XXIII

$$-\frac{dE}{dx} = \frac{2\pi e^4 N Z}{m v^2}\left[\ln \frac{m v^2 T}{2 I^2 (1-\beta^2)} - \ln 2\left\{2(1-\beta^2)^{\frac{1}{2}} - 1 + \beta^2\right\} + (1-\beta^2)\right] \quad (30)$$

where I is the average ionisation potential of the atoms concerned and is given approximately by $13.5\,Z$ electron volts. From equation (30) we see that the ratio of the rates of energy loss in diluted and in normal emulsions is

$$\frac{(dE/dx)_D}{(dE/dx)_N} = \frac{\sum (NZ)_D}{\sum (NZ)_N}\left[\frac{\ln A - \ln \overline{Z^2}_D - B}{\ln A - \ln \overline{Z^2}_N - B}\right] \quad (31)$$

where A and B are constants and $\overline{Z^2}$ is the mean value of Z^2 for a given emulsion. For fast particles $(v \to c)$ $B \to 0$.

For a normal emulsion equation (30) gives $(dE/dx)_N$ = [illegible] keV/micron, and, since $\sum(NZ)_{2D}/\sum(NZ)_N = 0.80$, $\sum(NZ)_{4D}/\sum(NZ)_N = 0.667$, $\overline{Z^2}_N = 445$, $\overline{Z^2}_{2D} = 224$ and $\overline{Z^2}_{4D} = 177$, we have $(dE/dx)_{2D} = 0.55$ keV/μ and $(dE/dx)_{4D}$ = [illegible] keV/μ.

In order to allow for the radiation loss the radiation length, L_R, was calculated from the equation (ref. 68)

$$\frac{1}{L_R} = \frac{4 N Z^2}{137} r_e^2 \ln\left(\frac{183}{Z^{1/3}}\right) \quad (32)$$

from which

$$\frac{(L_R)_D}{(L_R)_N} = \frac{\sum (NZ^2)_N \ln (183\, Z^{-1/3})_N}{\sum (NZ^2)_D \ln (183\, Z^{-1/3})_D} \quad (33)$$

Equation (32) gives $(L_R)_N = 2.94$ cm. and from equation (33) we find that $(L_R)_{2D} = 5.4$ cm. and $(L_R)_{4D} = 7.7$ cm. The average energy loss by radiation from an electron of initial energy E in a distance x is thus given by $\Delta E = E(1 - e^{-x/L_R})$.

Table XXIII

TABLE 23

Particle and Emulsion	Average Track Length (mm).	Ionisation Loss (MeV)	Radiation Loss (MeV)	Total Loss (MeV)
10 $\frac{MeV}{c}$ e's N	1.75	.613	.278	.89(1)
10 $\frac{MeV}{c}$ p's N	1.97	.690	.314	1.00(4)
15 $\frac{MeV}{c}$ e's N	2.35	.823	.568	1.39(1)
20 $\frac{MeV}{c}$ e's N	2.71	.950	.890	1.84(0)
20 $\frac{MeV}{c}$ e's X2	1.675	.460	.300	.76(0)
20 $\frac{MeV}{c}$ e's X4	1.73	.398	.216	.61(4)

$$-\frac{dE}{dx} = \frac{2\pi e^4 N Z}{m v^2}\left[\ln \frac{m v^2 T}{2\bar{I}^2(1-\beta^2)} - \ln 2\left\{2(1-\beta^2)^{1/2} - 1 + \beta^2\right\} + 1 - \beta^2\right] \quad (30)$$

where $\bar{I}$ is the average ionisation potential of the atoms concerned and is given approximately by 13.5 Z electron volts. From equation (30) we see that the ratio of the rates of energy loss in diluted and in normal emulsions is given by

$$\frac{(dE/dx)_D}{(dE/dx)_N} = \frac{\sum (NZ)_D}{\sum (NZ)_N}\cdot\left[\frac{\ln A/\overline{(Z^2)}_D - B}{\ln A/\overline{(Z^2)}_N - B}\right] \quad (31)$$

where A and B are constants and $\overline{Z^2}$ is the mean value of Z^2 for a given emulsion. For fast particles ($v \to c$) $B \to 0$.

For a normal emulsion equation (30) gives $(dE/dx) = 0.70$ keV/micron, and, since $\Sigma(NZ)_{x2}/\Sigma(NZ)_N = 0.80$, $\Sigma(NZ)_{x4}/\Sigma(NZ)_N = 0.667$, $\overline{Z^2}_N = 445$, $\overline{Z^2}_{x2} = 284$ and $\overline{Z^2}_{x4} = 177$, we have $(dE/dx)_{x2} = 0.55$ keV/μ and $(dE/dx)_{x4} =$ $\cdot 246$ keV/μ.

In order to allow for the radiation loss the radiation length, L_R, was calculated from the equation (Fermi[66])

$$\frac{1}{L_R} = \frac{4NZ^2}{137} \cdot r_e^2 \cdot \ln\left(\frac{183}{Z^{1/3}}\right) \quad (32)$$

from which

$$\frac{(L_R)_D}{(L_R)_N} = \frac{\sum (NZ^2)_N \ln\left(183/(Z^{1/3})_N\right)}{\sum (NZ^2)_D \ln\left(183/(Z^{1/3})_D\right)} \quad (33)$$

Equation (32) gives $(L_R)_N = 2.94$ cm. and from equation (33) we find that $(L_R)_{x2} = 5.4$ cm. and $(L_R)_{x4} = 7.7$ cm. The average energy loss by radiation from an electron of initial energy E in a distance x is then given by $\Delta E = E(1 - e^{-x/L_R})$.

Table XXIV

Table XXIV

TABLE 24

Particle & Emulsion	Cell-Size(μ)	Effective $p\beta c$ (MeV)	$K_{Expt.}$	$K_{Theo.}$	$Kc_{Expt.}$	Kc_{Th}
10 $\frac{MeV}{c}$ e's Normal	25	9.11	27.7 ± 0.6	23.1	20.9 ± 0.0'	20.2
	50		26.8 ± 0.8	24.5	21.7 ± 0.7	21.4
	100		26.1 ± 1.2	25.5	22.4 ± 0.9	22.8
	200		25.3 ± 1.7	26.6	24.0 ± 1.7	23.6
	400		25.3 ± 2.6	27.4	25.3 ± 2.6	24.7
10 $\frac{MeV}{c}$ p's Normal	25	9.00	25.6 ± 0.6	23.1	23.4 ± 0.6	20.2
	50		24.3 ± 0.8	24.5	22.3 ± 0.7	21.4
	100		23.0 ± 1.0	25.5	20.7 ± 0.9	22.8
	200		23.1 ± 1.5	26.6	23.1 ± 1.5	23.6
	400		22.1 ± 2.0	27.4	22.1 ± 2.0	24.7
15 $\frac{MeV}{c}$ e's Normal	50	13.61	27.5 ± 0.8	24.5	23.2 ± 0.7	21.4
	100		27.1 ± 1.2	25.5	24.4 ± 1.1	22.8
	200		27.1 ± 1.6	26.6	23.0 ± 1.6	23.6
	400		26.1 ± 2.5	27.4	26.2 ± 2.5	24.7
20 $\frac{MeV}{c}$ e's Normal	50	18.16	29.1 ± 0.8	24.5	24.0 ± 0.7	21.4
	100		27.3 ± 1.0	25.5	23.6 ± 1.0	22.8
	200		26.5 ± 1.5	26.6	23.1 ± 1.6	23.6
	400		25.4 ± 2.2	27.4	25.4 ± 2.2	24.7
20 $\frac{MeV}{c}$ e's X2	50	19.24	22.7 ± 0.7	20.2	16.7 ± 0.5	16.1
	100		20.8 ± 0.9	20.9	17.2 ± 0.7	16.7
	200		21.7 ± 1.3	21.5	20.2 ± 1.2	17.4
	400		22.7 ± 2.4	22.2	22.7 ± 2.4	18.3
20 $\frac{MeV}{c}$ e's X4	50	19.39	20.5 ± 0.7	16.7	14.4 ± 0.5	13.1
	100		19.6 ± 0.9	17.3	14.1 ± 0.7	13.6
	200		17.6 ± 1.3	17.8	13.7 ± 1.0	14.2
	400		20.3 ± 2.3	18.1	20.3 ± 2.3	14.7

Table XXIII gives the average lengths of each group of tracks and the corresponding energy losses. The corrected values of momentum obtained from these, and the corresponding scattering constants, together with the statistical standard deviations based on the number of observations used in each determination are given in Table XXIV.

Theoretical values of the scattering constants for comparison with the above results were obtained from the Molière theory. For normal G5 emulsion numerical values of the scattering constant have been obtained by Gottstein et al.[57] using Goldschmidt-Clermont's results[43]. The values so obtained are shown in fig. 35 of section 1.3.2. The value for fast electrons ($\beta = 1$) for a cell-size of 100μ ($\Omega_b = 310$) is $K_N = 25.5$.

For diluted emulsions the corresponding values of K were obtained in the following manner. Equation (25) of section 1.3.1 shows that $K = 2e^2(NZ^2)^{\frac{1}{2}}L$ so that $K_D/K_N = \Sigma(NZ^2)_D^{\frac{1}{2}}L_D/\Sigma(NZ^2)_N^{\frac{1}{2}}L_N$. Since $L = 1.45 - 0.8\,(\ln M)$ where M is the average number of collisions which a particle suffers (i.e. for the Molière theory $M = \Omega_b$), we have

$$\frac{K_D}{K_N} = \frac{\Sigma(NZ^2)_D^{\frac{1}{2}}}{\Sigma(NZ^2)_N^{\frac{1}{2}}} \cdot \left\{\frac{1.45 + 0.80[\ln(\Omega_b)_D]^{\frac{1}{2}}}{1.45 + 0.80[\ln(\Omega_b)_N]^{\frac{1}{2}}}\right\}$$

but $\Omega_b = \pi\delta^2/\Phi_{MIN}^2$ and $\delta \propto (NZ^2)^{\frac{1}{2}}$ and $\Phi_{MIN} \propto Z^{\frac{1}{3}}$. Therefore $\Omega_b \propto (NZ^{4/3})$, so that

$$\frac{K_D}{K_N} = \frac{\Sigma(NZ^2)_D^{\frac{1}{2}}}{\Sigma(NZ^2)_N^{\frac{1}{2}}} \left\{\frac{1.45 + 0.80[\ln\{\Omega_{b_N}\Sigma(NZ^{4/3})_D/\Sigma(NZ^{4/3})_N\}]^{\frac{1}{2}}}{1.45 + 0.80[\ln\Omega_{b_N}]^{\frac{1}{2}}}\right\} \quad (34)$$

As stated above, for $\beta = 1$ and $t = 100\mu$, $\Omega_b = 310$ so that, since $\Sigma(NZ^2)_{s2}^{\frac{1}{2}}/\Sigma(NZ^2)_N^{\frac{1}{2}} = 0.828$, and $\Sigma(NZ^{4/3})_{s1}/\Sigma(NZ^{4/3})_N = 0.695$, we have

$K_{x2}/K_N = 0.817$ and $K_{x2} = 20.9$. Similarly $\Sigma (NZ^2)_{x4} / \Sigma (NZ^2)^{\frac{1}{2}}_N = 0.750$ and $\Sigma (NZ^{4/3})_{x4} / \Sigma (NZ^{4/3})_N = 0.574$ giving $K_{x4}/K_N = 0.675$ and $K_{x4} = 17.3$.

The scattering constants corresponding to a restricted range of scattering angles were also derived from Molière's theory. This was done for various cell-sizes from 20 to 400μ. For each value of t Ω_b was obtained from Gottstein's curve[57] shown in fig. 49. The corresponding value of B was obtained from equation (19):- B - ln B = ln Ω_b - 0.115. Next the distribution of angles of scattering was found from equation (18):-

$$P(\phi)d\phi = \left[\left(\tfrac{2}{\pi^{1/2}}\right) e^{-\phi^2} + \left(\tfrac{1}{B}\right) f^1(\phi) + \left(\tfrac{1}{B^2}\right) f^2(\phi) \right] d\phi$$

using Molière's values of $f^1(\phi)$ and $f^2(\phi)$. The median of each distribution was then found and the ratio $K_c/K = \bar{\phi}_{cut}/\bar{\phi}$ determined for a cut at four times this median value.

Comparisons between the theoretical and experimental values of the scattering constants for each type of particle and emulsion used are shown in Table XXIV.

In fig. 50 $|\bar{\alpha}| p\beta c$ $(= K(t/100)^{\frac{1}{2}})$ is plotted against energy for electrons in normal emulsion (both cut and uncut). It can be seen that, as is expected from theory, there is no appreciable variation with energy. The dashed lines are drawn at the weighted mean value of $|\bar{\alpha}| p\beta c$ in each case. The variation of K and K_c with cell size is shown in fig. 51. It can be seen that for normal emulsion (fig. 51(a)) the agreement is reasonable for K_c but that there is considerable divergence between theory and experiment for the uncut values. The statistics for X2 and X4 diluted emulsions (fig. 51(b) and (c)) are poorer than those for the normal emulsion,

Table XXV.

The uncorrected $\bar{\alpha}$ values are shown, for each proton energy and each type of emulsion, in Table XXV. Noise corrections were applied to these results as for electrons, by measuring the apparent scattering of very fast particles in each type of emulsion with small cell-sizes. The

Table XXV.

TABLE 25

Energy (MeV)	Emulsion	Cell-Size (μ)	No. of Observations UNCUT	No. of Observations CUT	$\overline{\delta}_1$ (div.) UNCUT	$\overline{\delta}_1$ (div.) CUT
140	Normal	400	654	650	.948	.903
		800	311	307	2.73	2.58
	X2	400	326	316	.740	.678
		800	152	151	1.96	1.93
	X4	400	343	319	.732	.554
		800	162	155	1.92	1.71
68	Normal	200	1341	1287	.774	.658
		400	650	628	2.09	1.87
		800	305	298	5.86	5.44
	X2	200	799	773	.563	.504
		400	385	379	1.43	1.34
		800	177	173	3.72	3.49
	X4	200	741	702	.439	.369
		400	360	352	1.23	1.16
		800	170	166	3.24	3.05
49	Normal	200	730	706	.881	.791
		400	354	345	2.38	2.21
		800	169	167	7.17	6.94
	X2	200	514	477	.825	.738
		400	248	239	2.13	1.93
		800	115	115	5.85	5.85
	X4	200	657	624	.654	.538
		400	318	306	1.60	1.44
		800	148	148	4.28	4.21

measurements having been made only for one value of momentum (~ 20 MeV/c), but again the tendency of the experimental values of K to be larger than those predicted by the Molière theory is found. It is difficult to explain this discrepancy except on the assumption that, by chance, there were slightly more large single scatters in the tracks selected for measurement than are predicted by the probability laws. The effect of these large scatters would be most noticeable for small cell sizes and they would, of course, be eliminated from K_c.

The results of other authors with which the present results may be compared are (a) those of Gottstein et al. for 105 MeV positrons with a cell size of 200μ and for 185 MeV positrons with a cell size of 400μ, and (b) those of Voyvodic and Pickup for about 16.5 MeV electrons and positrons with a cell-size of 45μ. Only the uncut values of scattering constant obtained by these authors can be compared with the present results since different ~~cut off~~ cutting values were used in the different cases. It can be seen from fig. 51(a) that the agreement between the present results and the earlier ones is good for the larger cell sizes but that Voyvodic and Pickup's value for a 45μ cell size is closer to the theoretical value than is the present one. Further comparisons are made between theory and experiment in fig. 54, for both electrons and protons (see below).

(b) Protons.

The uncorrected $\overline{|\alpha|}$ values are shown, for each proton energy and each type of emulsion, in Table XXV. Noise corrections were applied to these results as for electrons, by measuring the apparent scattering of very fast particles in each type of emulsion with small cell-sizes. The measured values of N are given in Table XXV and the corrected values of $\overline{S}_{100}$, obtained by the same two methods as were used for the electrons and positrons, are given, together with the corresponding values of [illegible], in [illegible].

Checks for distortion were again made [illegible] of [illegible] values, taking account of their [illegible] for 150 MeV protons in X4 emulsion. It can be seen that no correction is required in this case.

Correction for inclination of the tracks to the x-direction of the microscope stage was also found to be unnecessary due to the straightness of the tracks and their more careful alignment before measurement.

The energy of the protons reaching the plates was calculated from the data supplied by the cyclotron operators (energy of protons leaving cyclotron = 148 ± 3 MeV) by correction for the loss of energy in the air between the exit port of the cyclotron and the box containing the plates (using the data given by Montgomery (87) on the loss of energy of protons in air) and, in the case of the lower energies, calculating the energy loss in the aluminium blocks interposed between the machine and the plates, (again using information from Montgomery). There were 267 cm. of air to be traversed before the plates were reached, giving an incident energy of 146.3 ± 3 MeV. The thinner aluminium absorber was 4.92 cm. thick, so the energy of the protons having penetrated it would be 78.5 MeV and on reaching the plates their energy would be 76.6 MeV. The thicker

Table XXVI

TABLE 26

Proton Energy (MeV)	Emulsion	Cell-Size (μ)	No. of Obsns.	$\overline{\epsilon}$ (div.)	Average (di
50	N	25	77	0.136	
"	X 2	"	154	0.127	
"	X 4	"	157	0.131	0.122 ±
100	N	"	154	0.102	
150	N	"	78	0.112	

measured values of $\bar{E}$ are given in Table XXVI and the corrected values of $\overline{|\delta|}$, obtained by the same two methods as were used for the electrons and positrons, are given, together with the corresponding values of $\overline{|\alpha|}$, in Table XXVII.

Checks for distortion were again made; the distribution of δ values (taking account of their signs) are shown in fig. 52 for 150 MeV protons in X4 emulsion. It can be seen that no correction is required in this case.

Correction for inclination of the tracks to the x-direction of the microscope stage was also found to be unnecessary due to the straightness of the tracks and their more careful alignment before measurement.

The energy of the protons reaching the plates was calculated from the data supplied by the cyclotron operators (energy of protons leaving cyclotron = 148 ± 3 MeV) by correction for the loss of energy in the air between the exit port of the cyclotron and the box containing the plates (using the data given by Montgomery (67) on the loss of energy of protons in air) and, in the case of the lower energies, calculating the energy loss in the aluminium blocks interposed between the machine and the plates, (again using information from Montgomery). There were 267 cm. of air to be traversed before the plates were reached, giving an incident energy of 146.3 ± 3 MeV. The thinner aluminium absorber was 4.92 cm. thick, so the energy of the protons having penetrated it would be 78.5 MeV and on reaching the plates their energy would be 76.6 MeV. The thicker

Table XXVII

aluminium block was 6.08 cm. thick giving a residual energy to the protons of 59 MeV. This corresponds, however, to a range in emulsion of 6.4 mm., whereas the measured range of the particles, whose tracks were used for the measurements, was about 12 mm. corresponding to an energy of 78 MeV. The latter value was used because the range energy relation is better known for emulsion than for aluminium. It was not possible to obtain a reliable value of the range of the 78 MeV protons in the emulsion because of the difficulty of finding tracks which stayed in the emulsion for the whole of their length. It appeared from the measured values of scattering constant however, that the energy value obtained from the theoretical energy loss in the aluminium was accurate in this case.

The effective energy of the protons was found from the experimental range-energy relation for protons in Ilford G5 emulsion, published by Wagner et al. ($E = 0.251\,R^{0.581}$) where E is in MeV and R is in microns. From this, by differentiation and substitution for R, we get $dE/dx = 0.058\,\beta^{-1.44}$ keV per micron. Assuming that this relationship also holds for C2 emulsions, whose composition is very similar to that of the G5 type, the initial rate of energy loss of the protons can be found from the value of β (0.508) corresponding to an energy of 146 MeV. This is 1.75 keV/μ and at this rate of loss the energy after travelling 4,000 μ (half of the average track length used in the measurements) would be 139 MeV. This corresponds to a value of β of 0.496 and an energy loss of

Table XXVII

TABLE 27

Energy (MeV).	Emulsion	Cell-Size (μ)	UNCUT $(\overline{\|\delta\|}^2_{m} - \bar{\epsilon}^2)^{1/2}$	UNCUT $t^{3/2}\left(\frac{\|\delta_2\|^2 - \|\delta_1\|^2}{t_2^3 - t_1^3}\right)^{1/2}$	UNCUT $100^{3/2}\left(\frac{\|\delta_2\|^2 - \|\delta_1\|^2}{t_2^3 - t_1^3}\right)^{1/2}$	CUT $(\overline{\|\delta\|}^2_{0} - \bar{\epsilon}^2)^{1/2}$	CUT $t^{3/2}\left(\frac{\|\delta_2\|^2 - \|\delta_1\|^2}{t_2^3 - t_1^3}\right)^{1/2}$	CUT $100^{3/2}(\ldots)$
	Normal	400	.940	.967	.225	.895	.914	.2
		800	2.73	-	.327	2.58	-	.3
	X 2	400	.730	.695	.174	.671	.684	.1
140		800	1.96	-	.234	1.93	-	.2
	X 4	400	.722	.670	.172	.540	.612	.1
		800	1.92	-	.229	1.71	-	.2
		200	.765	.733	.365	.647	.661	.3
	Normal	400	2.09	2.07	.499	1.87	1.93	.4
		800	5.86	-	.700	5.44	-	.6
		200	.550	.495	.263	.489	.469	.2
68	X 2	400	1.42	1.30	.339	1.34	1.22	.3
		800	3.72	-	.444	3.49	-	.4
		200	.422	.434	.204	.348	.415	.1
	X 4	400	1.22	1.14	.292	1.15	1.07	.2
		800	3.24	-	.387	3.05	-	.3
		200	.872	.798	.416	.781	.779	.3
	Normal	400	2.38	2.56	.569	2.21	2.49	.5
		800	7.17	-	.856	6.94	-	.8
		200	.816	.741	.390	.729	.665	.34
49	X 2	400	2.13	2.06	.509	1.93	2.06	.46
		800	5.85	-	.699	5.85	-	.69
		200	.643	.552	.307	.525	.506	.25
	X 4	400	1.60	1.50	.382	1.44	1.49	.34
		800	4.28	-	.511	4.21	-	.50

aluminium block was 6.68 cm. thick giving a residual energy of the protons of 39 MeV. This corresponds, however, to a range in emulsion of 6 mm. whereas the measured range of the particles whose tracks were used for the measurements was about 12 mm. corresponding to an energy of 58 MeV. The latter value was used because the range energy relation is better known for emulsion than for aluminium. It was not possible to obtain a reliable value of the range of the 76 MeV protons in the emulsion because of the difficulty of finding tracks which stayed in the emulsion for the whole of their length. It appeared from the measured values of scattering constant however, that the energy value obtained from the theoretical energy loss in the aluminium was accurate in this case.

The effective energy of the protons was found from the experimental range-energy relation for protons in Ilford C2 emulsion, published by Bradner et al. (68) :- $E = 0.251\ R^{0.581}$ where E is in MeV and R is in microns. From this, by differentiation and substitution for E, we get $dE/dx = 0.638\,\beta^{-1.44}$ keV per micron. Assuming that this relationship also holds for G5 emulsions, whose composition is very similar to that of the C2 type, the initial rate of energy loss of the protons can be found from the value of β (0.502) corresponding to an energy of 146 MeV. This is 1.75 keV/μ and at this rate of loss the energy after travelling 4,000μ (half of the average track length used in the measurements) would be 139 MeV. This corresponds to a value of β of 0.496 and an energy loss of

Table XXVIII

1.77 MeV/μ. Taking the average rate of energy loss as the mean of the initial and final rates we find an effective energy of 13[illegible].2 MeV and a corresponding value of $p\beta c$ of [illegible] MeV.

The formula for the energy loss of protons is given by equation(33)

$$-(dE/dx) = \{4\pi NZe^4/mv^2\}\{\ln(2mv^2/I(1-\beta^2)) - \beta^2\} \quad (33)$$

From this we see that for diluted emulsion the energy loss will be given by

$$\frac{(dE/dx)_D}{(dE/dx)_N} = \frac{\sum(NZ)_D}{\sum(NZ)_N}\left\{\frac{\ln(A/Z_D B) - \beta^2}{\ln(A/Z_N B) - \beta^2}\right\} \quad (34)$$

From which we find that for 2x diluted emulsions the rate of energy loss for 145 MeV protons is 0.[illegible]0 x 1.77 = 1.4[illegible] keV/μ and for 4x dilution the value is 0.67 x 1.77 = 1.19 keV/μ. The values of rate of energy loss, effective energy and corresponding $p\beta c$ are given for each energy and emulsion in Table XXVIII.

The experimental values of scattering constant, together with their standard deviations are shown in Table XXIX. Theoretical values were obtained from the Molière theory by a similar method to that used for the electrons. The value of α_1 was determined for each value of β from fig. 49 and, the appropriate value of K for normal emulsions having been obtained from Goldschmidt-Clermont's data (shown in fig. 36), the value of K_D/K_N was found from equation(34). The values of K_c for dilute emulsions were also obtained in the same way as for electrons. These theoretical values are also shown in Table XXIX.

The variation of K and K_c with cell size, t, is shown for each proton energy and each type of emulsion in fig. 53 in which th

Table XXVIII

Table XXIX

TABLE 28

Nominal Energy (MeV)	Emulsions	Average Track Length (mm)	Energy Loss (MeV)	Effective Energy (MeV)	Effec[illegible] pβc
	Normal	8	7.1	139.2	265
140	X 2	8	5.7	140.6	267
	X 4	8	4.7	141.6	269
	Normal	8	9.8	66.8	130
68	X 2	8	7.8	68.8	133
	X 4	8	6.8	69.8	135
	Normal	8	12.5	45.5	88.6
49	X 2	8	8.4	49.6	97.0
	X 4	8	8.0	50.0	97.4

1.79 keV/μ. Taking the average rate of energy loss as the mean of the initial and final rates we find an effective energy of 139.2 MeV and a corresponding value of $p\beta c$ of 265 MeV. The formula for the energy loss of protons is given by Fermi[65] as

$$-(dE/dx) = (4\pi NZe^4/mV^2)\left[\ln\left\{2mV^2/I(1-\beta^2)\right\} - \beta^2\right] \quad (35)$$

from this we see that for diluted emulsion the energy loss will be given by

$$\frac{(dE/dx)_D}{(dE/dx)_N} = \frac{\sum (NZ)_D B \left\{\ln (A/Z_D B) - \beta^2\right\}}{\sum (NZ)_N B \left\{\ln (A/Z_N B) - \beta^2\right\}} \quad (36)$$

from which we find that for X2 diluted emulsions the rate of energy loss for 146 MeV protons is 0.80 x 1.77 = 1.42 keV/μ and for X4 dilution the value is 0.67 x 1.77 = 1.19 keV/μ. The values of rate of energy loss, effective energy and corresponding $p\beta c$ are given for each energy and emulsion in Table XXVIII.

The experimental values of scattering constant, together with their standard deviations are shown in Table XXIX. Theoretical values were obtained from the Molière theory by a similar method to that used for the electrons. The value of Ω_b was determined for each value of β from fig. 49 and, the appropriate value of K for normal emulsions having been obtained from Goldschmidt-Clermont's data (shown in fig. 35), the value of K_D/K_N was found from equation (34). The values of K_C for dilute emulsions were also obtained in the same way as for electrons. These theoretical values are also shown in Table XXIX.

The variation of K and K_c with cell size, t, is shown for each proton energy and each type of emulsion in fig. 53 in which the

Table XXIX

Table XXIX

TABLE 29

Nominal Energy (MeV)	Emulsion	Cell-Size (μ)	Effective $p\beta c$ (MeV)	$K_{Expt.}$	$K_{Theo.}$	$Kc_{Expt.}$
141	Normal	400	265	30.0 ± 0.8	28.6	25.6 ± 0.8
		800		32.0 ± 1.2	29.4	26.0 ± 1.2
	X 2	400	267	23.4 ± 0.8	23.4	21.5 ± 0.8
		800		22.2 ± 1.2	24.0	22.0 ± 1.2
	X 4	400	269	23.1 ± 0.8	19.5	17.3 ± 0.7
		800		21.7 ± 1.1	19.8	19.4 ± 1.1
68	Normal	200	130	30.0 ± 0.6	28.0	25.3 ± 0.6
		400		31.9 ± 0.8	28.9	25.6 ± 0.8
		800		31.7 ± 1.2	29.8	24.0 ± 1.1
	X 2	200	133	24.7 ± 0.6	22.8	21.9 ± 0.5
		400		22.6 ± 0.7	23.7	21.3 ± 0.7
		800		22.7 ± 1.0	24.5	19.8 ± 1.0
	X 4	200	135	19.9 ± 0.7	19.0	16.1 ± 0.4
		400		19.8 ± 0.7	19.6	18.6 ± 0.6
		800		18.4 ± 1.1	20.4	17.5 ± 0.9
49	Normal	200	88.6	27.1 ± 0.7	28.1	24.2 ± 0.7
		400		26.2 ± 1.0	29.0	24.2 ± 0.9
		800		27.6 ± 1.4	29.9	27.0 ± 1.4
	X 2	200	97.0	25.9 ± 0.6	23.0	21.9 ± 0.8
		400		25.6 ± 0.9	23.8	21.3 ± 1.0
		800		25.0 ± 1.1	24.6	23.0 ± 1.0
	X 4	200	97.4	22.6 ± 0.6	19.1	18.4 ± 0.5
		400		19.9 ± 0.9	19.7	17.9 ± 0.7
		800		18.8 ± 1.1	20.5	18.6 ± 1.0

smooth curves represent Molière's results. In fig. 54 the scattering constants are plotted against the corresponding values of Ω_b, as was done by Gottstein et al. (57), and the results summarised in their paper are included in this figure which incorporates the present results for both electrons and protons.

It can be seen that the agreement between theory and experiment is as good for the present results as for those of other authors (though in the case of K_c, as mentioned earlier, a direct comparison is not strictly possible owing to the slightly different cutting procedure adopted by previous authors).

2.4 Single Scattering.

The effort involved in measuring with reasonable statistical accuracy the single scattering of electrons and positrons of about 10 MeV energy is, compared with that required for multiple scattering measurements on the tracks of these particles, so great that from the outset it was decided to concentrate the available labour on a single energy value and on one type of emulsion. The single scattering measurements were therefore made only on tracks of 10 MeV/c electrons and positrons in normal emulsions. In this way a comparison of the single scattering of electrons and positrons under identical conditions could be made and the use of the lowest energy value and of the densest scattering medium ensured the highest possible rate of collection of single scattering events.

2.4.1 Measurements.

In the course of this work three Cooke, Troughton and Sims M4000 microscopes were used, the alignment of the plates on the microscope stages being carried out in a manner similar to that used for the multiple scattering measurements. The conditions governing the acceptance of tracks for measurement were:-

(1) that the direction of travel in the plane of the emulsion (i.e. in a plane parallel to the stage of the microscope) and just below the emulsion surface must be within 15° of the x-direction of the microscope stage which in the setting up process had been

arranged to be parallel to the incident direction of travel of particles from the analyser.

(2) that the angle of dip into the emulsion after processing should not, at the point of entry into the emulsion, be more than 15°.

(3) that the length of the track must not be less than 700μ if it left the emulsion at the lower surface or 500μ if it re-emerged from the upper surface.

The first and second conditions above are similar to those for the multiple scattering measurements. The third is less severe than the corresponding conditions for multiple scattering, where, in order to obtain reasonable statistics for the 151 determinations on individual tracks, it was necessary to have a minimum track length of 1,500μ.

A further visual check was made of all tracks satisfying the above conditions to ensure that, in the opinion of the observer, they had a degree of multiple scattering consistent with an energy of 10 MeV.

When the single scattering investigation was started the method of measurement was as follows. An examination was made along the length of each accepted track from the point at which it entered the emulsion, until a single scattering event was found with a change of direction (in space) of 20° or more, or until a 2,000μ length of the track had been examined. This limit to the length of track scanned was applied in order to restrict the energy range of tracks whose single scatters were accepted - in 2,000μ of emulsion the particles used in this investigation would lose, by ionisation alone, about 2 MeV. Since the magnitude of the change of direction in space could not be accurately estimated by inspection, any scattering event in which the change of direction in the plane of the microscope stage was 10^{o} or more, or in which a sudden change in the rate of dip into the emulsion was detectable, was recorded and those events which on calculation of the change of direction in space gave a value less than 20^{o} were later removed from the record.

When an acceptable scattering event was found the change of direction, ϕ, in the plane of the microscope stage and the rate of dip of the track into the emulsion before and after the scattering, α_1 and α_2, were measured. The change of direction in the plane of the stage was measured directly by means of the goniometer attachment to the microscope eye-piece to an accuracy of 0.25^{o}. The angles of dip were measured by means of the microscope's calibrated fine focus control, the change in depth of the track from the emulsion surface over a horizontal distance of 50μ along the track being found. The fine focus control carried a scale reading to 0.5μ and a table was prepared giving the angles of dip in unprocessed emulsion for each value of depth change in 0.5μ steps, assuming a shrinkage factor of 2.3.

The change of direction in space, θ, was found from the measured values of ϕ, α_1 and α_2 by means of the equation

$$\text{Cos}\,\theta = \text{Sin}\,\alpha_1\,\text{Sin}\,\alpha_2 + \text{Cos}\,\alpha_1\,\text{Cos}\,\alpha_2\,\text{Cos}\,\phi \qquad (37)$$

which may be proved by simple geometry with reference to fig. 55 which shows a scattering event. The actual evaluation of θ was greatly facilitated by the use of a special chart ("The Sigsby Hydrographic Chart", obtained from the Physics Department, the University of Bristol) from which, ϕ, α_1 and α_2 having been set up, θ could be read off directly.

When a scatter of 20° or more had been found in a given track, the distance from the point at which the particle entered the emulsion to that at which the scatter occurred was measured along the track by means of the calibrated eyepiece scale. In this measurement the dip of the track into the emulsion was ignored (i.e. the projection of the track's length onto the surface of the emulsion was measured) since the measurement of the true length would have been extremely laborious and this simplification introduced only a small correction factor (Sec α). Correction for this dip was applied after all the measurements had been made by determining the average angle of dip of each group of tracks measured.

Originally, after one scattering event had been found in a track the track was abandoned. In this way no track was examined after it had suffered a scatter of about 20° or more and so the inclusion of a scattering event in a track produced by a particle which had previously lost, by radiation in an earlier scatter, an appreciable amount of energy was avoided. The inclusion of such events would of course have given too high a value of scattering cross section since, for relativistic energies this cross section is proportional to $1/E^2$.

A histogram was constructed in which the observed number of scattering events in a given angular interval was plotted against the size of the angle of scattering. The ordinates of the histogram were proportional to the scattering cross section averaged over the angular interval concerned (neglecting for the moment the various corrections which it was necessary to apply to the observed results), and the "scattering coefficient" could be obtained for a given interval by dividing the number of scattering events in that interval by the total track length in which they occurred. The cross section for scattering could then be obtained by dividing this coefficient by the number of scattering nuclei per cc. of emulsion. (This information was supplied by Ilford Ltd.).

This method of measurement at first worked reasonably well and a difference between the cross sections for scattering of electrons and positrons began to emerge from the measurements, as shown by fig. 56. From this graph it can be seen that the divergence between the electron and positron cross sections appears to increase for angles less than 20°. Because of this it appeared desirable to include angles smaller than 20° in the study. The measurements were therefore extended to include all scattering events in which θ was greater than 10°. (Any event in which a noticeable change in either the rate of dip or in the horizontal angle of direction occurred was measured up).

When this was done the length of track along which it was necessary to search before a single scatter equal to or greater than the minimum size for acceptance was found was greatly reduced (for small angles the cross section varies as $1/\sin^4 \theta/2$ so that the cross section at 10° is roughly 16 times as great as that at 20°.) The distance scanned along each track was in fact found to be only a few tens of microns and as the original method of measurement whereby the portion of a track occurring after the first scatter was not examined was maintained , only these first few tens of microns were examined in each track.

The results so obtained gave practically identical values of scattering cross section for positrons and electrons, as can be seen from fig. 57. This unexpected result was explained on the grounds that the observer was not now examining a sufficiently long length of track to be able to judge reliably whether the multiple scattering was of the magnitude to be expected for a 10 MeV particle. This lack of proper track selection would result in the inclusion of "background" tracks which happened to lie in the required direction and since these would be mainly stray electrons and positrons scattered into the plate from the material surrounding it during exposure they would be of the same nature for both sets of emulsions (i.e. those into which electrons had been fired and those with positrons in them). The cross section for scattering of the background particles would therefore be the same for each set of plates, and the two curves might be expected to run together, if there were a sufficiently high proportion of stray tracks amongst those measured.

A careful re-examination of some of the tracks accepted in the above measurements suggested that this explanation was very probably correct and it was therefore decided that an actual measurement of multiple scattering rather than a rough visual estimation of its magnitude would have to be made for all tracks accepted for measurement so as to exclude those not of the correct energy value. The previous section of this work (that on multiple scattering) had indicated that this procedure would effectively eliminate background tracks. Unfortunately however, it would also greatly decrease the rate of collection of data. In view of this and the evidence from other authors (referred to in section 1.2.1) that the loss of energy on scattering was very small, it was decided that all single scatters greater than 10° in the first 2,000μ of those tracks which satisfied the acceptance criteria would be included in the measurements.

The procedure now employed was, therefore, that any track satisfying the acceptance criteria was measured for multiple scattering and, if it was found to have a value of $|\bar{\delta}_1|_{c,T}$ within $\pm$ 40% of the value determined for 10 MeV electrons in the previous work, it was then examined for single scattering events. All the scatters found in the first 2,000μ, or in the total length if this was less than 2,000μ, were recorded provided that they were of at least the minimum size for acceptance.

This method of measurement was used for a considerable time in the examination of the plates exposed to the beam of the 30 MeV synchrotron, but the necessity for the multiple scattering measurement on each track caused a great reduction in the speed of accumulation of data and made the work rather arduous. Eventually it was recognised that a new exposure of plates was required and that if possible the experimental conditions for this exposure should be such that the background of stray tracks would be so small that there would be no necessity to make a multiple scattering measurement in order to verify that each track examined was produced by a particle of the required energy.

The new exposures were made in the manner described in section 2.1.2 using the 1 MeV H.T. set. In these exposures increased densities of the required tracks were obtained with reduced background intensities (the plates were found on examination to have about two required tracks per field of view of the microscope, compared with 0.1 for the original synchrotron plates). Tests were made in which observers, after looking at a track decided whether it was of the required energy value, their decision then being checked by a multiple scattering measurement on the track in question. These tests showed that it was now possible to dispense with the multiple scattering measurements, the decision of the observers being, after some training, quite reliable. This method of measurement was adopted for all the work in which these new plates were used and it appeared to give satisfactory results.

The limit on the speed of collection of results was now set by the time taken to measure, and to convert into change of direction in space, the various angles at each scattering event. Because the cross section increases so rapidly with decreasing angle of scatter, most of the scatters measured were of small angle and eventually it was realised that reasonable statistics could be obtained for the larger angles of scattering only if the rate of collection of data was increased by raising the minimum size of scatter accepted. It was therefore decided to fix a limit of 25^{o} for these measurements.

2.4.2 Correction of experimental results

Before the experimentally determined cross sections could be compared with theory and with other experimental determinations, it was necessary for certain corrections to be applied. Three main corrections were considered, namely that to allow for the difficulty of resolving two scattering events occurring very close together along the length of a track (the "double scattering" correction), that to correct for the increased possibility of missing a scattering event when a large change in the angle of dip into the emulsion occurs (the "azimuthal angle" correction) and that to allow for the escape of particles from the emulsion before their tracks were of the minimum length required for them to be accepted for measurement (the "escape" correction).

(a) Correction for double scattering.

In all measurements of single scattering there is a finite probability that two separate scattering events, occurring close together along a track will escape resolution and be interpreted as a single event. A theoretical consideration of the correction required to allow for this effect was obtained as long ago as 1922 by Wentzel (69) for the case of scattering in thin foils. The adaptation of Wentzel's method to the present case is rather involved, the main complication being due to the variation, in the present case, of the quantity equivalent to "foil thickness" in Wentzel's paper.

Wentzel calculated $J_n(\phi)$, the probability that after suffering n collisions in a foil, a particle should emerge in a direction making an angle between ϕ and $\phi + d\phi$ with the incident direction. Limiting our consideration to double scattering, we have, from Wentzel's paper,

$$J_2(\phi) = \int_0^{\pi} d\phi_1 \cdot F(0, \phi_1) \times \frac{F(\phi_1, \phi)}{\mathrm{Cos}\,\phi_1} \times D_2$$

where $D_2 = \int_0^{\pi} dz_0 \,\mathrm{exp.}\left[-\mu z_0 (1 - \mathrm{Sec}\,\phi_1)\right] \times \int_0^{d} dz_1 \,\mathrm{exp.}$ $\left[-\mu z_1 (\mathrm{Sec}\,\phi_1 - \mathrm{Sec}\,\phi)\right] \times \mathrm{exp.}\,(-\mu d\,\mathrm{Sec}\,\phi)$ in which ϕ_1 is the direction of the scattered particle (relative to the incident direction) after the first scatter, caused by a nucleus at a depth z_0 in the foil; ϕ is the angle after the second scatter, by a nucleus at a depth z_1, d is the thickness of the foil, $F(0, \phi_1)$ is the probability of single scattering from direction 0 to direction ϕ_1, and $F(\phi_1, \phi)$ the corresponding probability for scattering from ϕ_1 to ϕ.

is some angle above which the probability of scattering is very small and μ is given by πNR^2 where N is the number of scattering nuclei per c.c. and R is their effective radius.

If μd (Sec γ - 1) $\ll$ 1 the above expressions are considerably simplified. In order to avoid divergence of the integrals a lower limit, ω, must be set to the range of size of ϕ_1 - Wentzel took $\omega = 1^\circ$. He showed that for a Rutherford distribution of single scattering ω is given by $Ctg^2\, \omega/2 = \mu/\alpha$ ($\alpha = \pi N (Ze^2 / mv^2)^2$), so that in the present case, for $\omega = 1^\circ$ and $d = 5 \times 10^{-3}$ cm. (the size of d is discussed later), we have μd (Sec γ - 1) = 0.[illegible] for $\gamma = 55^\circ$. Since the probability of scattering through angles greater than 55° in a distance of 50 microns will be very small we may take the above condition to be satisfied and we now have, according to Wentzel, $J_2(\phi) = \frac{d^2}{2} e^{-\mu d}\, \Phi_2(\phi)$ where $\Phi_2(\phi) = \int_0^{\pi} F(0, \phi_1) \times F(\phi_1, \phi)\, d\phi_1$.

Assuming that Rutherford's theory of single scattering applies we have $F(0, \phi_1) = \dfrac{\cos \phi_1/2}{\sin^3 \phi_1/2}$ and

$$F(\phi_1, \phi) = \frac{2\alpha \sin\phi (1 - \cos\phi_1 \cos\phi)}{|\cos\phi_1 - \cos\phi|^3} \text{ for } |\phi_1 - \phi| > \omega .$$

In a medium such as a nuclear emulsion the foil thickness d is replaced by the minimum separation along the track for which two scattering events ϕ_1 and ϕ_2 can be resolved and this distance depends upon ϕ_1 since if ϕ_1 is small the resolution of these two events is more difficult for a given value of d than when ϕ_1 is large. To allow for this we may put $d = a/\sin\phi_1$

a being the perpendicular displacement of the scattered track, after a distance d, from the initial direction. It is reasonable to assume that this displacement will be independent of ϕ_1.

In the present case therefore, $d = a \operatorname{Cosec} \phi_1$ where a was found by an estimation of the minimum separation of various sizes of single scatters which could just be resolved, to be of the order of 10^{-4} cm.

Therefore

$$J_2(\phi) = \frac{a^2 \alpha^2}{2} \int_0^{\pi} \frac{\operatorname{Sin}\phi (1 - \operatorname{Cos}\phi_1 \operatorname{Cos}\phi) \exp. (-\mu a \operatorname{Cosec}\phi_1)}{(\operatorname{Sin}^4 \phi_1/2) \operatorname{Sin}\phi_1 \, |\operatorname{Cos}\phi_1 - \operatorname{Cos}\phi|^3} \, d\phi_1$$

$$= \frac{a^2 \alpha^2}{2} \int_0^{\pi} y \, d\phi_1 \qquad (38) \text{ for } |\phi_1 - \phi| \geqslant \omega.$$

and for $\phi_1 = \phi \geqslant \omega/2$ it can be shown that

$$J_2(\phi) = \frac{a^2 \alpha^2}{2} \int_0^{\pi} \frac{(\operatorname{Ctg}^2 \omega/2 + 3 + 2\operatorname{Ctg}^2\phi_1)(\operatorname{Ctg}^2 \omega/2 - \operatorname{Ctg}^2 \phi_1)}{6\pi (\operatorname{Sin}^4 \phi_1/2) \operatorname{Sin}\phi_1} \times$$

$$\times \exp\left(-\mu a (\operatorname{Sec}\phi_1)\right) \times d\phi_1 \qquad (39)$$

The integration must be performed graphically and when this is done the variation of y with ϕ_1 is found to be that shown in fig. 58 for the cases of $\phi = 20^\circ$ and $\phi = 10^\circ$. From these curves and the simple Rutherford expression for $J_1 (10^\circ)$, we find the correction factors for double scattering $J_1 (10^\circ) / J_1 (10^\circ) + J_2 (10^\circ) = 0.92$ and $J_1 (20^\circ) / J_1 (20^\circ) + J_2 (20^\circ) = 0.96$.

As will be shown later these factors are not sufficient to remove the "hump" which was found in the experimental curve of cross section versus angle of scattering at the region 10° to 20°

A different method of calculating the double scattering correction was devised by Dr. H. Muirhead, Mr. I. S. Hughes and the present author. This method has the following basis. Suppose that in a given track we have a scatter through an angle θ_1 followed after a distance x by one through an angle θ_2. Then, if $x > a\,\mathrm{Cosec}\,\theta_1$ each scatter will be recorded, but if $x \leq a\,\mathrm{Cosec}\,\theta_1$ we shall record (a) too few (b) the correct number or (c) too many scatters in the angular range Θ to Θ^1 according to which of the following conditions apply:-

(1) for $\theta_1 < \Theta$ or $> \Theta^1$, a) if $\theta_2 < \Theta$ or $> \Theta^1$ our value of $N_s(\Theta \to \Theta^1)$ is too high by one if R_{θ_1,θ_2} lies between Θ and Θ^1.

b) if $\Theta < \theta_2 < \Theta^1$ our value of $N_s(\Theta \to \Theta^1)$ is too low by one if R_{θ_1,θ_2} does not lie between Θ and Θ^1.

(2) for $\Theta < \theta_1 < \Theta'$, a) for all values of θ_2 our value of $N_s(\Theta \to \Theta^1)$ is too low by one if $R_{\theta_1\theta_2}$ does not lie between Θ and Θ^1.

b) for $\Theta < \theta_1 < \Theta^1$ our value of $N_s(\Theta \to \Theta^1)$ is too low by a further one if R_{θ_1,θ_2} does not lie between Θ and Θ^1.

In these conditions above, $N_s(\Theta \to \Theta^1)$ is the number of scatters recorded for the angular interval Θ to Θ^1 and R_{θ_1,θ_2} is the resultant angle formed by θ_1 and θ_2 when these are unresolved.

The true number of scatters N_T is therefore related to the apparent number N_A by the relationship

$N_A[1 + P(1_a) - P(1_b) - P(2_a) - P(2_b)]N_T$ where $P(1_a)$ etc. are the probabilities of the occurrence of conditions 1a etc. These are given by

$$P(1a) = \left[\Sigma_{\alpha}^{\Theta} P(\theta_1) + \Sigma_{\Theta'}^{180^\circ} P(\theta_1)\right]\left[\Sigma_{\alpha}^{\Theta} P_x(\theta_2) + \Sigma_{\Theta'}^{180^\circ} P_x(\theta_2)\right] P(\phi) \qquad (40)$$

$$P(1_b) = \left[\Sigma_{\alpha}^{\Theta} P(\theta_1) + \Sigma_{\Theta'}^{180^\circ} P(\theta_1)\right] \Sigma_{\Theta}^{\Theta'} P_x(\theta_2) \times \left(1 - P(\phi)\right) \qquad (41)$$

$$P(2_a) = \Sigma_{\Theta}^{\Theta'} P(\theta_1) \Sigma_{\alpha}^{180^\circ} P_x(\theta_2) \times \left(1 - P(\phi)\right) \qquad (42)$$

$$P(2_b) = \Sigma_{\Theta}^{\Theta'} P(\theta_1) \Sigma_{\Theta}^{\Theta'} P_x(\theta_2) \times \left(1 - P(\phi)\right) \qquad (43)$$

with the condition that $P(1a)$, $P(1b)$, $P(2a)$ and $P(2b)$ all equal zero for $\theta_1 > \sin^{-1} a/x$, and where α is the lower limit of the range of θ_1 and θ_2 and $P(\phi)$ is the probability of R_{θ_1,θ_2} lying in the range Θ to Θ^1.

The evaluation of the above probabilities is an extremely long and tedious process. However, numerical results were obtained for the range 10° to 15° giving a correction factor of ~ 0.9. This result confirms that obtained from the application of Wentzel's work.

For the larger angular intervals the corrections for double scattering will be much smaller than that for the 10° to 15° interval because of the greatly increased ability which an observer has to resolve two scattering events when each of them is quite large.

(b) Azimuthal angle correction.

When a scattering event occurs in which the dip of the track into the emulsion undergoes a large change, the possibility of missing the scatter increases. The effect of this is greatest for the smallest angular interval examined and for the largest. For the small angle interval the effect is important because a scatter with, say $10^{\circ} < \theta < 15^{\circ}$ may be missed altogether if ϕ (the projection of the angle of scatter onto the plane of the emulsion) is small (as it must be if the change of dip is large). For large angles the importance of this effect arises from the fact that a large change in dip together with a large change in ϕ may make the scattered track difficult to locate so that the event may be interpreted as a stopping of the incident particle and not as a scatter.

The effect was investigated in the present work in the following way. A number of scatters in which θ was greater than 25° were carefully measured up and the angle, A, between the plane of the microscope stage and the projection of the scattered track on a plane perpendicular to the incident direction (see fig. 59) was then given by the relationship $\text{Cos } A = \text{Sin}\,\phi / \text{Cos}\,\alpha_1 \text{ Tan } \theta$. (The value of A was in fact obtained by setting up the appropriate values of α_1, α_2 and ϕ in a model of the scattering event from which A could be directly read off). This projected "azimuthal" angle should have an isotropic distribution provided that scatters with all values of change in angle of dip are detected with the same efficiency. Any anisotropy in the distribution of the azimuthal angle may therefore be regarded as a measure of the degree to which those events in which a large change of dip occurs are lost.

The observed distribution of the azimuthal angle is shown in fig. 60 for electrons and for positrons, no distinction being made between positive and negative values of A. It can be seen from the histograms of this figure that for electrons the distribution falls off for values of A from 60° to 90°, the fall-off being, as expected, most noticeable for scatters with large ($> 50^{\circ}$) or small (25° to 35°) values of θ. For positrons the fall-off is limited to the small values of θ. The absence of any fall-off for the large angles of scatter in this case is attributed to the fact that the background was much lower in the plates exposed to positrons with the H.T set than in those exposed to electrons. The reason for this was that for the electron exposures a deuteron beam was used in the accelerator and consequently quite a heavy background of scattered protons was found in the plates, caused by the stray neutrons associated with this beam. For the positron exposures, however, as mentioned in section 2.1.2., a proton beam was used so that this background was eliminated. It was checked experimentally that the number of tracks appearing to stop abruptly in the plates increased with the heaviness of the plate background.

The correction factor to allow for the loss of traks which caused this anisotropy was found by counting the number of tracks for each interval of θ, lying in the range $0^{\circ} < A < 60^{\circ}$, for which no fall-off was noticeable. From this number the

Tables XXX & XXXI

Table 30

	ELECTRONS			POSITRONS		
Angular Interval	25-35°	35-50°	> 50°	25-35°	35-50°	> 50°
Expected Number of Scatters	84	25.5	18	43.5	27	16.5
Actual Number	65	22	13	32	22	16.0
Correction Factor	1.29	1.16	1.38	1.36	1.23	1.00

TABLE 31

t_1 (microns)	50	100	150	200	250	300	350	400	450
G (ψ = 10°)	443.3	394.4	345.7	313.8	250	203.7	154.8	120.4	92.2
G (ψ = 13.5°)	440	391.6	343.7	296.3	250	205.5	164.1	129.1	106.6

number to be expected for the interval $0° < A < 90°$ was calculated and the ratio of the actual number of events found in this interval divided by the expected number gave the correction factor for the particular range of θ concerned.

The values of correction factor so obtained are shown in Table XXX. It can be seen at once from these figures that the effect is of a considerable size and this fact coupled with the necessarily rather poor statistics involved in its derivation is an unfortunate feature of this section of the work. The only ameliorating consideration is that the corrections for electrons and for positrons are of similar magnitude, so that the ratio of positrons to electron cross section will not be too sensitive to this effect.

c) Correction for escape of particles from the emulsion.

(i) Escape from the upper surface.

In order to be accepted for measurement it was necessary for a track, if it re-emerged from the upper surface of the emulsion, to have a total projected length in the plane of the emulsion of at least 500μ. A track which after being scattered at a point near the surface, left the emulsion before its projected length had reached $500\ \mu$ was thus not accepted for measurement. Since tracks could escape measurement in this was only if they were scattered, a correction must be applied or too low a value of cross section would be obtained.

The correction factor necessary to allow for this effect was evaluated in the present work in the following manner. Suppose that all the incident tracks may be represented by parallel straight lines entering the emulsion at an angle ψ and suppose that in its first 500 μ of projected length no track suffers more than one scatter of measureable size. If a particle travels a distance l_1 (projected length $t_1 = l_1 \cos\psi$) before being scattered, then in order to be accepted for measurement it must travel a further l_2, whose projection is t_2, where $t_1 + t_2 \geqslant 500$ μ. l_2 is, of course, a function of l_1, of ψ and of the angle through which the particle is scattered.

All tracks having a total projected length of 500 μ will end on the curved part of one of a series of cylinders whose radii are given by $t_2 = 500 - t_1$. Also, for a given value of θ the scattered track will lie along the surface of a cone of half angle θ and with its axis along the incident direction, as shown in fig. 61. The probability of escape is then given by the area of surface of that part of the cone which passes out of the surface of the emulsion inside the cylinder divided by the total area of surface of the cone. This probability is given by $\phi s/\pi$ where ϕs is as shown in fig. 61b. Seen from above, the cylinder appears as a circle of radius t_2 and the base of the cone appears as an ellipse intersecting this circle at the points B' and B'' shown in figs. 61b. and c.

Φ is the projection onto the emulsion surface of ϕs. It can be shown that all possible values of θ are covered by this

θ \ t_1 (μ)	50	100	150	200	250	300	350	400	450	500	$\bar{\phi}$
5°	0	0	0	0	0	0	0	0	0	0	0
10°	0	0	0	0	0	0	0	0	0	0	0
15°	0	0	0	0	0	0	0	0	0	0	0
20°	42.3	35.1	15.0	0	0	0	0	0	0	0	9.24
25°	54.3	48.6	40.1	25.9	0	0	0	0	0	0	16.90
30°	62.0	57.4	51.2	42.3	26.4	0	0	0	0	0	23.93
35°	67.0	63.2	58.3	51.3	40.3	17.1	0	0	0	0	29.72
40°	70.8	67.6	63.2	57.4	48.7	33.6	0	0	0	0	34.13
45°	73.8	70.3	67.1	62.0	54.3	42.7	5.1	0	0	0	37.61
50°	76.4	73.7	70.2	65.6	59.0	48.7	29.6	0	0	0	42.32
55°	78.4	75.9	72.8	68.5	62.5	55.6	37.5	0	0	0	44.91
60°	80.2	77.9	74.9	71.0	65.4	57.1	45.3	0	0	0	46.98
65°	81.8	79.7	76.8	72.8	67.9	60.1	47.5	21.1	0	0	50.77
70°	85.3	82.5	78.5	74.9	69.9	62.6	50.8	28.3	0	0	55.95
75°	84.7	82.7	80.1	76.6	71.8	64.8	53.6	33.5	0	0	54.78
80°	86.0	84.0	81.4	78.0	75.4	66.3	55.7	37.0	0	0	56.38
85°	87.2	85.3	82.7	79.4	74.2	68.1	57.7	39.9	0	0	57.45
90°	88.4	86.3	84.0	80.7	76.1	69.5	59.5	41.9	0	0	58.64

Table XXXII

TABLE 32.

$t_1 (\mu)$	50	100	150	200	250	300	350	400	450	500	$\overline{\Phi}_s$	$P_s(\theta)$
θ						Φ_s						
5°	0	0	0	0	0	0	0	0	0	0	0	0
10°	0	0	0	0	0	0	0	0	0	0	0	0
15°	0	0	0	0	0	0	0	0	0	0	0	0
20°	42.3	33.1	15.0	0	0	0	0	0	0	0	9.04	.050
25°	54.5	48.6	40.1	25.8	0	0	0	0	0	0	16.90	.094
30°	62.0	57.4	51.2	42.3	26.4	0	0	0	0	0	23.93	.133
35°	67.0	63.2	58.3	51.3	40.3	17.1	0	0	0	0	29.72	.165
40°	70.8	67.6	63.2	57.4	48.7	33.6	0	0	0	0	34.13	.190
45°	73.8	70.9	67.1	62.0	54.5	42.7	5.1	0	0	0	37.61	.209
50°	76.4	73.7	70.2	65.6	59.0	48.7	29.6	0	0	0	42.32	.235
55°	78.4	75.8	72.8	68.5	62.5	53.6	37.5	0	0	0	44.91	.249
60°	80.2	77.9	74.9	71.0	65.4	57.1	43.3	0	0	0	46.98	.261
65°	81.8	79.7	76.8	72.8	67.9	60.1	47.5	21.1	0	0	50.77	.282
70°	83.3	81.2	78.5	74.9	69.9	62.6	50.8	28.3	0	0	59.95	.294
75°	84.7	82.7	80.1	76.6	71.8	64.8	53.6	33.5	0	0	54.78	.304
80°	86.0	84.0	81.4	78.0	73.4	66.5	55.7	37.0	0	0	56.20	.312
85°	87.2	85.3	82.7	79.4	74.2	68.1	57.7	39.9	0	0	57.45	.319
90°	88.4	86.5	84.0	80.7	76.1	69.5	59.3	41.9	0	0	58.64	.326

figure, the ellipse becoming a straight line for $\theta = 90^\circ$. For any given value of t_2 there is a corresponding value of scattering angle (say θ') for which the scattered particles can just not escape no matter where they lie on the cone, i.e. the cone just touches the cylinder and B' and B" coincide. In this case if the radius of the base of the cone is x, we have

$$\sin\theta' = x/l_2 = (t_1 + t_2)\sin\psi/(t_2^2 + t_1^2 \tan^2\psi)^{1/2} \text{ so that}$$

$$\sin\theta' = 500 \sin\psi \,/\, \left\{ (500 - t_1)^2 + t_1^2 \tan^2\psi \right\}^{1/2} \qquad (44)$$

In the general case we see by reference to fig. 63b that $\cos\phi_s = K_s/R_s$ and it can be shown by simple geometry that

$$\cos\phi_s = \left[\frac{t_1}{\{t_1^2 + 500\cos^2\psi(500 - 2t_1)\}^{1/2} \sin\theta} + \cos\theta \right] \tan\psi \qquad (45$$

This expression reduces to equation (44) for the case in which $\cos\phi_s = 1$. Putting $\left\{t_1^2 + 500\cos^2\psi(500 - 2t_1)\right\}^{1/2} = G$ we find that G is almost independent of the value of ψ. This is shown in Table XXXI where G is calculated for $\psi = 10^\circ$ and 13.5°. Since we may take G to be independent of ψ, $\cos\phi_s$ is proportional to $\tan\psi$. In Table XXXII the values of ϕ_s are given for all values of θ, in five degree intervals and all possible values of t_1 in 50 µ intervals. The last two columns of this table give the mean value of ϕ_s averaged over all values of t_1 for each value of θ, and the corresponding value of $P_s(\theta) = \phi_s/\pi$.

(ii) Escape from the lower surface (into the glass backing).

Similar considerations apply in this case as in the case just considered, but now the thickness of the emulsion enters the calculations. The conditions are shown in fig. 64, and the escape probability is in this case $P_G(\theta) = \phi_G/\pi$. $\cos_G = K_G/R_G$

TABLE 33

θ \ L (μ)	50	100	150	200	250	300	350	400	450	500	550	600	650
20	28.6	20.8	0	0	0	0	0	0	0	0	0	0	0
30	50.4	47.6	44.2	39.8	34.6	27.5	21.7	0	0	0	0	0	0
40	57.7	55.7	53.7	50.7	47.9	45.4	38.2	31.3	21.4	0	0	0	0
50	61.0	59.2	57.2	51.1	52.8	49.4	45.7	41.0	35.1	27.1	29.7	0	0
60	61.4	60.6	59.1	57.0	54.9	52.2	48.9	45.3	40.3	34.3	26.3	15.1	0
70	61.8	60.4	59.2	57.1	55.2	52.6	49.7	46.2	41.9	36.3	29.6	21.3	9.2
80	60.5	59.8	57.8	56.1	54.1	51.7	41.9	45.6	41.3	36.1	29.4	21.1	10.6
90	58.2	56.9	55.5	53.7	51.7	49.3	46.4	42.9	38.6	33.1	26.2	17.0	0

Table XXXIII

TABLE 33

$t_1(\mu)$	50	100	150	200	250	300	350	400	450	500	550	600	650	700
θ	ϕ_G													
20	28.6	20.8	0	0	0	0	0	0	0	0	0	0	0	0
30	50.4	47.6	44.2	39.8	34.6	27.5	21.7	0	0	0	0	0	0	0
40	57.7	55.7	53.7	50.7	47.5	43.4	38.2	31.3	21.4	0	0	0	0	0
50	61.0	59.2	57.2	51.1	52.8	49.4	45.7	41.0	35.1	27.1	29.7	0	0	0
60	61.4	60.6	59.1	57.0	54.9	52.2	48.9	45.3	40.3	34.3	26.3	15.1	0	0
70	61.8	60.4	59.2	57.1	55.2	52.6	49.7	46.2	41.9	36.3	29.6	21.3	9.2	0
80	60.5	59.8	57.8	56.2	54.1	51.7	41.9	45.6	41.3	36.1	29.4	21.1	10.6	0
90	58.2	56.9	55.5	53.7	51.7	49.3	46.4	42.9	38.6	33.1	26.2	17.0	0	0

and again it can be shown that

$$\cos\phi_G = \frac{1}{1 + \{(L_G - t_1)/(d - t_1 \tan\psi)^2\}^{\frac{1}{2}} \sin\theta \cos\psi} - \frac{\tan\psi}{\tan\theta} \quad (46)$$

The acceptance condition in this case was that the track must be at least 700 μ long (i.e. $L_G = 700$ μ). Putting this value together with d = 400 μ and $\psi = 13.5^{\circ}$ we get the values of ϕ_G shown in Table XXXIII together with the corresponding values of $P_G(\theta)$.

(iii) Application of the Correction.

If n tracks enter the surface of a given area of emulsion and these tracks have in their first 500 μ of length a total of N_θ scatters in which the angle of scatter is θ, no track having more than one such scatter, then the number of such tracks escaping will be $N_\theta\left(P_s(\theta) + P_G(\theta)\right)$ and the total number of tracks escaping for all values of θ is

$\sum N_\theta\left(P_s(\theta) + P_G(\theta)\right)$ or $\int N_\theta\left(P_s(\theta) + P_G(\theta)\right) d\theta$.

Thus the number of tracks accepted for measurement is $n - \sum N_\theta P_T(\theta)$ where $P_T(\theta) = P_s(\theta) + P_G(\theta)$. The number of scatters of value θ missed is $N_\theta P_T(\theta)$.

The true mean free path for scattering is $\lambda_T = n \times L/N_\theta$ and the observed value is $\lambda_M = \{n - \sum N_\theta P_T(\theta)\}\, L/N_\theta\left(1 - P_T(\theta)\right)$, so that $\lambda_T = \lambda_M\left(1 - P_T(\theta)\right)/\left(1 - \sum \frac{N_\theta}{n} P_T(\theta)\right)$ (47)

Table XXXIV shows the values of $\frac{N_\theta}{n} P_T(\theta)$ for two angular intervals, and it can be seen that in both cases this quantity is so much less than unity that it can be ignored. Making this simplification we have corrections.

$$\lambda_T = \lambda_M \, (1 - P_T(\theta)) \qquad (48) \qquad \text{or}$$

$$\sigma_T = \sigma_M / (1 - P_T(\theta)) \qquad (49)$$

The effect of different angles of dip of the incident tracks was investigated by calculating $P_T(\theta)$ for $\psi = 13.5^\circ$ and for $\psi = 10^\circ$. The results so obtained are shown in fig. 63 and it can be seen that there is very little difference in the values of $P_T(\theta)$ for the two values of ψ. This is to be expected since with increasing ψ $P_s(\theta)$ decreases while $P_\theta(\theta)$ increases by about the same amount, as is shown in fig. 64.

The correction factors given in equations (48) and (49) are only applicable to the cross section determined from the first 500 μ of each track accepted for measurement. The cross section determined from the whole of each accepted length of track will require a smaller correction, the value of which will depend on the average length of the tracks since the cross section determined from all except the first 500 μ will not require any correction.

In order to apply the above correction therefore it was necessary to determine the number of scatters in the first 500 μ of each track. This was easily done since the position of each scatter on the tracks had been noted. The number of scatters in all the first 500 microns was so small however, that it was felt desirable to apply a modified correction to longer track lengths. For this reason the scatters occurring in the first 1000 μ [illegible] application of the

Tables XXXIV & XXXV.

TABLE 34

θ	$20 - 25^{\circ}$	$85 - 90^{\circ}$
N_{θ}/n	1.01×10^{-2}	1.68×10^{-4}
P_t	0.112	0.537
$\frac{N_{\theta}}{n} \cdot P_t$	1.1×10^{-3}	9.10^{-5}

TABLE 35

Type of Particle	Angular Interval	No. of Scatters in 1st. 1000 μ's	No. of Scatters not in 1st 1000 μ's	Correction Factor for 1st 1000 μ's	Corrected No. in 1st. 1000 μ's	Corrected Total No.
	$25 - 35^{\circ}$	37	18	1.14	42.2	60.2
Electrons	$35 - 50^{\circ}$	4	11	1.24	5.02	16.02
	$50 - 100^{\circ}$	4	5	1.35	5.41	10.41
	$25 - 35^{\circ}$	15	14	1.14	17.1	31.1
Positrons	$35 - 50^{\circ}$	8	7	1.24	9.9	16.9
	$50 - 100^{\circ}$	4	3	1.35	5.41	8.41

$$\lambda_T = \lambda_M \; (1 - P_T(\theta)\;) \qquad (48) \quad \text{or}$$

$$\sigma_T = \sigma_M/(1 - P_T\,(\theta)\;) \qquad (49)$$

The effect of different angles of dip of the incident tracks was investigated by calculating $P_T(\theta)$ for $\psi = 13.5^o$ and for $\psi = 10^o$. The results so obtained are shown in fig. 63 and it can be seen that there is very little difference in the values of $P_T\;(\theta)$ for the two values of ψ. This is to be expected since with increasing θ $P_s\;(\theta)$ decreases while $P_G\;(\theta)$ increases by about the same amount, as is shown by fig. 64.

The correction factors given in equations (48) and (49) can be applied only to the measured value of cross section determined from the first 500 μ of each track accepted for measurement. The cross section determined from the whole of each accepted length of track will require a smaller correction, the value of which will depend on the average length of the tracks since the cross section determined from all except the first 500 μ will not require any correction.

In order to apply the above correction therefore it was necessary to determine the number of scatters in the first 500 μ of each track. This was easily done since the position of each scatter on the tracks had been noted. The number of scatters in all the first 500 microns was so small however, that it was felt desirable to apply a modified correction to larger track lengths. For this reason the scatters occuring in the first 1000 μ were used for the application of the correction.

If the true number of scatters occuring in all the first 500 microns is N_T and the number of these detected is N_A, then except for certain considerations mentioned below, the true number in all the first 1000 microns will be $2N_T$ and the detected number will be $N_A + N_T$, since none will be missed in the second 500 µ of each track by this process (if a track reaches a length of 500 µ it is accepted). The correction factor to be applied to the cross section determined from the first 1000 µ is therefore $2N_T / (N_T + N_A)$. Therefore,

$$f_{1000} = \frac{2f_{500}}{1 + f_{500}} \qquad (50)$$

As mentioned above the number of scatters in the first 1000 µ of a given track will not on the average be twice the number in the first 500 µ because (a) the energy of the track is lower for the second 500 µ than for the first 500 µ and (b) the track has a certain probability of ending before it has completed the second 500 µ. The correction required for the first effect is small since the rate of loss of energy on the particle producing the track is small. The correction to allow for the second effect can be found experimentally by finding the distribution of length of tracks greater than 500 µ. This was done and it was found that 92.1% of these tracks stayed in the emulsion for the second 500 µ. The required correction factor now becomes $f_{1000} = \frac{f_{500}\,(1 + .921)}{.921\, f_{500} + 1}$ (51)

The correction factor so obtained is shown in Table XXXV.

Table XXXVI

(d) Other corrections.

Apart from the three effects already mentioned, it was necessary to apply corrections to the experimental results to allow for the fact that the tracks were not parallel to the emulsion surface so that the distance from the start of a track to the point at which a scatter occured was greater than the measured length and also for the fact that the energy of the particles producing the tracks was not exactly the same for all the plates.

The first effect was allowed for by measuring the lengths of a sample consisting of 481 tracks. These were divided into groups according to their lengths with [illegible] intervals and the correction factor to allow for the reduction of length due to dip was calculated for each group. By applying to each correction a weighting factor determined by the number of tracks in the interval to which the factor was applied a mean correction factor was determined. It was found to be 1.04.

To allow for the different energies of the particles in different plates (due to exposure at different times under different conditions), all the energies were corrected to 10 MeV using the relation $\sigma_1/\sigma_2 = (E_2/E_1)$. The energies of the particles in each set of plates and the corresponding correction factors are shown in Table XXXVI.

2.4.3 Experimental results.

(a) Plates exposed to 30 MeV synchrotron.

The results of measurements with the first batch of plates (those exposed to the 30 MeV synchrotron) are shown in figs. 65 and 66. In the first of these the uncorrected results are

Table XXXVI

TABLE 36

Type of Particles	Incident Energy (MeV)	Energy Loss in Plate(MeV)	Effective Energy E (MeV)	Correction Factor $(E/10)^2$
Synchrotron Electrons	9.5	-0.82	8.68	0.75
Synchrotron Positrons	9.5	0.83	8.67	0.75
H.T. Set Electrons	10.64	0.78	9.86	0.97
H.T. Set Postrons	10.72	0.78	9.94	0.99

Table XXXVI

(d) Other corrections.

Apart from the three effects already mentioned, it was necessary to apply corrections to the experimental results to allow for the fact that the tracks were not parallel to the emulsion surface so that the distance from the start of a track to the point at which a scatter occured was greater than the measured distance, and also for the fact that the energy of the particles producing the tracks was not exactly the same for all the plates.

The first effect was allowed for by measuring the lengths of a sample consisting of 481 tracks. The tracks were divided into groups according to their lengths with 200 μ intervals and the correction factor to allow for the reduction of length due to dip was calculated for each group. By applying to each correction a weighting factor determined by the number of tracks in the interval to which the factor was applied a mean correction factor was determined. It was found to be 1.04.

To allow for the different energies of the particles in different plates (due to exposure at different times under different conditions), all the energies were corrected to 10 MeV using the relation $\sigma_1/\sigma_2 = (E_2/E_1)^2$. The energies of the particles in each set of plates and the corresponding correction factors are shown in Table XXXVI.

2.4.3 Experimental results.

(a) Plates exposed to 30 MeV synchrotron.

The results of measurements with the first batch of plates (those exposed to the 30 MeV synchrotron) are shown in figs. 65 and 66. In the first of these the uncorrected results are shown, expressed as a ratio to the first Mott approximation for the cross section (the line in this figure merely joins together the experimental points). Fig. 66 shows the results after the corrections described above have been applied. Here the solid curve represents the best theoretical values of the cross section - the modified "α^4" formula with finite nuclear size correction referred to in section 1.2.1 - the values for the constituents of nuclear emulsion have been obtained by interpolation by the present author. The theoretical values also are expressed as a ratio to the first Mott approximation.

The results are based on measurements of 66 cm. of electron - and 53 cm. of postron - track. The errors associated with the experimental points in these figures are the statistical standard deviations and the numbers in brackets by each point are the numbers of scattering events on which the points are based.

In fig. 65 the small angle "hump" referred to in section 2.4.2. can be seen and it is clear that the double scattering correction factor of ~ 0.9 is insufficient to remove this hump. The part not accounted for by this correction is attributed to "spill-over" from the smallest angular interval (5° - 10°) which was measured simply to ensure that no scatters in the 10° to 15° interval were missed. There were approximately five times as many scatters in the 5° - 10° interval as in the 10° - 15° one and because of the small magnitude of the angles concerned it was difficult to measure them accurately. It was therefore possible for a small percentage of those angles which were in fact slightly less than 10^{o} to be measured as slightly greater and vice versa. Because of the greater number of scatters in the first interval this effect would result in a nett increase in the number of scatters recorded in the second interval so that it could account for the phenomenon observed. For the larger angular intervals the increased accuracy of measurement and greater size of the intervals make the effect of much less importance. In view of these considerations and the fact that all the other published work indicated that no unusual features were to be expected for small angles it was felt that the points representing the 10^{o} to 15^{o} interval should not be included in the corrected results.

The corrected results for electrons agree reasonably with the theoretical values but in the case of the positrons the agreement with theory (in this case Yadav's positron version of the "α^{4}" formula with finite nuclear size correction) is less satisfactory. Also the statistical uncertainty of these results is rather large.

b. Plates exposed with H.T. set.

It was in view of the rather unsatisfactory nature of these results that the decision mentioned earlier, to expose new plates and concentrate on the higher values of scattering angle, was taken. The results obtained with these plates, the examination of which was completed after the present author had left the Natural Philosophy Department, represent the most recent experimental information obtained in this work. The results were obtained from 381 cm. of electron tracks and 517 cm. of those of positrons both these values having been corrected for dip into the emulsion. The investigation was limited to angles of scattering greater than 25°, as mentioned earlier, and 155 such events were found in the electron tracks and 168 in the positron ones, the expected numbers being respectively 186 and 207. The discrepancy between the observed and expected numbers is entirely accounted for by the various corrections described earlier, as can be seen from fig. 67 where the corrected results are displayed in the same manner as were the earlier ones in fig. 66 and where the experimental cross section values are seen to be generally higher than the theoretical values.

The agreement between theory and experiment is within the statistical error, except for the 35 - 50° interval, for both the electrons and the positrons, although this uncertainty is still, unfortunately, quite large.

Results obtained by other authors are available for comparison with those given above only in the case of electrons. The work of Lyman, Hanson and Scott[17] is probably the most accurate yet performed in this energy region. The most suitable of these authors' results for comparison with the present ones are those obtained with silver scattering foils, and in fig. 68 the comparison is made. The results of Lyman et al. are divided by the McKinley and Feshbach improved "$\propto^4$" cross section[3] for silver with finite nuclear size correction[17] and the present results are divided by the corresponding values for nuclear emulsion both for a uniform spatial distribution of nuclear charge (σ_{EXPT}/σ_U) and for a uniform surface distribution (σ_{EXPT}/σ_S).

It can be seen that the present results because of their cosiderable statistical errors cannot definitely be said to favour one type of distribution rather than the other, but they do agree reasonably well with theory and with the earlier results.

The absence of other experimental results on the scattering of positrons in this energy region means that comparison can be made only with theory. In fig. 67 the original Yadav (point nucleus) results (6) are given together with the modified ones obtained by Elton and Parker (16) for a uniform distribution of charge throughout a finite spherical nucleus. It can be seen that the results appear slightly to favour a point nucleus.

One advantage of an experiment of the type described here is that, as mentioned earlier, it enables a comparison of electron and positron scattering to be made under very similar conditions. In fig. 69 Elton and Parker's curve of σ^-/σ^+ (given as fig. 13 in 1.2.1) is reproduced with the results of the present work added. It can be seen that in this case, due to the much larger finite nuclear size effect of electrons, the results show a definite nuclear size effect and, if anything, support a shell, rather than a uniform, distribution, though the large statistical error again makes it difficult to draw definite conclusions.

2.5. Conclusion.

The objectives of the work herein described were, as described earlier:-

(1) To obtain experience in the technique of measurement of multiple scattering of tracks in photographic emulsions and to check the observers' measurements of such scattering by comparison of their values of the scattering constants of various particles in a given type of emulsion with previously published values for the same types of particle and medium. The values obtained in the present work have been found to agree reasonably well with the previously published values and with the theoretical values.

(2) To obtain for the first time values of the scattering constants of diluted emulsions and to compare the values so obtained with those predicted by theory. Again reasonable agreement has been found.

(3) To examine the single scattering of electrons and positrons in nuclear emulsion and to determine the variation of the scattering cross section with the angle of scattering to establish whether the finite size of the nucleus affected this variation. In the case of electrons marked evidence of this effect has been found, but for positrons, for which the effect is expected to be much smaller, no effect at all has been found.

As mentioned above the rather poor statistical accuracy which is an almost inevitable feature of methods of measurement such as that described here, as compared to methods employing Geiger counters as detectors of the scattered particles, impose severe limits to the interpretation which may be made of the results. However, it is felt that the objectives may, especially in the case of multiple scattering, be said to have been achieved.

The lack of statistical accuracy is the main disadvantage of such a study as has been described here, compared with work such as that of Lyman, Hanson and Scott described above. The advantage of the present method of study lies in its comparative simplicity. In the present work, apart from the very short period during which the plates were being exposed, only either one or two graduates were employed in the work together with either two or three microscopists. Its demands on labour and other resources were therefore slight. The work of Lyman, Hanson and Scott, which is a fairly typical example of a Geiger counter experiment, involved a much greater amount of skilled labour in the construction of the scattering apparatus for a time comparable with that taken in the collection of the present results. Once this apparatus had been pefected, of course, a great many scattering problems could be undertaken in a very short time.

It is almost certainly true to say that if the results herein presented were to be obtained starting at the present time, following the publication of details of the Geiger counter detector apparatus, and if sufficient funds and labour were available, it would be much preferable to constmct such an apparatus rather than to tackle the problem with photographic plates. This is not, however, felt to condemn the use of the method described in this thesis at the time at which this work was begun and under the conditions then prevailing.

REFERENCES.

1. Mott, Proc. Roy. Soc., 124A, 425 (1929); 135A, 429 (1932).
2. Urban, Zeits. f. Phys., 119, 67 (1942).
3. McKinley and Feshbach, Phys. Rev., 74, 1759 (1948)
4. Bartlett and Watson, Proc. Amer. Acad. Arts & Sci., 74, 53 (1940).
5. Feshbach, Phys. Rev., 88, 295 (1952).
6. Yadav, Proc. Phys. Soc., 65A, 672 (1952).
7. Massey, Proc. Roy. Soc., 181A, 14 (1942).
8. Acheson, Phys. Rev., 82, 488 (1951).
9. Rose, Phys. Rev., 73, 279 (1948).
10. Feshbach, Phys. Rev., 84, 1206 (1951).
11. Bodmer, Proc. Phys. Soc., 66A, 1041 (1953).
12. Elton, Proc. Phys. Soc., 63A, 1115 (1950).
13. Parzen, Phys. Rev., 80, 261 and 355 (1950).
14. Feenberg, Phys. Rev., 59, 593 (1941).
15. Hofstadter, Fechter and McIntyre, Phys. Rev., 92, 978 (1953).
16. Elton and Parker, Proc. Phys. Soc., 66A, 428 (1953).
17. Lyman, Hanson and Scott, Phys. Rev., 84, 626 (1951).
18. Miller, Ann. Phys., 14, 531 (1932).
19. Mohr, Proc. Roy. Soc., 182A, 189 (1943).
20. Parker, Proc. Phys. Soc., 66A, 881 (1953).
21. Schwinger, Phys. Rev., 73, 416 (1948); 76, 790 (1949).
22. Elton and Robertson, Proc. Phys. Soc., 65A, 145 (1952).
23. Randels, Chao and Crane, Phys. Rev., 68, 62 (1945).
24. Champion and Roy, Proc. Phys. Soc., 61, 532 (1948).
25. Van de Graaff, Buechner and Feshbach, Phys. Rev. 69, 452 (1946); 72, 678 (1947).
26. Paul and Reich, Zeits. f. Phys., 131, 326 (1952).
27. Pidd, Hammer and Raka, Phys. Rev., 92, 436 (1953).
28. Wilson, Phys. Rev., 88, 350 (1952).
29. Schiff, Phys. Rev., 92, 988 (1953).
30. Barker and Champion, Proc. Roy. Soc., 168A, 159 (1938); Phys. Rev., 55, 111 (1939)
31. Le Prince Ringuet, Ann. de Phys., (11), 7, 5 (1937).
32. Sen Gupta, Proc. Phys. Soc., 51, 355 (1939).
33. Bothe, Zeits. f. Naturforsch., 4A, 88 (1949).
34. Cusack, Phil. Mag., 43, 671 (1952).
35. Howatson and Atkinson, Phil. Mag., 42, 1136 (1951).
36. Roy and Groven, Phys. Rev., 87, 619 (1952).
37. Lipkin, Phys. Rev., 85, 517 (1952).
38. Lasich, Aust. Journ. Sci. Res., 1A, 249 (1948).
39. Fowler and Oppenheimer, Phys. Rev., 54, 320 (1938).
40. Williams, Proc. Roy. Soc., 169A, 531 (1938); Phys. Rev., 58, 292 (1940).
41. Goudsmit and Saunderson, Phys. Rev., 57, 24 (1940); 58, 36 (1940).
42. Molière, Zeits. f. Naturforsch., 3A, 78 (1948).
43. Goldschmidt-Clermont, Nuovo Cim., 7, 331 (1950).
44. Bethe, Phys. Rev., 89, 1256 (1953).
45. Lewis, Phys. Rev., 78, 526 (1950).
46. Spencer and Blanchard, Phys. Rev., 91, 240 (1953).

47. Snyder and Scott, Phys. Rev., 76, 220 (1949).
48. Rossi and Greisen, Rev. Mod. Phys., 13, 240 (1941).
49. Corson, Phys. Rev., 83, 217 (1951); 84, 605 (1951).
50. Hanson, Lanzl, Lyman and Scott, Phys. Rev., 84, 634 (1951).
51. Kulchitsky and Latychev, Phys. Rev., 61, 254 (1942).
52. Groetzinger, Berger and Ribe, Phys. Rev., 77, 584 (1950).
53. Groetzinger, Berger and Ribe, Phys. Rev., 85, 78 (1952).
54. Fowler, Phil. Mag., 41, 169 (1950).
55. McDiarmid, Phys. Rev., 84, 851 (1951).
56. Voyvidoc and Pickup, Phys. Rev., 85, 91 (1952).
57. Gottstein, Menon, Mulvey, O'Ceallaigh and Rochat, Phil. Mag., 42, 708 (1951).
58. Menon, O'Ceallaigh and Rochat, Phil. Mag., 42, 932 (1951).
59. O'Ceallaigh and Rochat, Phil. Mag., 42, 1050 (1951).
60. Gottstein and Mulvey, Phil. Mag., 42, 1089 (1951).
61. Menon and Rochat, Phil. Mag., 42, 1232 (1951).
62. Rutherford, Chadwick and Ellis, "Radiations from Radio-active Substances (C.U.P.) p.43.
63. Montgomery, "Cosmic Ray Physics" (Princeton Univ. Press, 1949), p.34.
64. Dilworth, Occhialini and Payne, Nature, 163, 102 (1948).
65. Fermi, "Nuclear Physics" (Univ. Chicago Press), p. 30.
66. Fermi, "Nuclear Physics" (Univ. Chicago Press), p. 47.
67. Montgomery, "Cosmic Ray Physics" (Princeton Univ. Press, 1949) p.350.
68. Bradner, Smith, Barkas and Bishop, Phys. Rev., 77, 462 (1950).
69. Wentzel, Ann. der Phys., 69, 335 (1922).
70. Champion, Proc. Roy. Soc., A146, 83 (1934) and A153, 353 (1936).
71. Skobelzyn and Stepanowa, Nature, 137, 456 (1936).
72. Stepanowa, Phys. Zeits. Sowjet. 12, 550 (1937).
73. Bonisov et al. C. R. de Lacad. Sci. U.S.S.R., 26, 142 (1940).
74. Bleuler et al Phys. Rev., 61, 95 (1942).
75. Bleuler et al, Helv. Phys. Act., 15, 613 (1942).
76. Zuber Helv. Phys. Act. 11, 370 (1938).
77. Stepanowa Journ. Phys. U.S.S.R., 1,204 (1939).
78. Klarman and Bothe Zeits. f. Phys. 101, 489 (1936).
79. Sigrist, Helv. Phys. Act. 16, 471 (1943).
80. Sen Gupta, Proc. Phys. Soc., 51, 355 (1939).
81. Berger, Lord and Schein, Phys. Rev., 83, 850 (1951).

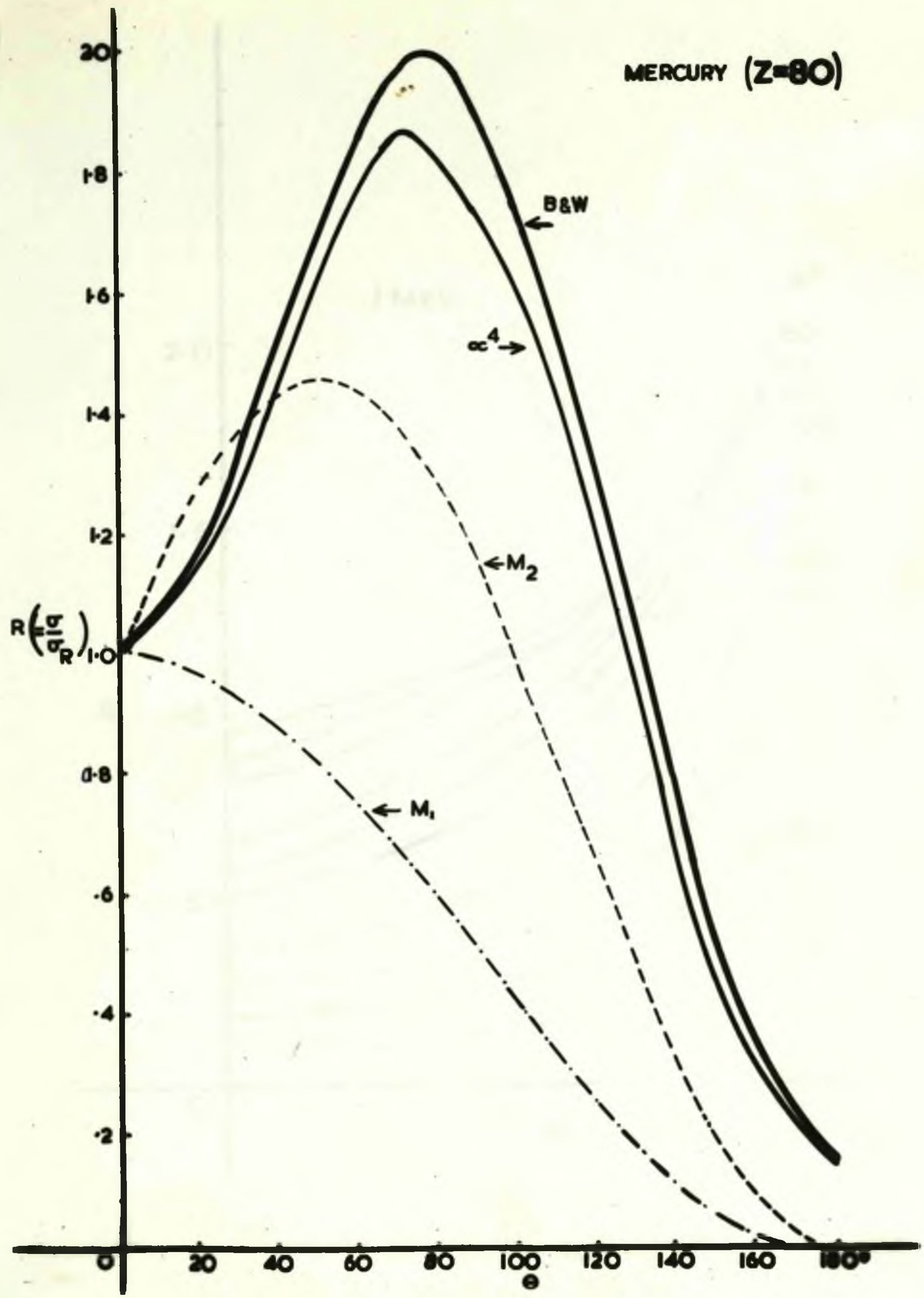

MERCURY (Z=80)
2·0
1·8
1·6
1·4
1·2
1·0
0·8
·6
·4
·2
R $\left(=\frac{\sigma}{\sigma_R}\right)$
B&W
α^4
M_2
M_1
0
20
40
60
80
100
120
140
160
180°
θ

Fig 1

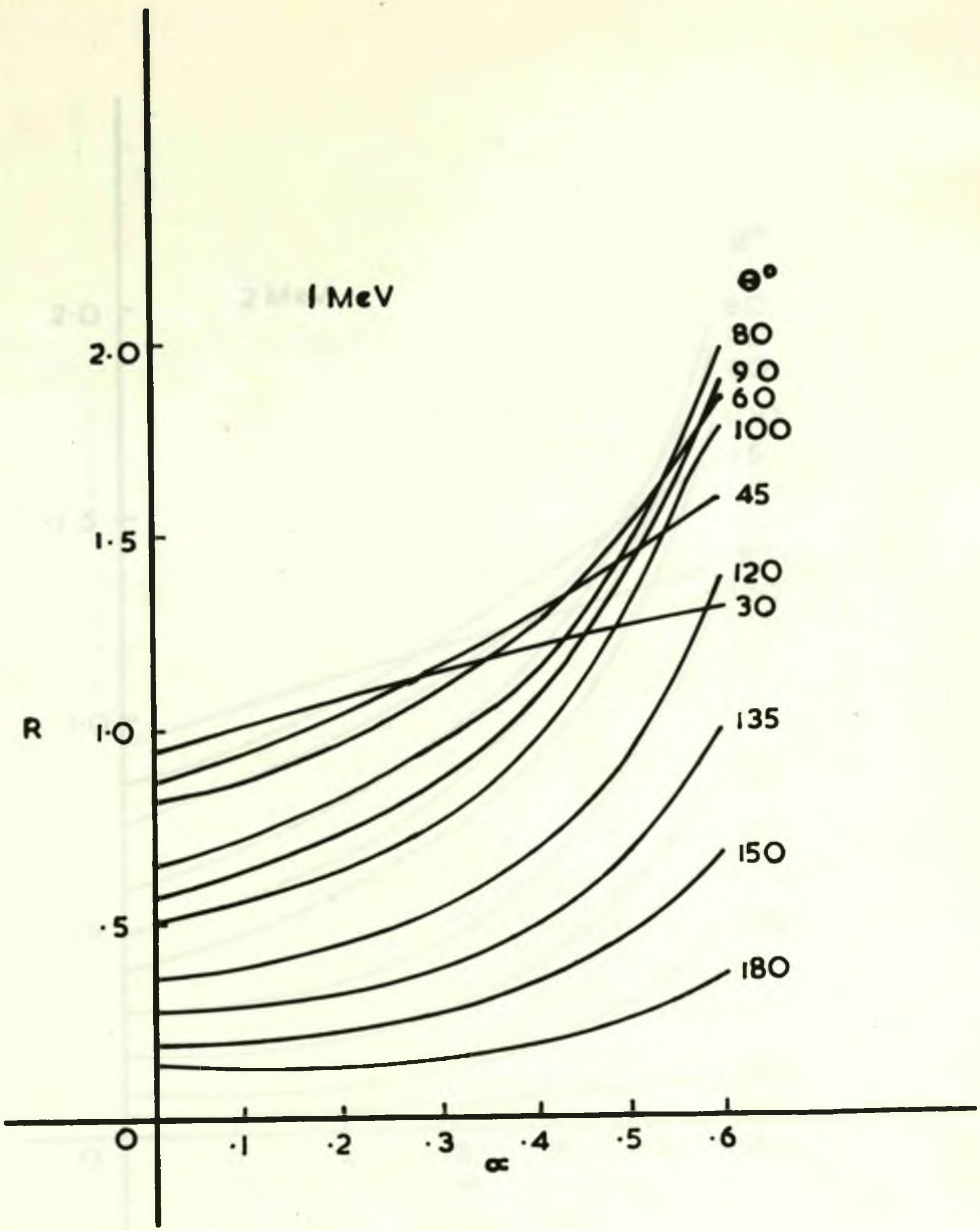

Fig 2a

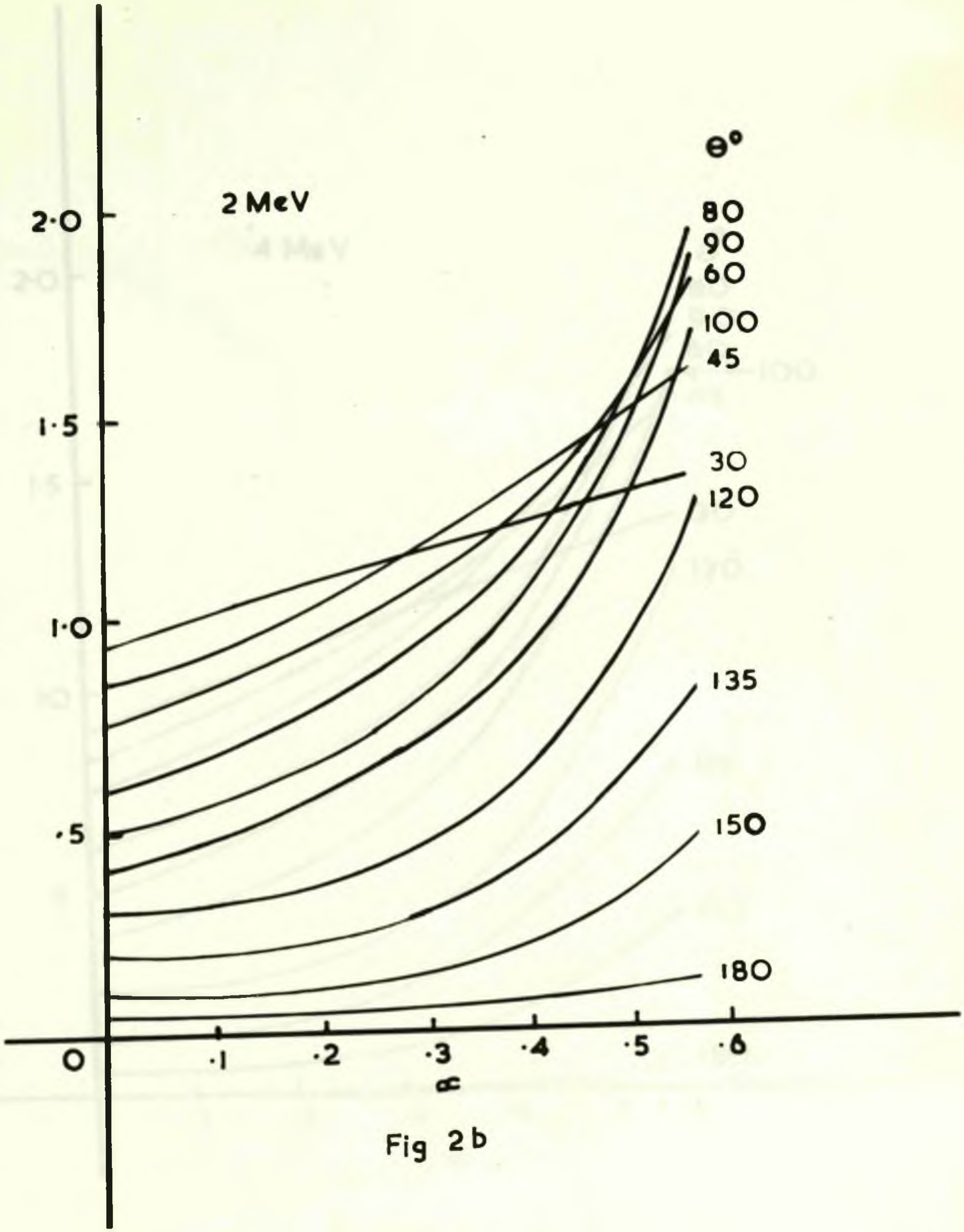

Fig 2b

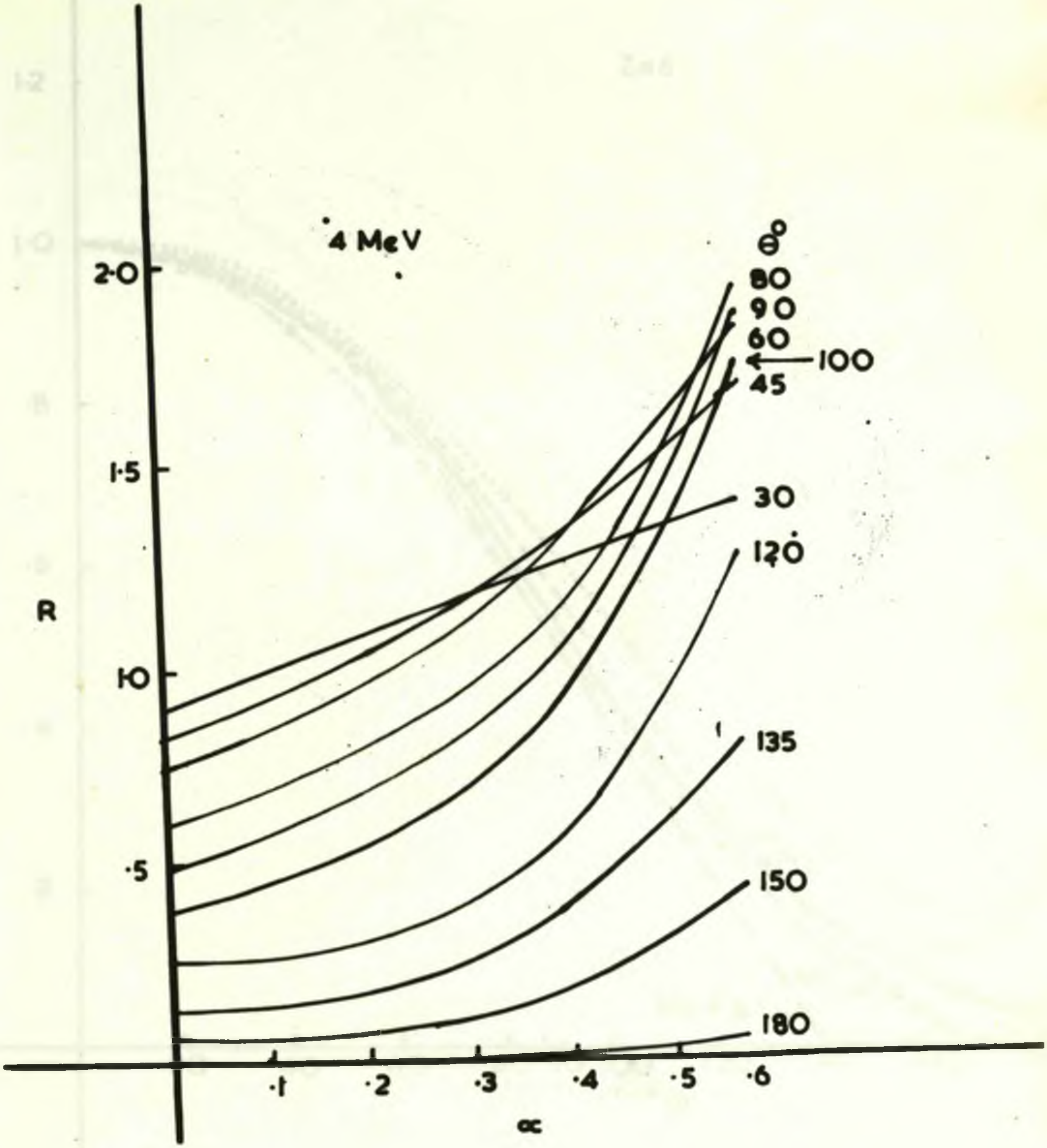

4 MeV
θ°
80
90
60
100
45
30
120
135
150
180
R
2·0
1·5
1·0
·5
·1
·2
·3
·4
·5
·6
α

Fig 2c

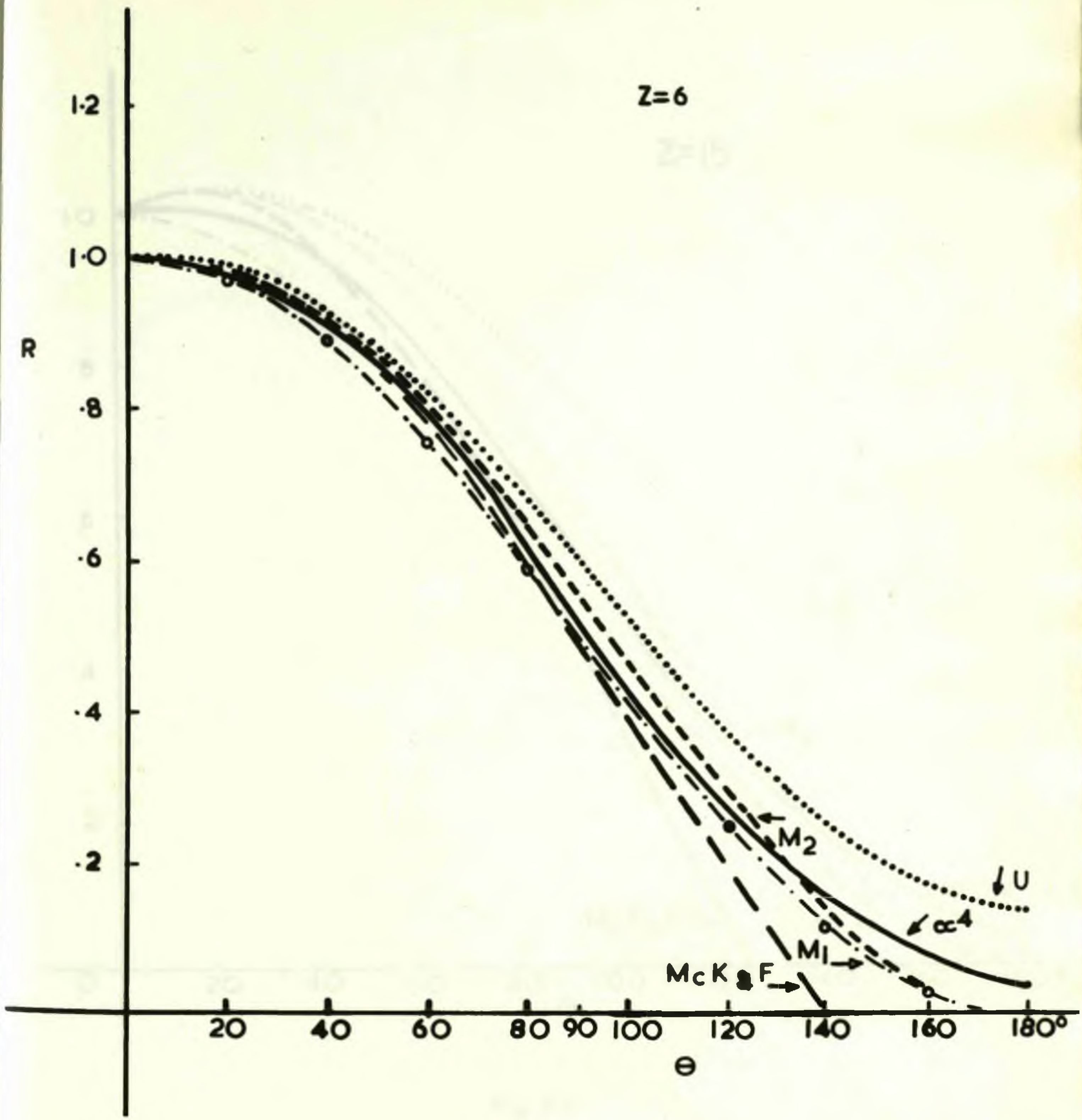

Fig 3a

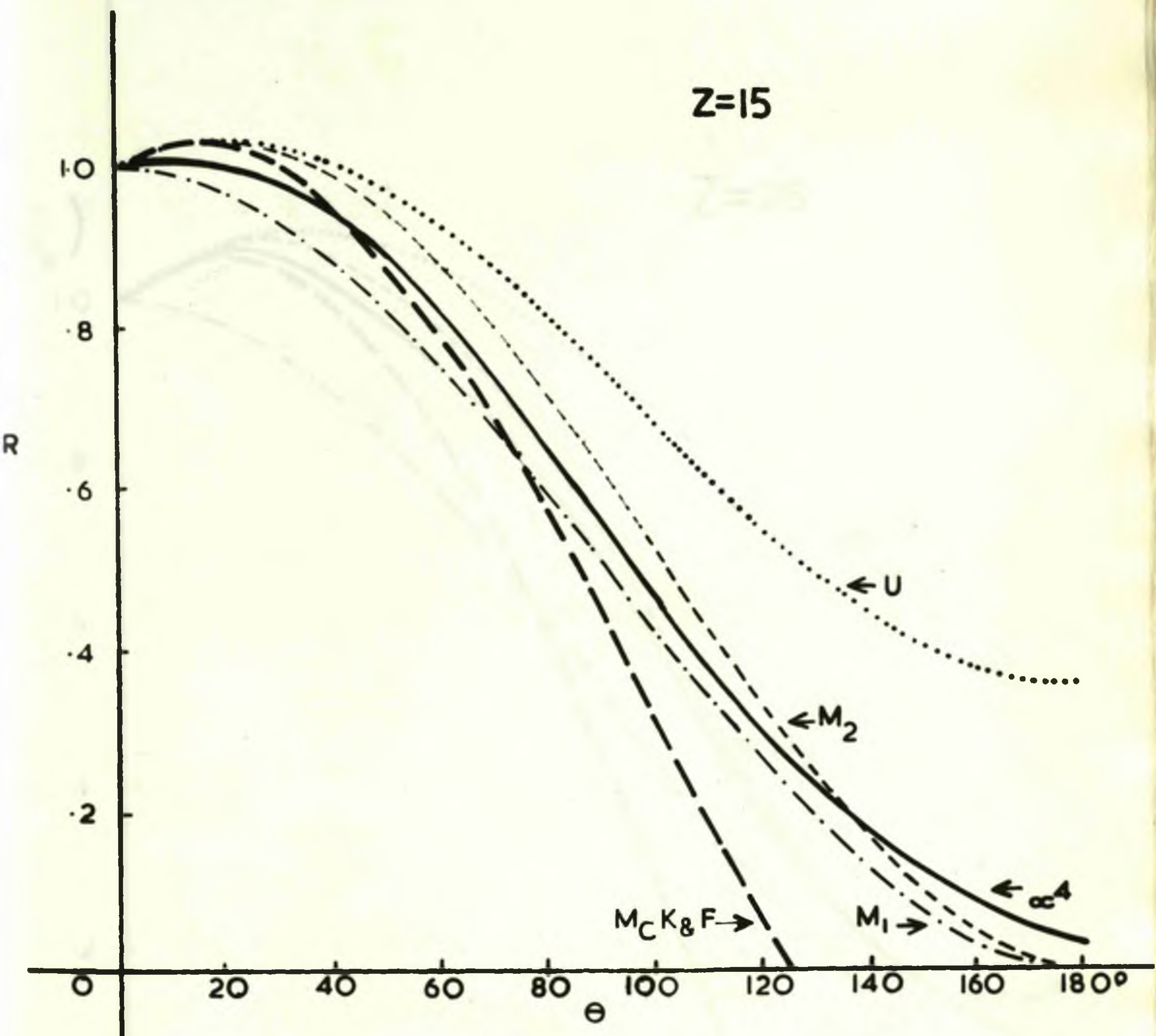

Fig 3b

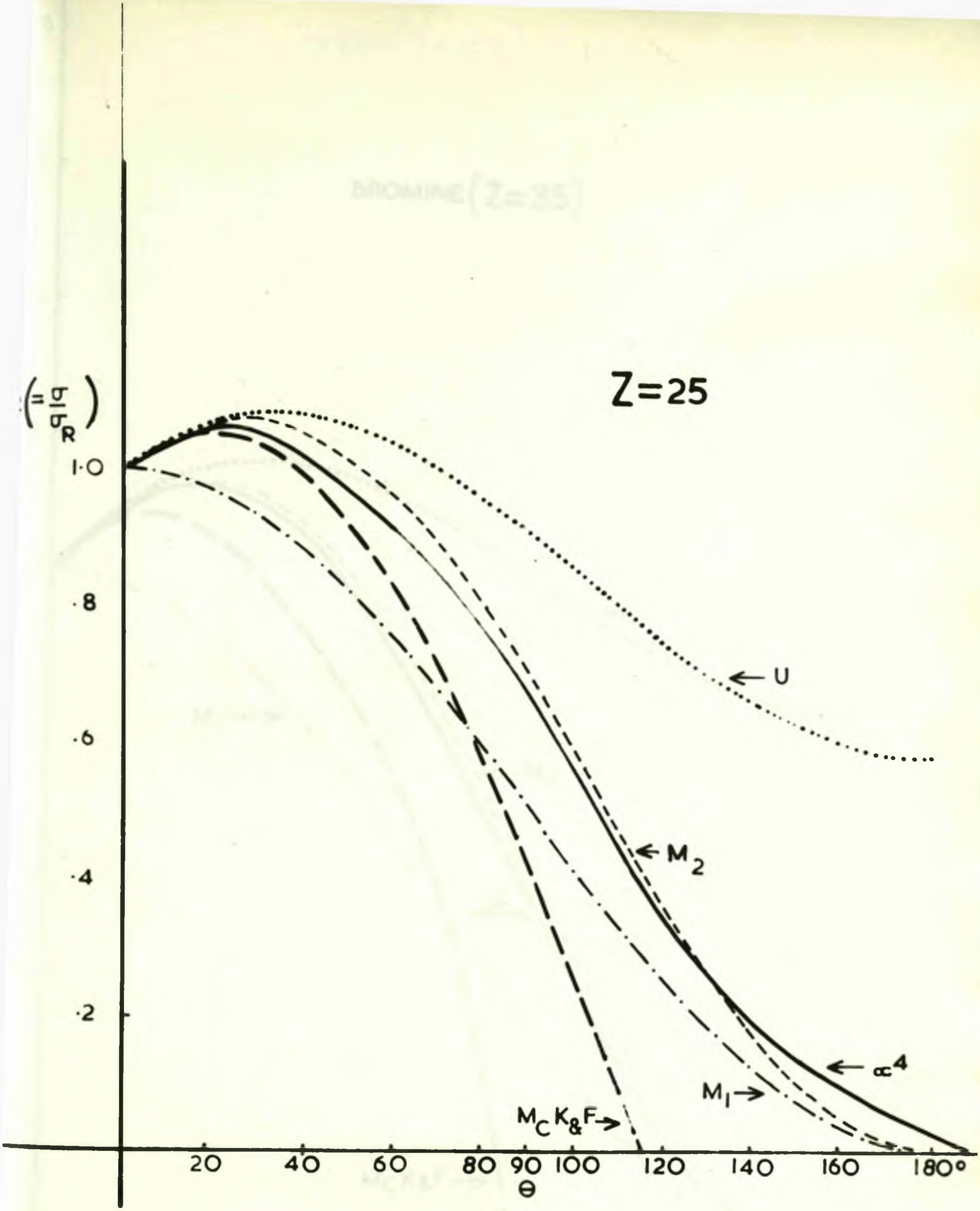

$\left(\frac{b}{b_R}\right)$
Z=25
1·0
·8
·6
·4
·2
← U
← M_2
← α^4
M_1 →
M_C K & F →
20
40
60
80
90
100
120
140
160
180°
θ

Fig 3c

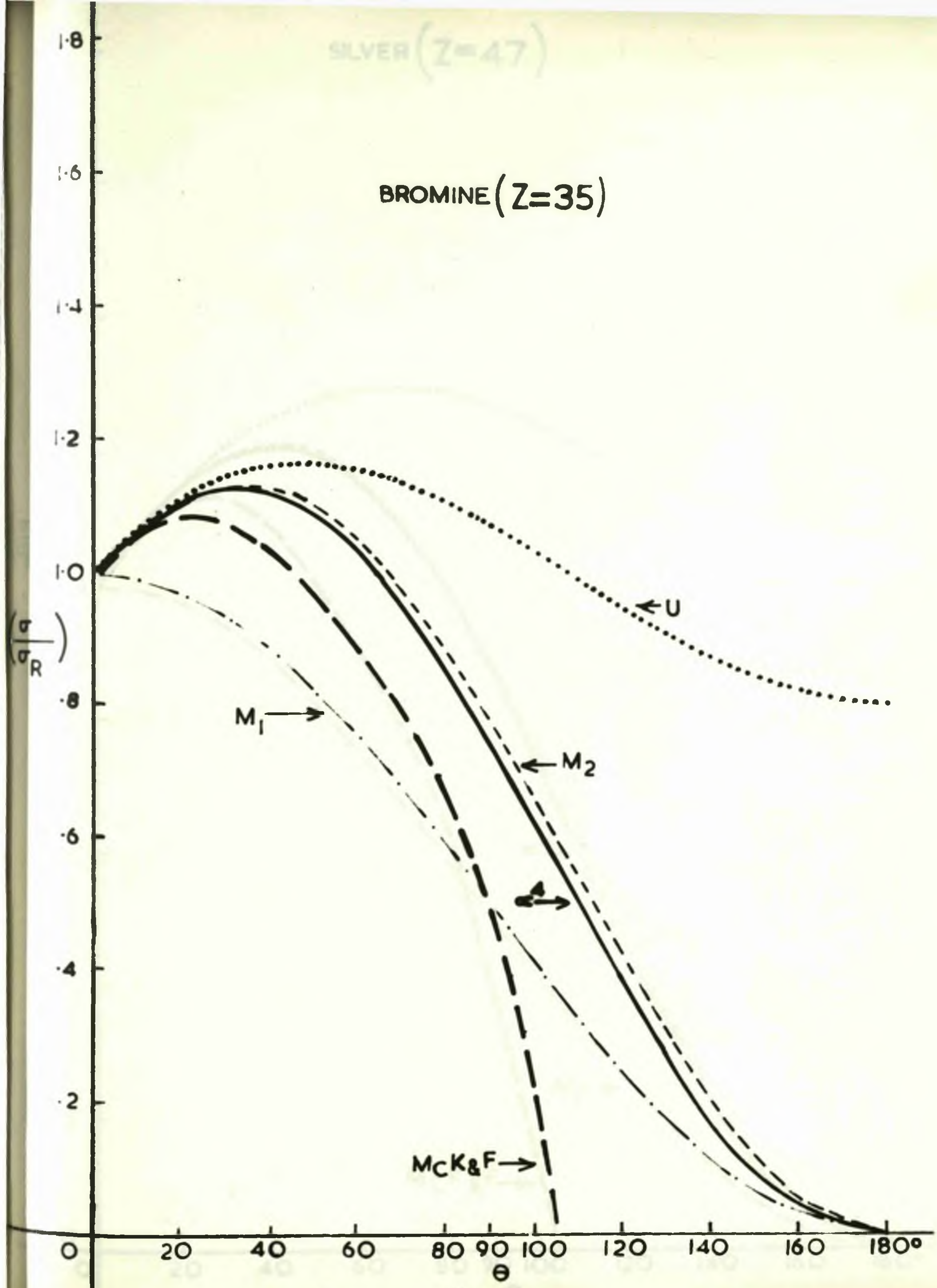

BROMINE (Z=35)
1·8
1·6
1·4
1·2
1·0
·8
·6
·4
·2
$\left(\frac{\sigma}{\sigma_R}\right)$
U
M_1
M_2
McK & F
0
20
40
60
80
90
100
120
140
160
180°
θ

Fig 4a

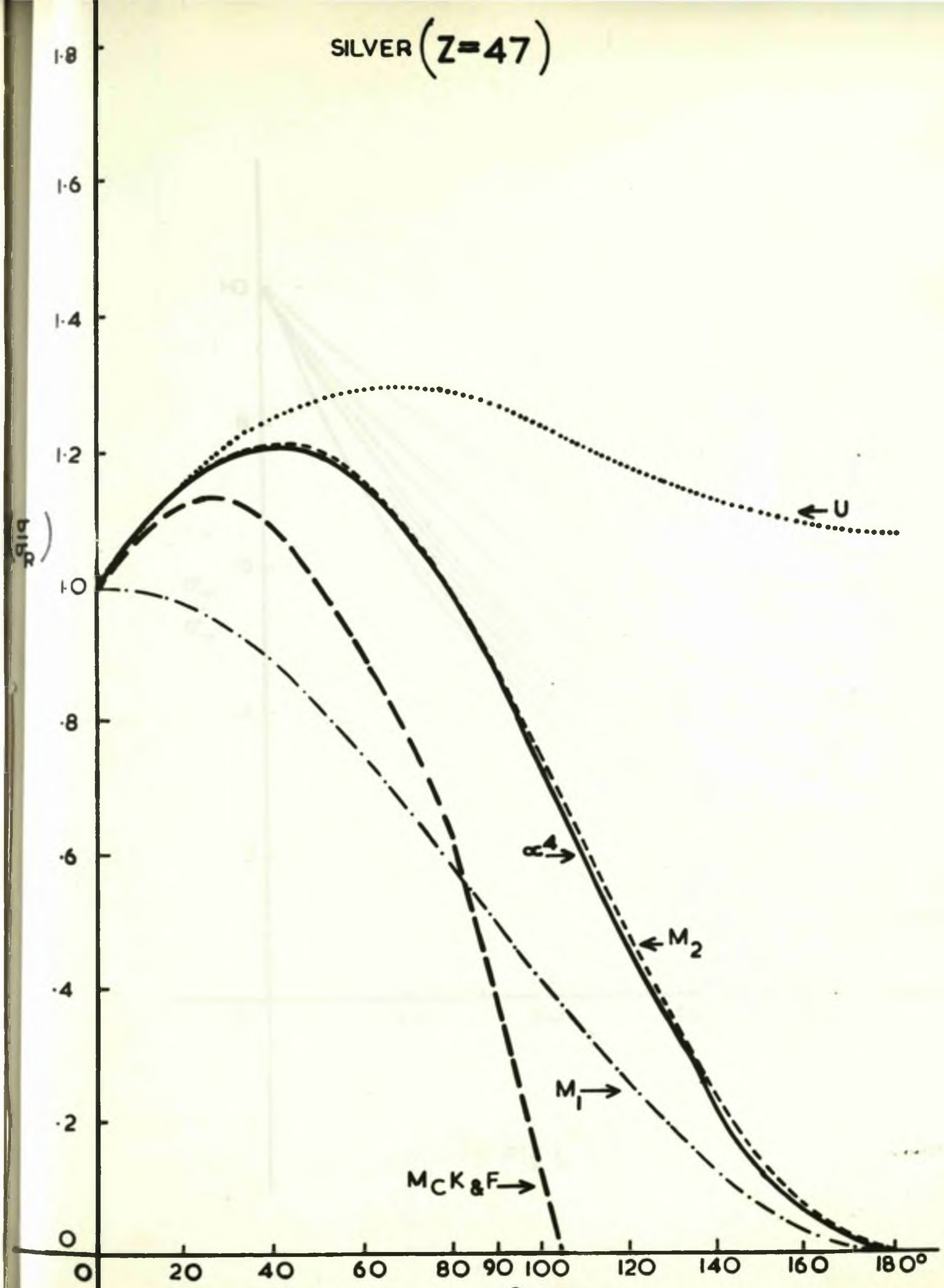

SILVER (Z=47)
1·8
1·6
1·4
1·2
1·0
·8
·6
·4
·2
0
U
α^4
M_2
M_1
$M_C K_\& F$
0
20
40
60
80
90
100
120
140
160
180°
θ

Fig 4b

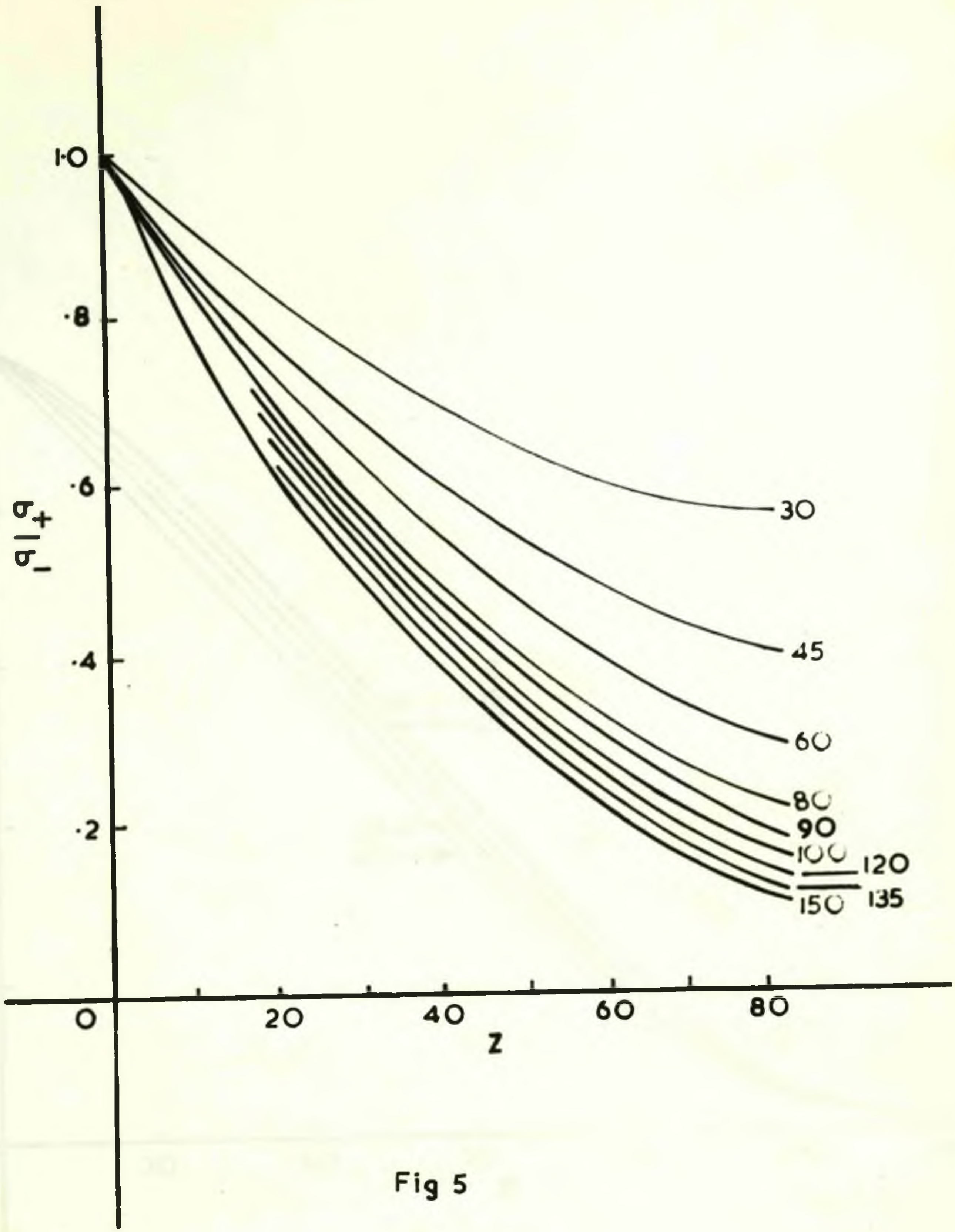

Fig 5

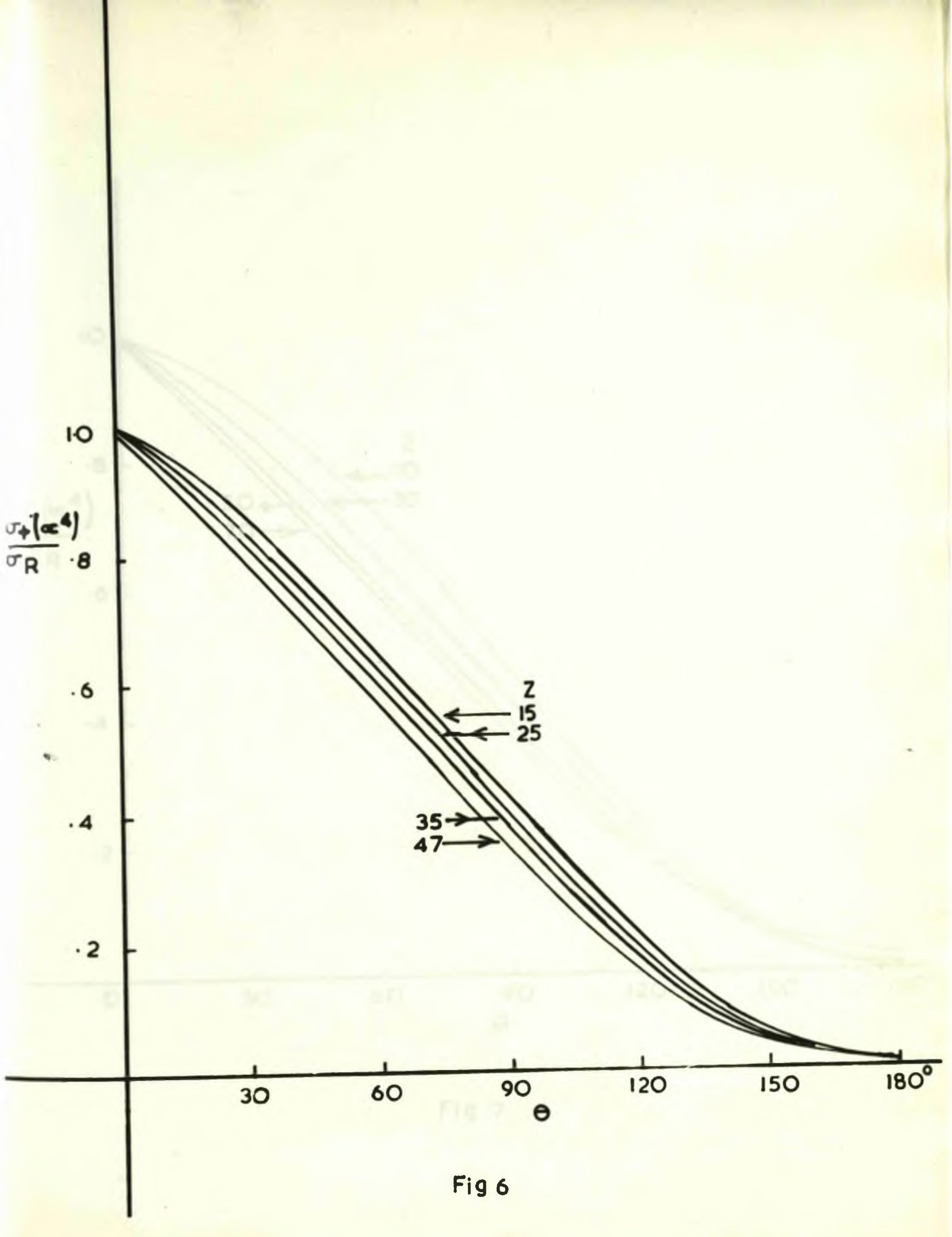

$\frac{\sigma_+(\alpha^4)}{\sigma_R}$
1·0
·8
·6
·4
·2
Z
15
25
35
47
30
60
90
120
150
180°
θ

Fig 6

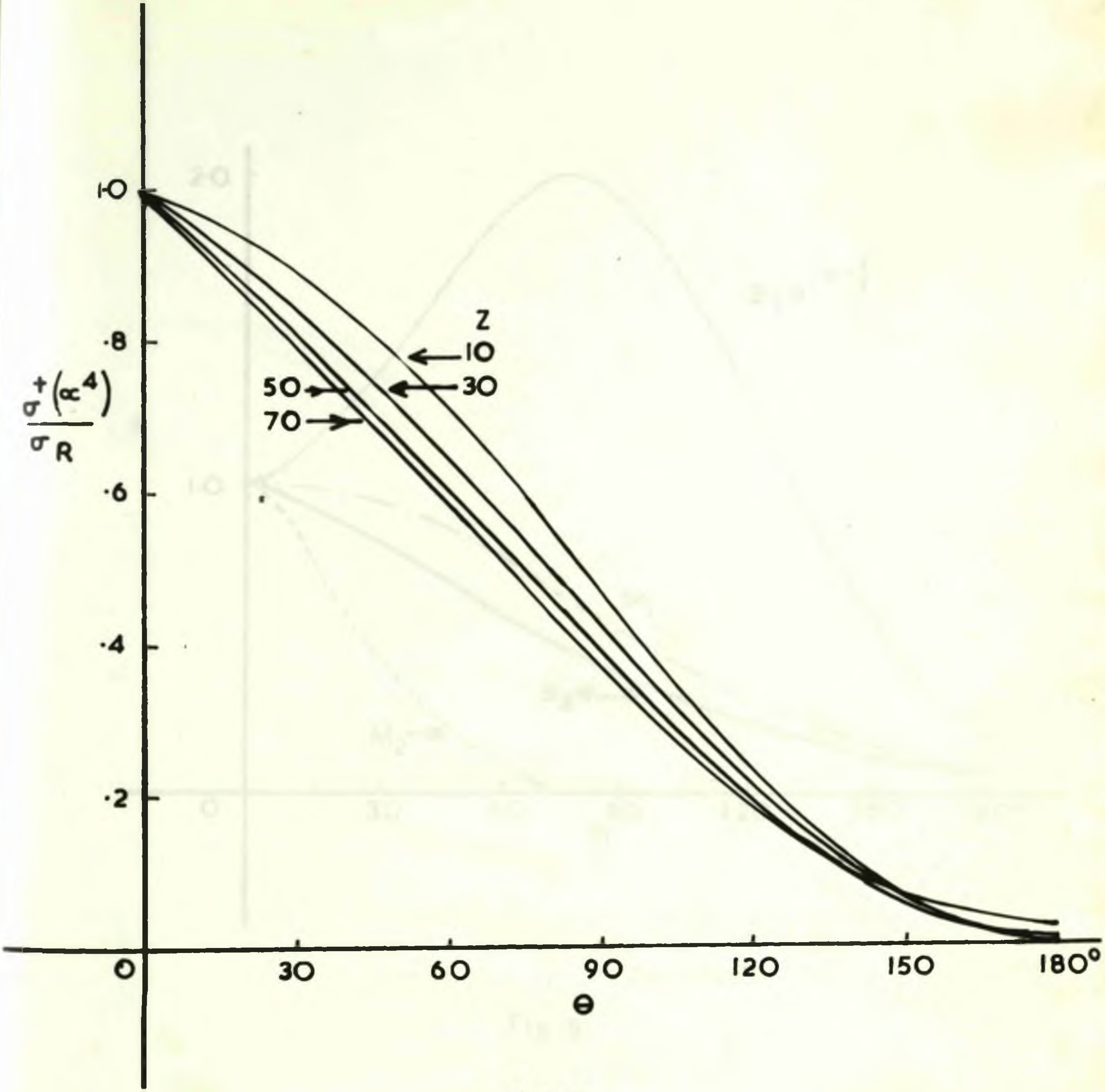

1·0
·8
·6
·4
·2
$\frac{\sigma^{+}(\alpha^{4})}{\sigma_{R}}$
Z
10
30
50
70
0
30
60
90
120
150
180°
θ

Fig 7

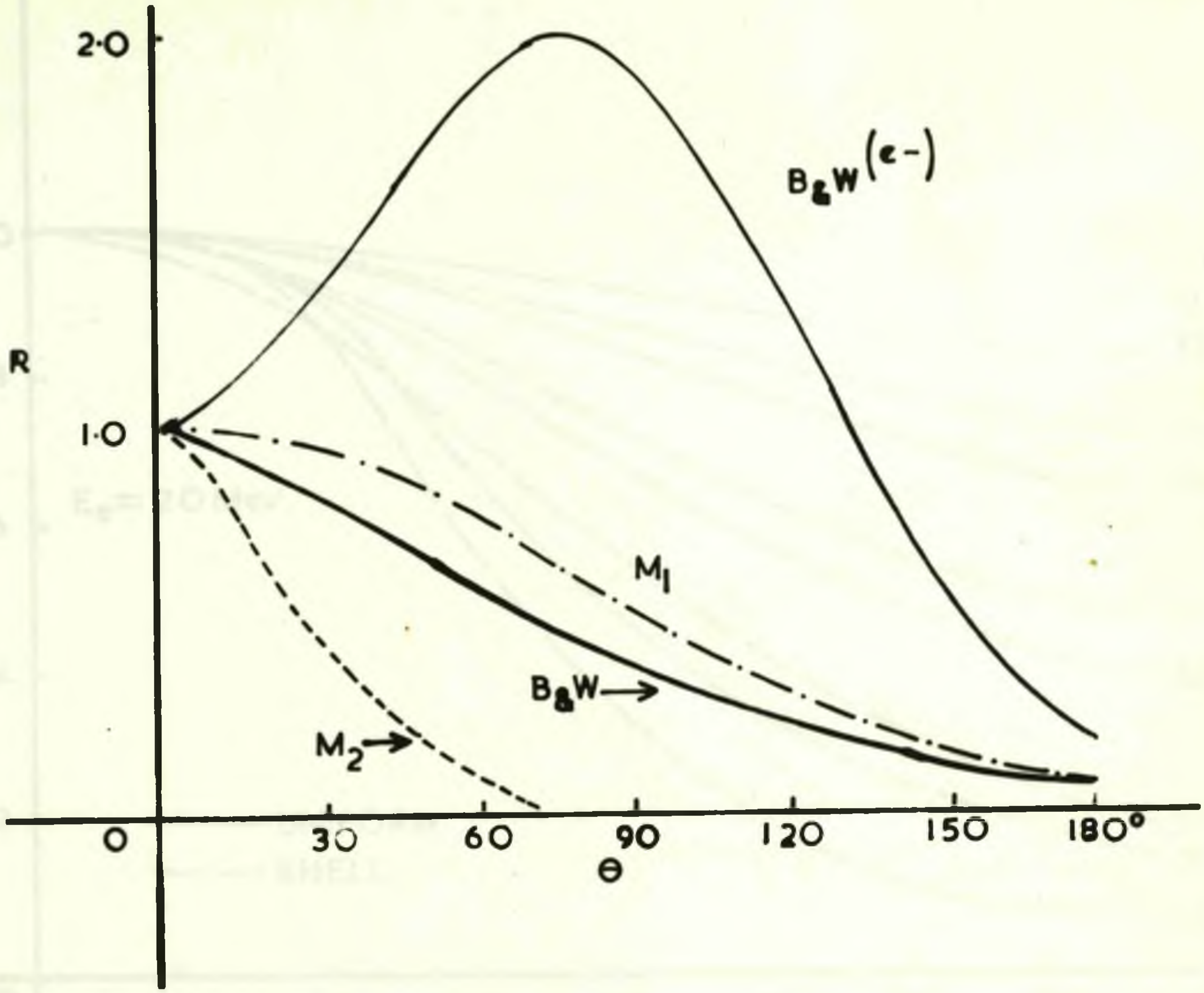

Fig 8

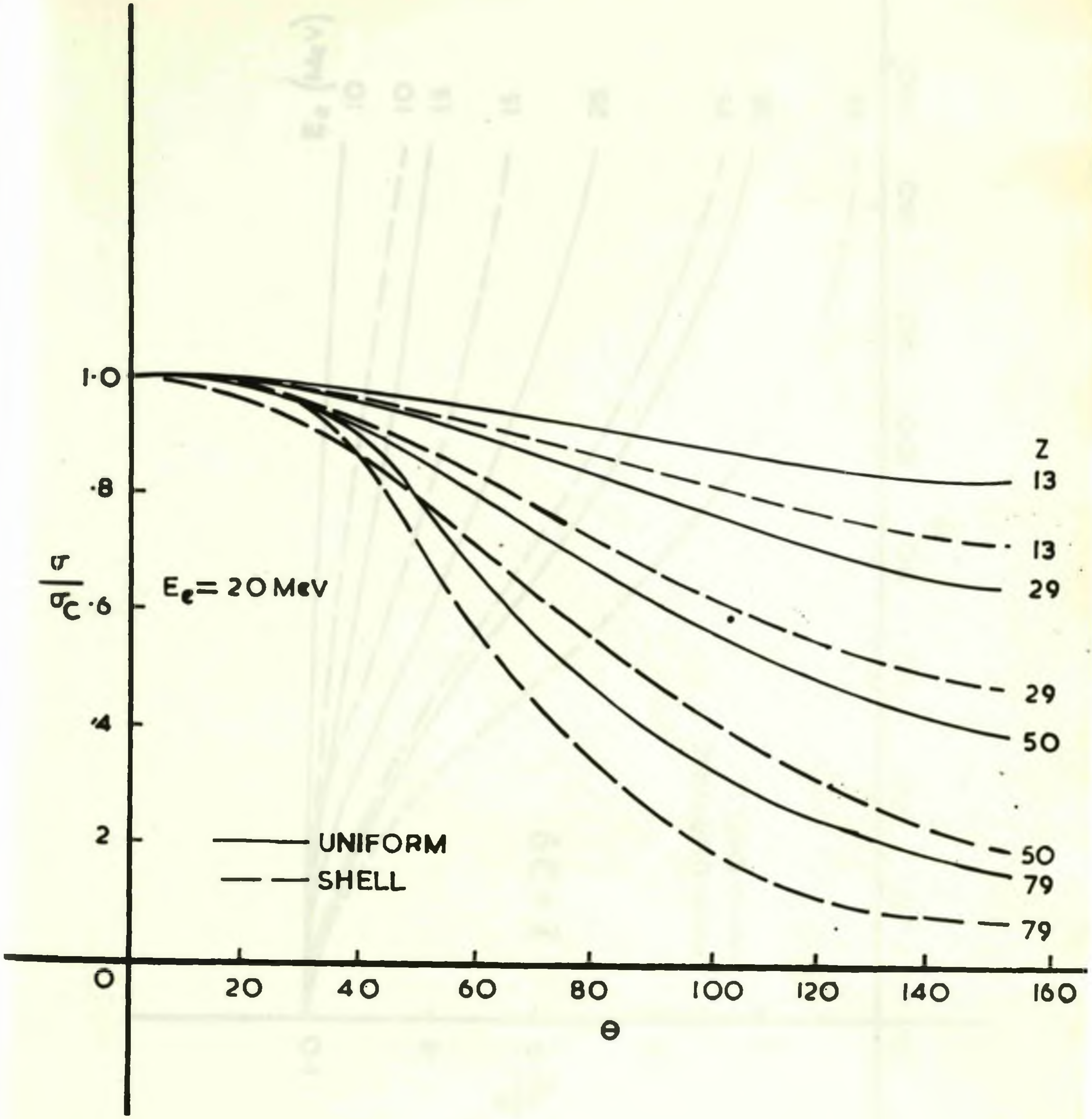

1·0
·8
$\frac{\sigma}{\sigma_C}$ ·6
·4
2
0
E_e= 20 MeV
UNIFORM
SHELL
Z
13
13
29
29
50
50
79
79
20
40
60
80
100
120
140
160
θ

Fig 9a

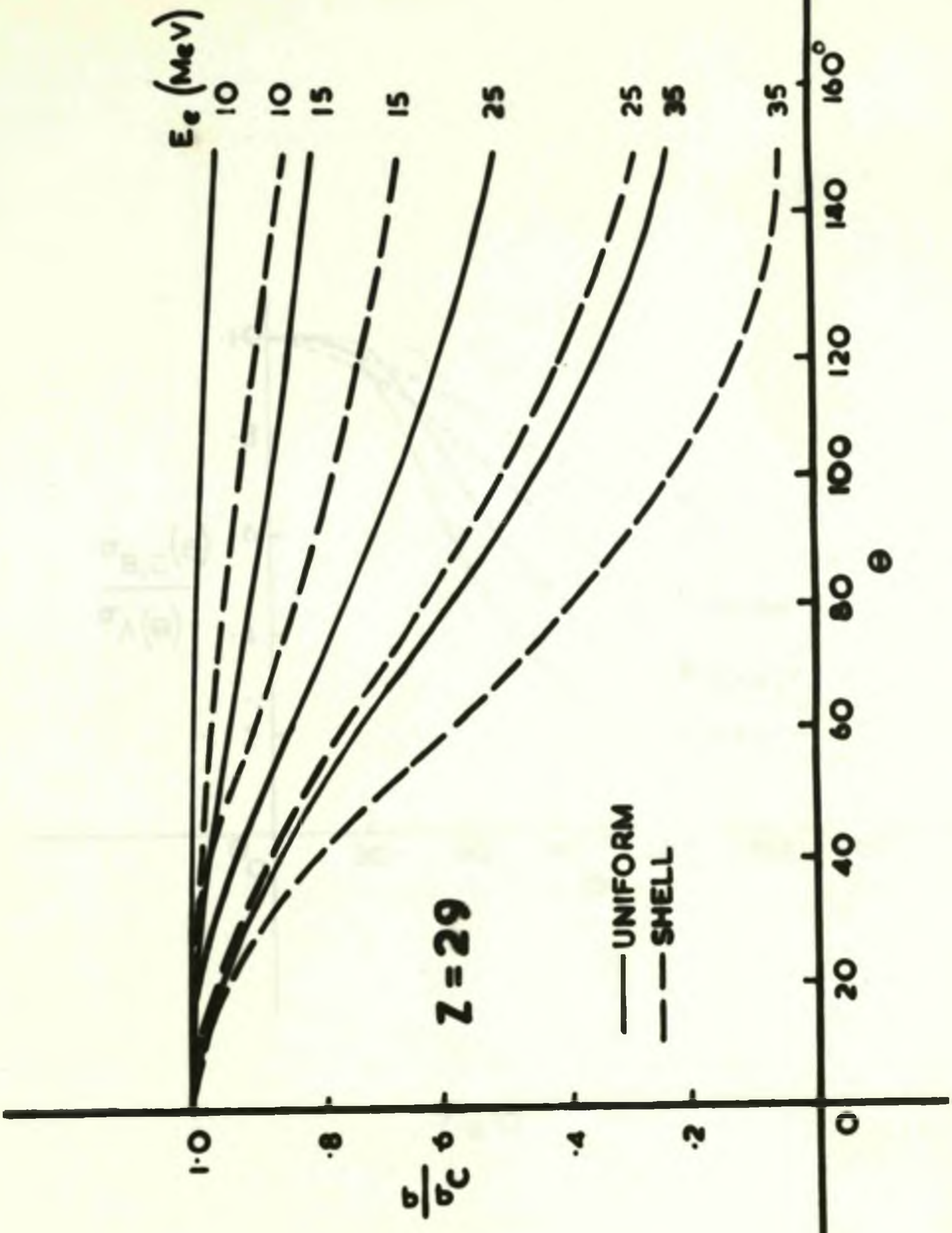

E_e (MeV)
10
10
15
15
25
25
35
35
Z = 29
UNIFORM
SHELL
σ/σ_C
1·0
·8
·6
·4
·2
0
20
40
60
80
100
120
140
160°
θ

Fig 9b

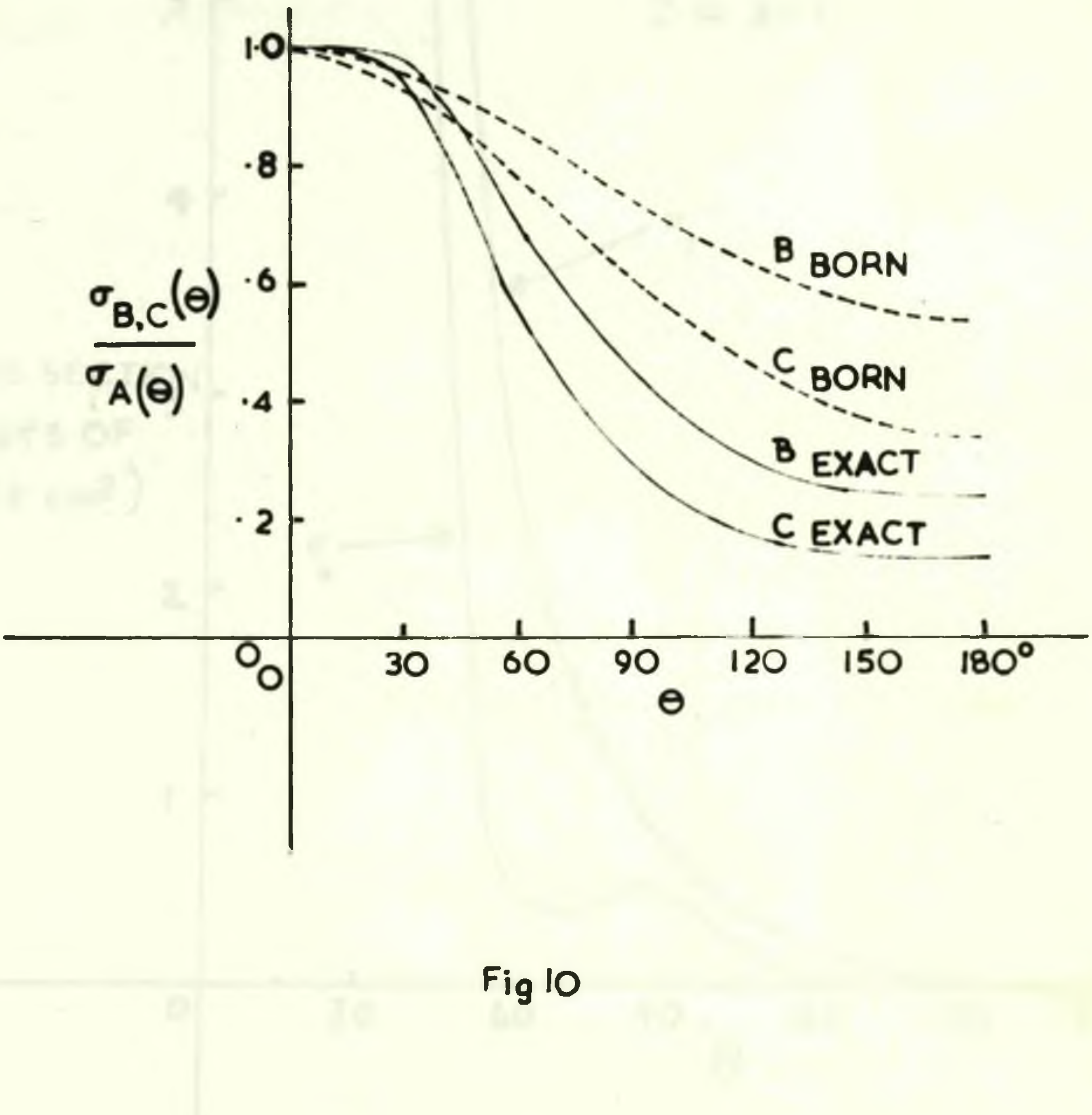

1·0
·8
·6
·4
·2
$\frac{\sigma_{B,C}(\Theta)}{\sigma_A(\Theta)}$
B BORN
C BORN
B EXACT
C EXACT
0
30
60
90
120
150
180°
Θ

Fig 10

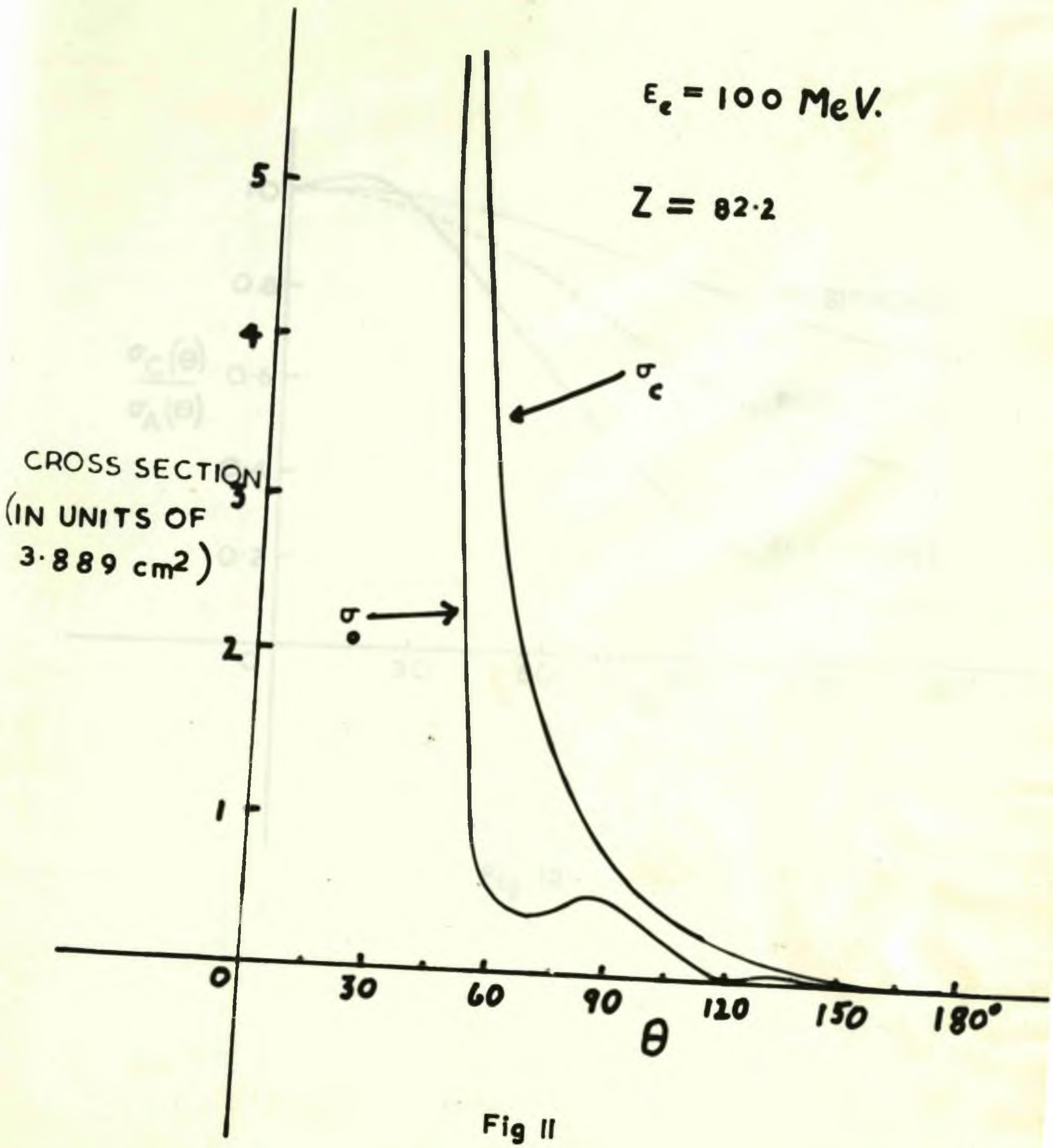

$E_e = 100$ MeV.
$Z = 82{\cdot}2$
CROSS SECTION (IN UNITS OF $3{\cdot}889$ cm^2)
σ_c
σ_0
5
4
3
2
1
0
30
60
90
120
150
180°
θ

Fig II

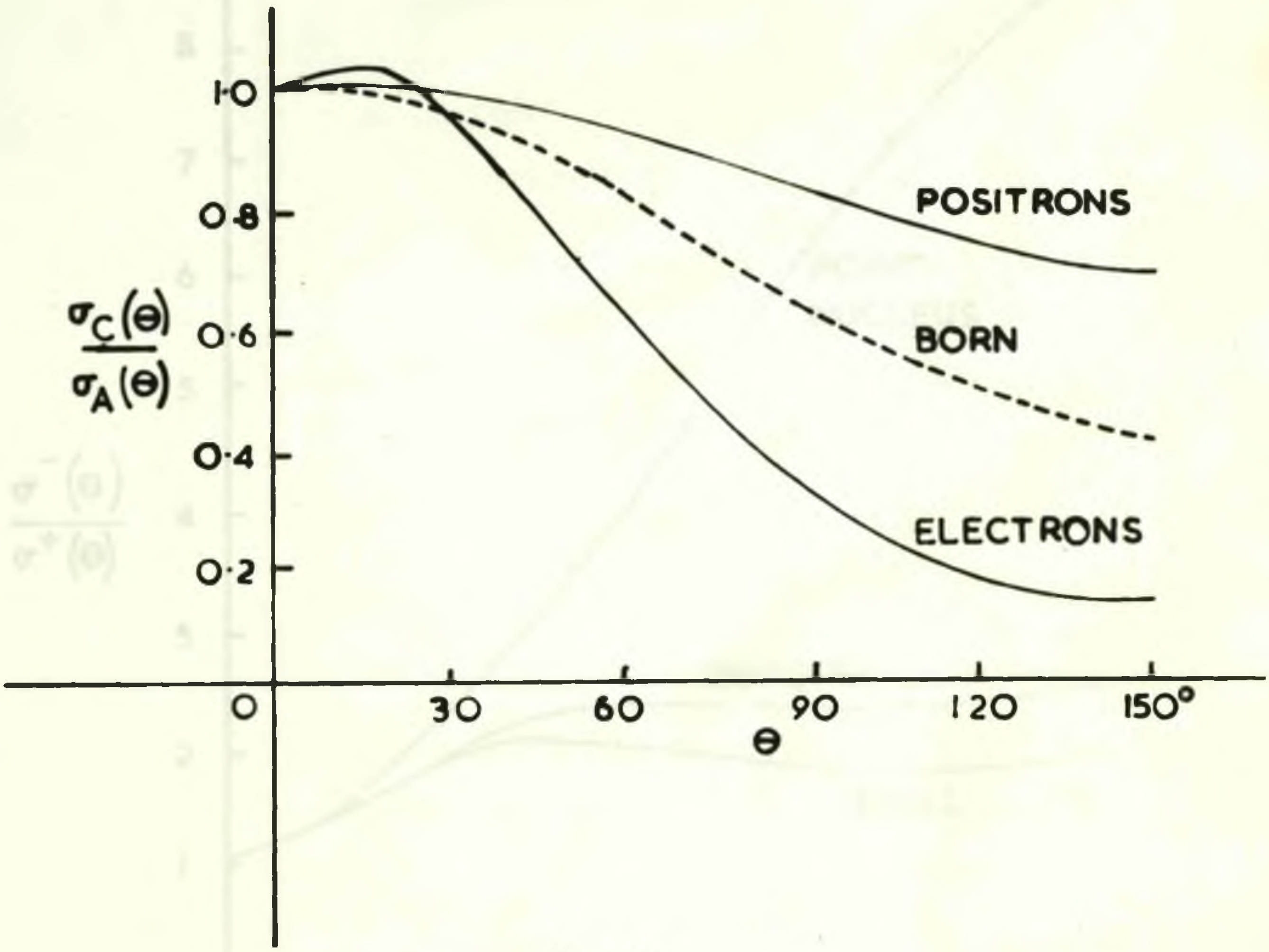
1·0
0·8
0·6
0·4
0·2
$\frac{\sigma_C(\theta)}{\sigma_A(\theta)}$
POSITRONS
BORN
ELECTRONS
0
30
60
90
120
150°
θ

Fig 12

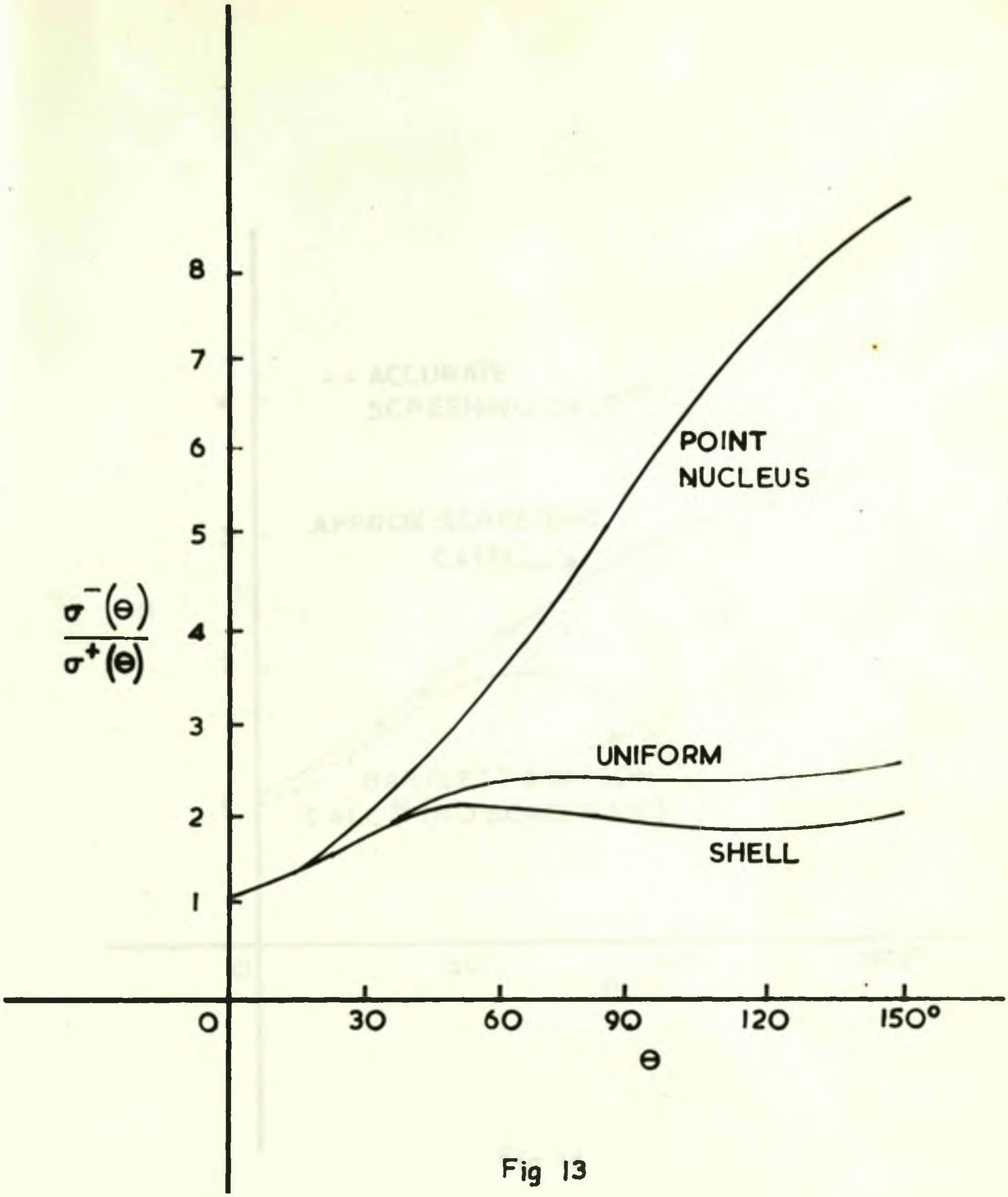

$\frac{\sigma^-(\theta)}{\sigma^+(\theta)}$
8
7
6
5
4
3
2
1
POINT NUCLEUS
UNIFORM
SHELL
0
30
60
90
120
150°
θ

Fig 13

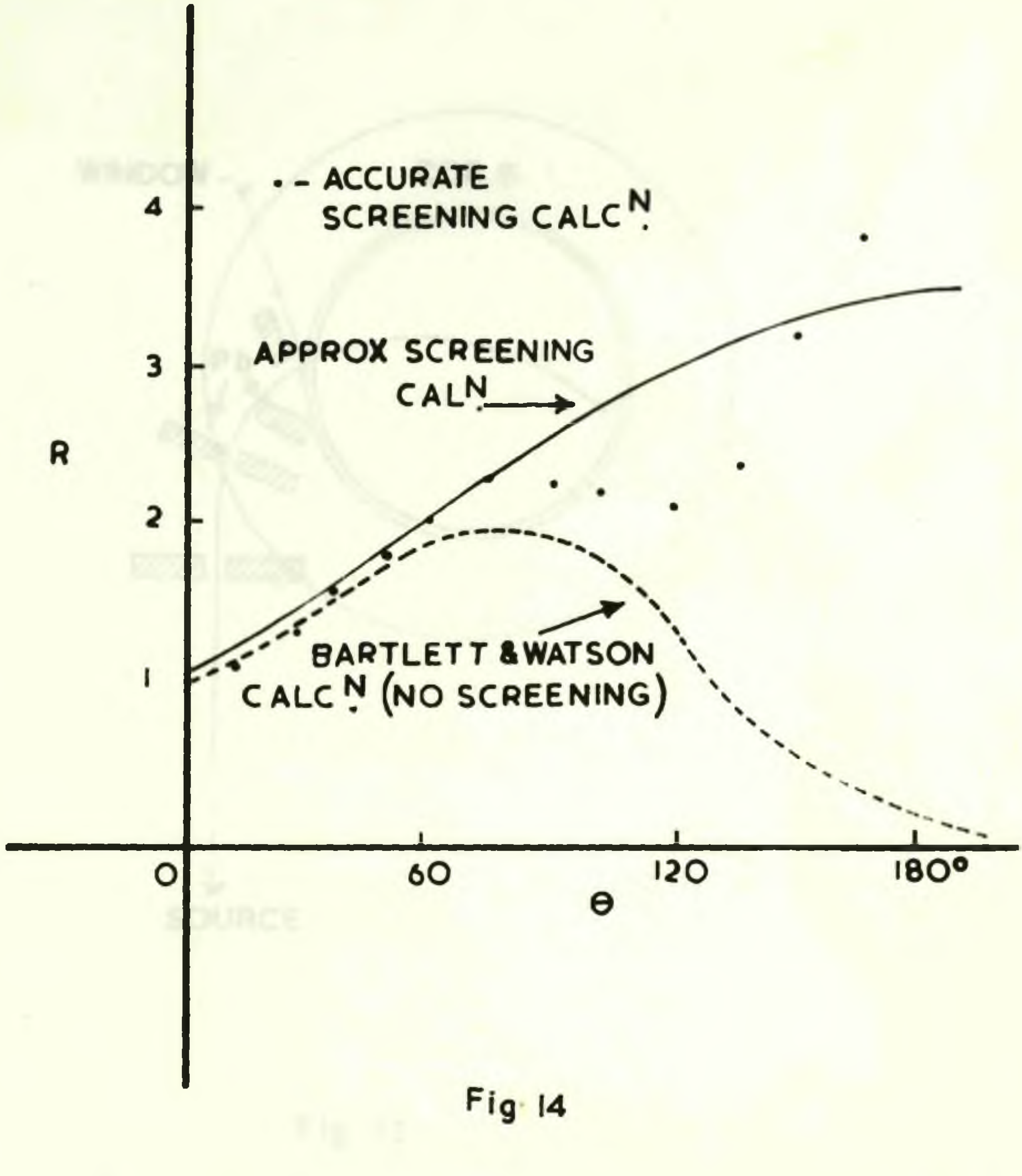

• - ACCURATE
SCREENING CALC N.
APPROX SCREENING
CAL N.
BARTLETT & WATSON
CALC N. (NO SCREENING)
R
4
3
2
1
0
60
120
180°
θ

Fig 14

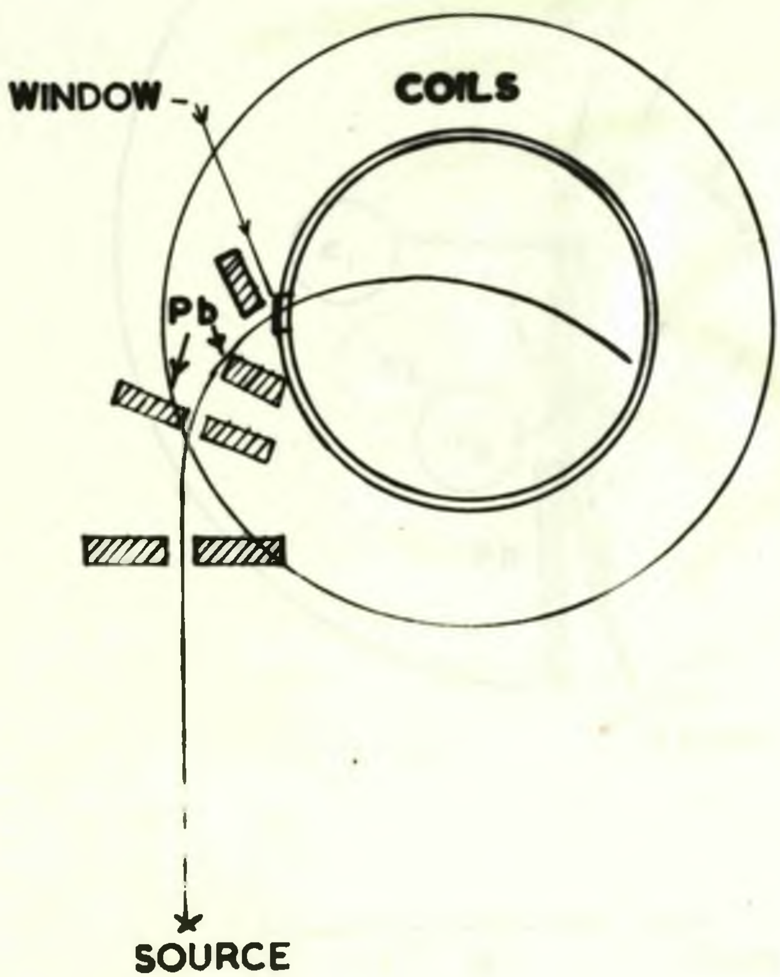

Fig 15

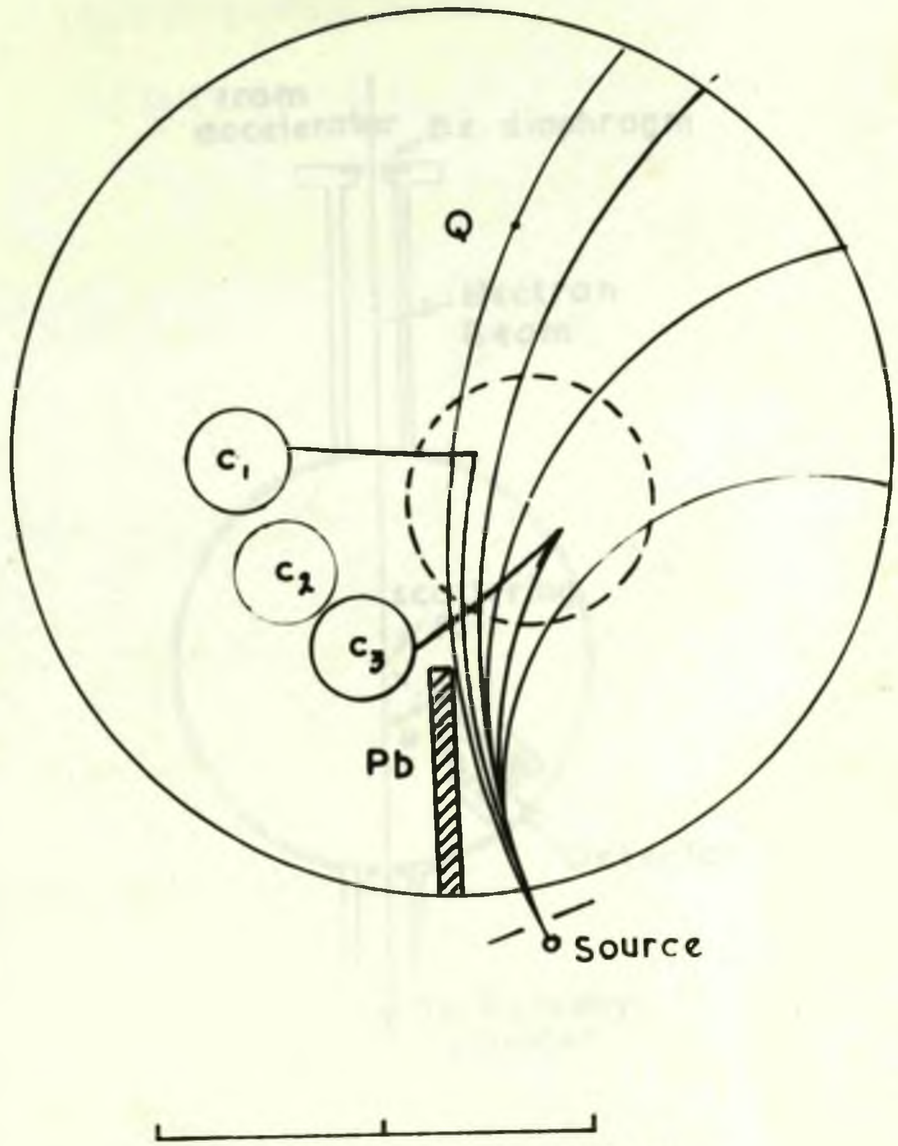

Fig 16

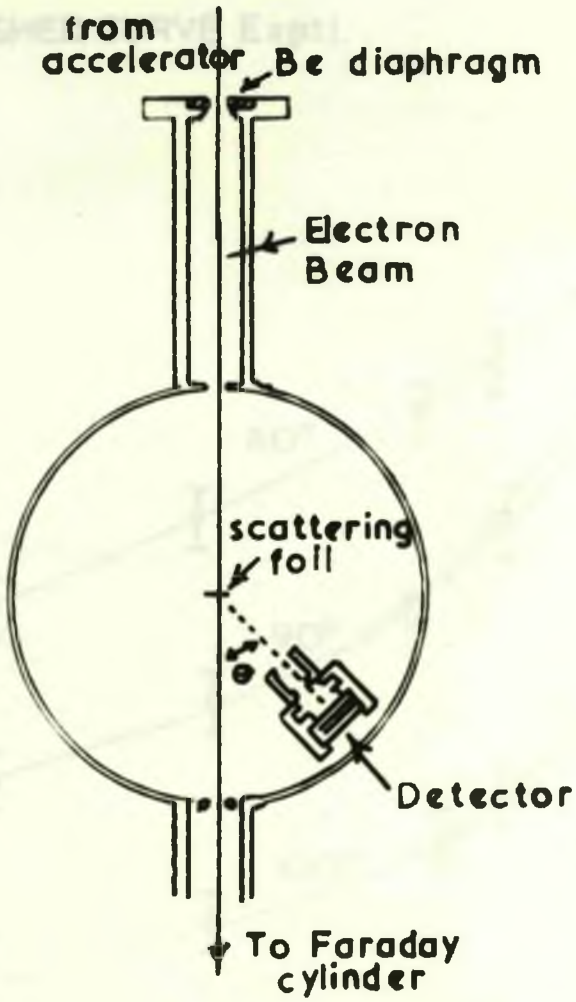

from
accelerator
Be diaphragm
Electron
Beam
scattering
foil
θ
Detector
To Faraday
cylinder

Fig 17

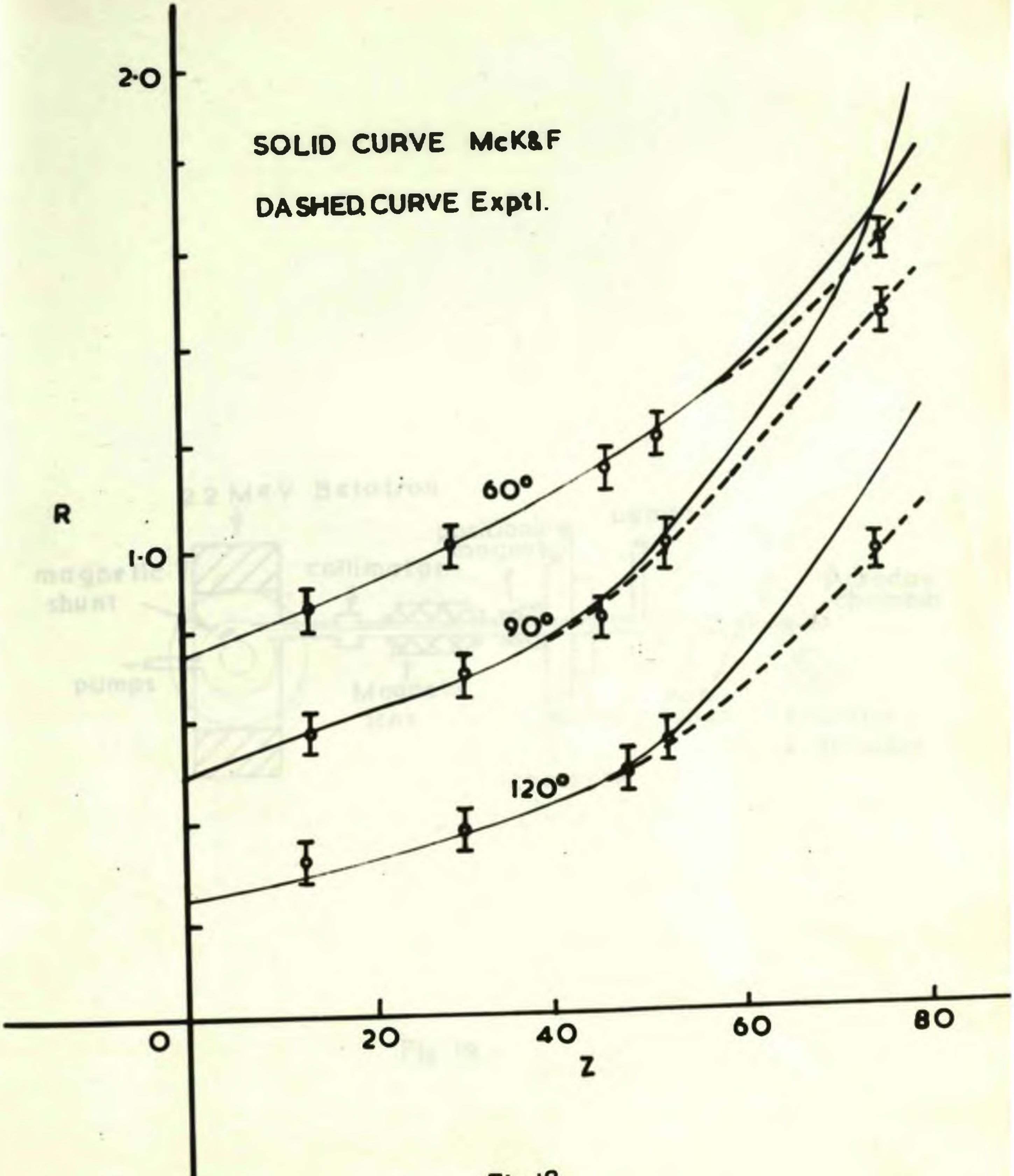

2·0
SOLID CURVE McK&F
DASHED CURVE Exptl.
60°
90°
120°
R
1·0
O
20
40
60
80
Z

Fig 18

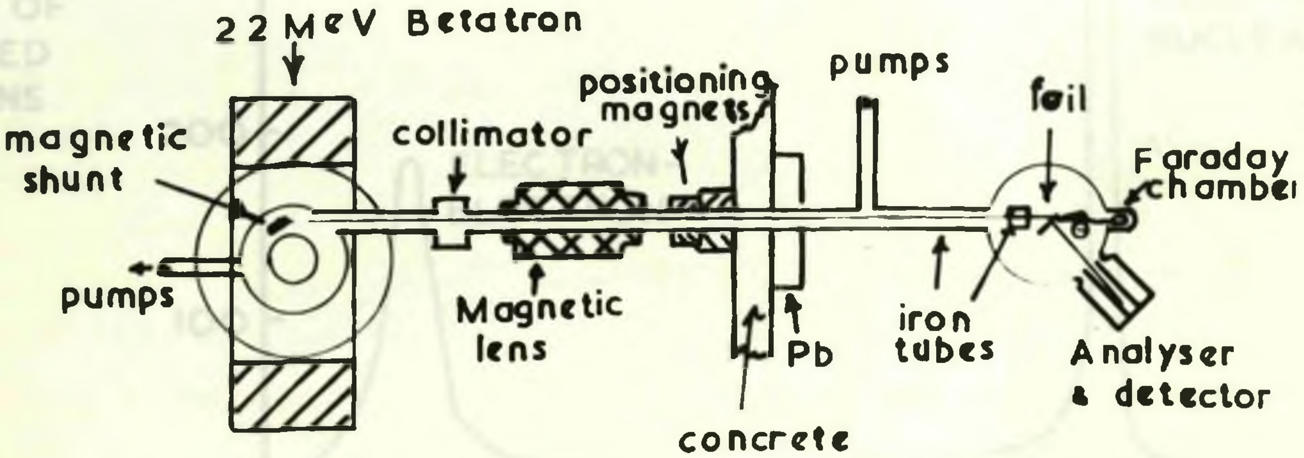

22 MeV Betatron
magnetic shunt
pumps
collimator
Magnetic lens
positioning magnets
concrete
Pb
pumps
iron tubes
foil
Faraday chamber
Analyser & detector

Fig 19

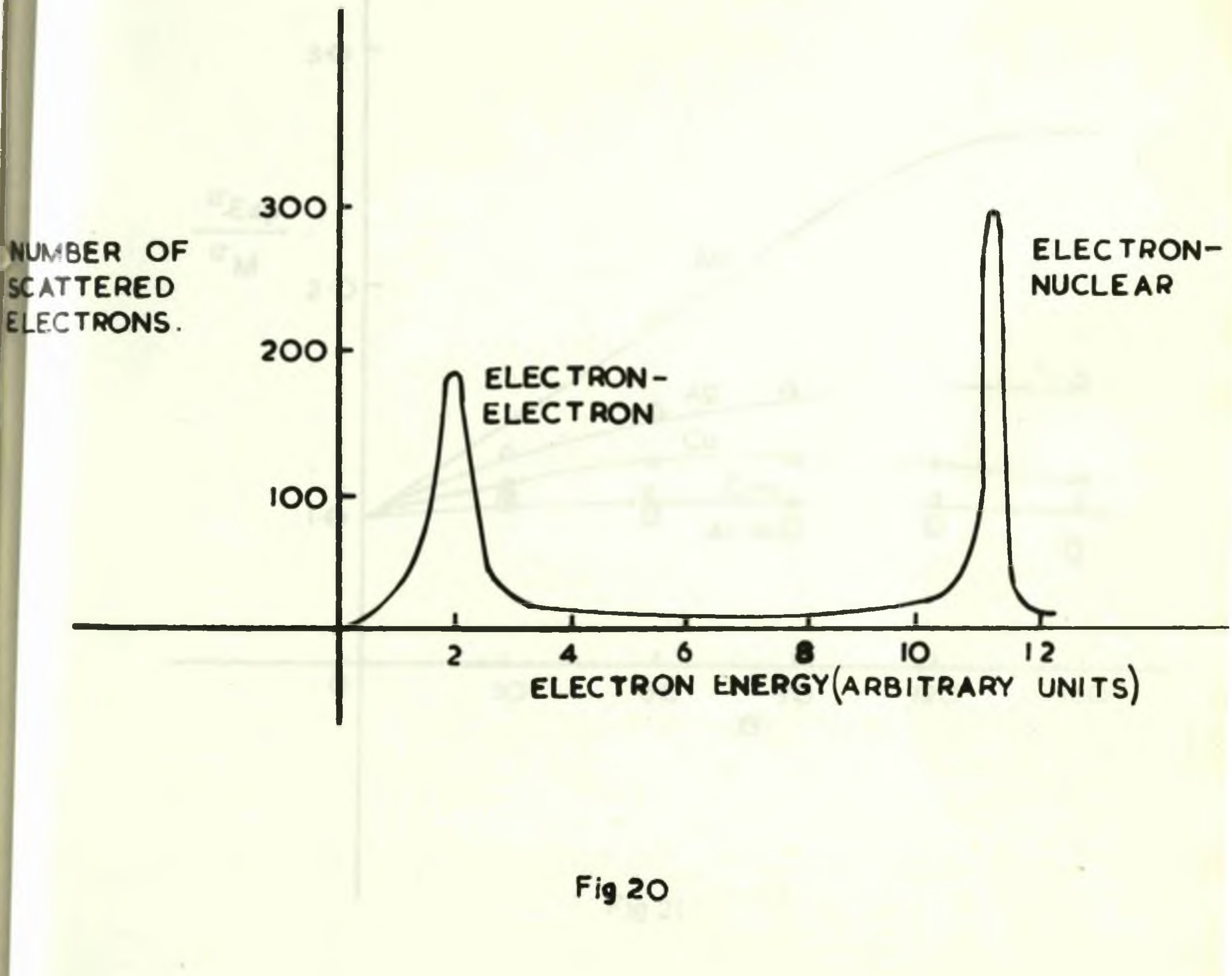

300
200
100
NUMBER OF SCATTERED ELECTRONS.
ELECTRON-ELECTRON
ELECTRON-NUCLEAR
2
4
6
8
10
12
ELECTRON ENERGY(ARBITRARY UNITS)

Fig 20

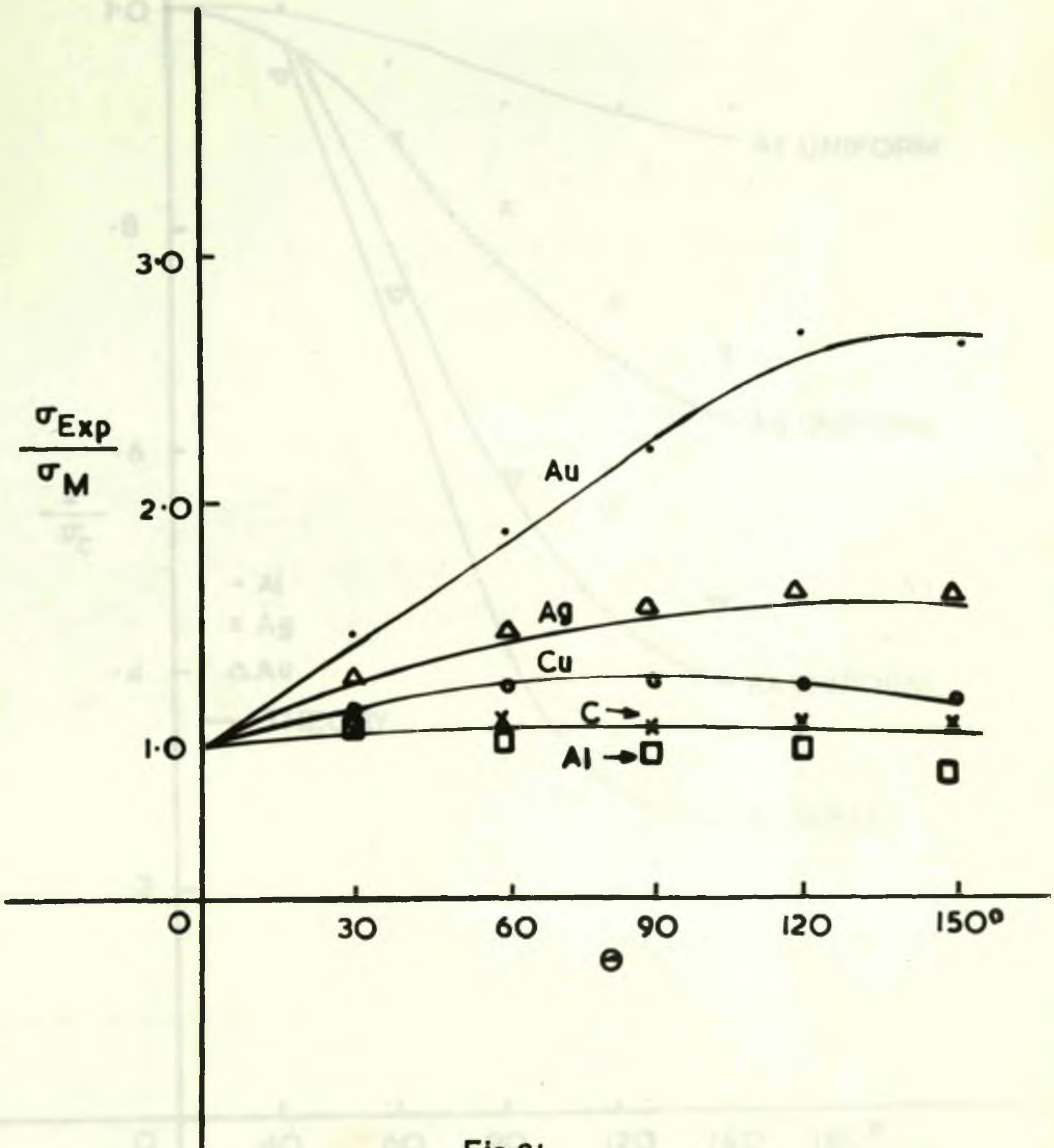

Fig 21

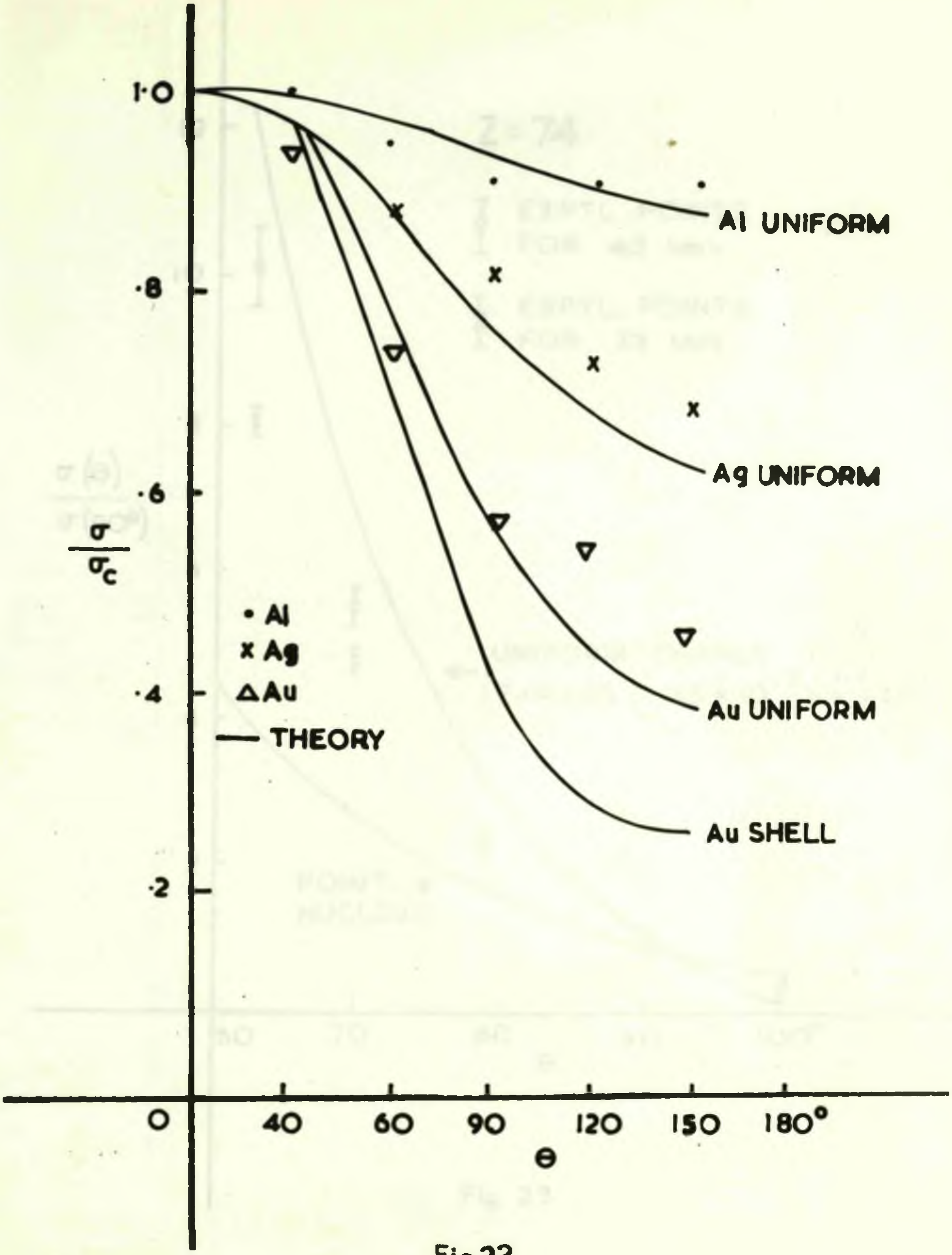

1·0
·8
·6
·4
·2
σ / σc
• Al
x Ag
△ Au
— THEORY
Al UNIFORM
Ag UNIFORM
Au UNIFORM
Au SHELL
0
40
60
90
120
150
180°
θ

Fig 22

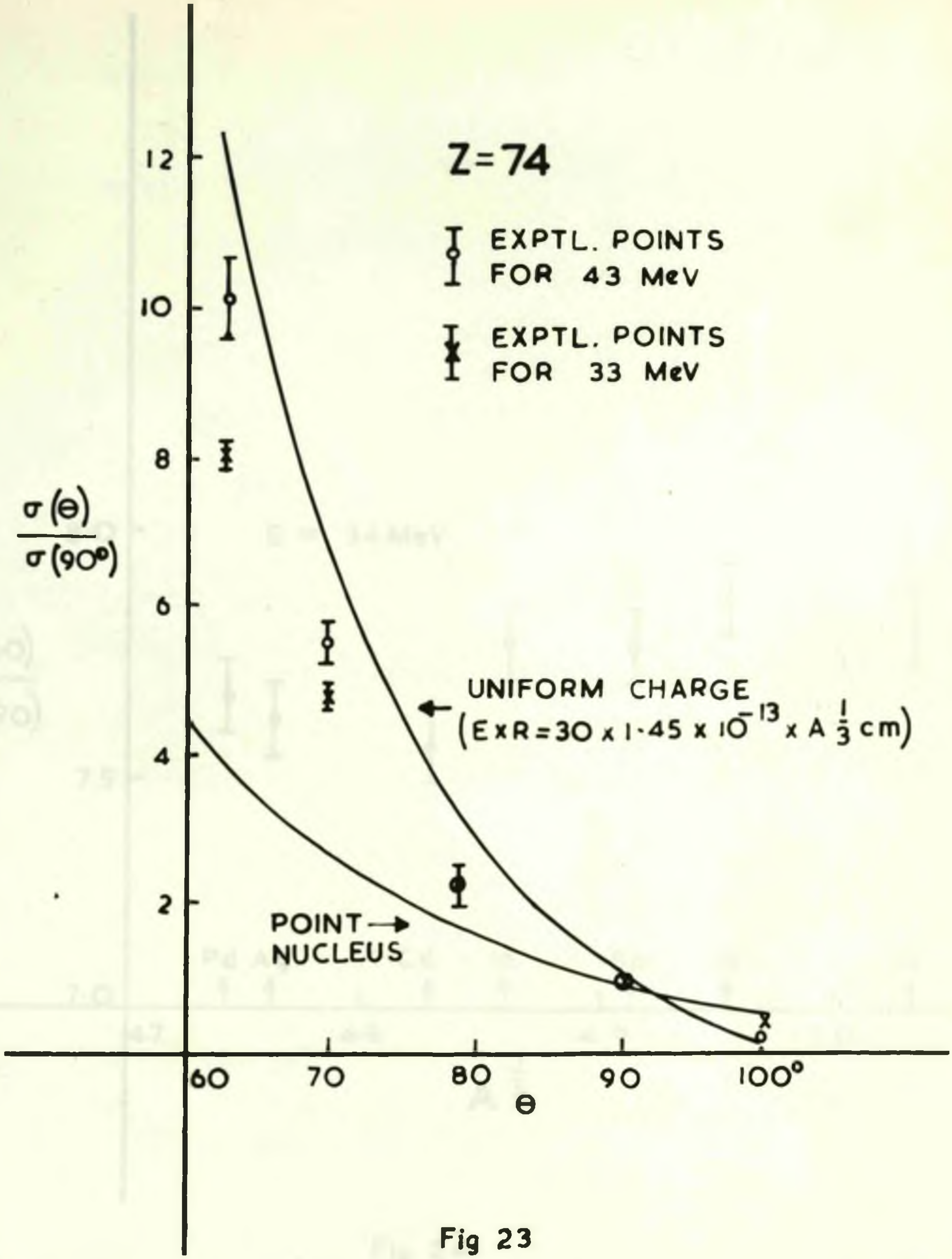

Z=74
EXPTL. POINTS
FOR 43 MeV
EXPTL. POINTS
FOR 33 MeV
σ(Θ)
σ(90°)
UNIFORM CHARGE
(E×R=30×1·45×10⁻¹³×A⅓ cm)
POINT →
NUCLEUS
12
10
8
6
4
2
60
70
80
90
100°
Θ

Fig 23

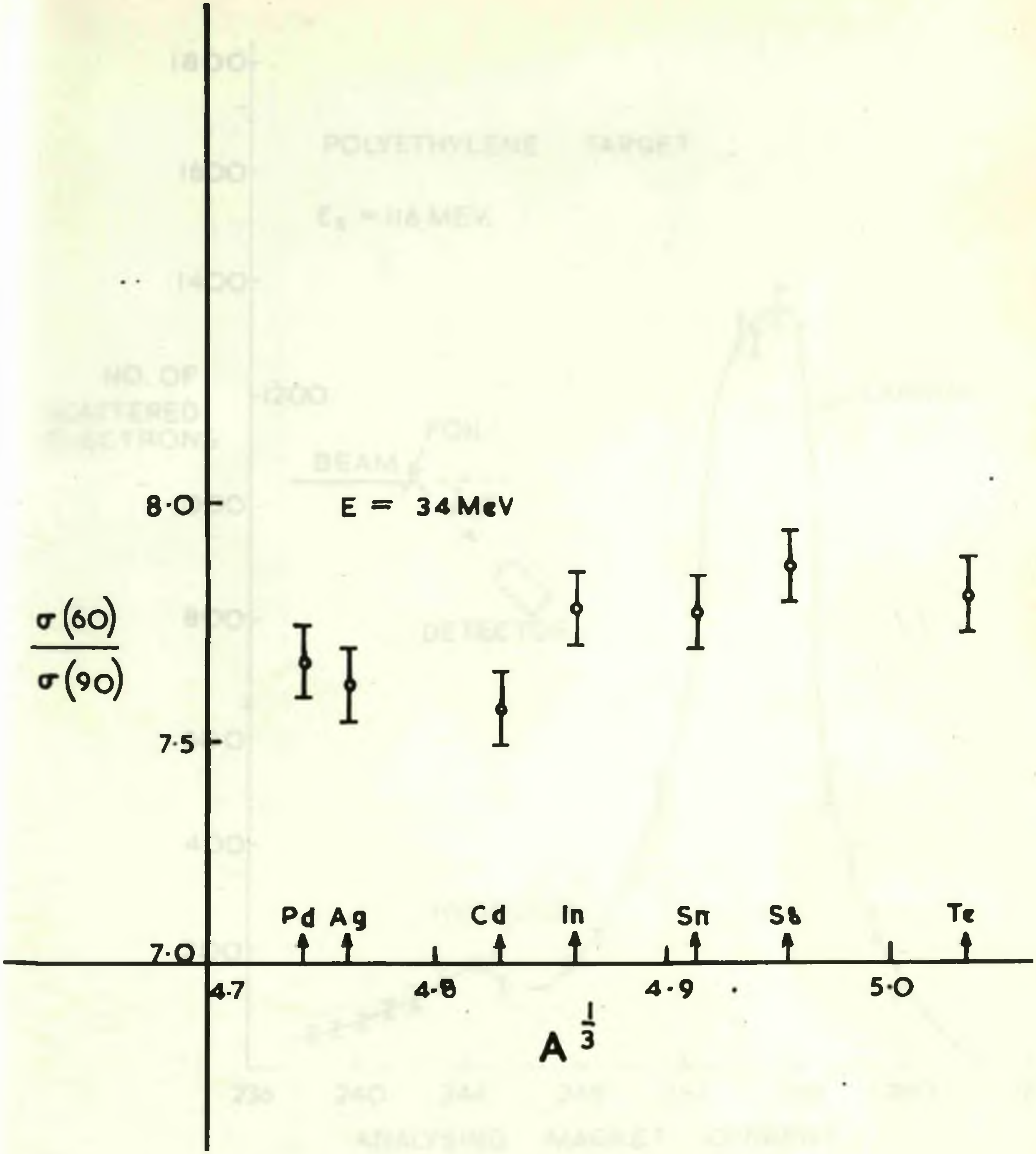

Fig 24

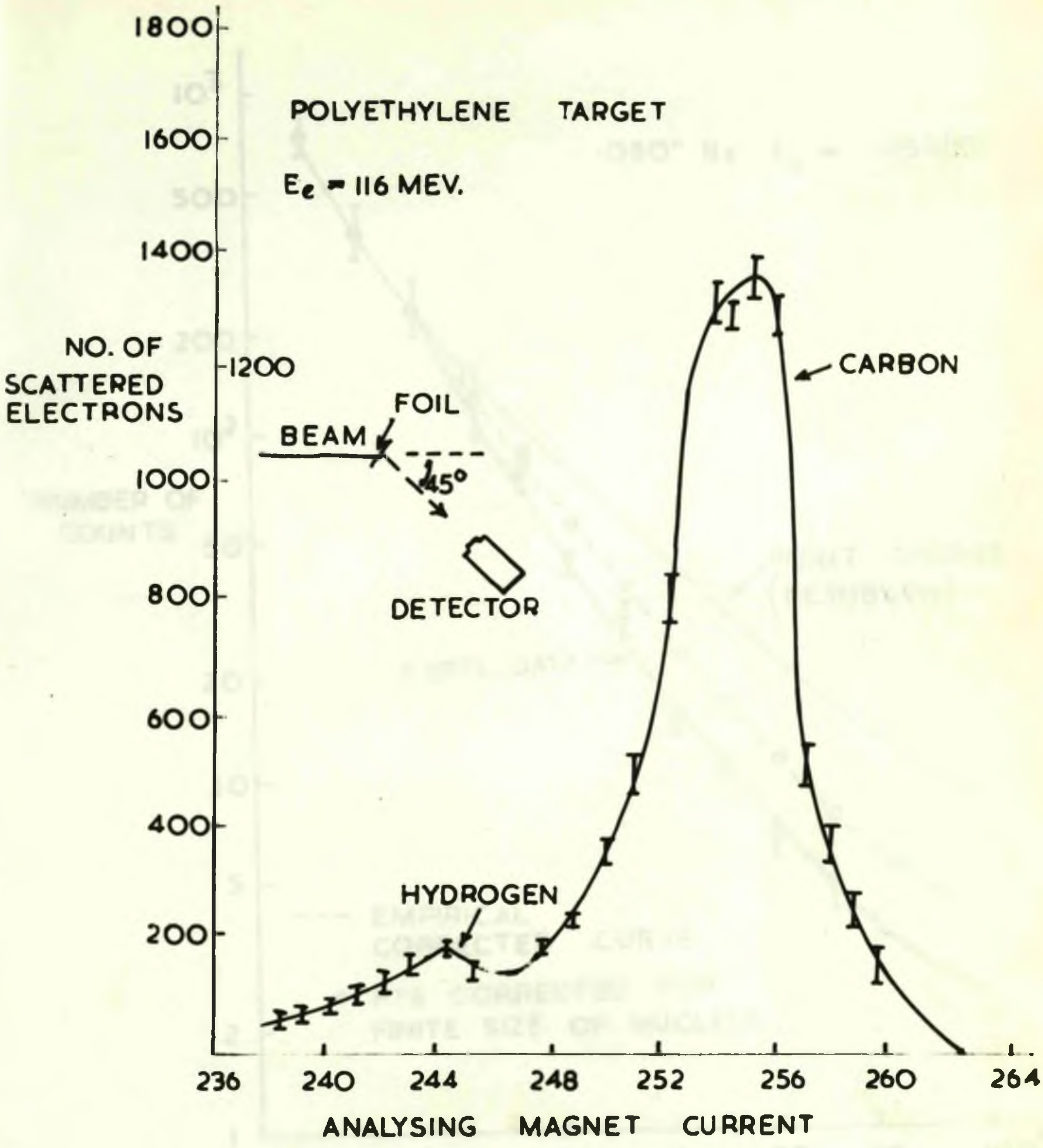
1800
1600
1400
1200
1000
800
600
400
200
POLYETHYLENE TARGET
E_e = 116 MEV.
NO. OF
SCATTERED
ELECTRONS
FOIL
BEAM
45°
DETECTOR
CARBON
HYDROGEN
236
240
244
248
252
256
260
264
ANALYSING MAGNET CURRENT

Fig 25

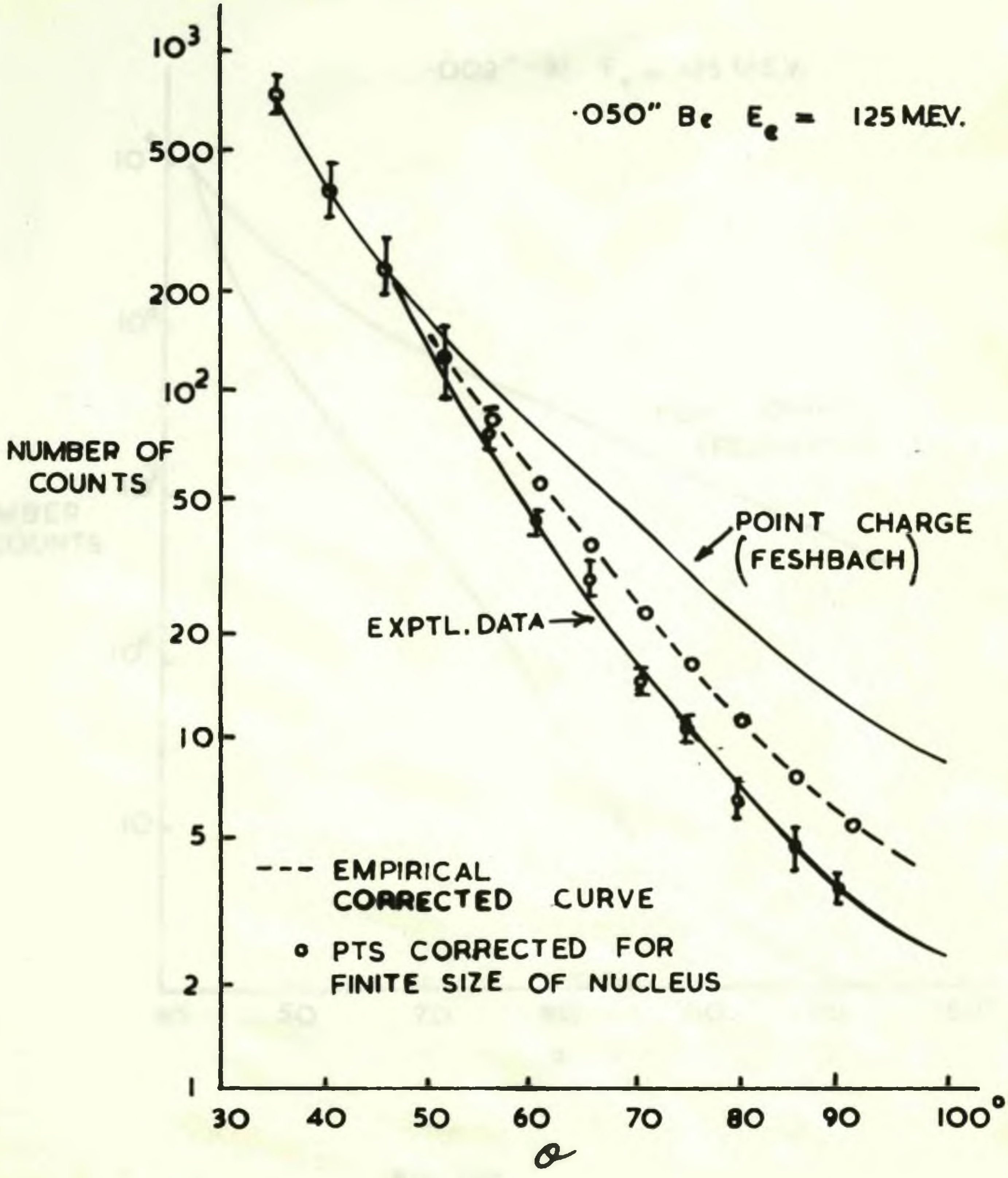
·050" Be E_e = 125 MEV.
NUMBER OF COUNTS
10^3
500
200
10^2
50
20
10
5
2
1
POINT CHARGE (FESHBACH)
EXPTL. DATA
--- EMPIRICAL CORRECTED CURVE
o PTS CORRECTED FOR FINITE SIZE OF NUCLEUS
30
40
50
60
70
80
90
100°
θ

Fig 26a

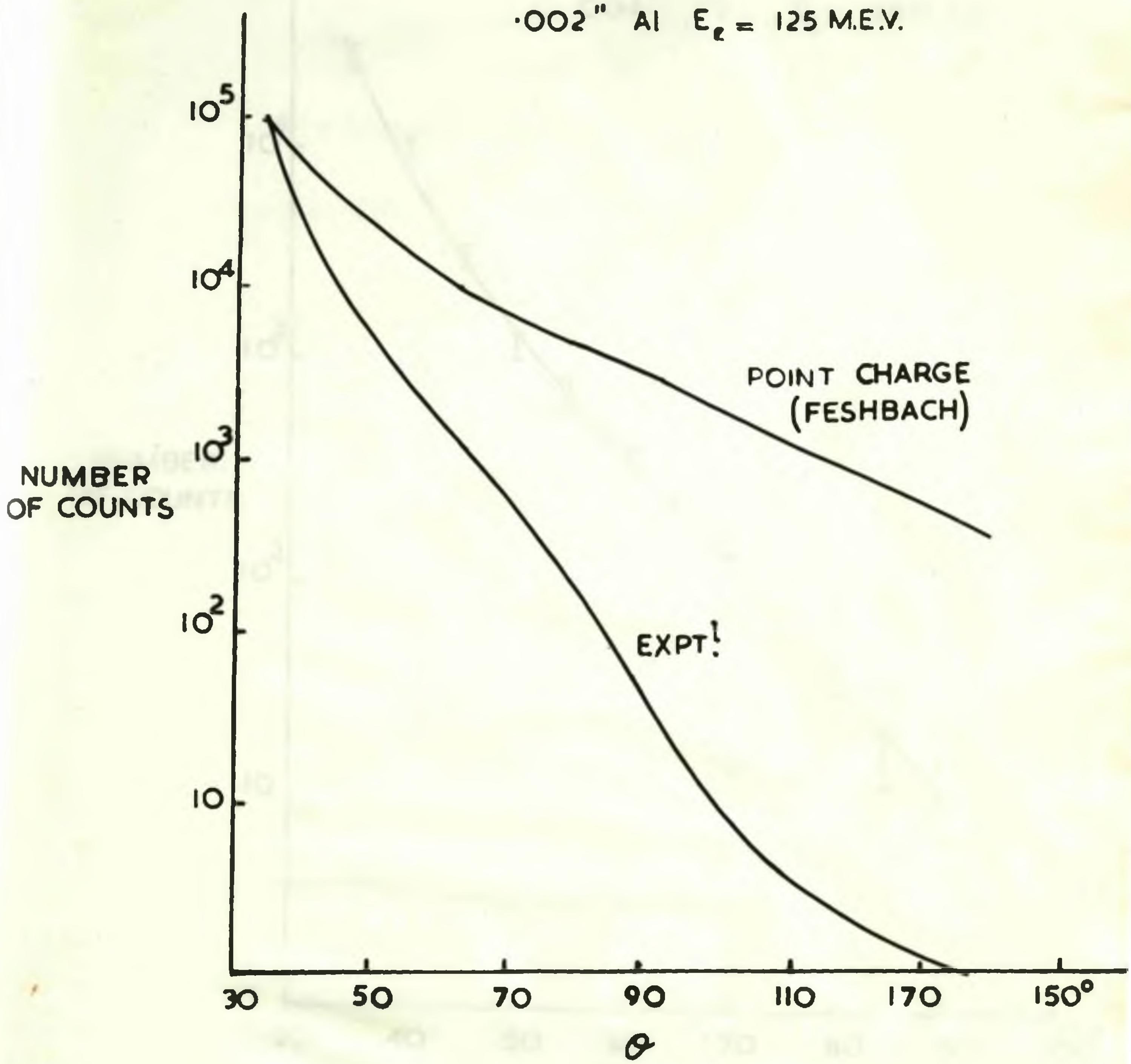
·002" Al E_e = 125 M.E.V.
10^5
10^4
10^3
10^2
10
NUMBER OF COUNTS
POINT CHARGE (FESHBACH)
EXPT!
30
50
70
90
110
170
150°
θ

Fig 26b

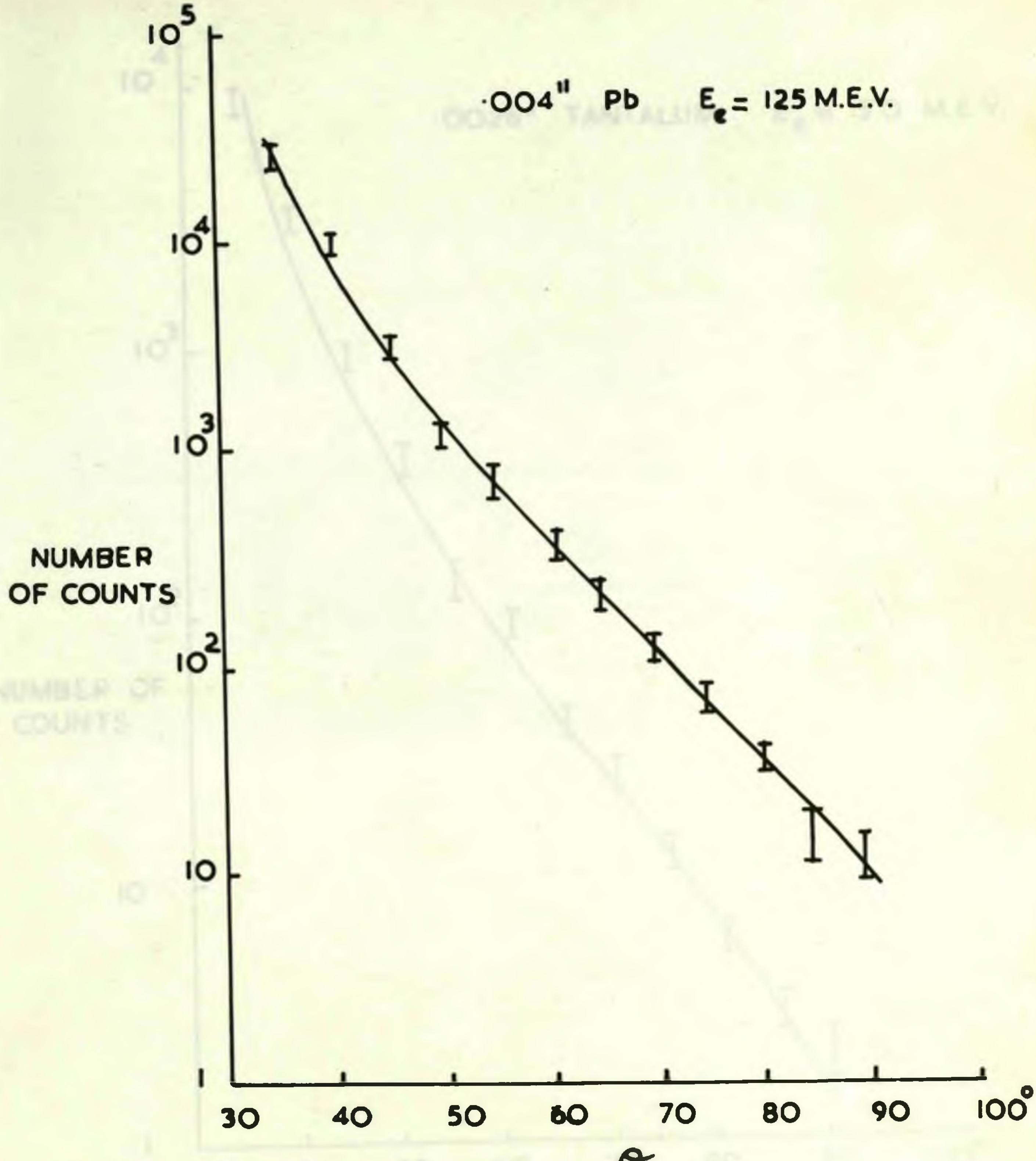

·004" Pb E_e = 125 M.E.V.
NUMBER OF COUNTS
10^5
10^4
10^3
10^2
10
1
30
40
50
60
70
80
90
100°
θ

Fig 26c

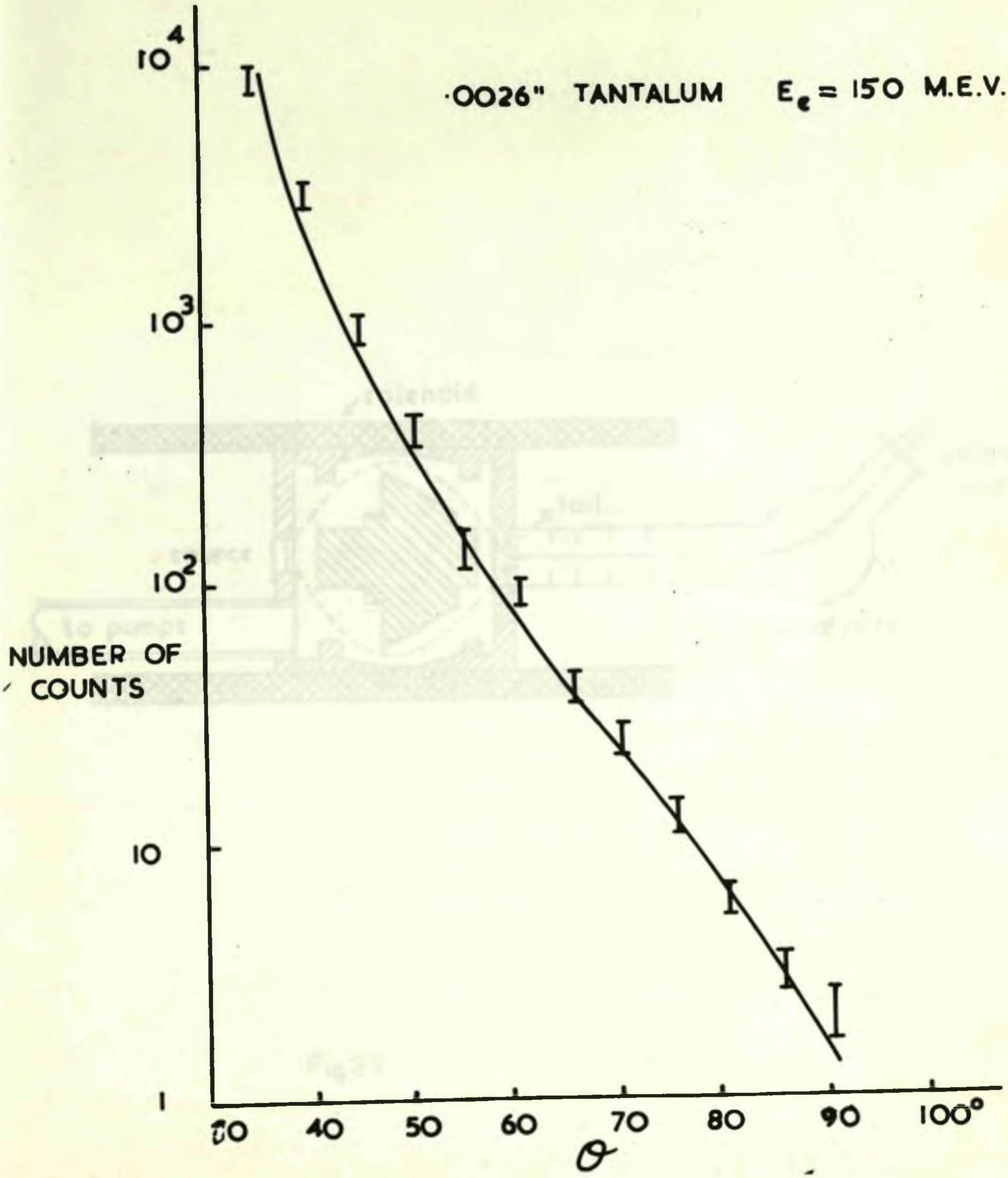
·0026" TANTALUM E_e = 150 M.E.V.
10^4
10^3
10^2
10
1
NUMBER OF COUNTS
30
40
50
60
70
80
90
100°
θ

Fig 26 d

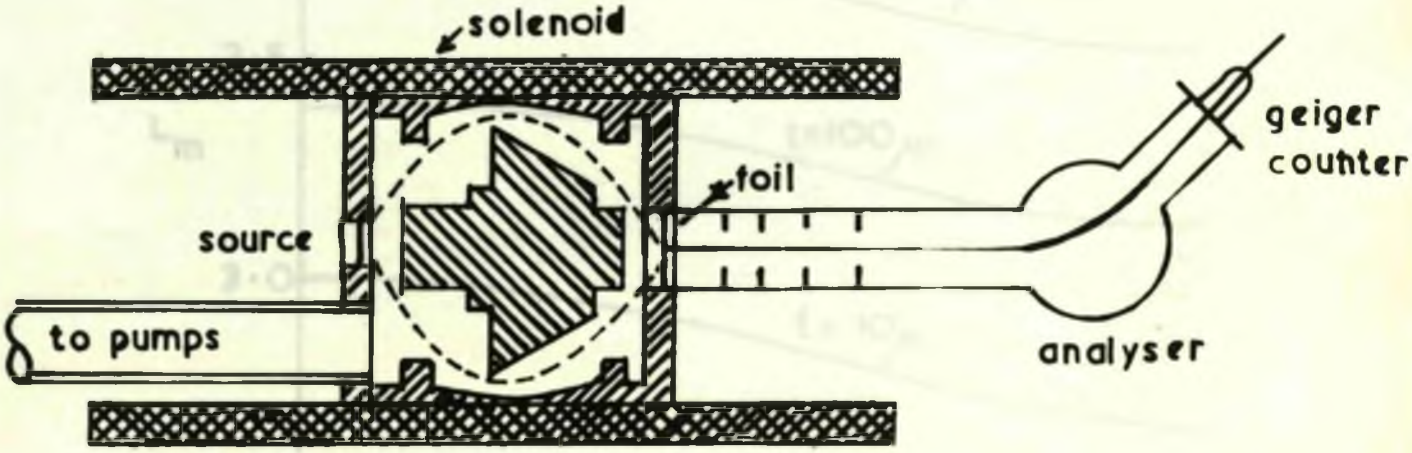

Fig 27

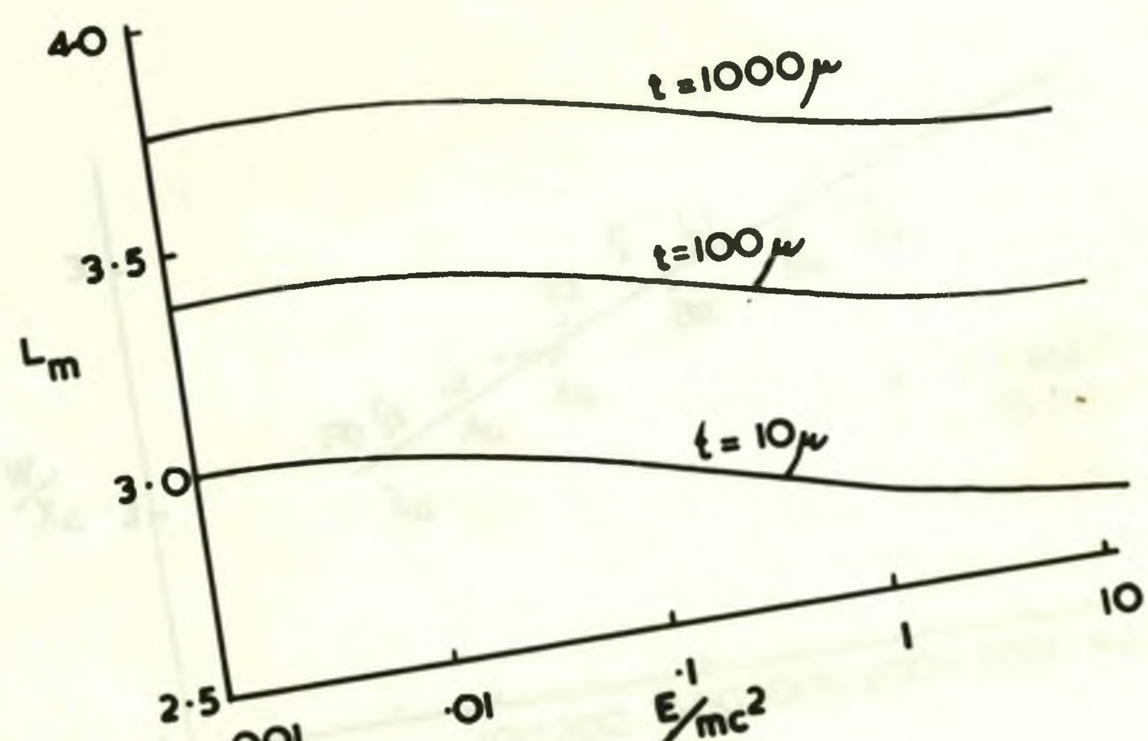

Fig 28

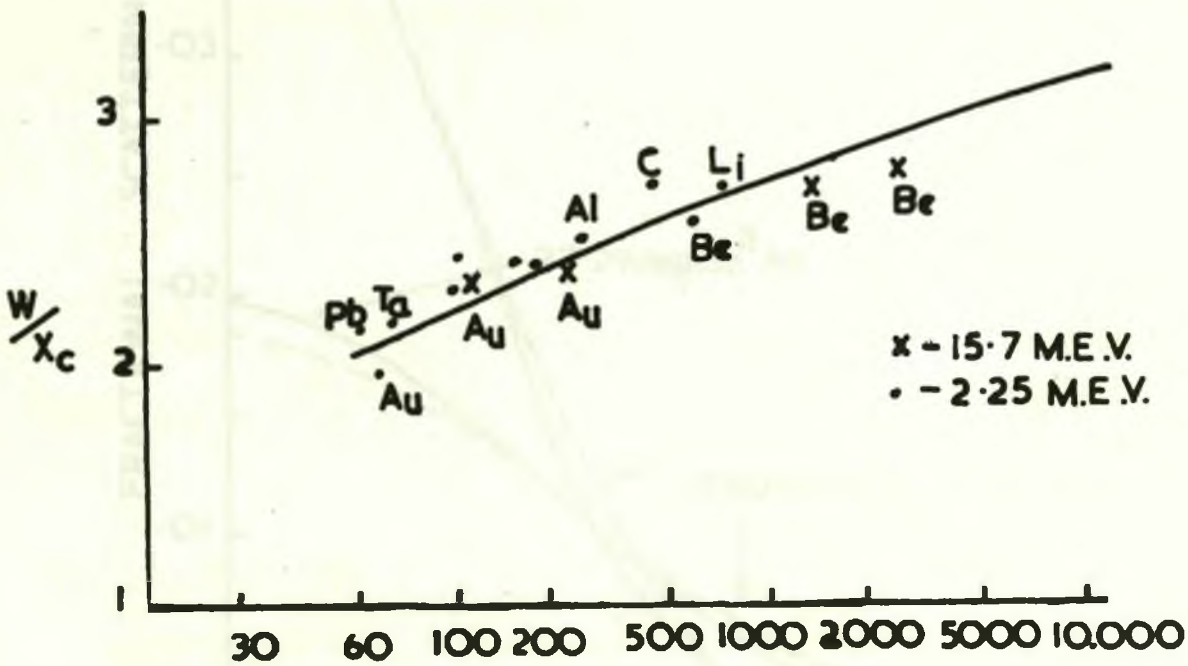
W/Xc
3
2
1
Pb
Ta
Au
Au
Au
Al
C
Li
Be
Be
Be
30
60
100
200
500
1000
2000
5000
10.000
x - 15·7 M.E.V.
• - 2·25 M.E.V.

Fig 29

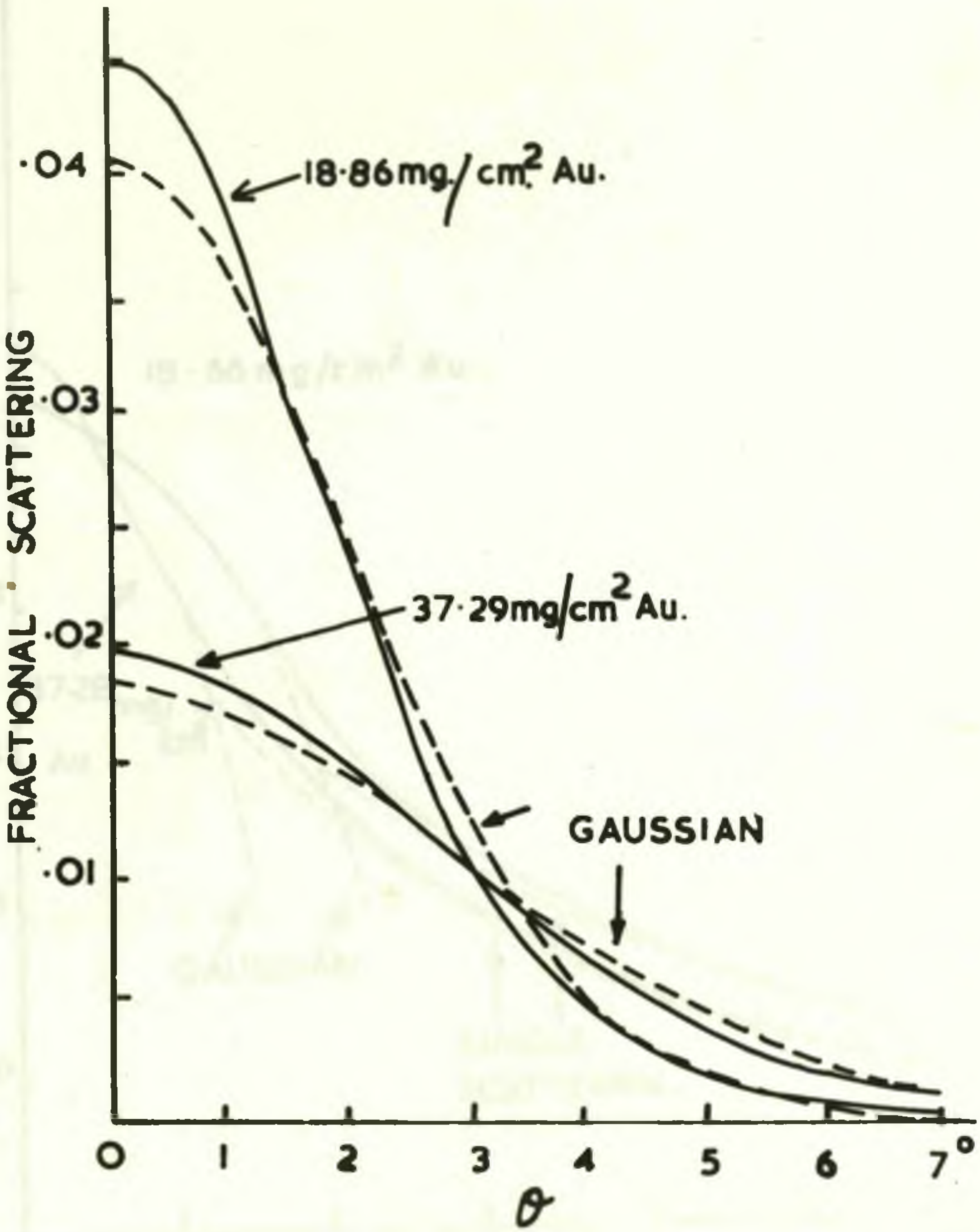

·04
·03
·02
·01
FRACTIONAL SCATTERING
18·86mg./cm.^{2} Au.
37·29mg/cm^2 Au.
GAUSSIAN
0
1
2
3
4
5
6
7°
θ

Fig 30

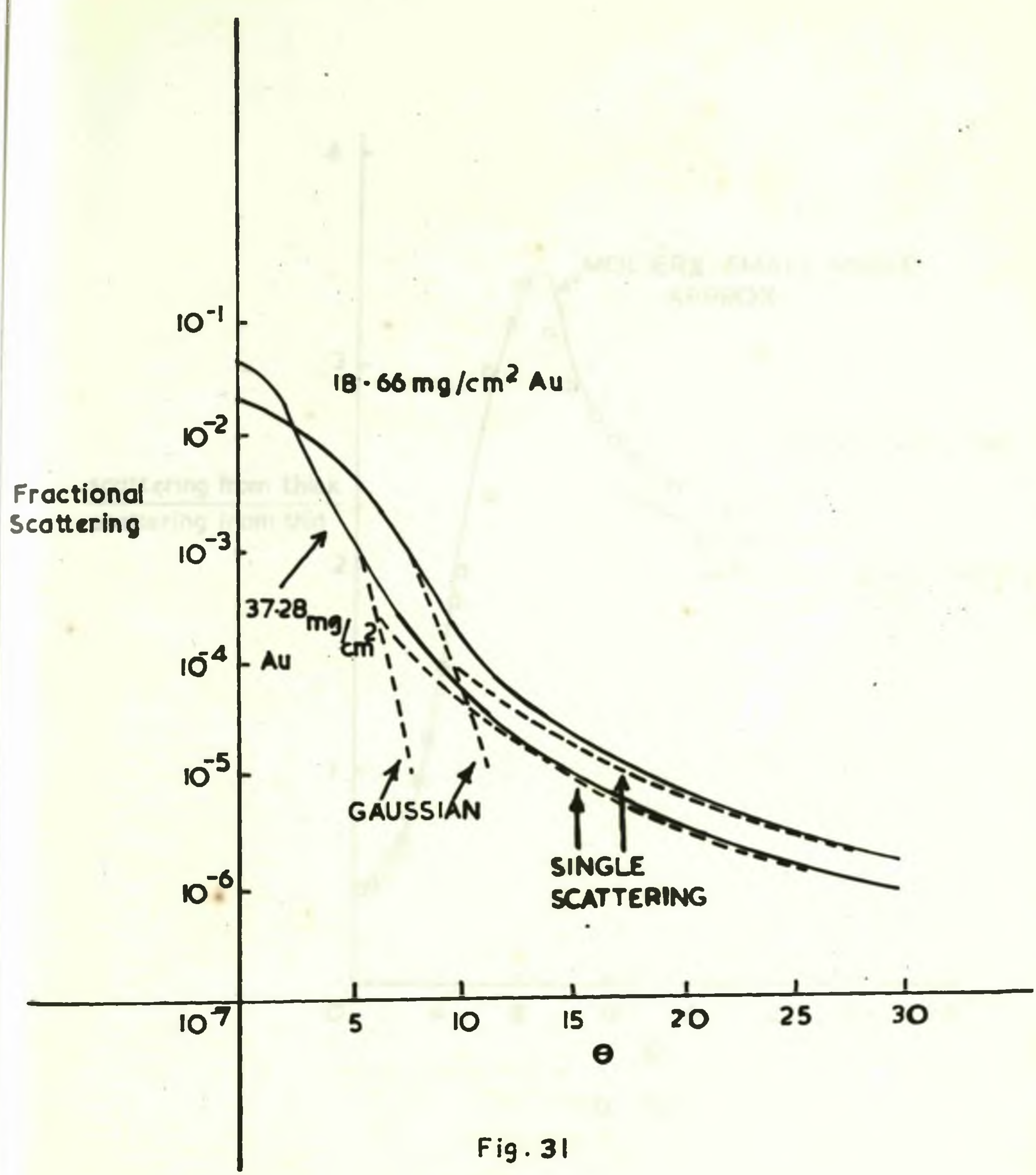

Fractional Scattering
10^{-1}
10^{-2}
10^{-3}
10^{-4}
10^{-5}
10^{-6}
10^{-7}
18·66 mg/cm² Au
37·28 mg/cm² Au
GAUSSIAN
SINGLE SCATTERING
5
10
15
20
25
30
θ

Fig. 31

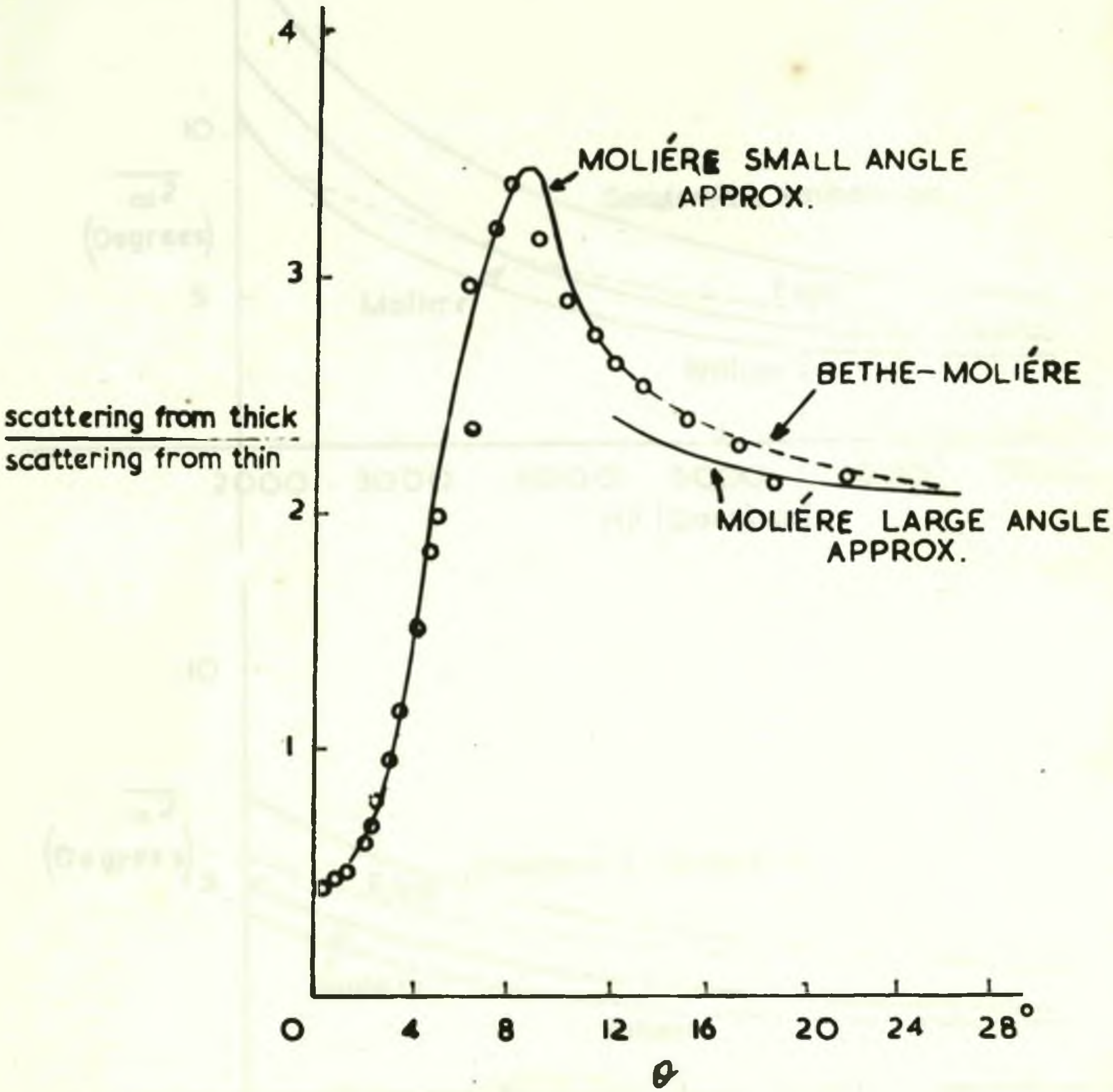

MOLIÉRE SMALL ANGLE APPROX.
BETHE-MOLIÉRE
MOLIÉRE LARGE ANGLE APPROX.
scattering from thick / scattering from thin
4
3
2
1
0
4
8
12
16
20
24
28°
θ

FIG. 32

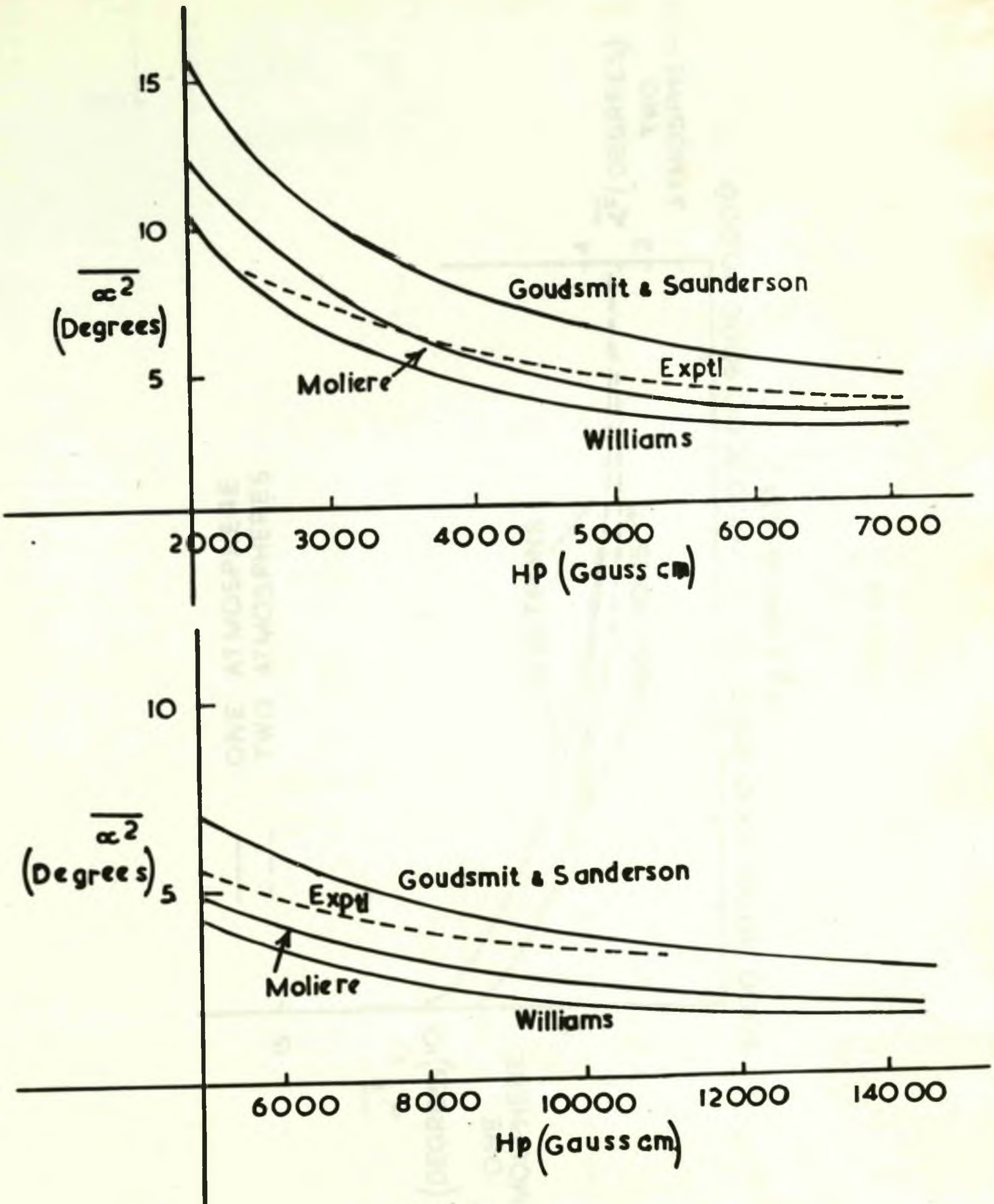

15
10
5
$\overline{\alpha^2}$ (Degrees)
Goudsmit & Saunderson
Exptl
Moliere
Williams
2000
3000
4000
5000
6000
7000
Hp (Gauss cm)
10
$\overline{\alpha^2}$ (Degrees)
5
Goudsmit & Sanderson
Exptl
Moliere
Williams
6000
8000
10000
12000
14000
Hp (Gauss cm)

Fig.33

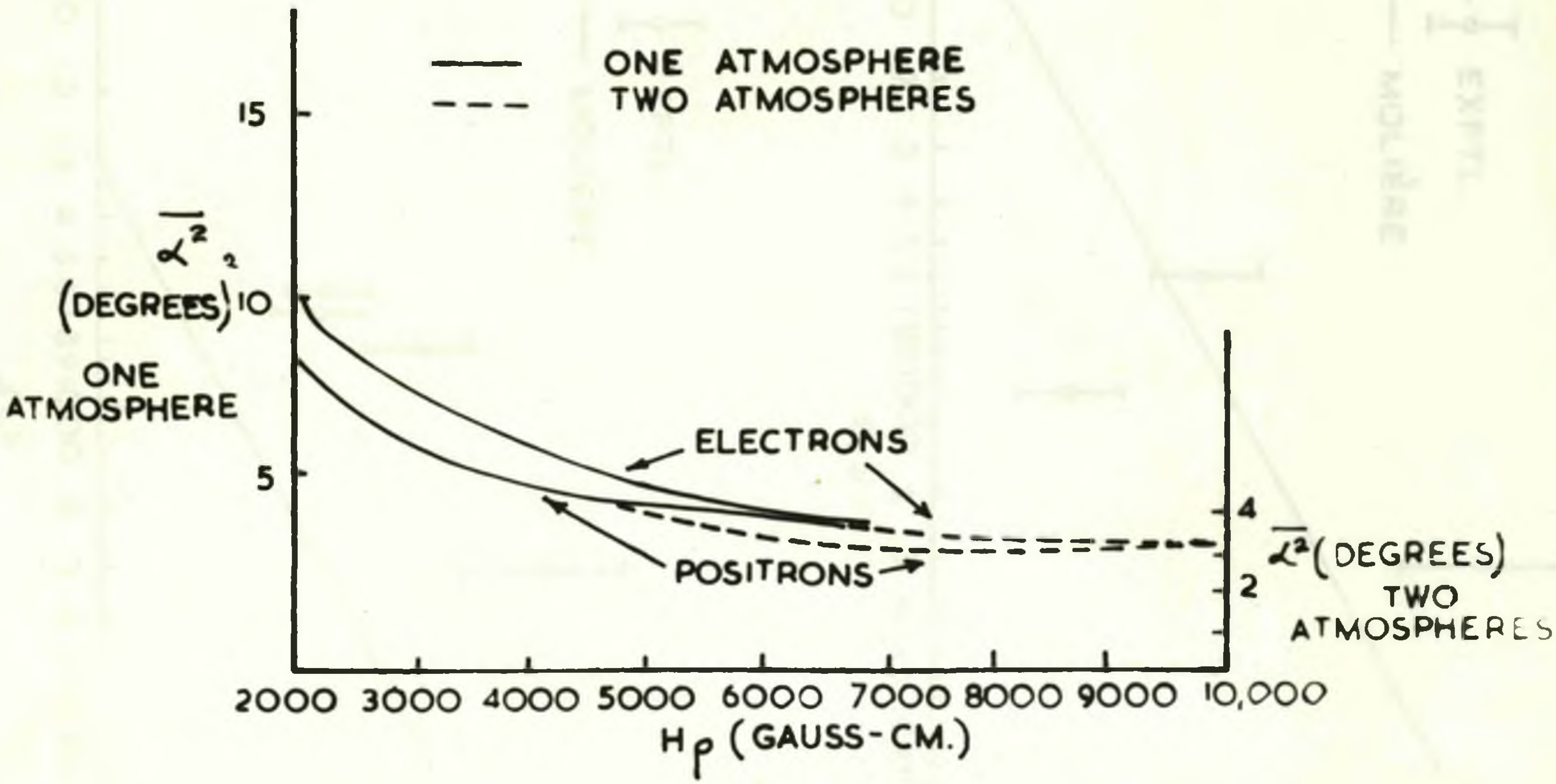

ONE ATMOSPHERE
TWO ATMOSPHERES
15
10
5
$\overline{\alpha^2}$ (DEGREES)^2
ONE ATMOSPHERE
ELECTRONS
POSITRONS
4
2
$\overline{\alpha^2}$ (DEGREES)
TWO ATMOSPHERES
2000
3000
4000
5000
6000
7000
8000
9000
10,000
$H\rho$ (GAUSS-CM.)

FIG. 34

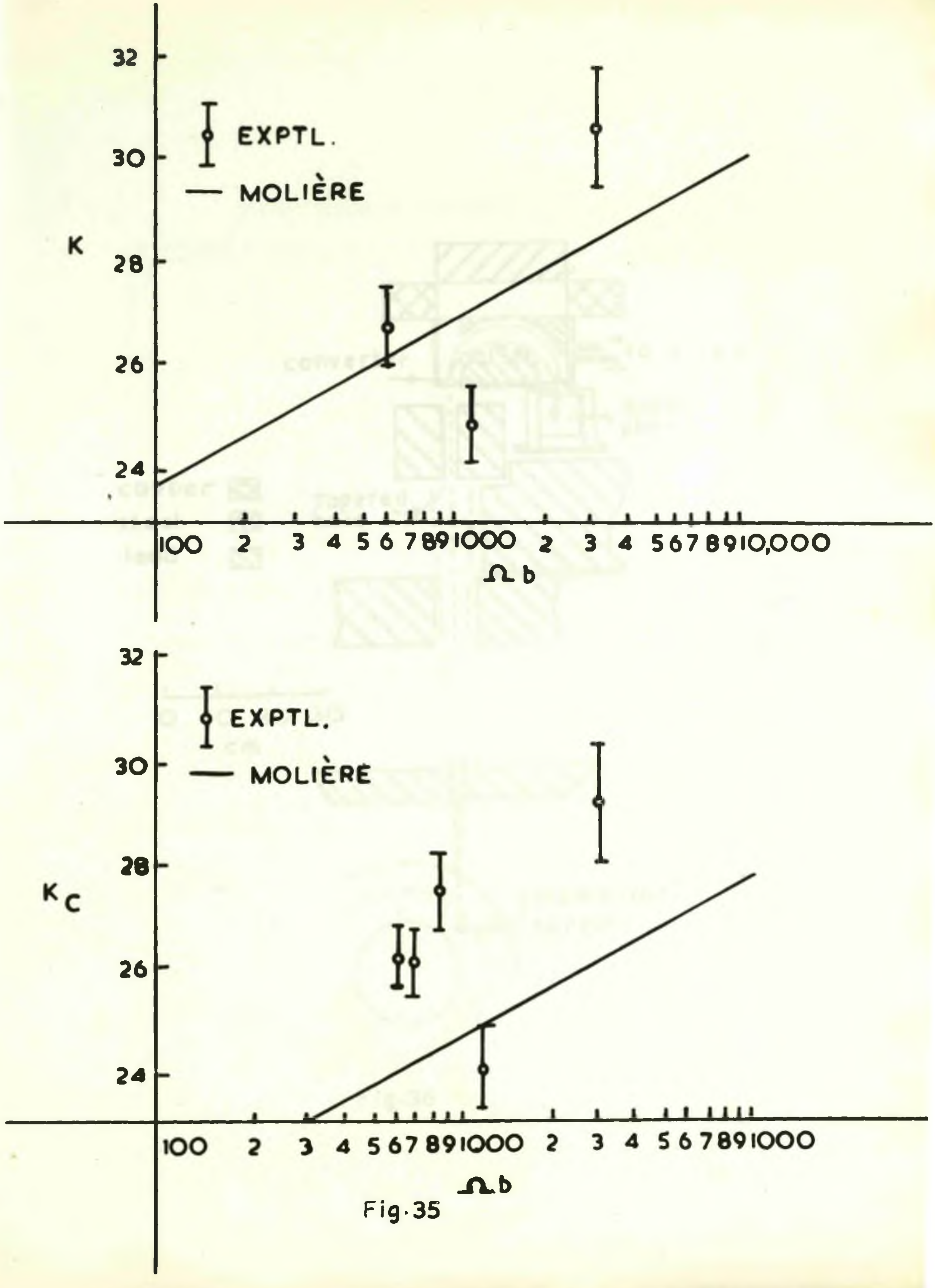
EXPTL.
MOLIÈRE
K
32
30
28
26
24
100 2 3 4 5 6 7 8 9 1000 2 3 4 5 6 7 8 9 10,000
Ωb
EXPTL.
MOLIÈRE
K_C
32
30
28
26
24
100 2 3 4 5 6 7 8 9 1000 2 3 4 5 6 7 8 9 1000
Ωb

Fig. 35

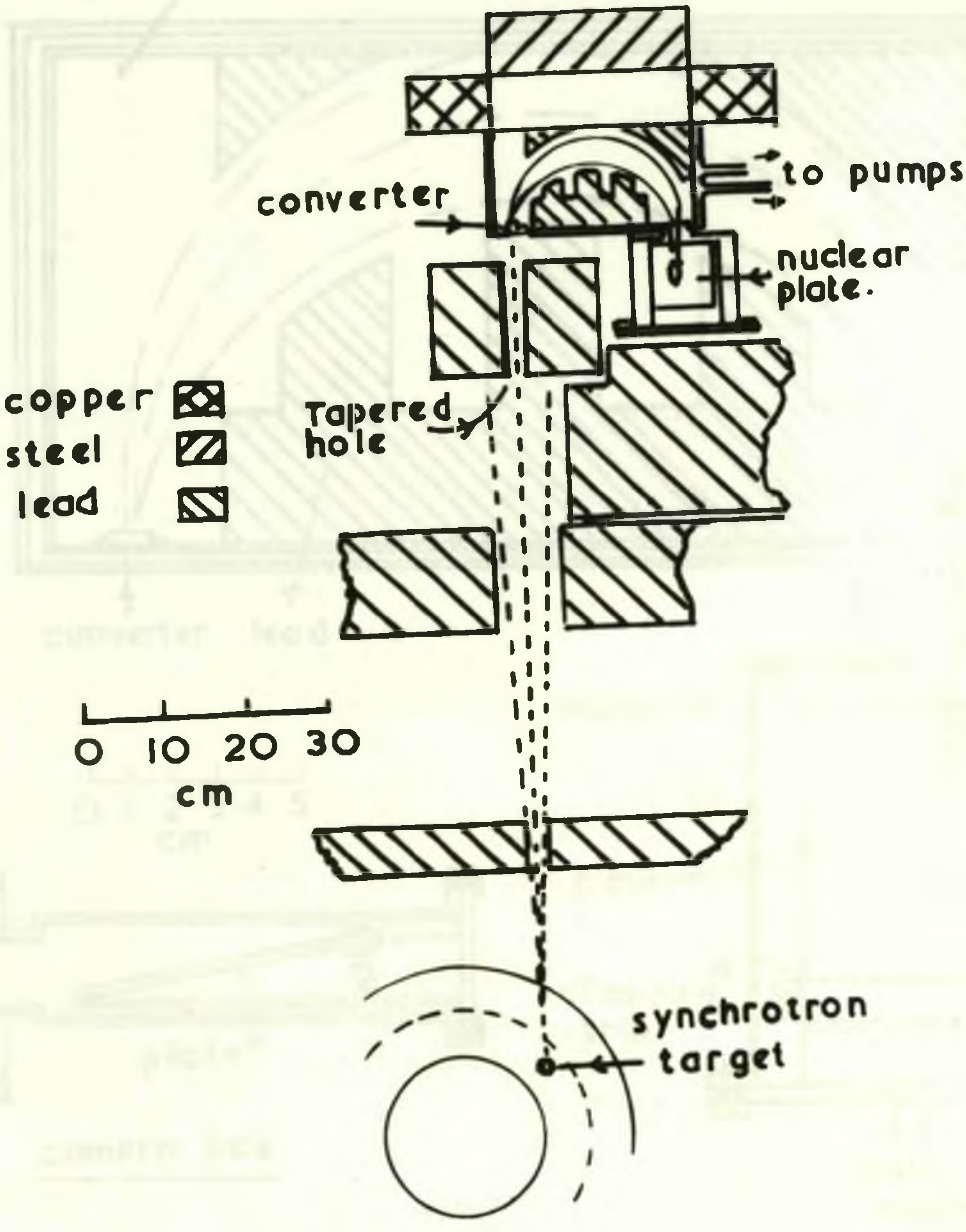
to pumps
converter
nuclear plate.
copper
steel
lead
Tapered hole
0 10 20 30
cm
synchrotron target

Fig.36

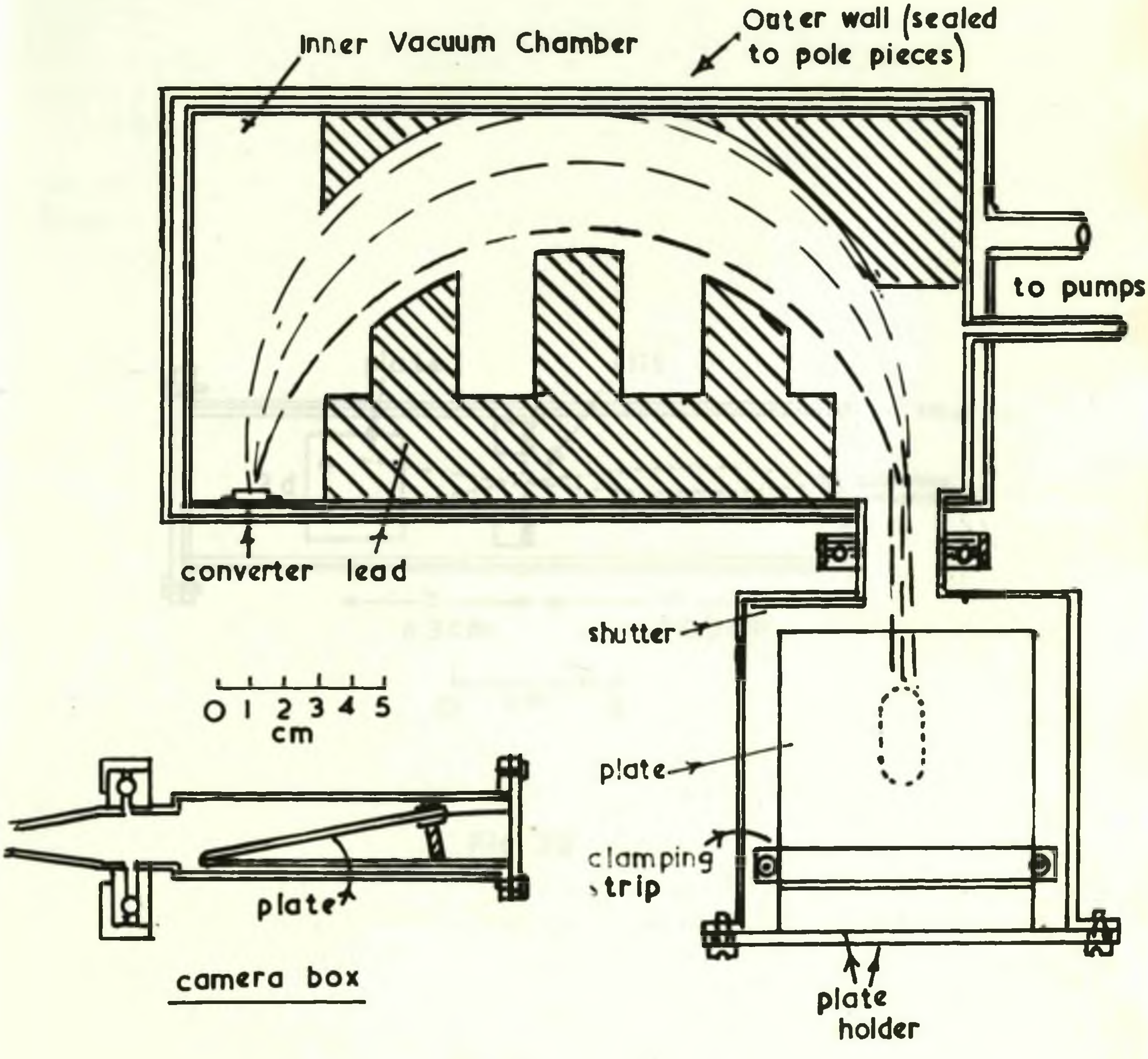

Inner Vacuum Chamber
Outer wall (sealed to pole pieces)
to pumps
converter
lead
shutter
0 1 2 3 4 5
cm
plate
clamping strip
plate
camera box
plate holder

Fig. 37

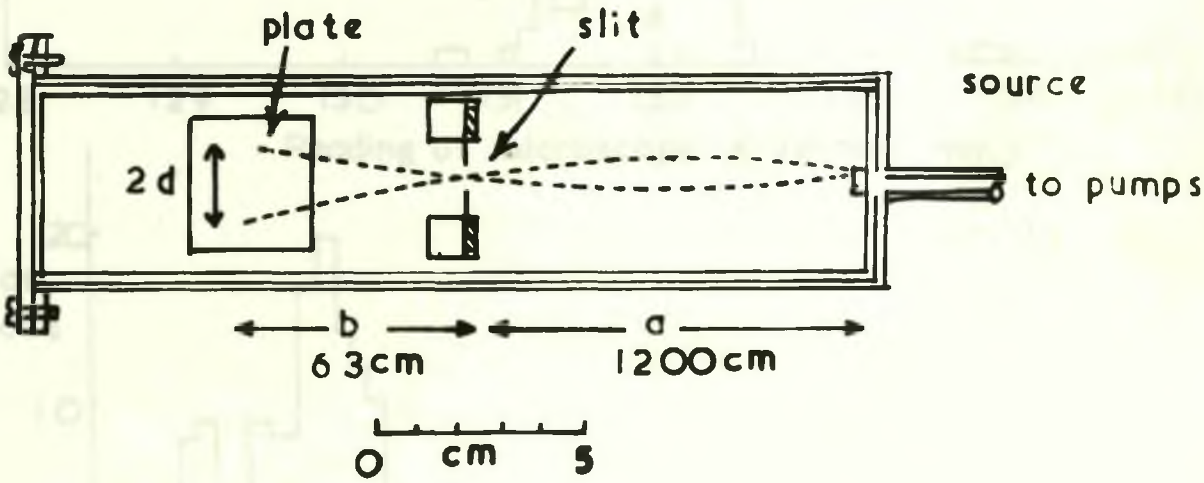

Fig. 38

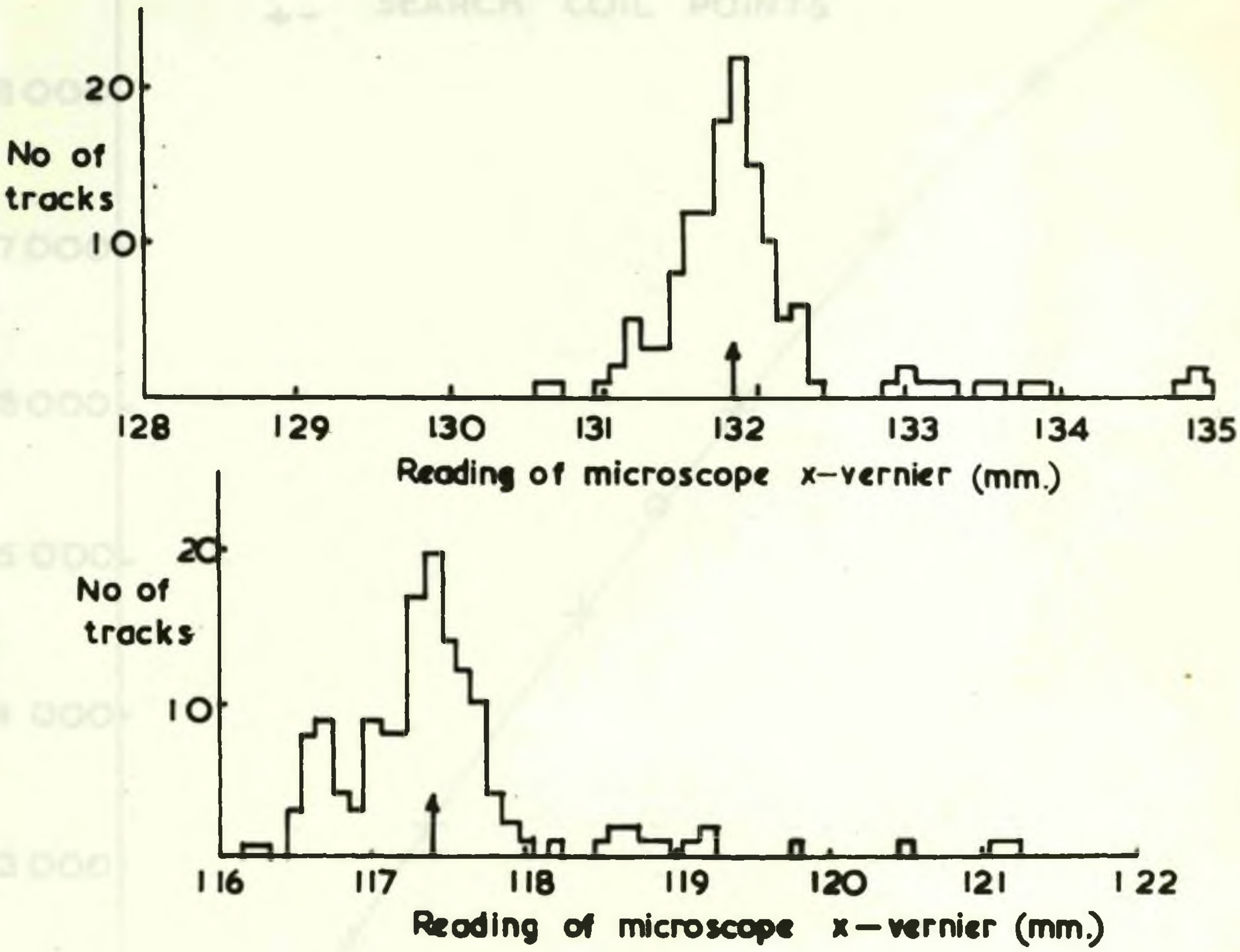

20
No of
tracks
10
128
129
130
131
132
133
134
135
Reading of microscope x-vernier (mm.)
20
No of
tracks
10
116
117
118
119
120
121
122
Reading of microscope x-vernier (mm.)

Fig. 39

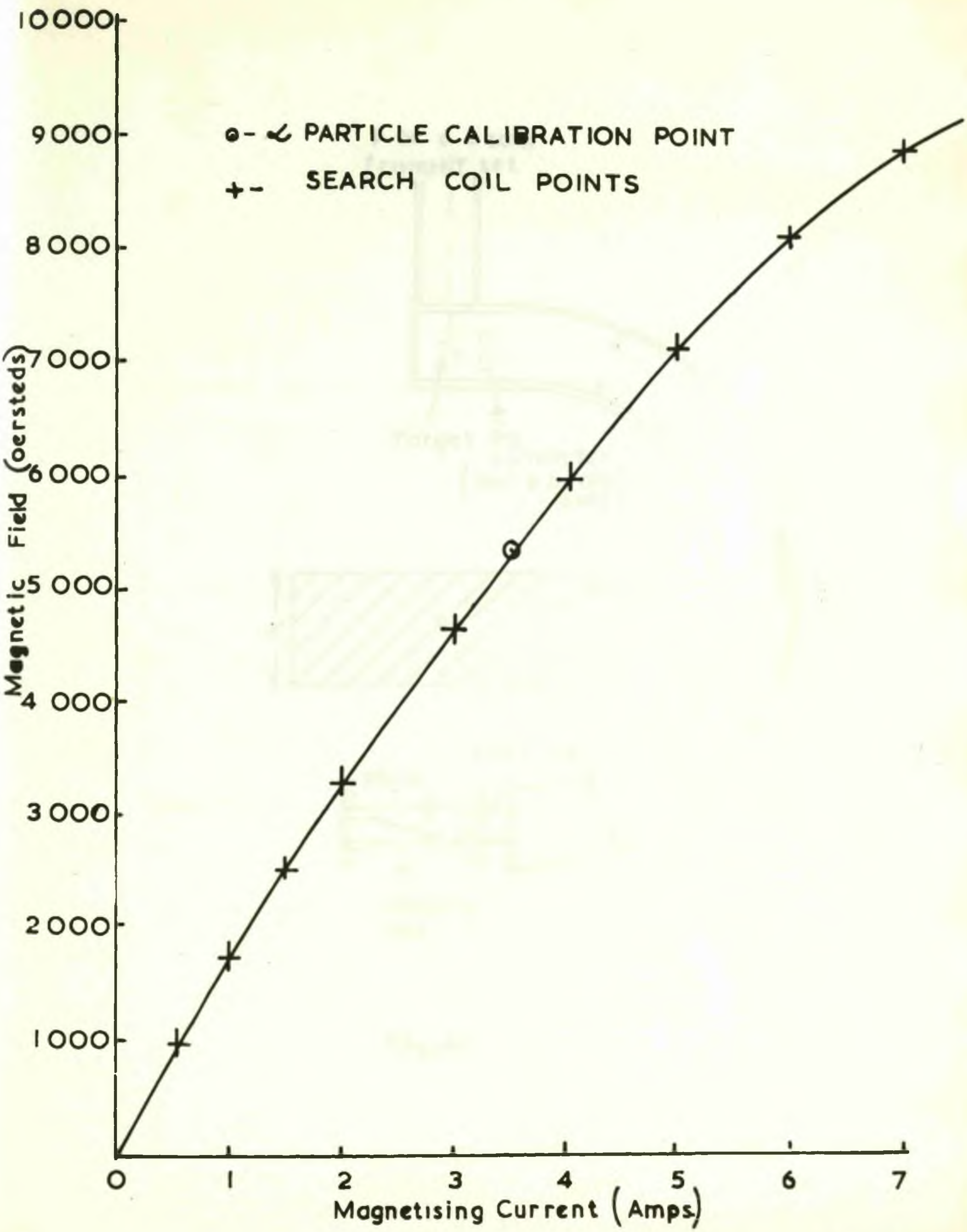

10000
9000
8000
7000
6000
5000
4000
3000
2000
1000
0
1
2
3
4
5
6
7
⊙ - α PARTICLE CALIBRATION POINT
+ - SEARCH COIL POINTS
Magnetic Field (oersteds)
Magnetising Current (Amps)

Fig. 40

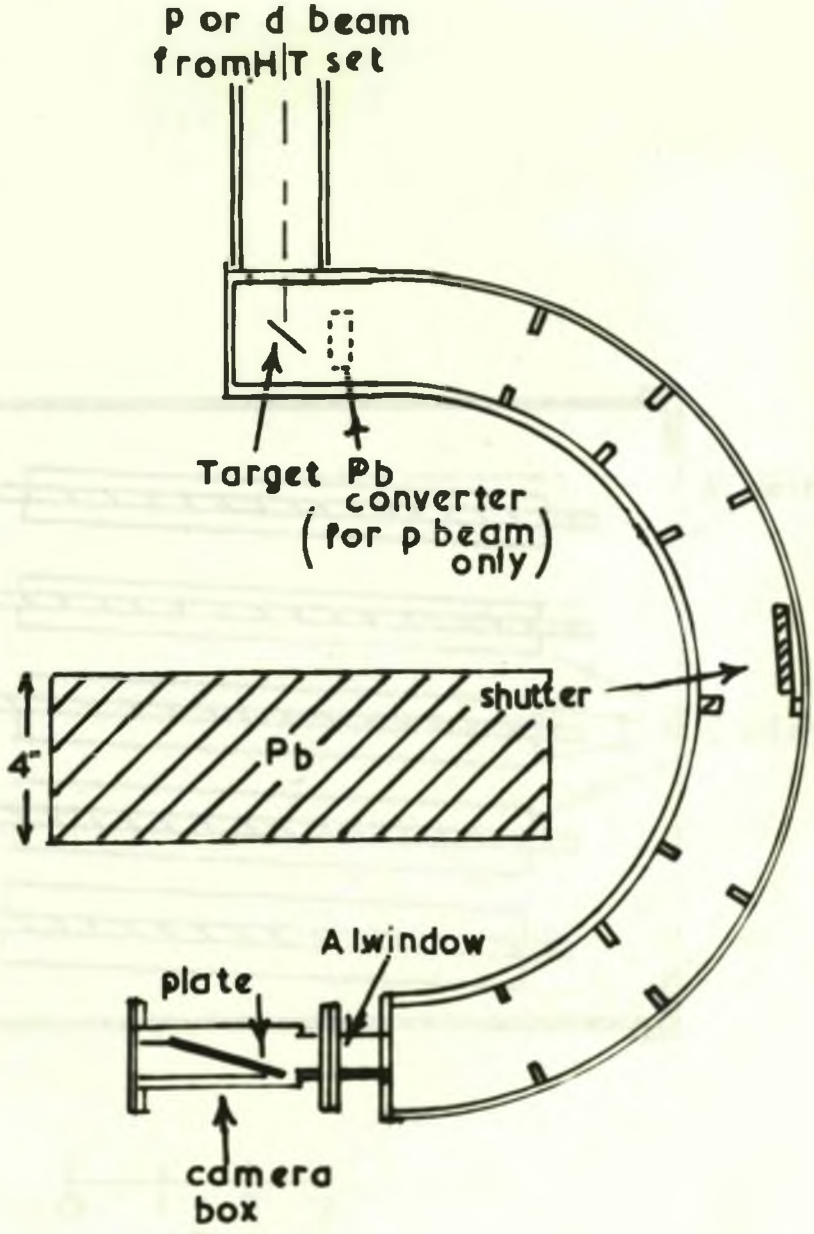
p or d beam
from H|T set
Target
Pb
converter
(for p beam only)
shutter
Pb
4"
Al window
plate
camera box

Fig. 41

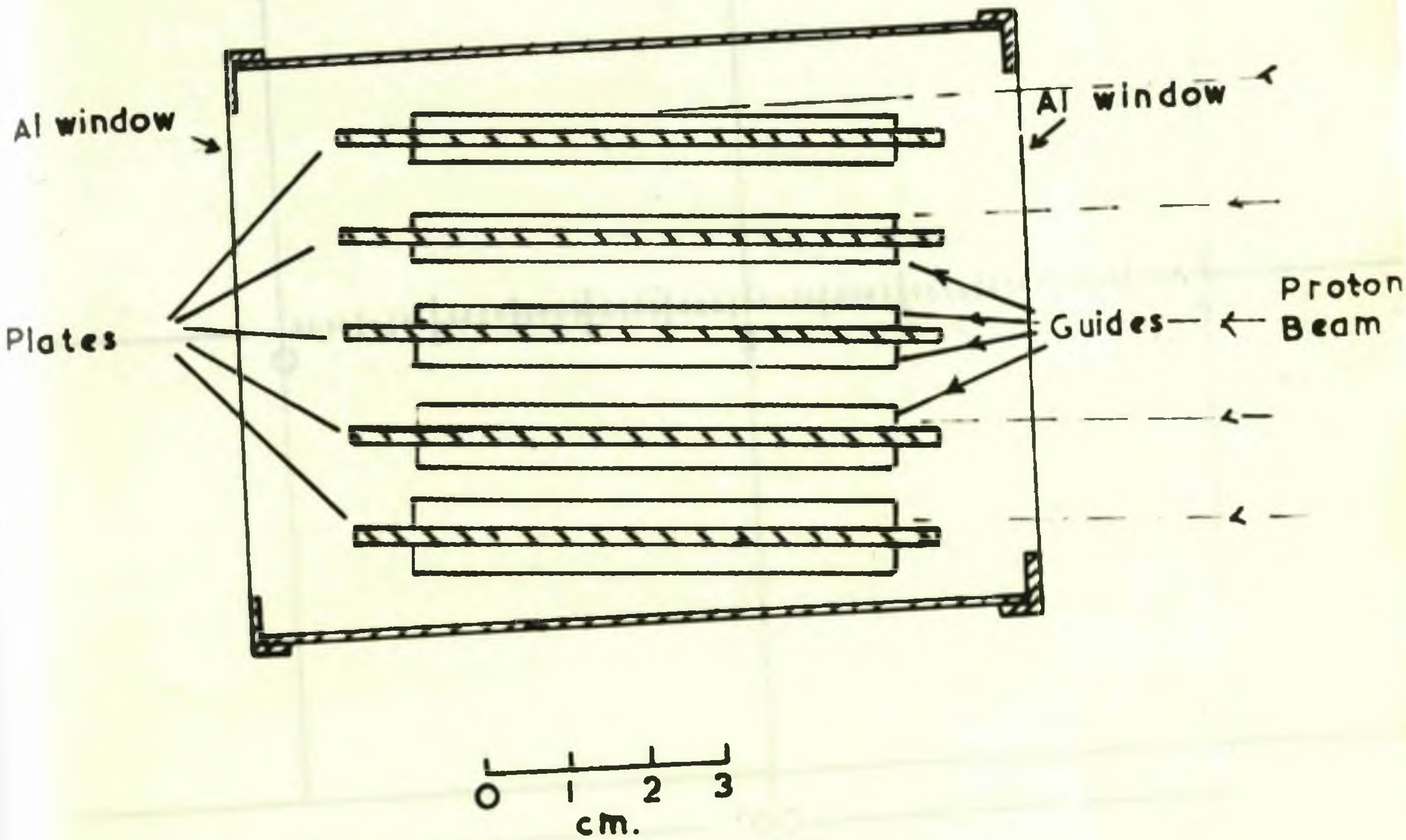

Fig. 42

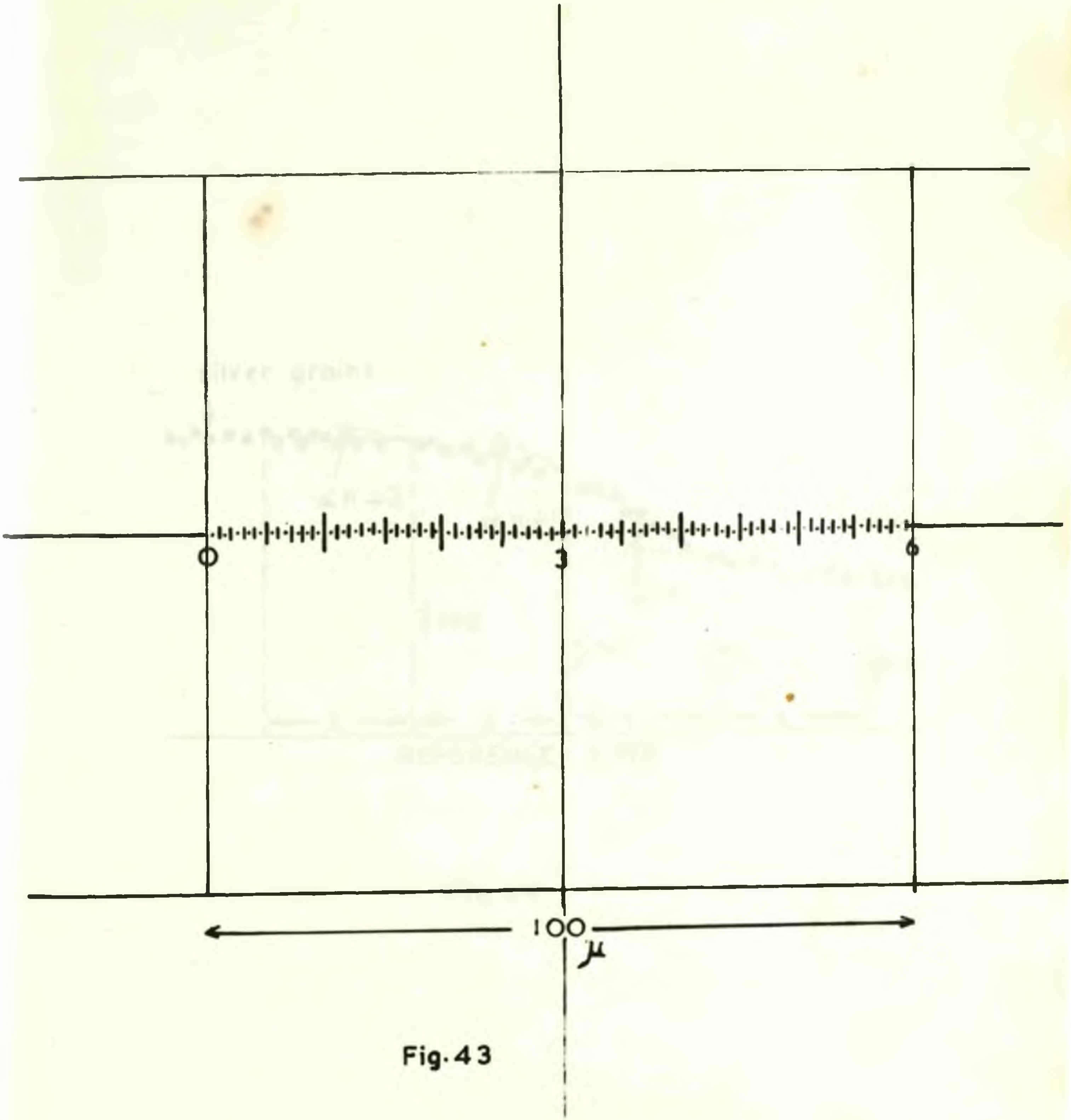

Fig. 43

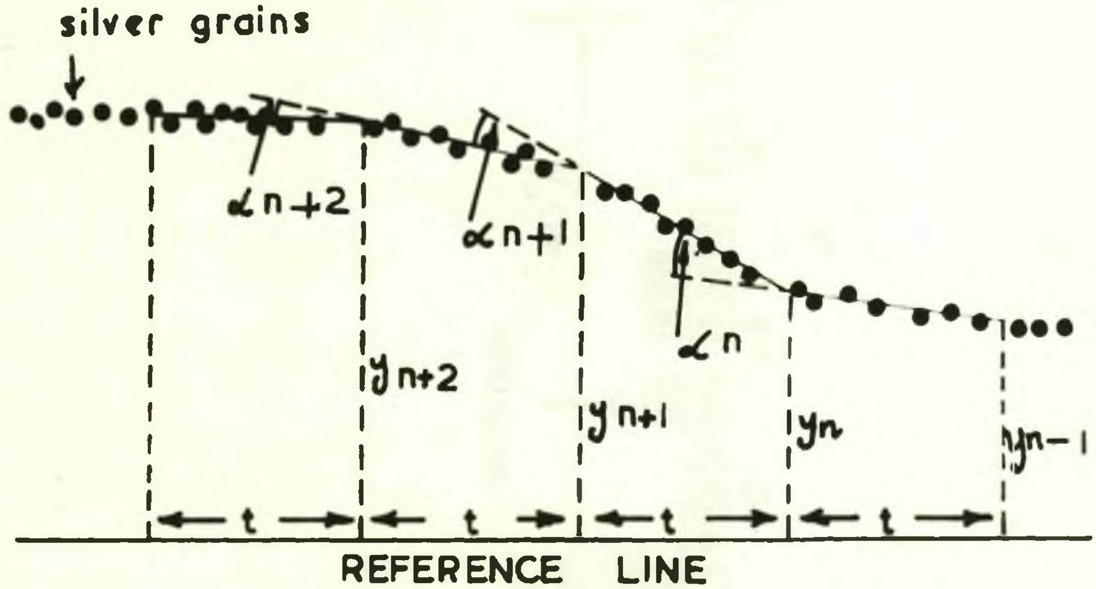

Fig. 44

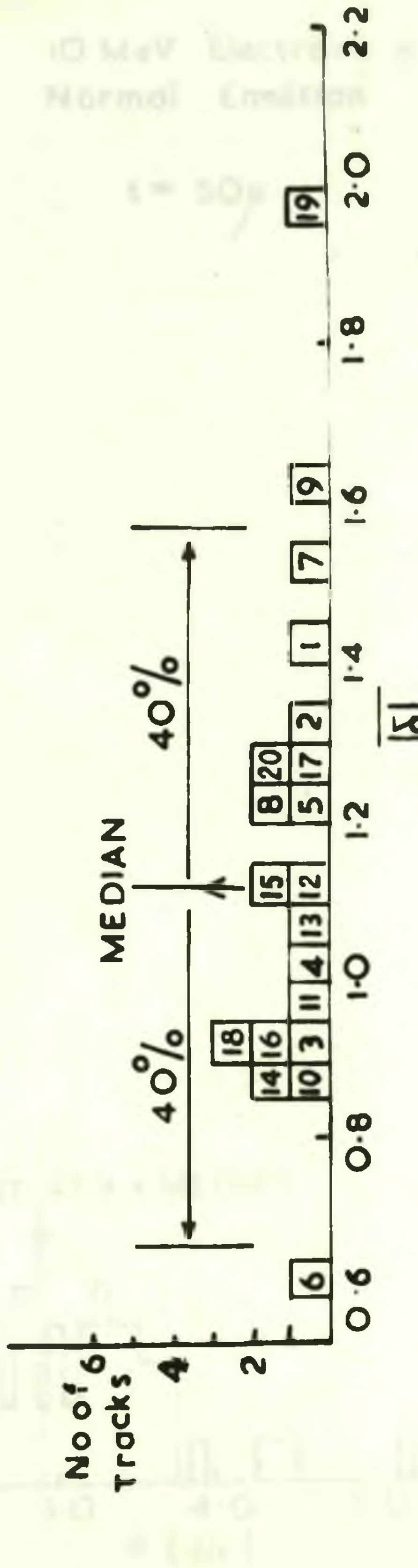
No. of Tracks
6
4
2
0·6
0·8
1·0
1·2
1·4
1·6
1·8
2·0
2·2
$\overline{|\delta|}$
MEDIAN
40%
40%
6
10
14
3
16
18
11
4
13
12
15
5
8
17
20
2
1
7
9
19

Fig.4 5

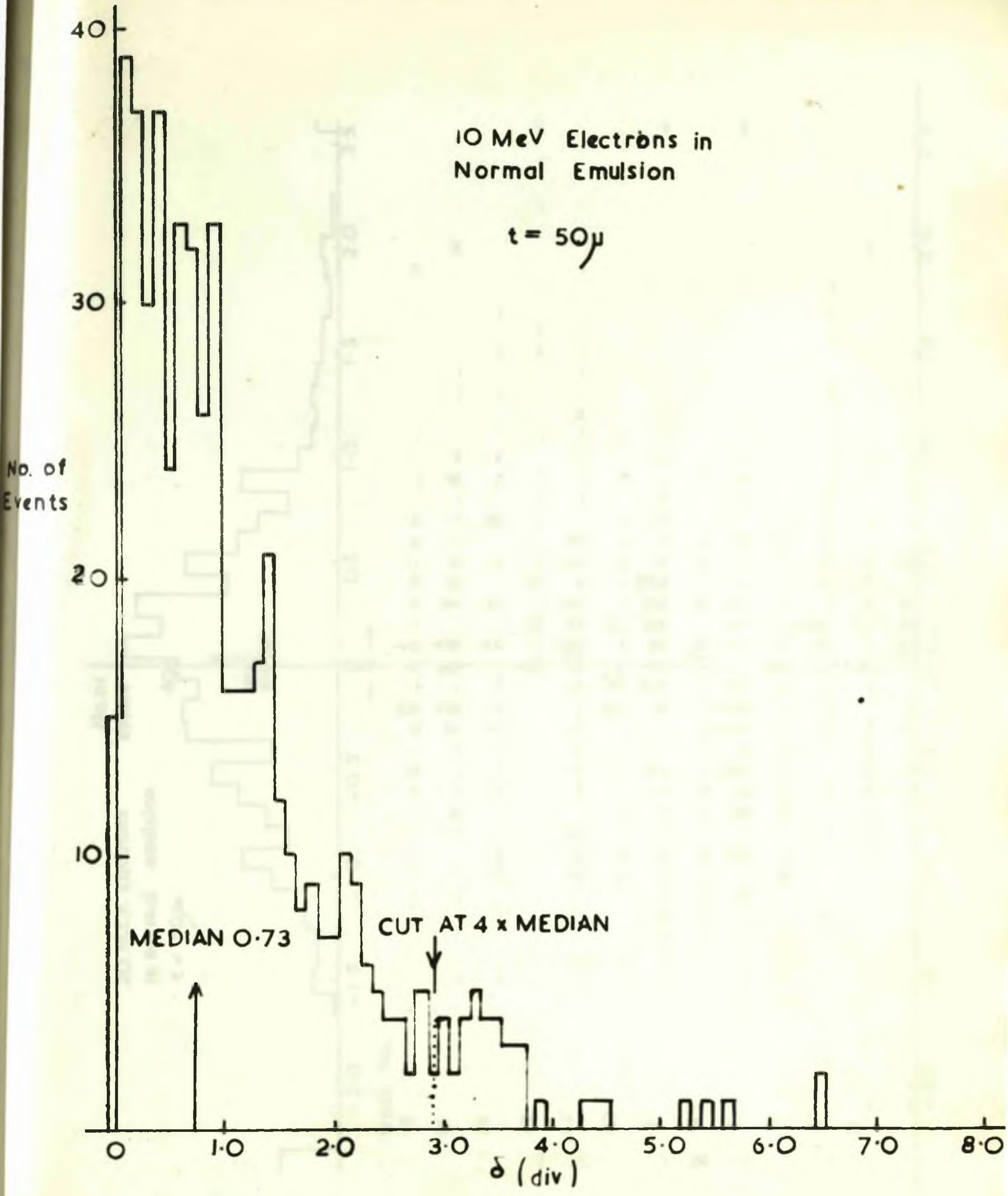

10 MeV Electrons in Normal Emulsion
t = 50μ
No. of Events
MEDIAN 0·73
CUT AT 4 x MEDIAN
δ (div)
0
1·0
2·0
3·0
4·0
5·0
6·0
7·0
8·0
10
20
30
40

Fig. 46

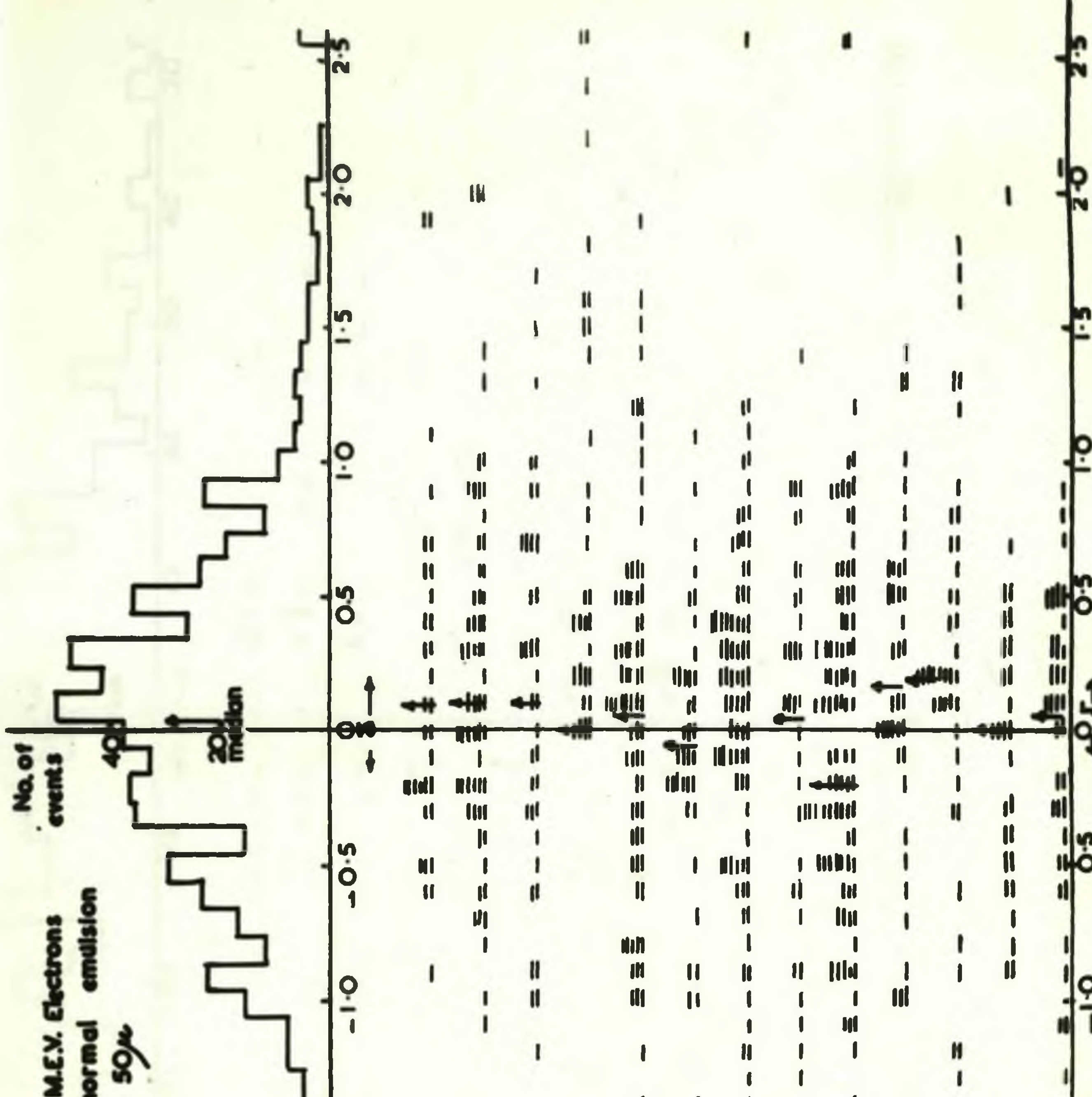
20 M.E.V. Electrons
in normal emulsion
t = 50μ
No. of events
40
20
median
track No.
15
14
13
12
11
10
9
8
7
6
5
2
1
−2·0
−1·5
−1·0
−0·5
0
0·5
1·0
1·5
2·0
2·5

Fig. 47a

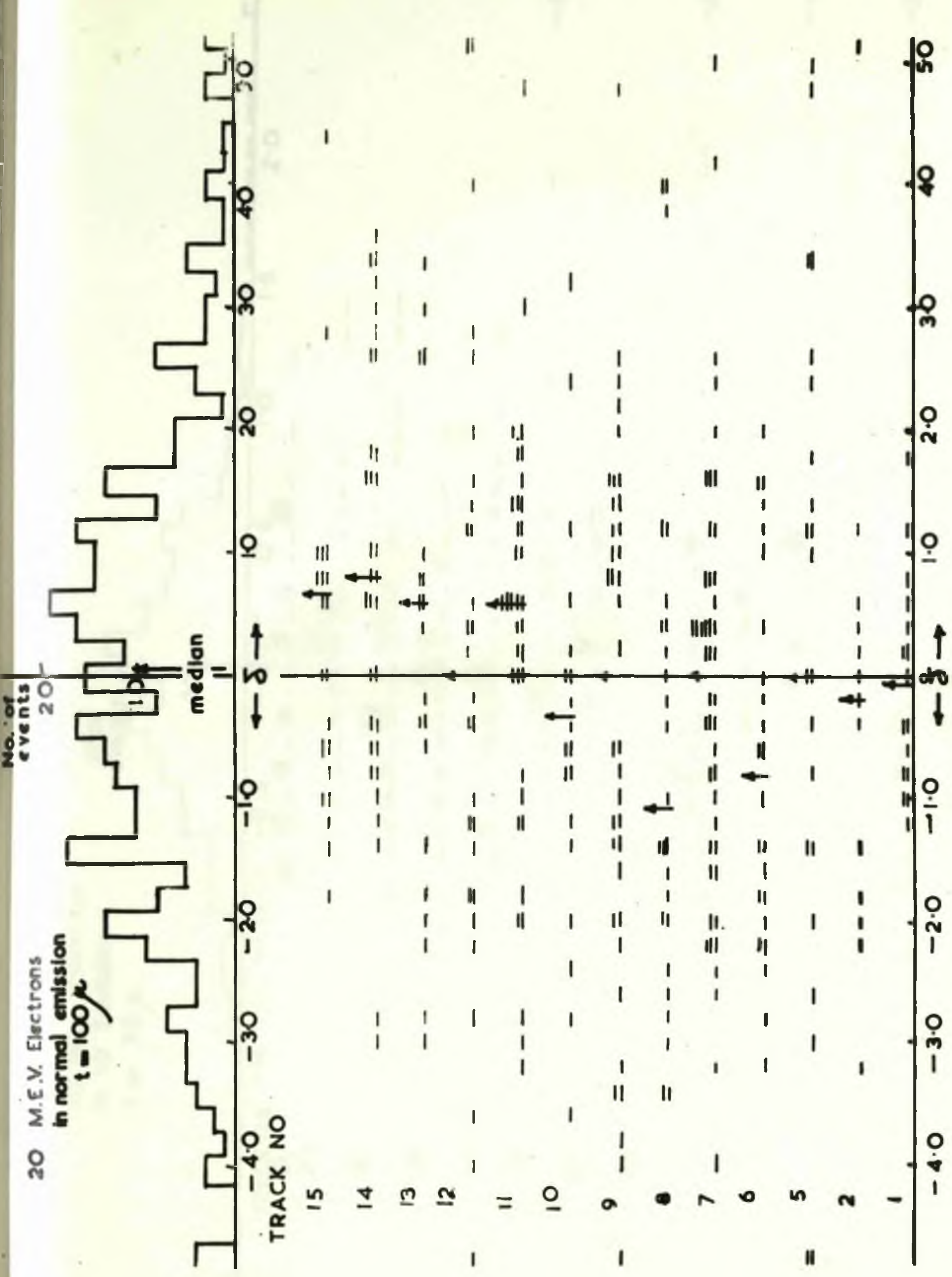
20 M.E.V. Electrons
in normal emission
t=100μ
No. of events
TRACK NO
median

Fig. 47b

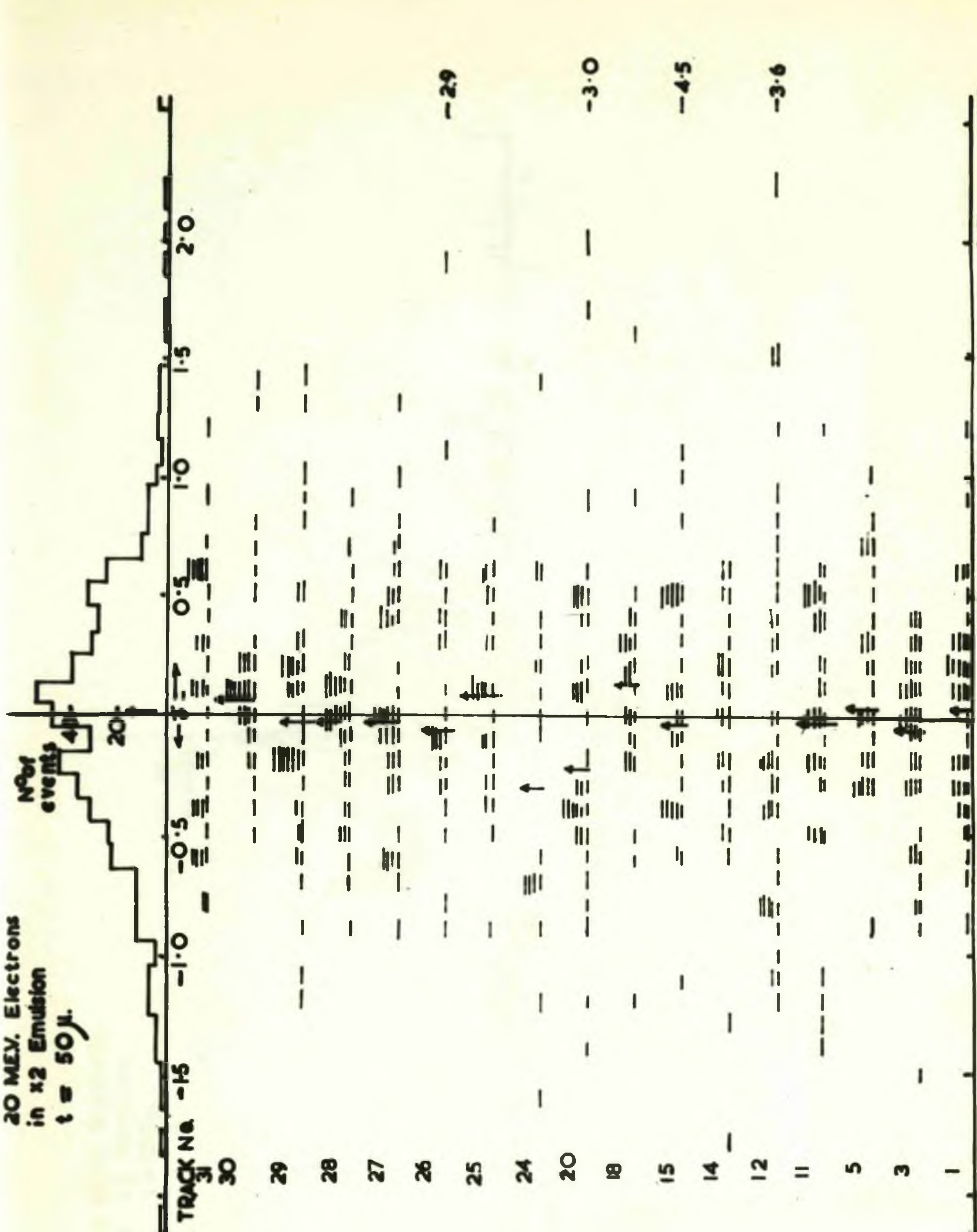
20 MEV. Electrons
in x2 Emulsion
t = 50μ.
Nº of events
TRACK No.
31
30
29
28
27
26
25
24
20
18
15
14
12
11
5
3
1
-2·9
-3·0
-4·5
-3·6
-2·0
-1·5
-1·0
-0·5
0
0·5
1·0
1·5
2·0
2·5
20
40
δ

Fig.47c

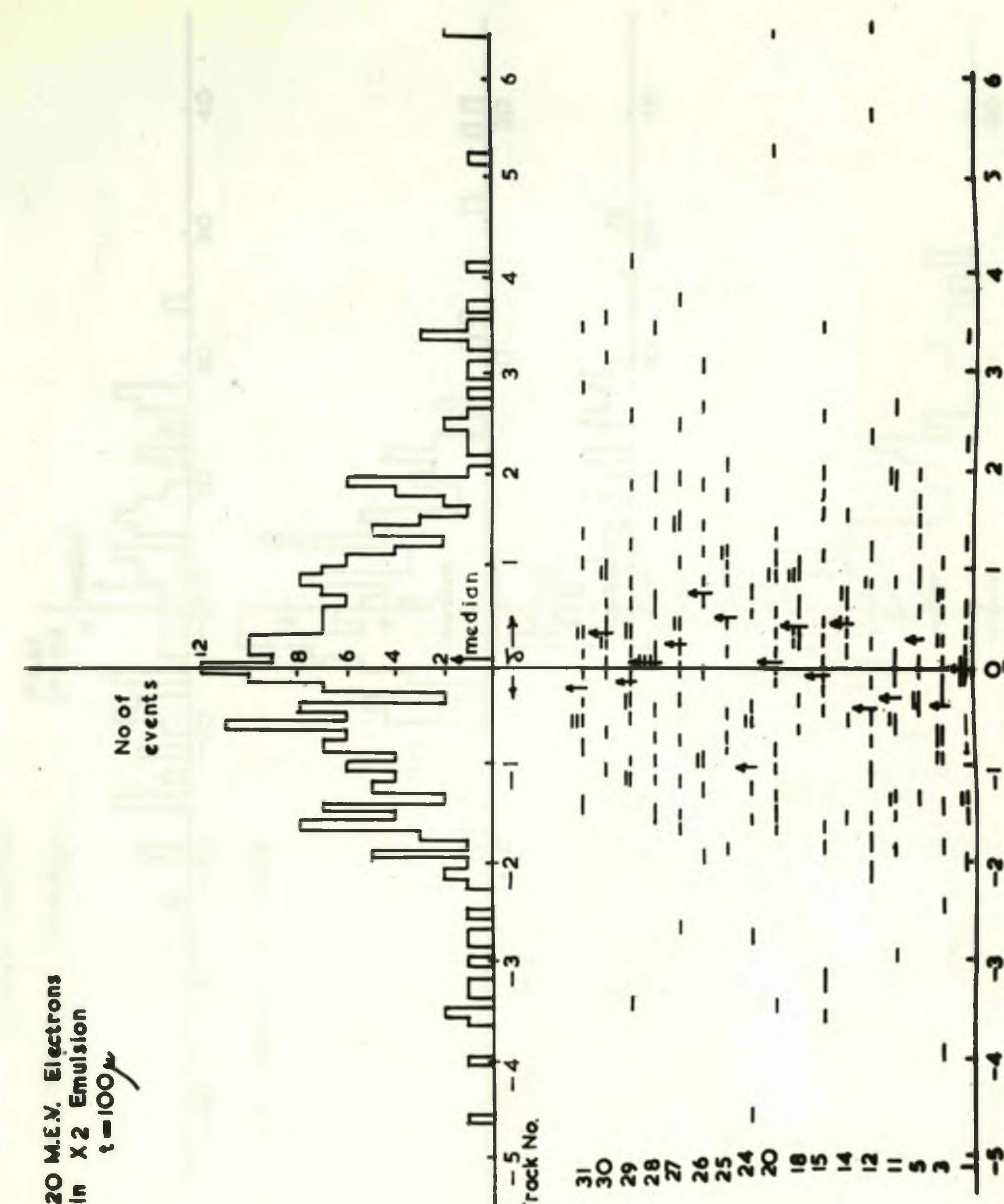
20 M.E.V. Electrons
In X2 Emulsion
t=100μ
No of events
median
δ
Track No.

Fig. 47d

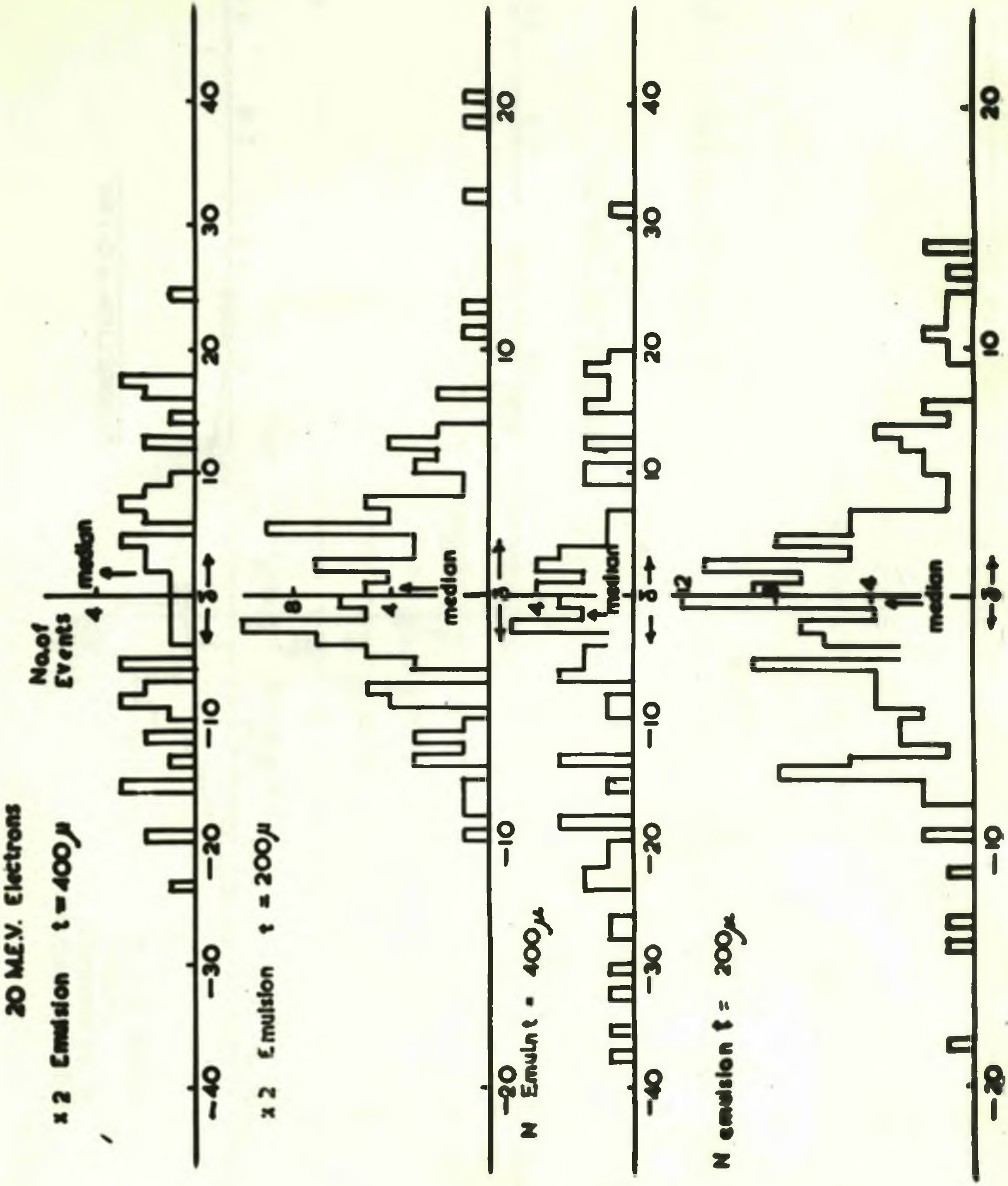

20 M.E.V. Electrons
x 2 Emulsion t = 400μ
x 2 Emulsion t = 200μ
N Emulsn t = 400μ
N emulsion t = 200μ
No.of Events
median

Fig.47e

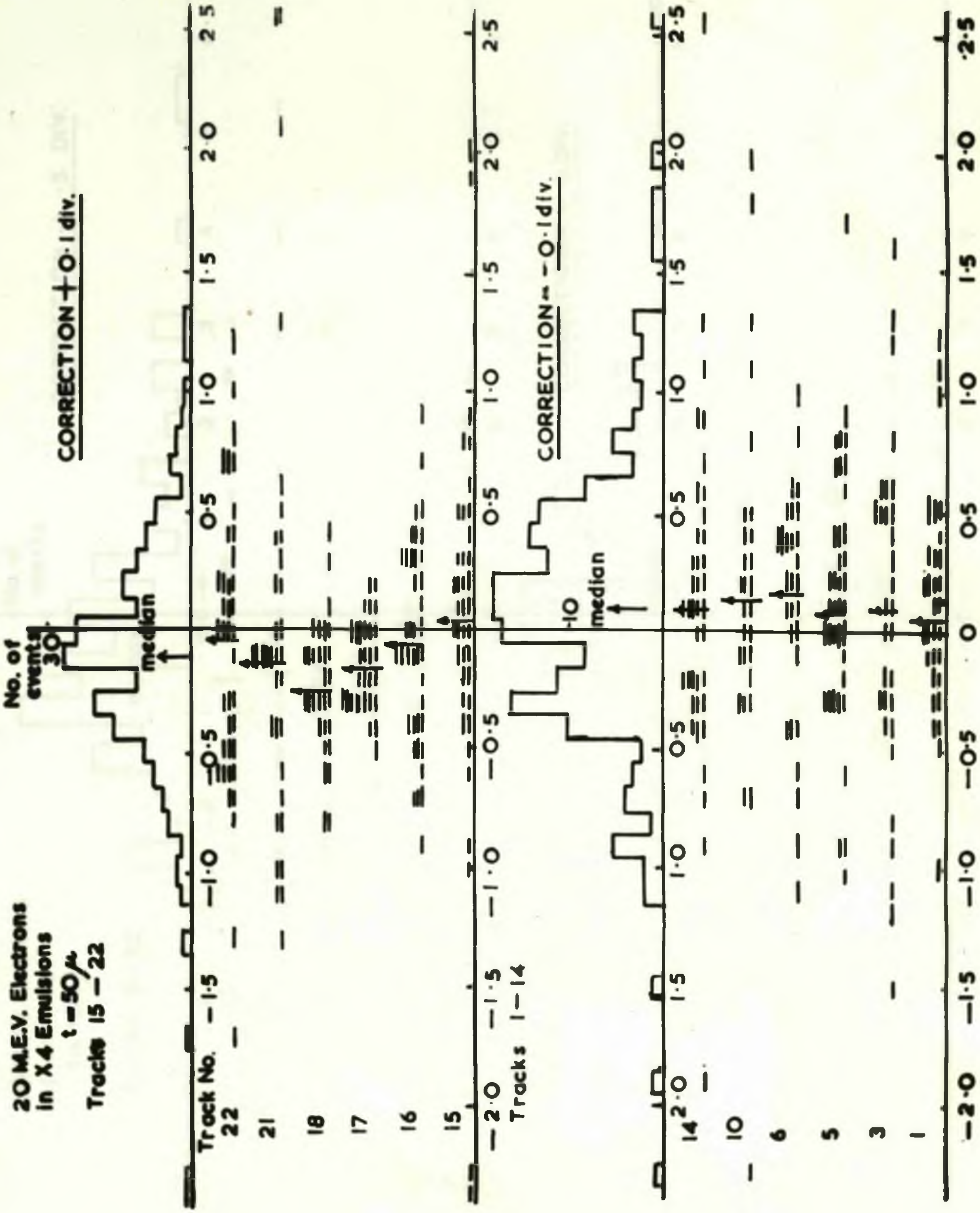
20 M.E.V. Electrons
in X.4 Emulsions
t = 50 μ
Tracks 15 – 22
CORRECTION + 0·1 div.
No. of events
30
median
Track No.
Tracks 1 – 14
CORRECTION = − 0·1 div.
median

Fig·48a

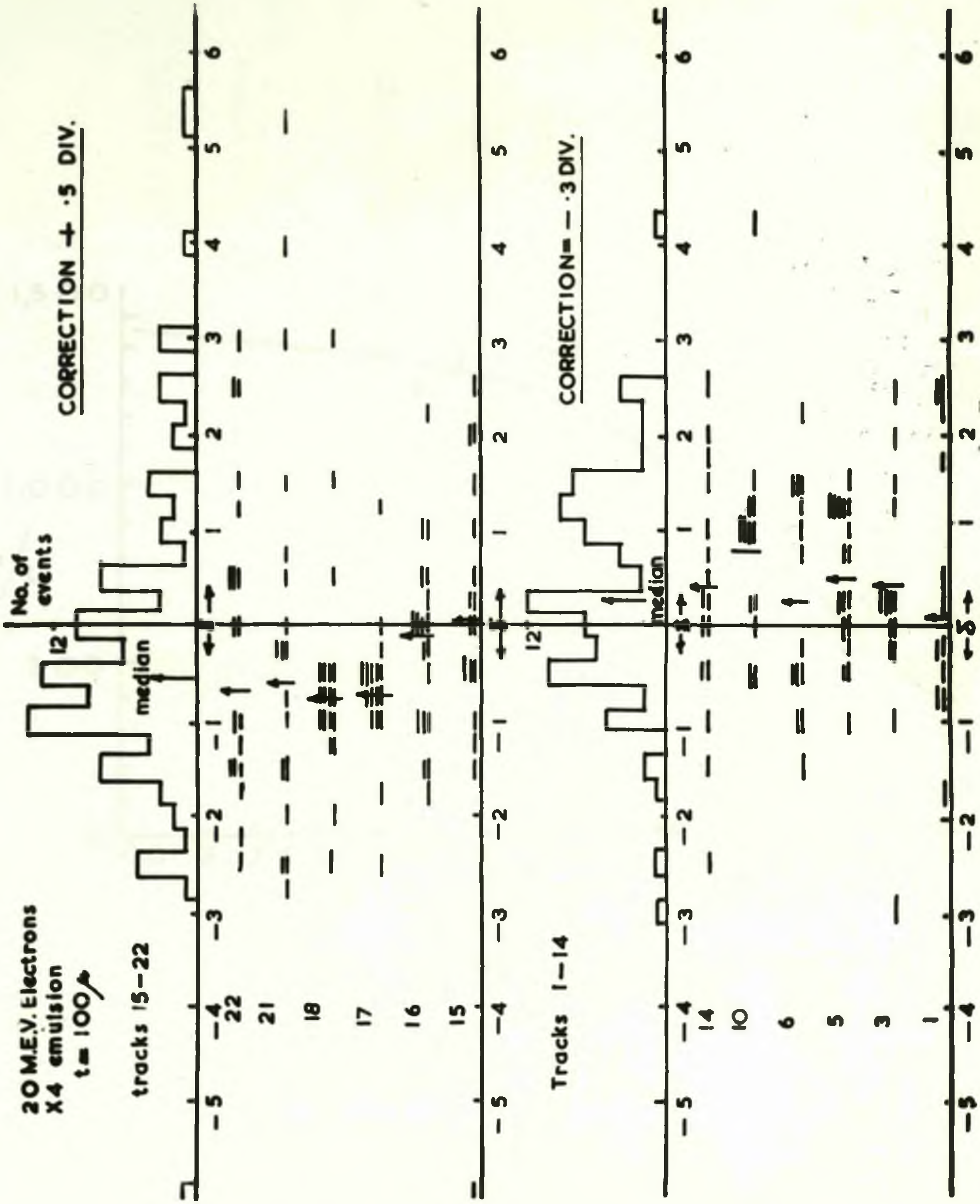
20 M.E.V. Electrons
X4 emulsion
t= 100μ
tracks 15–22
Tracks 1–14
CORRECTION + ·5 DIV.
CORRECTION= – ·3 DIV.
No. of events
median
12

Fig. 48b

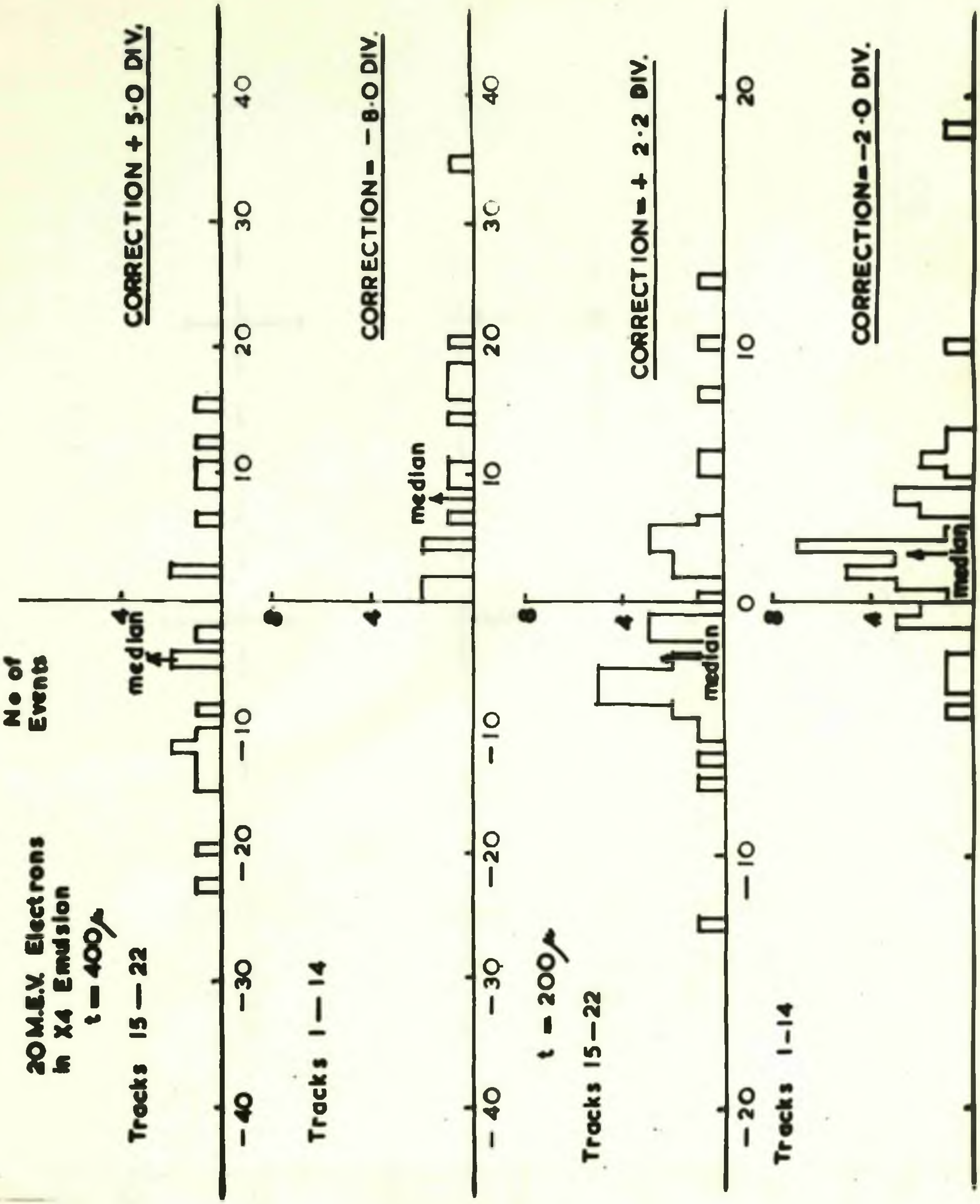
20 M.E.V. Electrons
in X4 Emulsion
t = 400μ
Tracks 15 — 22
No of Events
median
CORRECTION + 5·0 DIV.
Tracks 1 — 14
median
CORRECTION = −8·0 DIV.
t = 200μ
Tracks 15—22
median
CORRECTION = + 2·2 DIV.
Tracks 1-14
median
CORRECTION = −2·0 DIV.

Fig.48c

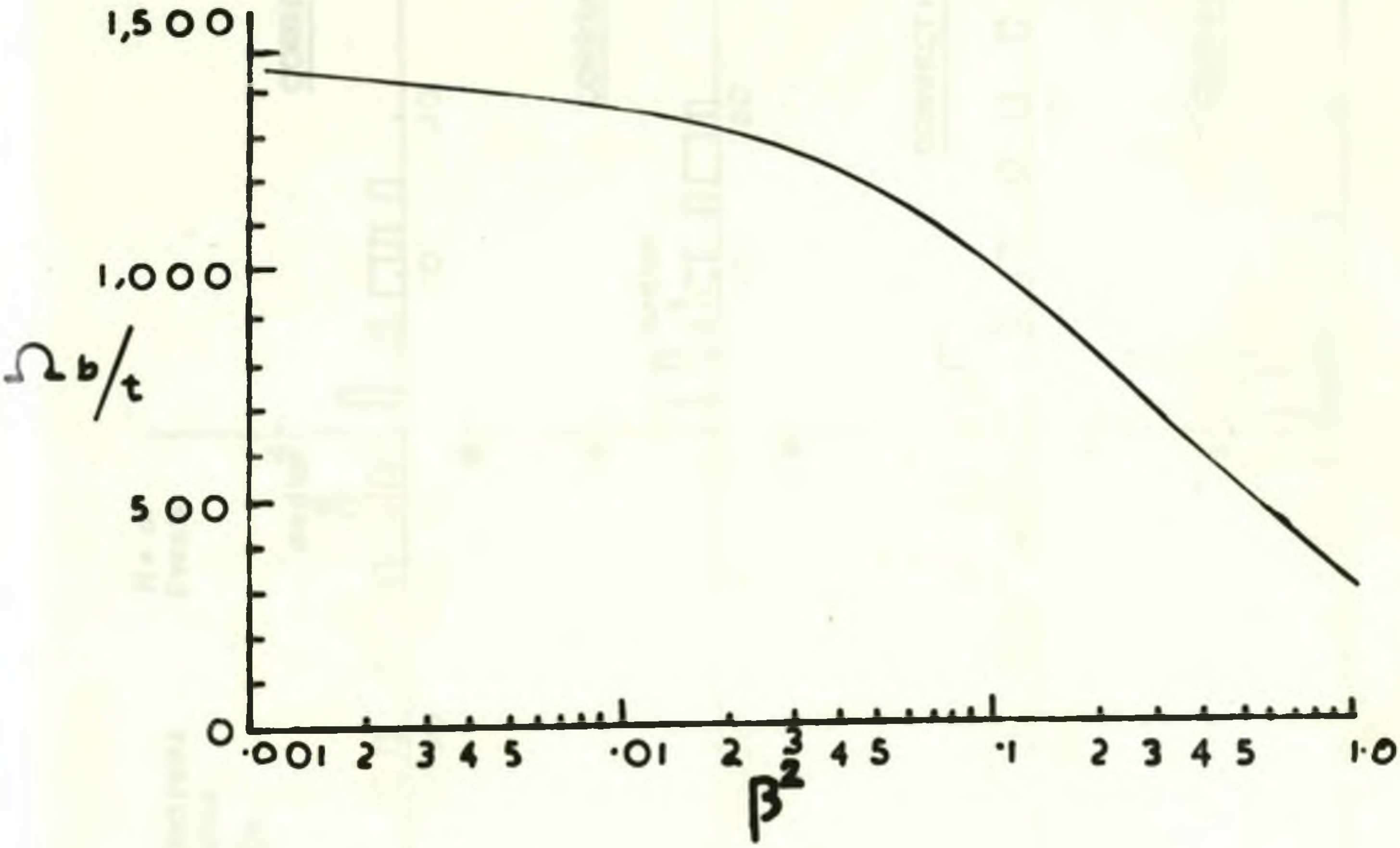

Fig. 49

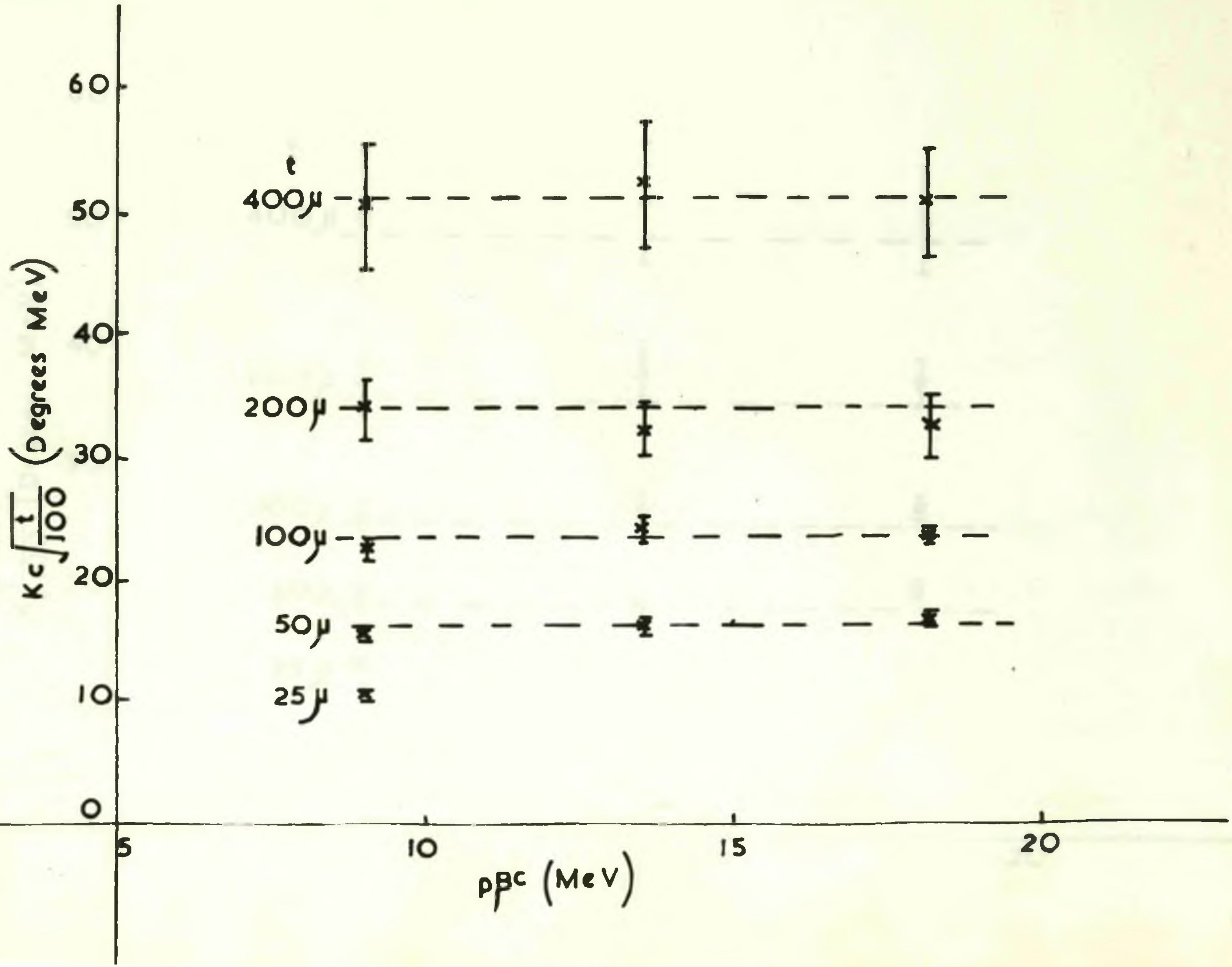

60
50
40
30
20
10
0
5
10
15
20
t
400μ
200μ
100μ
50μ
25μ
Kc √(t/100) (Degrees MeV)
pβc (MeV)

Fig. 50a

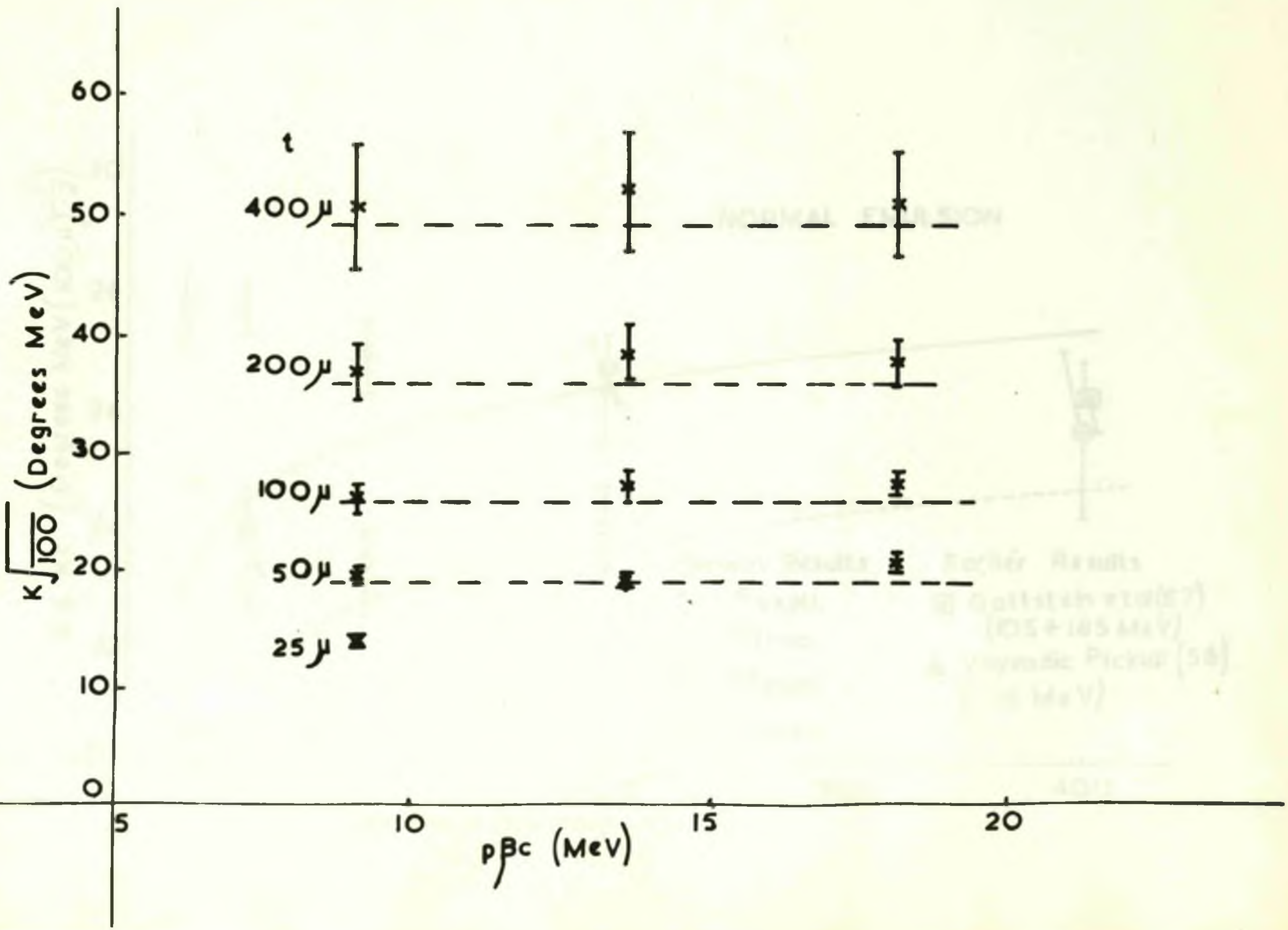

$K\sqrt{100}$ (Degrees MeV)
60
50
40
30
20
10
0
t
400μ
200μ
100μ
50μ
25μ
5
10
15
20
pβc (MeV)

Fig. 50b

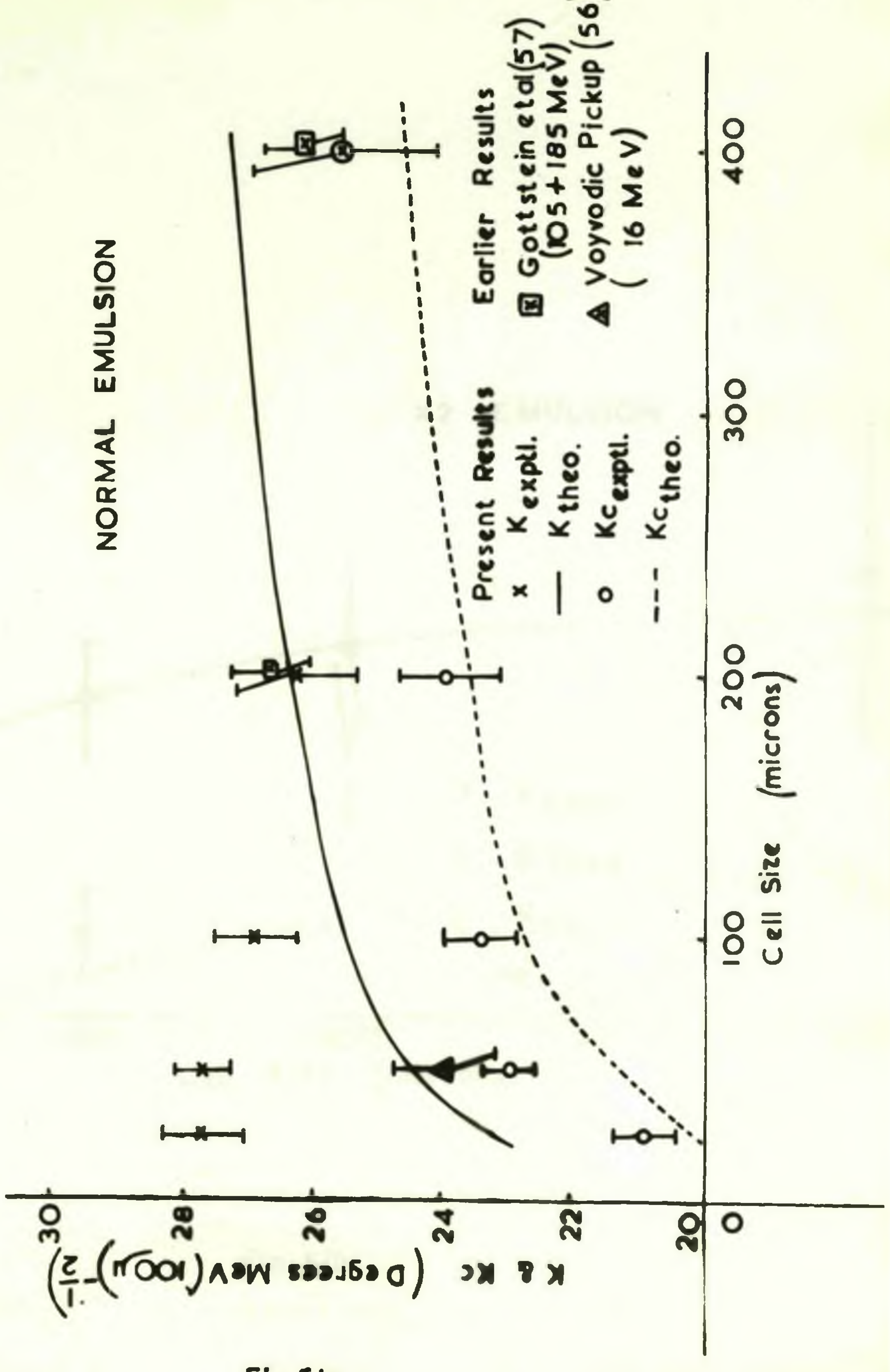
NORMAL EMULSION
Present Results
x $K_{exptl.}$
— $K_{theo.}$
o $Kc_{exptl.}$
--- $Kc_{theo.}$
Earlier Results
Gottstein et al (57) (105+185 MeV)
Voyvodic Pickup (56) (16 MeV)
K & Kc (Degrees MeV $(100\mu)^{-\frac{1}{2}}$)
Cell Size (microns)
0
100
200
300
400
20
22
24
26
28
30

Fig. 51a

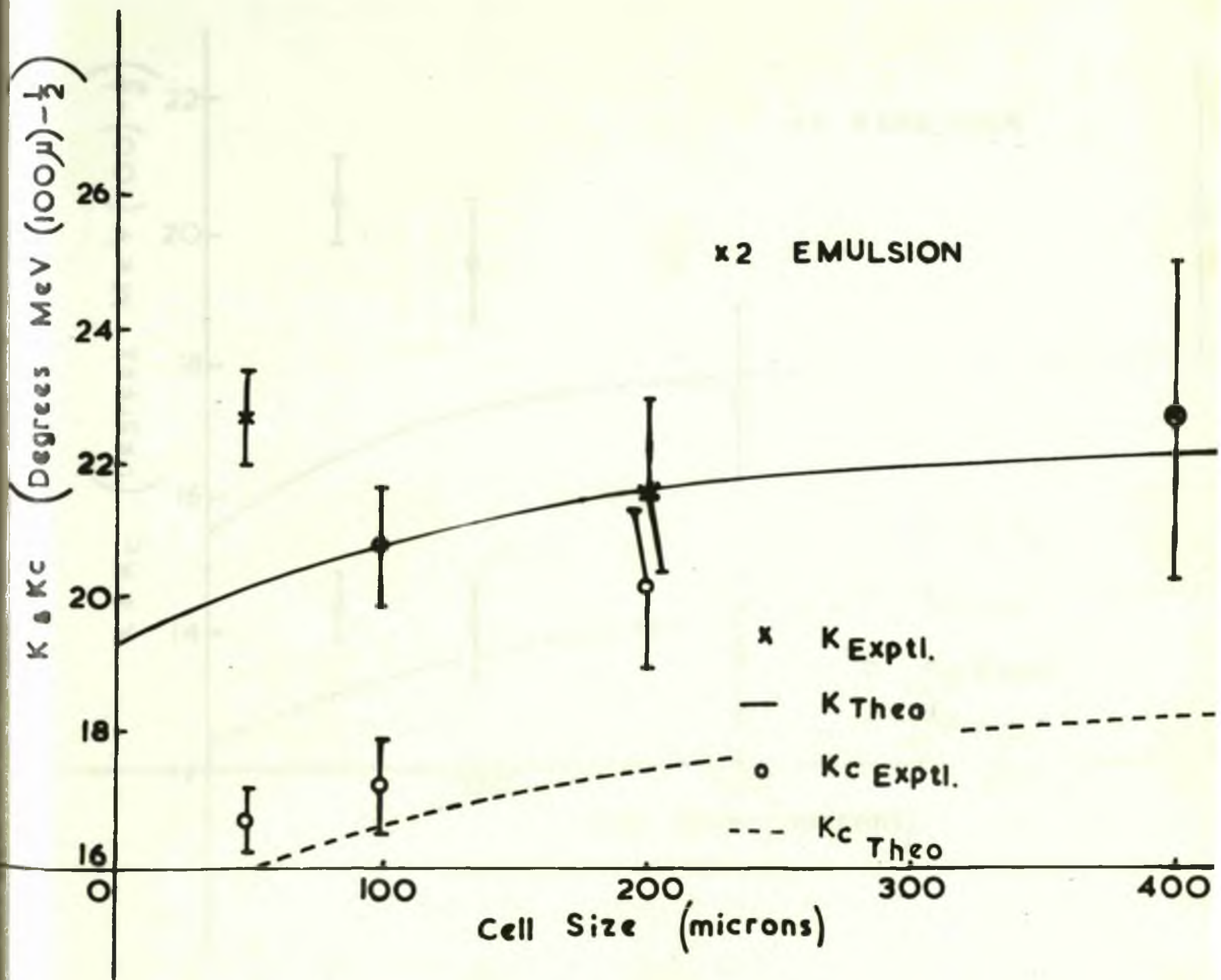

K & Kc (Degrees MeV (100μ)-½)
26
24
22
20
18
16
x2 EMULSION
x K Exptl.
K Theo
o Kc Exptl.
Kc Theo
0
100
200
300
400
Cell Size (microns)

Fig. 51b

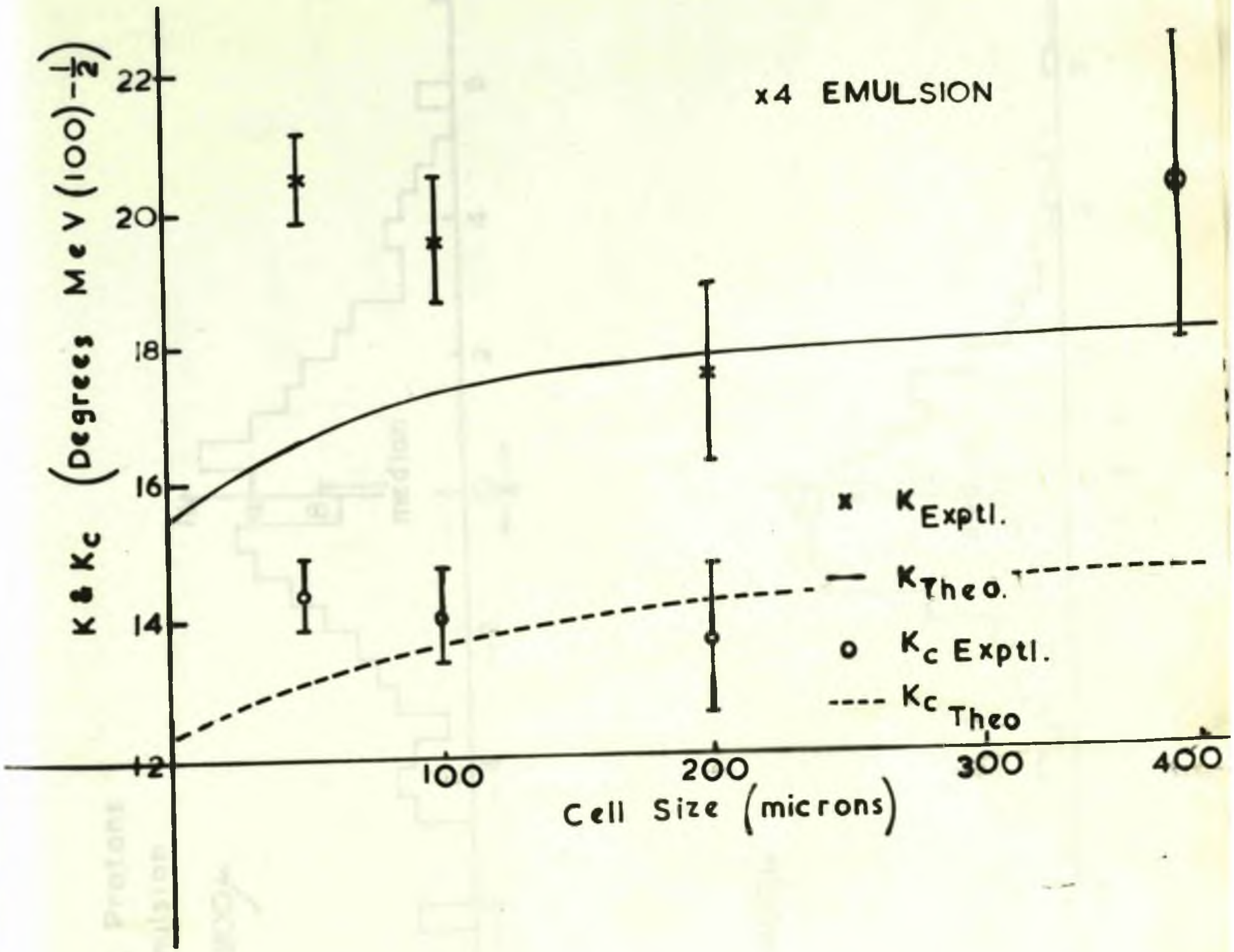
x4 EMULSION
K & Kc (Degrees MeV (100)^-1/2)
22
20
18
16
14
12
100
200
300
400
Cell Size (microns)
x K Exptl.
— K Theo.
o Kc Exptl.
---- Kc Theo

Fig. 51c

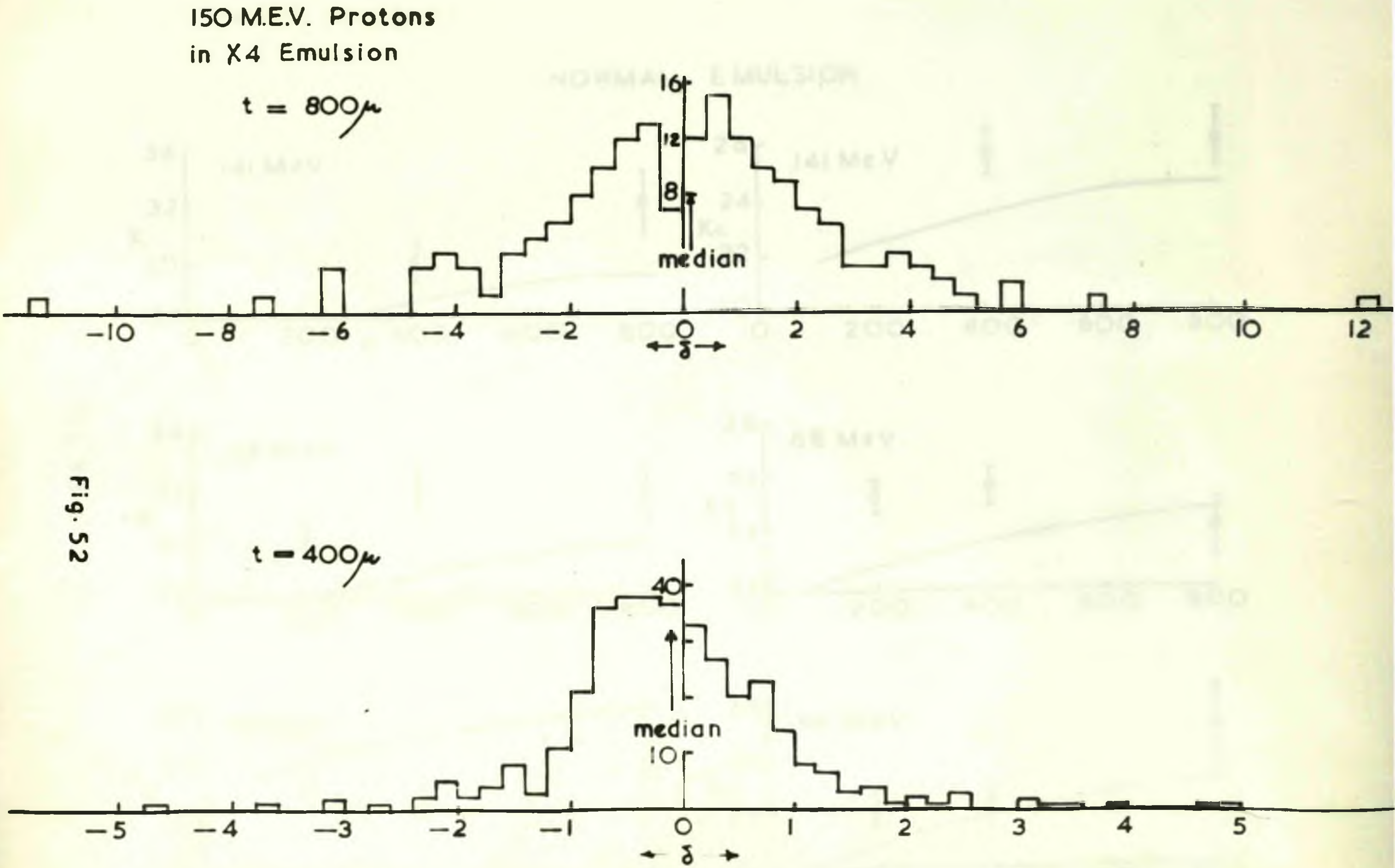
150 M.E.V. Protons
in X4 Emulsion
t = 800μ
16
12
8
median
-10
-8
-6
-4
-2
0
2
4
6
8
10
12
δ
t = 400μ
40
median
10
-5
-4
-3
-2
-1
0
1
2
3
4
5
δ

Fig. 52

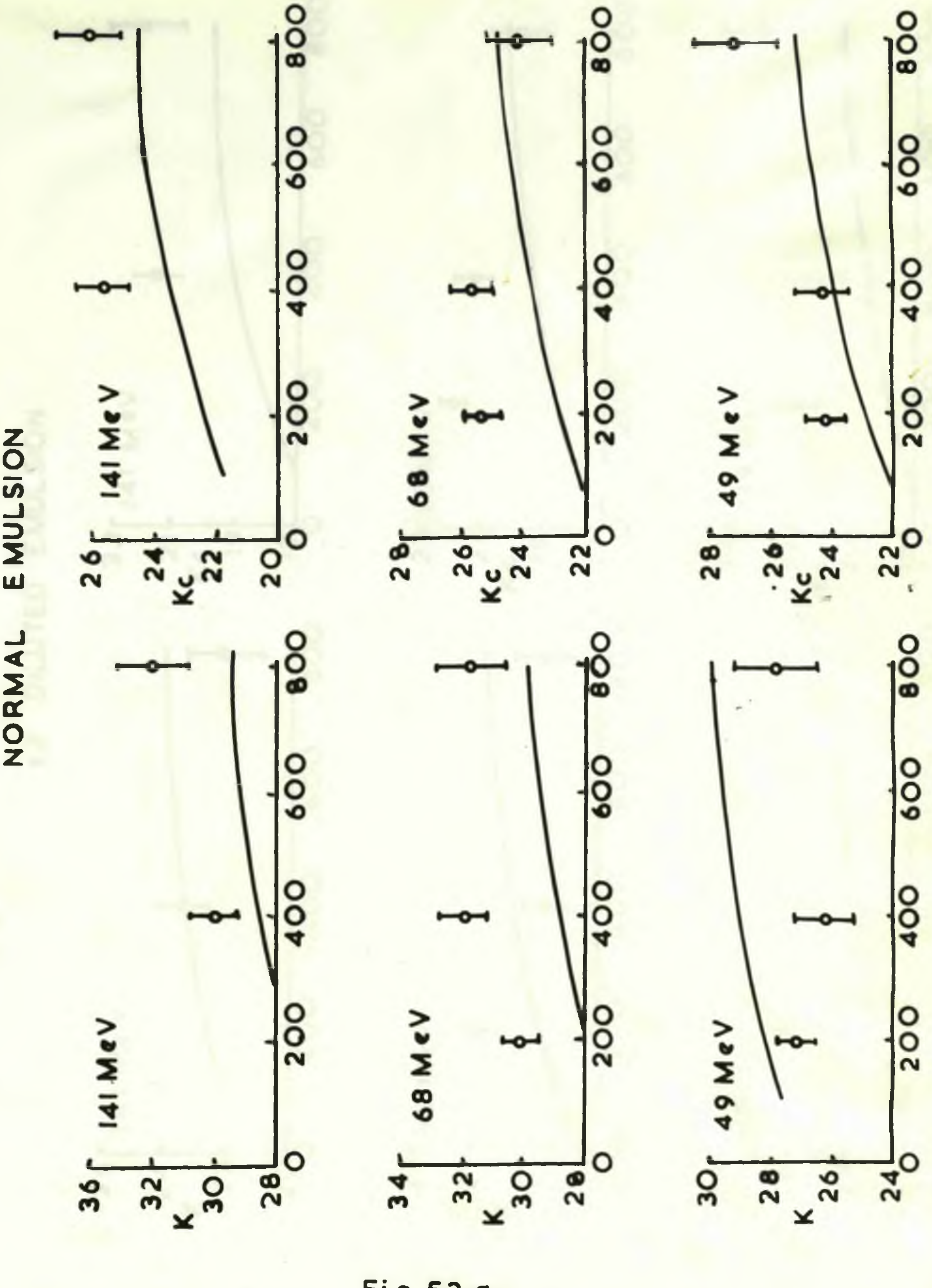

Fig 53 a

Fig 53 a

x2 DILUTED EMULSION

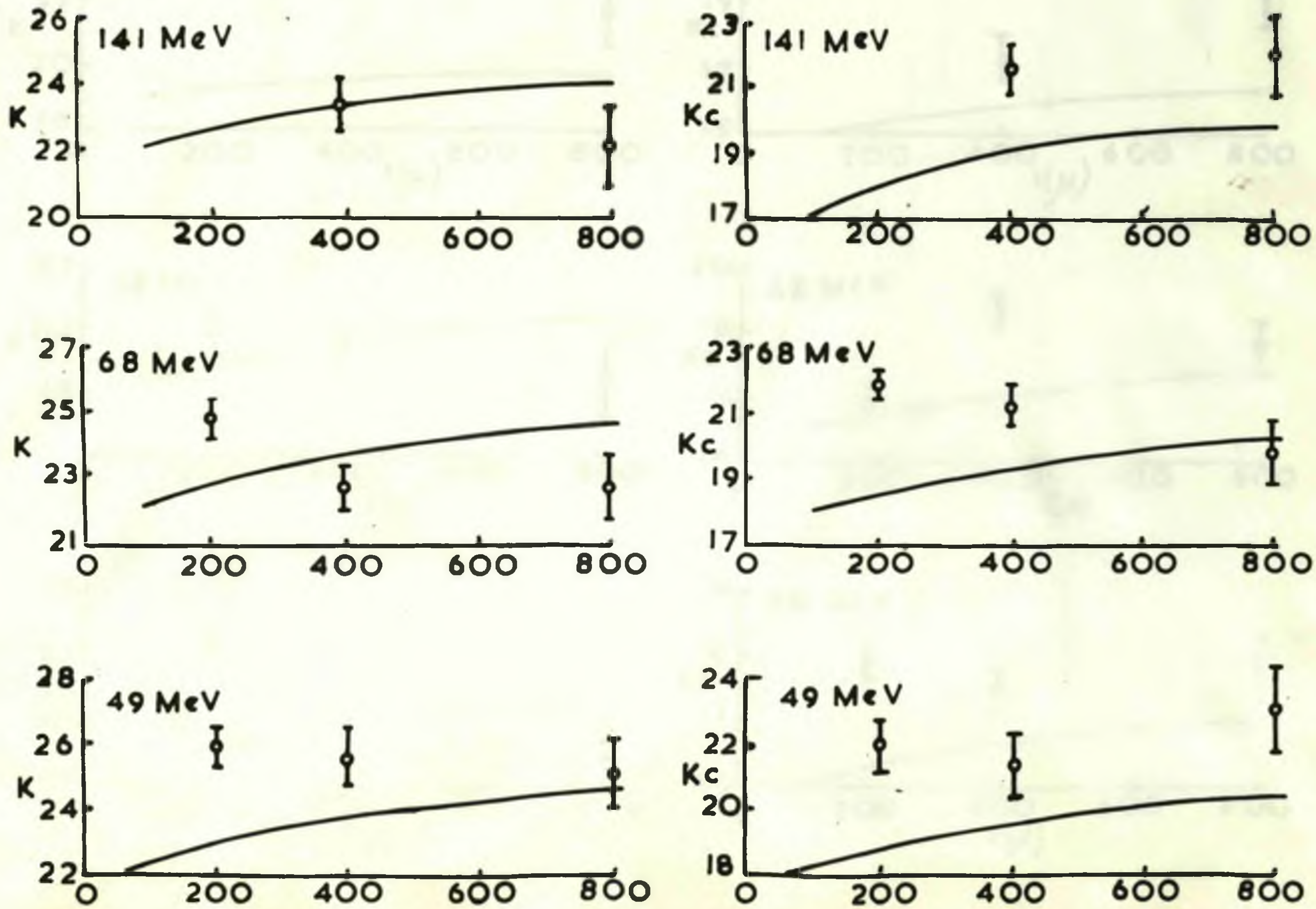

Fig 53 b

Fig 53 b

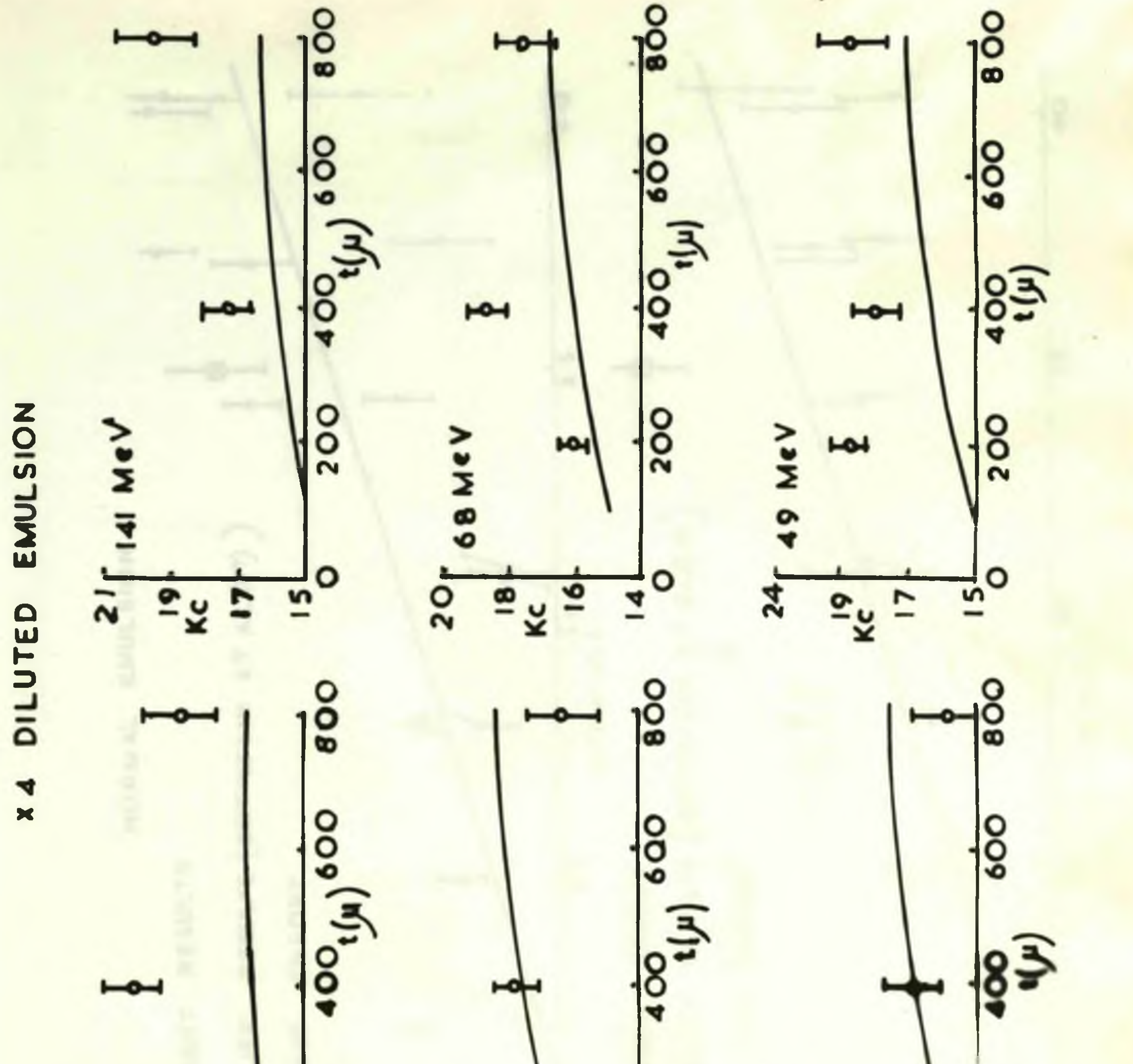

Fig. 53c

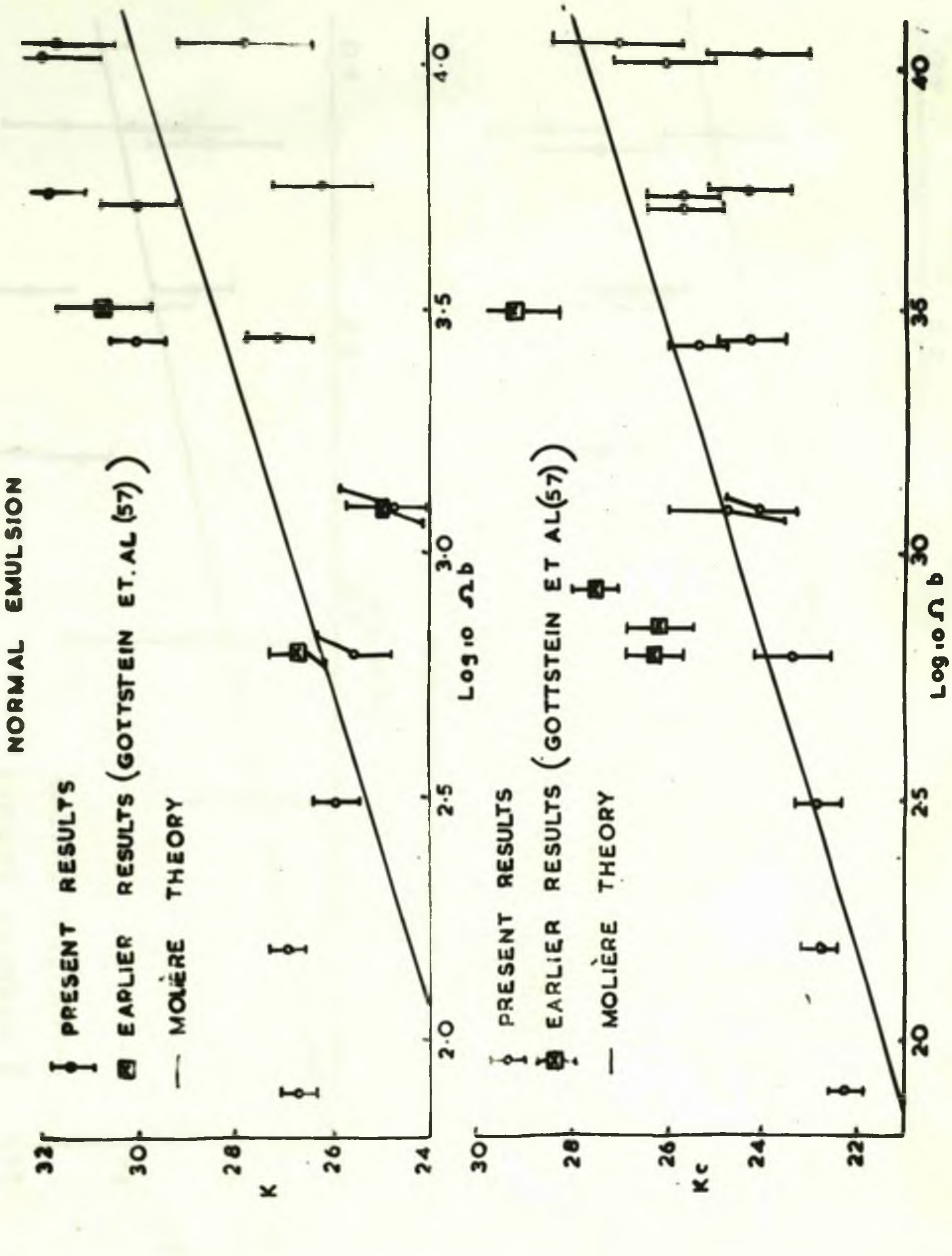

NORMAL EMULSION
PRESENT RESULTS
EARLIER RESULTS (GOTTSTEIN ET. AL (57))
MOLIÈRE THEORY
K
Kc
Log10 Ωb
32
30
28
26
24
22
2·0
2·5
3·0
3·5
4·0

Fig. 54a

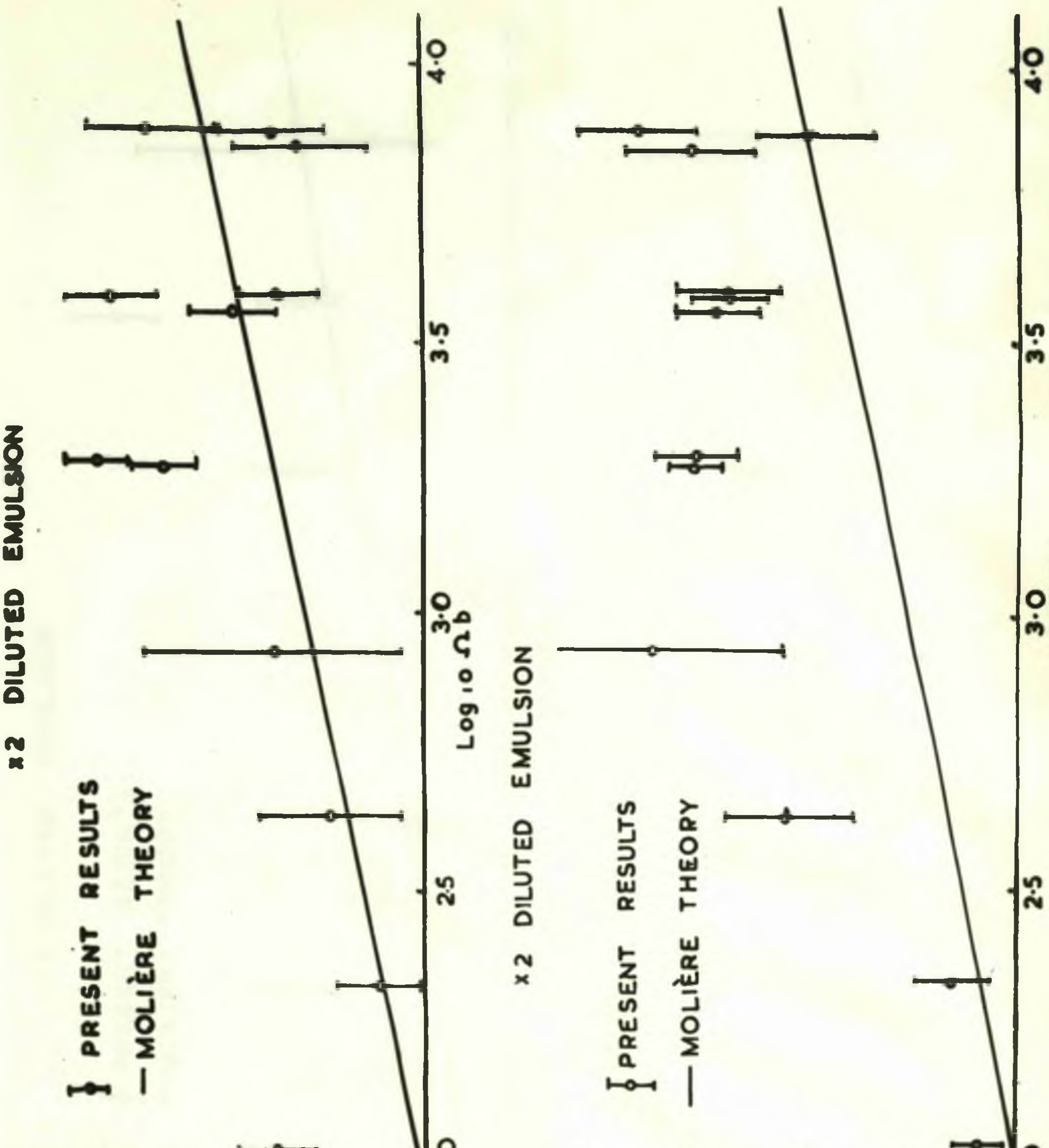
x 2 DILUTED EMULSION
PRESENT RESULTS
— MOLIÈRE THEORY
K
26
24
22
20
2·0
2·5
3·0
3·5
4·0
Log₁₀ Ωb
x 2 DILUTED EMULSION
PRESENT RESULTS
— MOLIÈRE THEORY
Kc
24
22
20
18
16
2·0
2·5
3·0
3·5
4·0
Log₁₀ Ωb

Fig 54 b

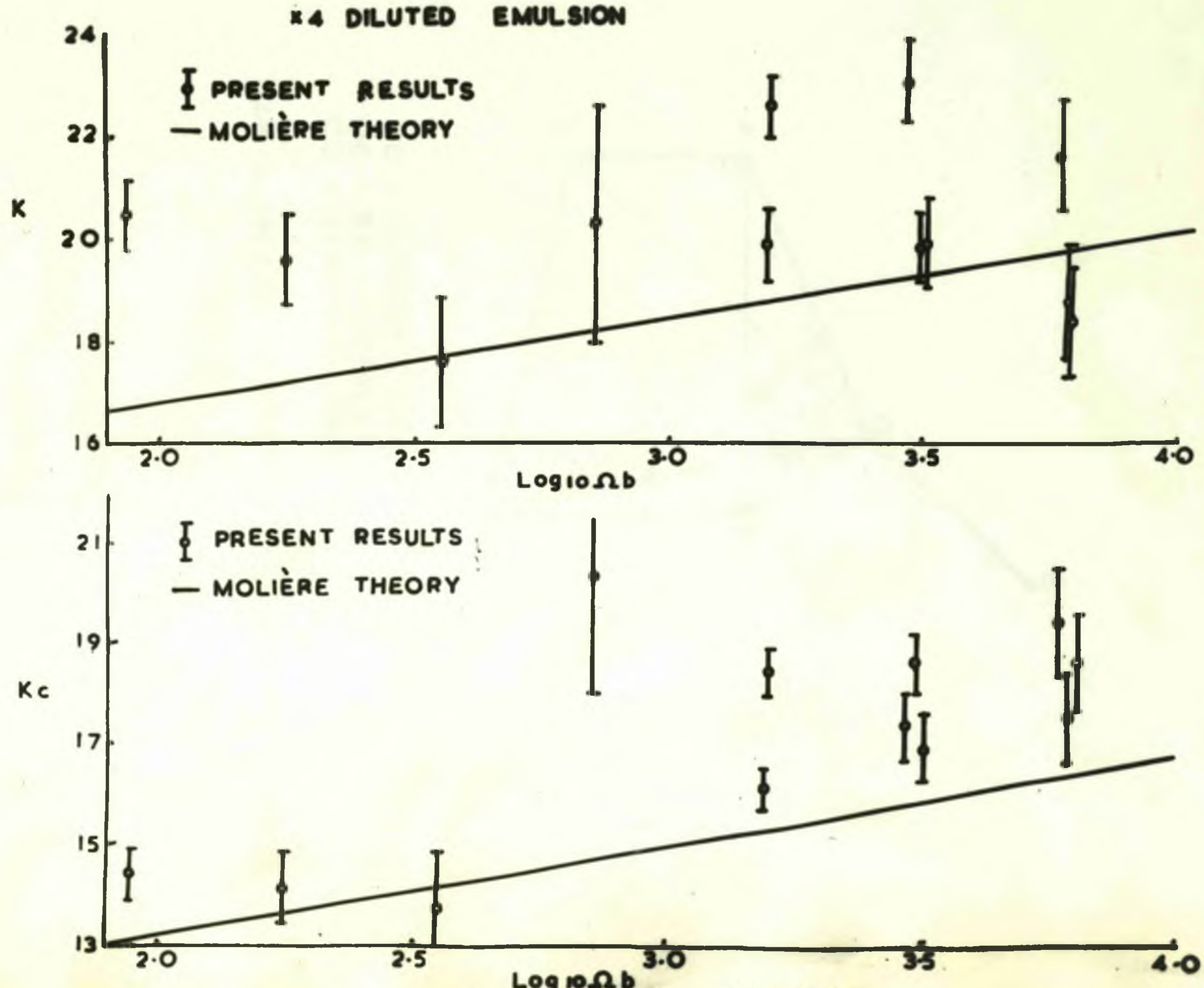

Fig 54c

Fig 54c

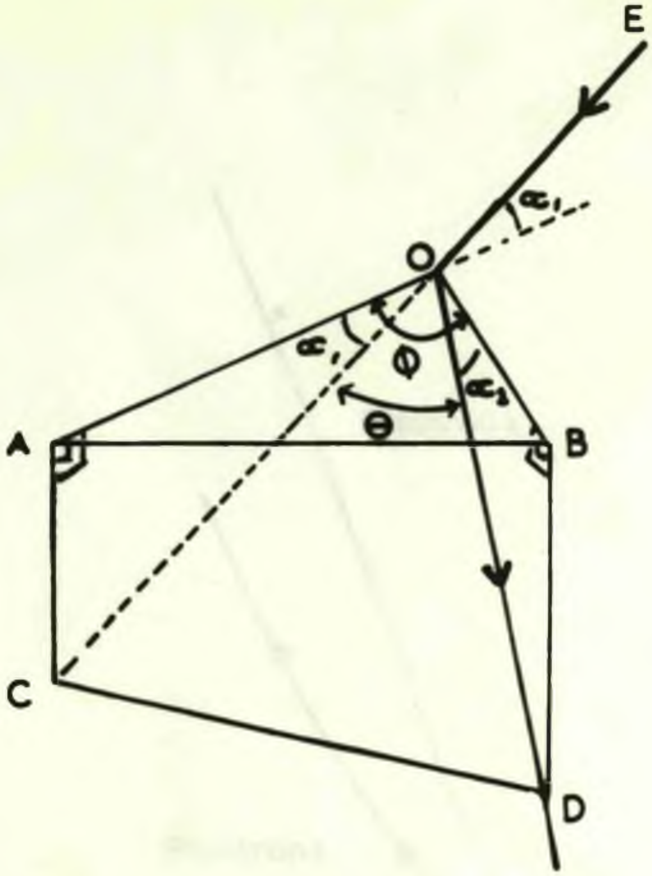

EO = INCIDENT TRACK
OC = EO CONTINUED
OD = SCATTERED TRACK

OAB = PLANE PARALLEL TO EMULSION SURFACE

Fig. 5.5

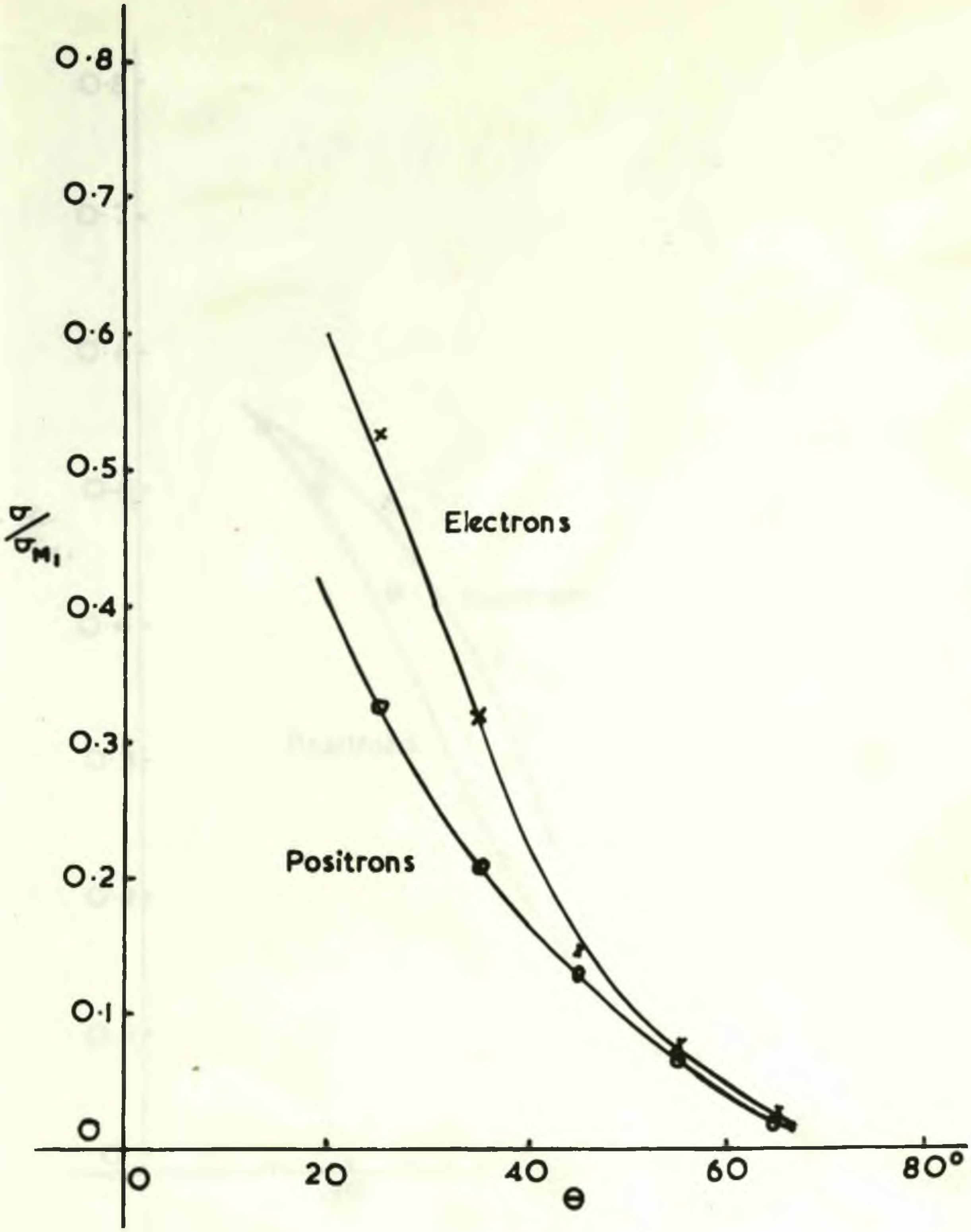

Fig 56

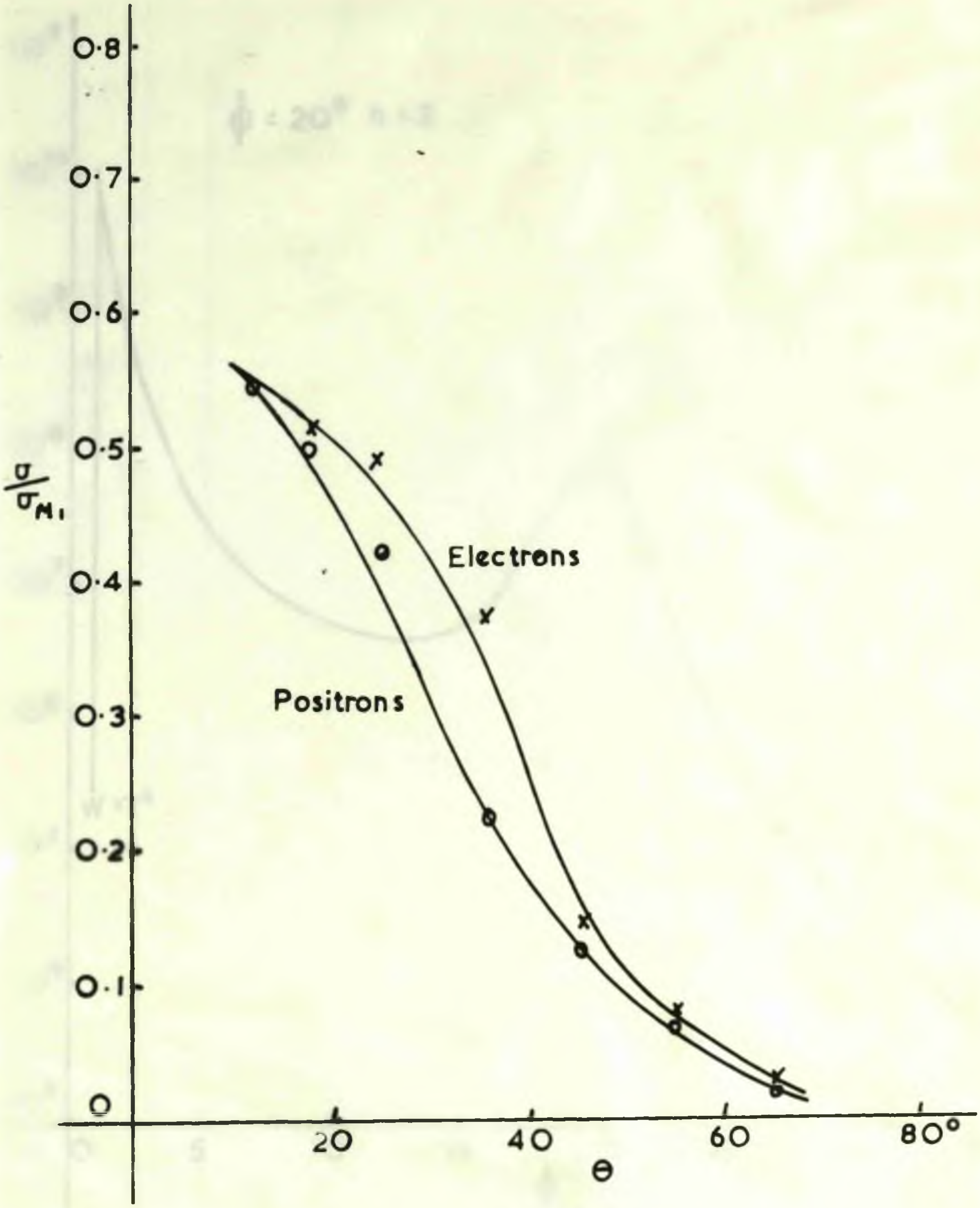

Fig 57

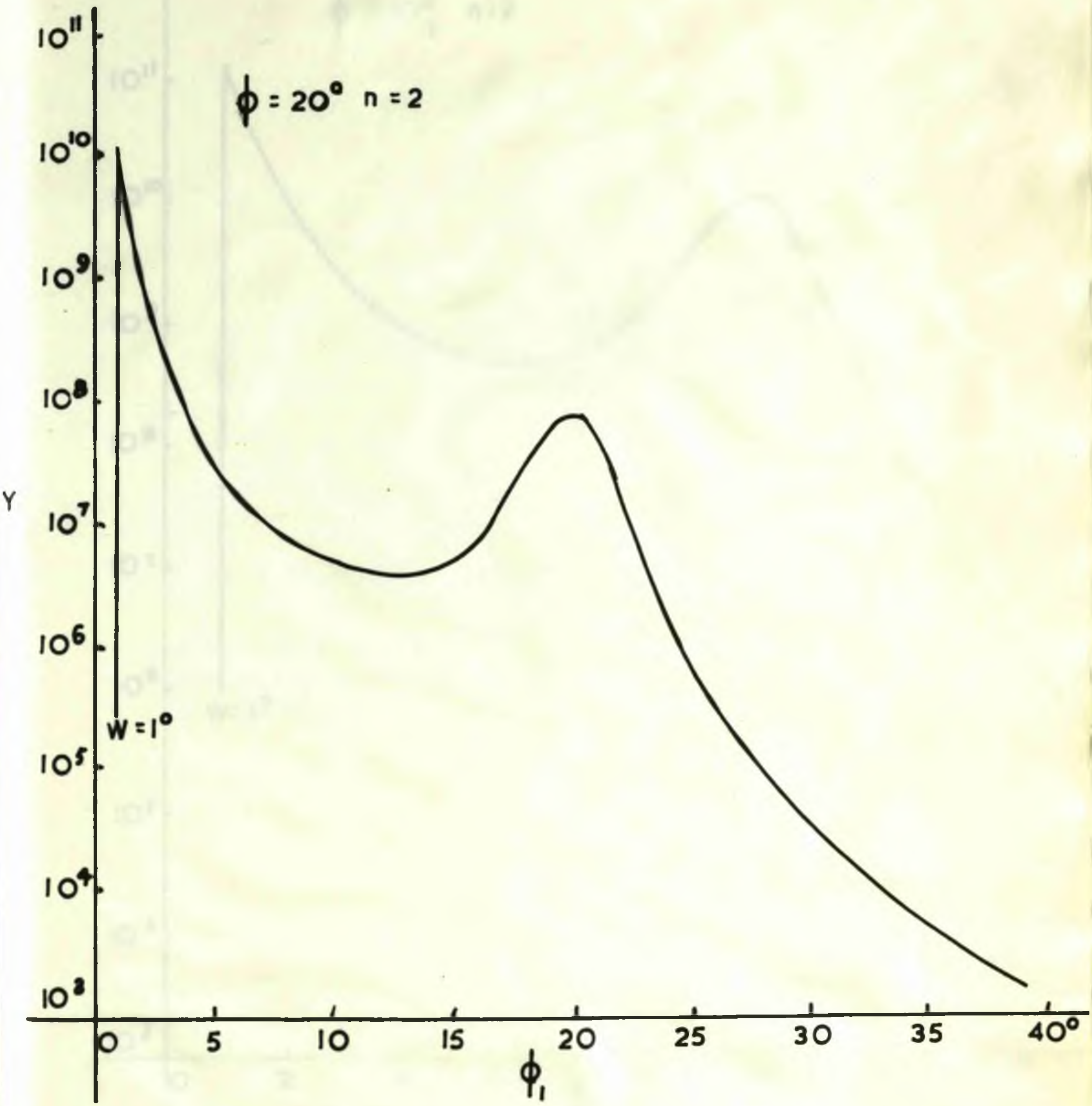

$\phi = 20^{\circ}$ n = 2
10^{11}
10^{10}
10^{9}
10^{8}
Y
10^{7}
10^{6}
W = 1°
10^{5}
10^{4}
10^{3}
0
5
10
15
20
25
30
35
40°
ϕ_1

Fig 58 a

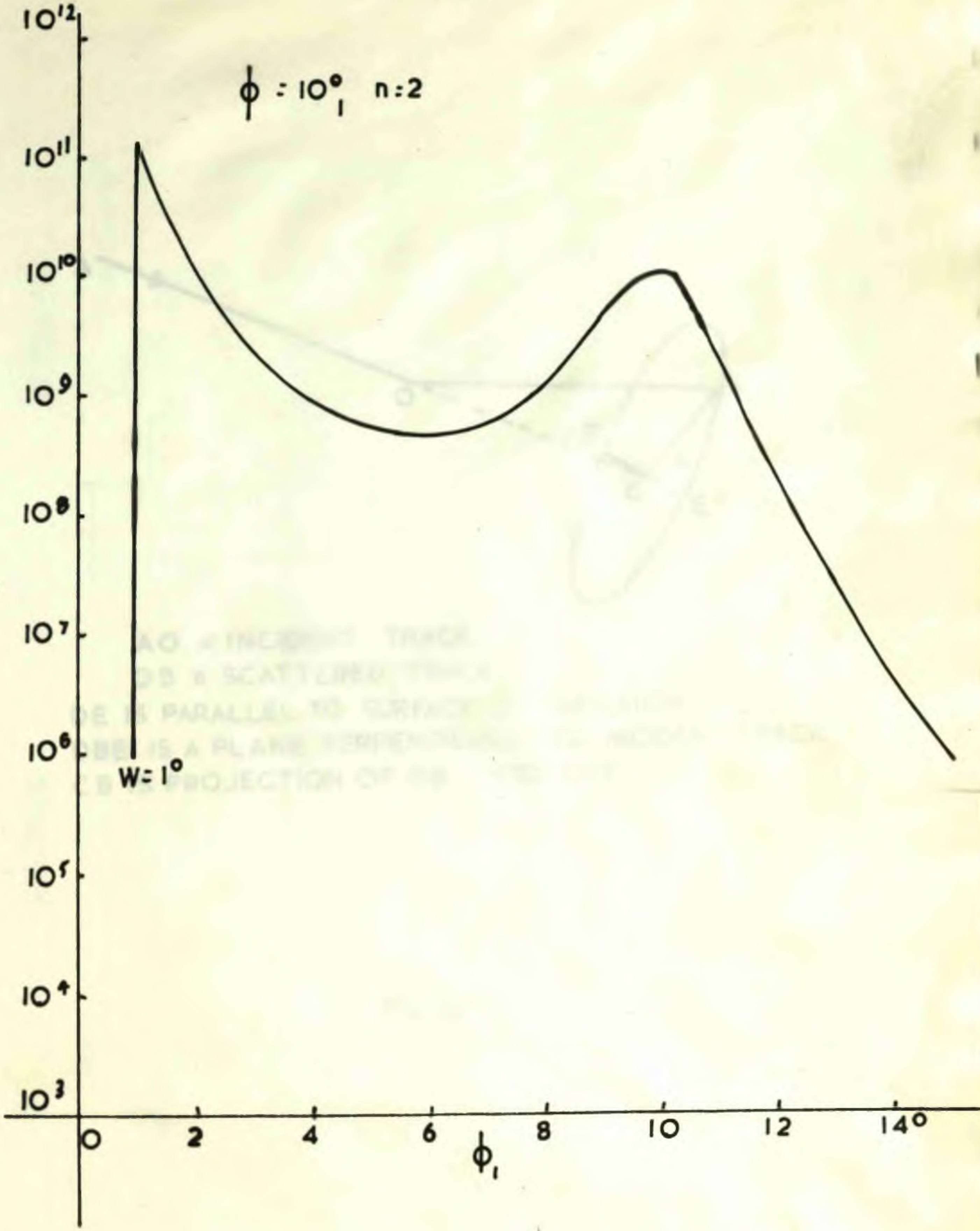

$\phi_1 = 10^\circ$ $n = 2$
10^{12}
10^{11}
10^{10}
10^9
10^8
Y
10^7
10^6
$W = 1^\circ$
10^5
10^4
10^3
0
2
4
6
8
10
12
14°
ϕ_1

Fig 58 b

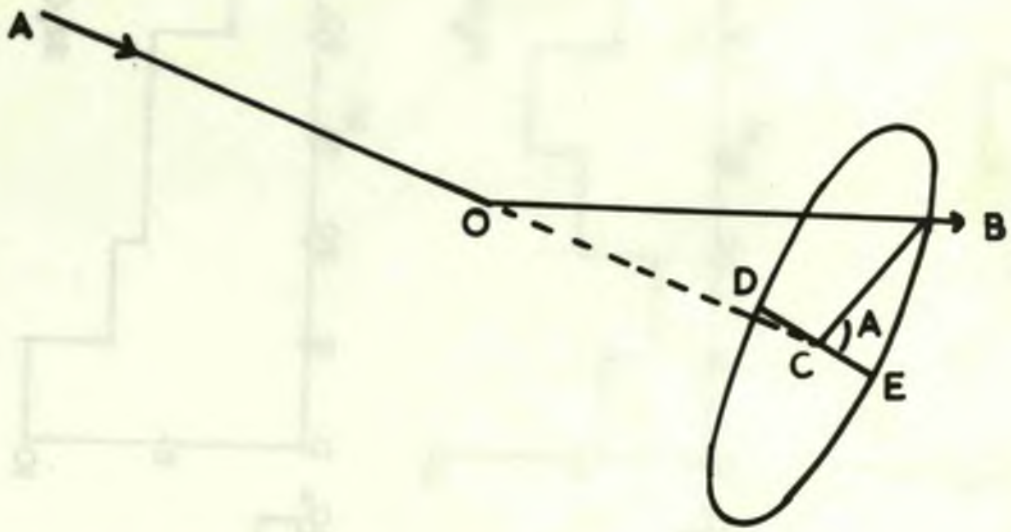

AO = INCIDENT TRACK
OB = SCATTERED TRACK
DE IS PARALLEL TO SURFACE OF EMULSION
DBE IS A PLANE PERPENDICULAR TO INCIDENT TRACK.
CB IS PROJECTION OF OB ONTO DBE

Fig. 59

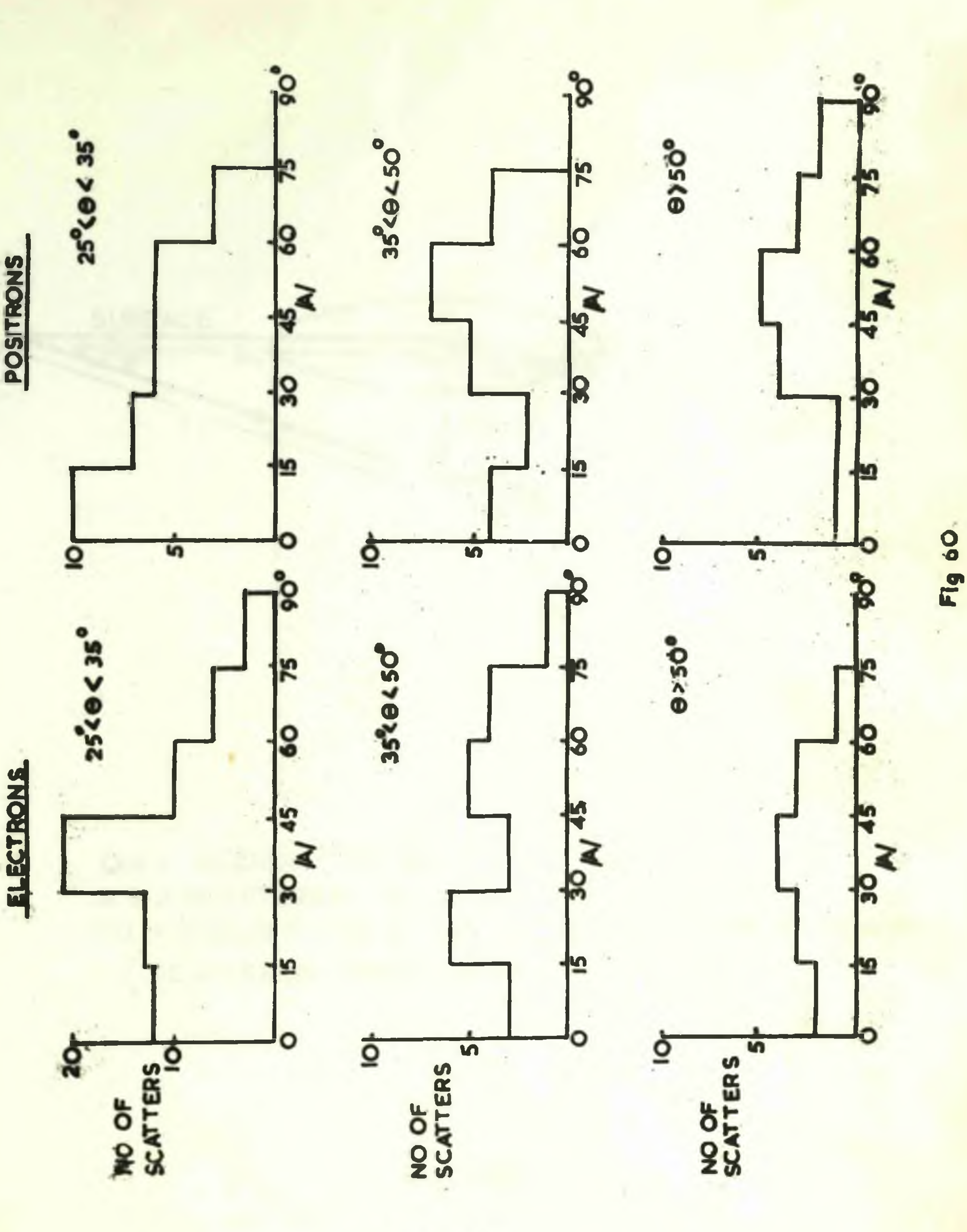

ELECTRONS
POSITRONS
25°<θ<35°
35°<θ<50°
θ>50°
NO OF SCATTERS
|λ|
0
15
30
45
60
75
90°
5
10
20
Fig 60

Fig 60

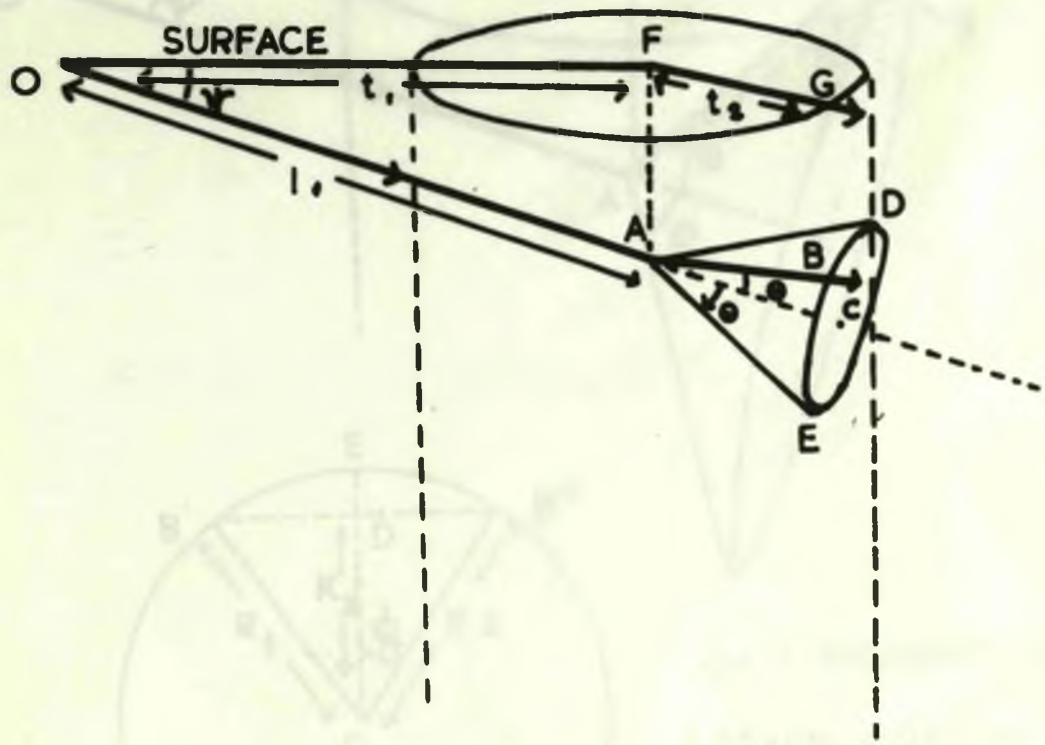

OA = INCIDENT TRACK
AB = SCATTERED TRACK
FG = PROJECTION OF AB ONTO SURFACE OF EMULSION
(SCATTERED TRACK NOT LOST)

Fig. 61a

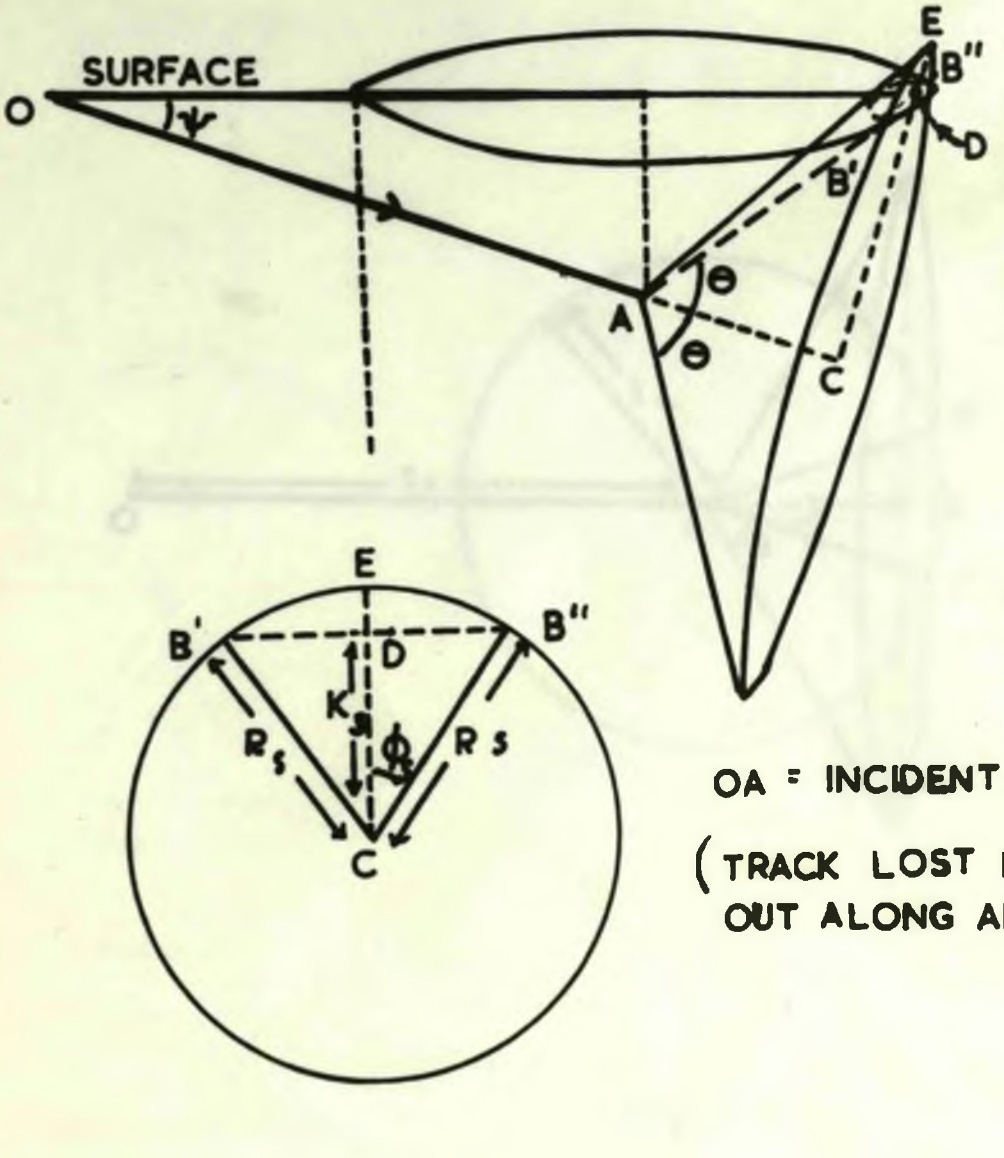

OA = INCIDENT TRACK

(TRACK LOST IF SCATTERED OUT ALONG ARC B'EB'')

Fig. 61b

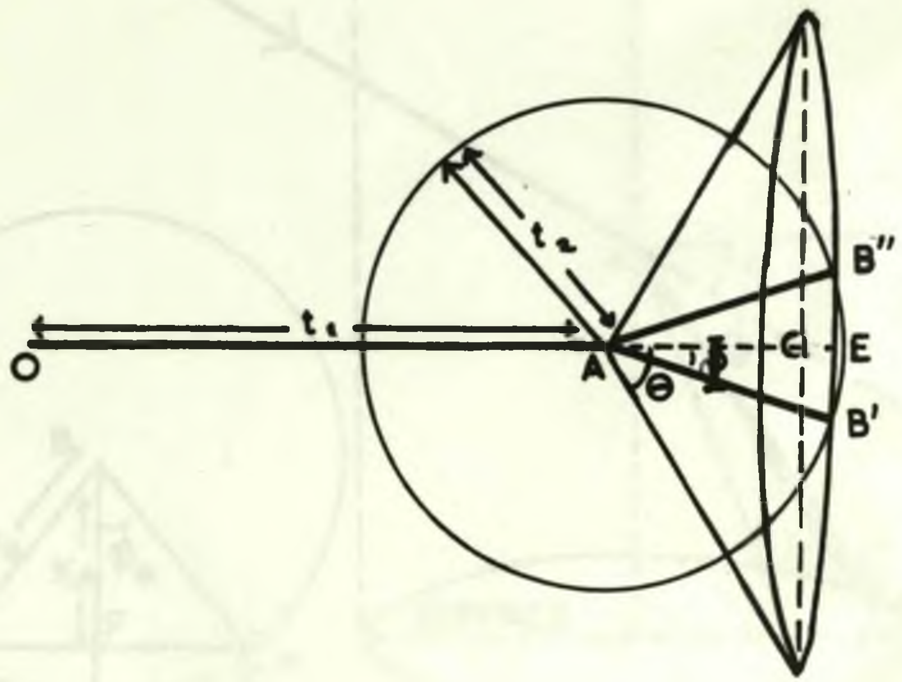

Fig. 61c

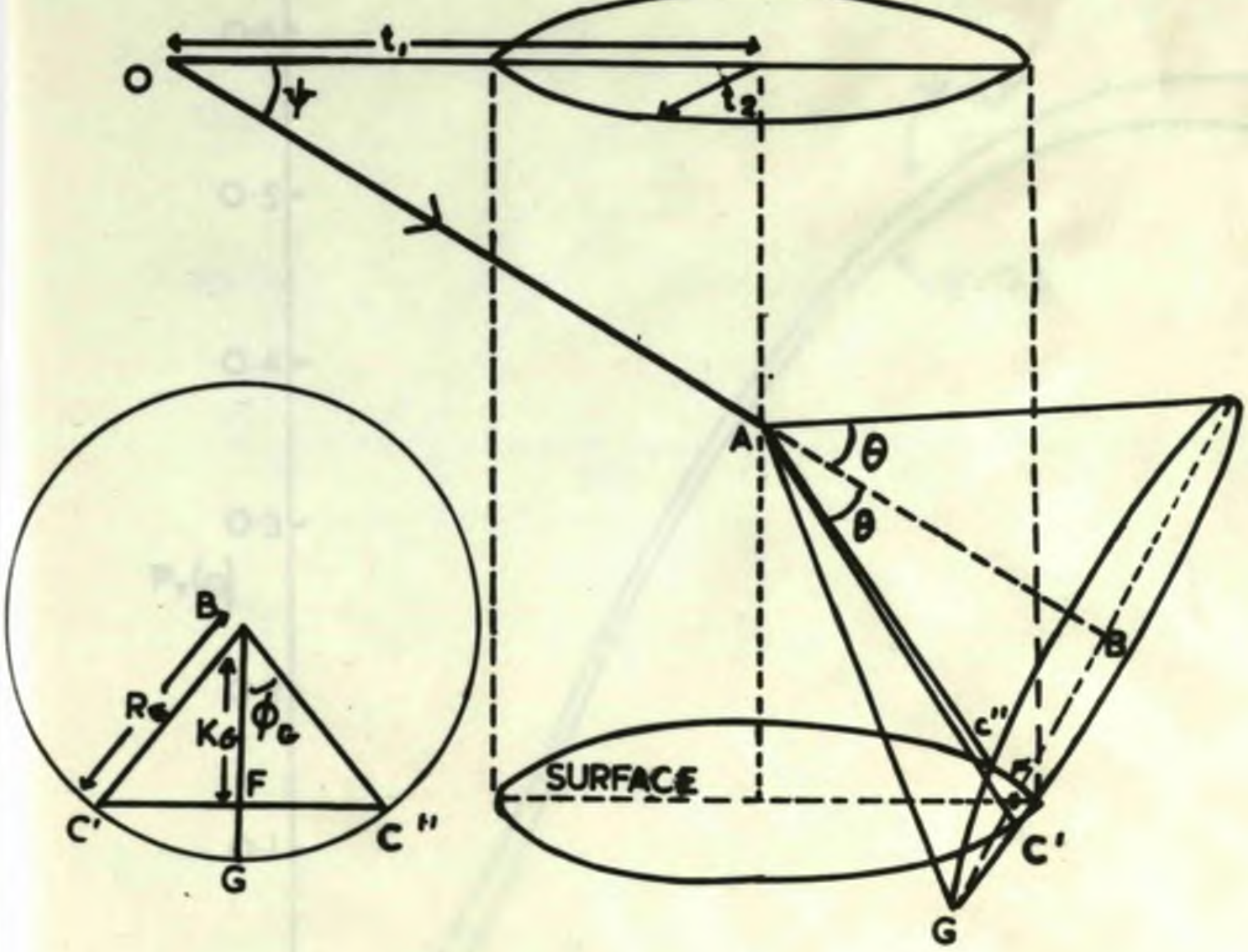

OA = INCIDENT TRACK
(TRACK LOST IF SCATTERED
OUT ALONG ARC C'GC")

Fig. 62

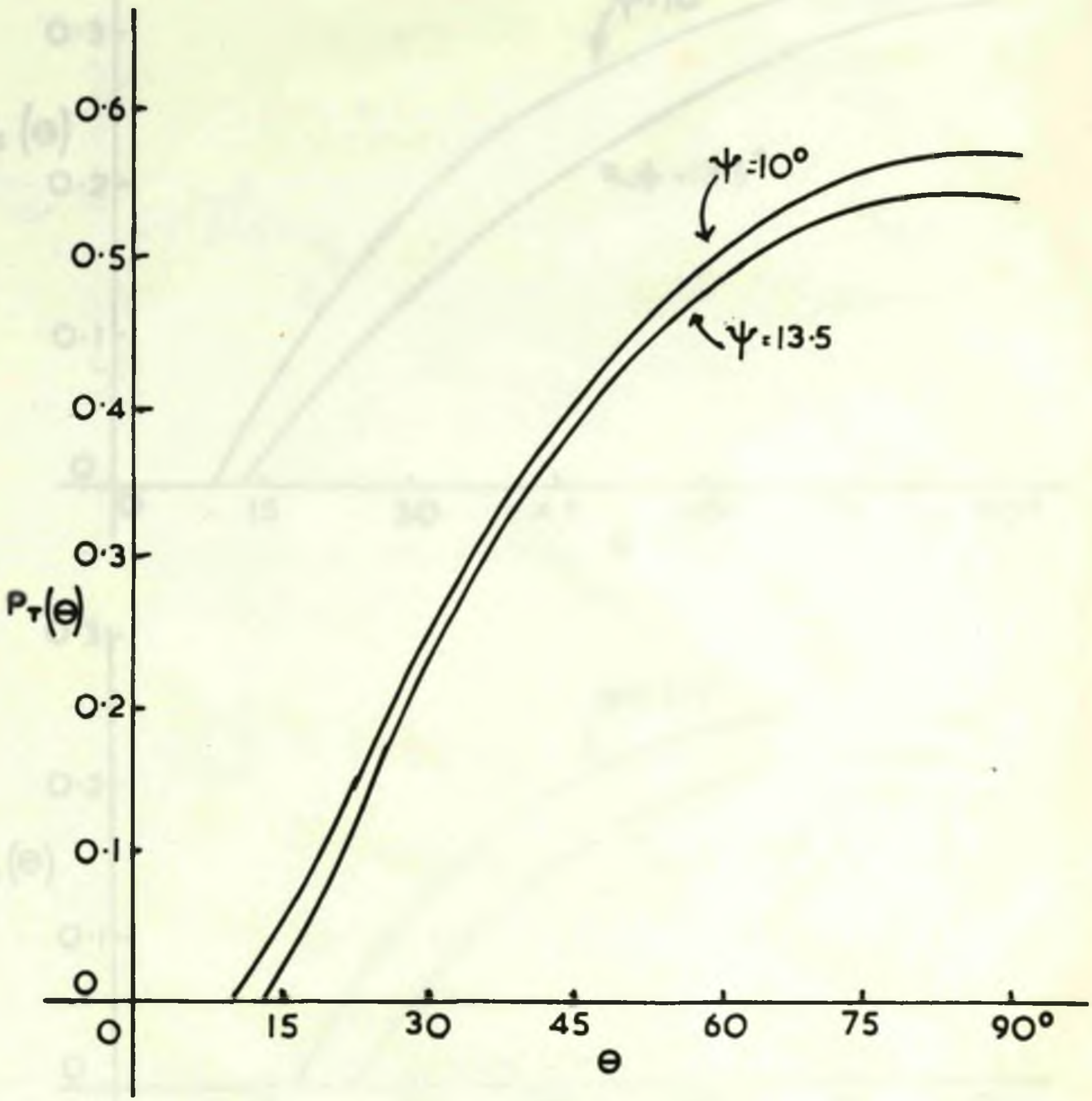

Fig 63

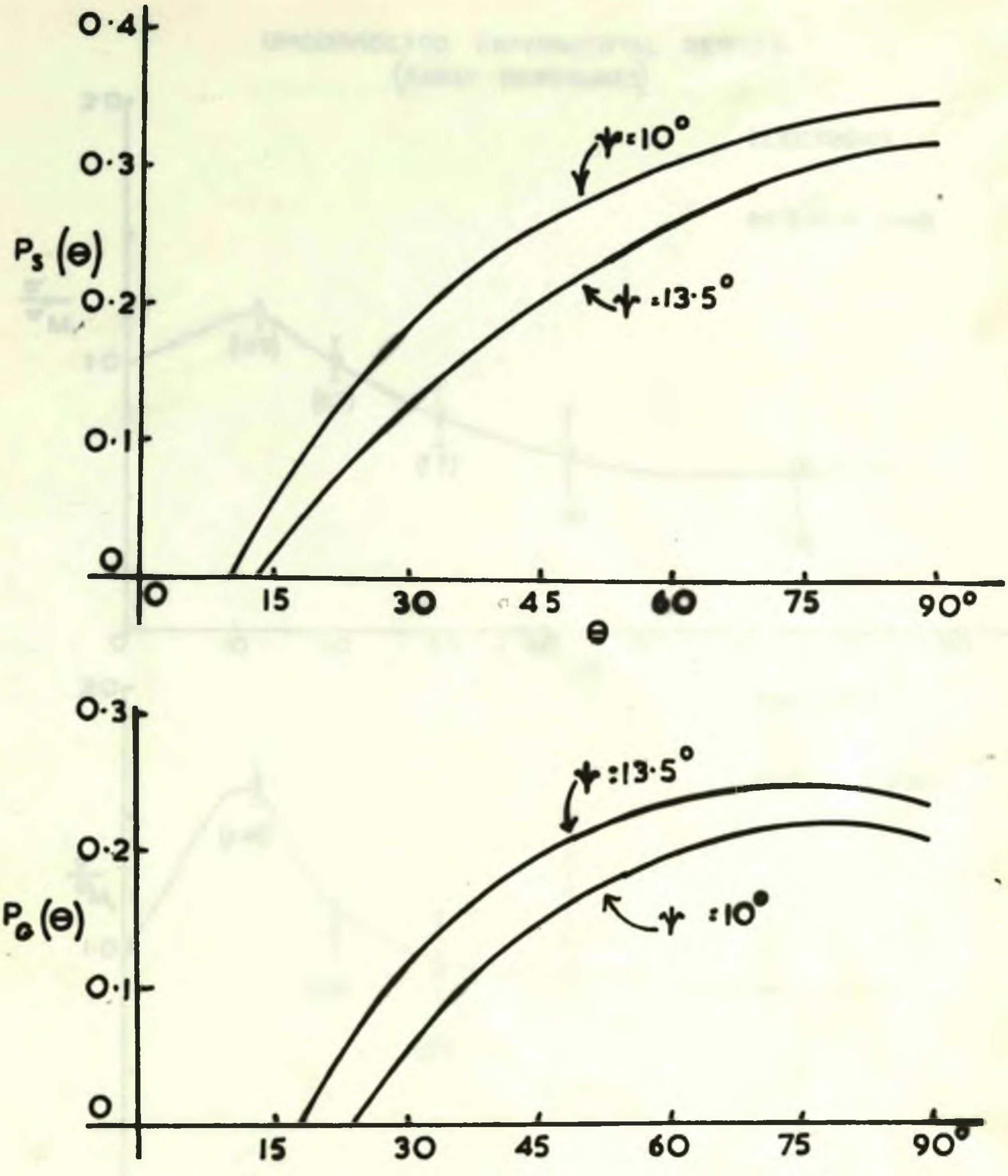
0·4
0·3
0·2
0·1
0
$P_s(\theta)$
$\psi = 10°$
$\psi = 13·5°$
0 15 30 45 60 75 90°
θ
0·3
0·2
0·1
0
$P_\theta(\theta)$
$\psi = 13·5°$
$\psi = 10°$
15 30 45 60 75 90°

Fig 64

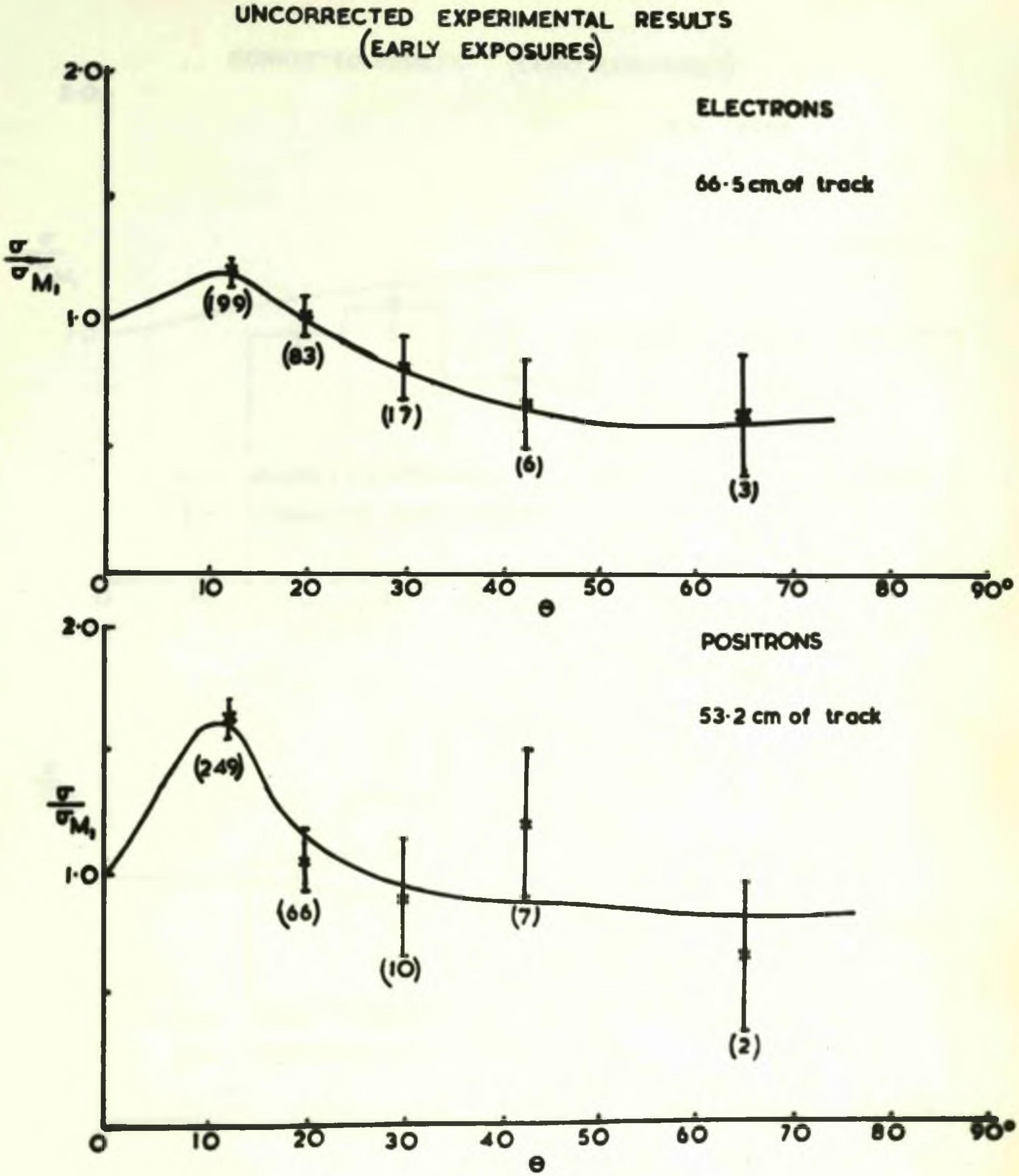

UNCORRECTED EXPERIMENTAL RESULTS
(EARLY EXPOSURES)
ELECTRONS
66·5 cm of track
(99)
(83)
(17)
(6)
(3)
POSITRONS
53·2 cm of track
(249)
(66)
(10)
(7)
(2)
2·0
1·0
0
10
20
30
40
50
60
70
80
90°
θ

Fig 65

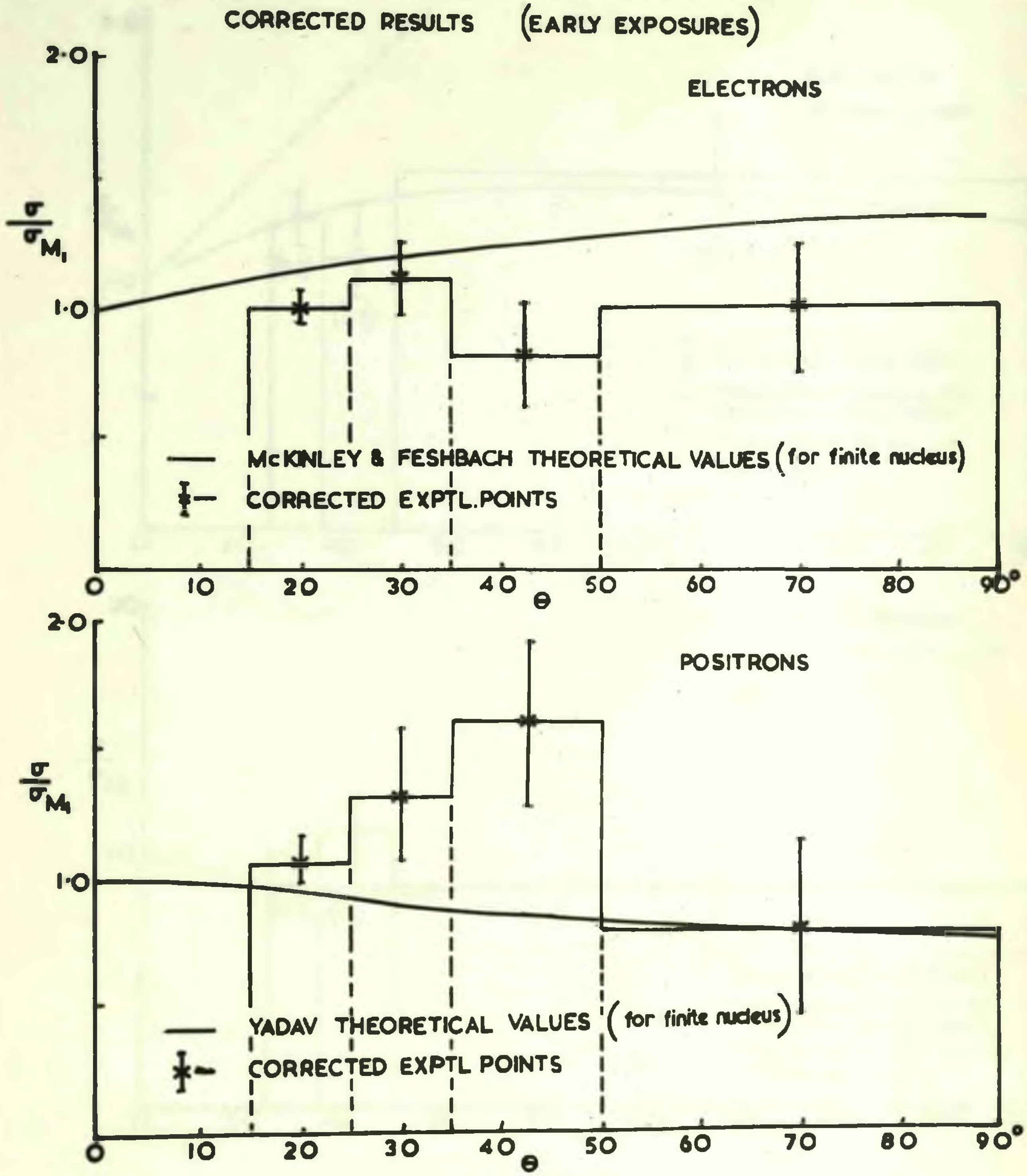

CORRECTED RESULTS (EARLY EXPOSURES)
ELECTRONS
2·0
1·0
σ / σ_{M_1}
McKINLEY & FESHBACH THEORETICAL VALUES (for finite nucleus)
CORRECTED EXPTL. POINTS
0
10
20
30
40
50
60
70
80
90°
θ
POSITRONS
YADAV THEORETICAL VALUES (for finite nucleus)
CORRECTED EXPTL POINTS

Fig 66

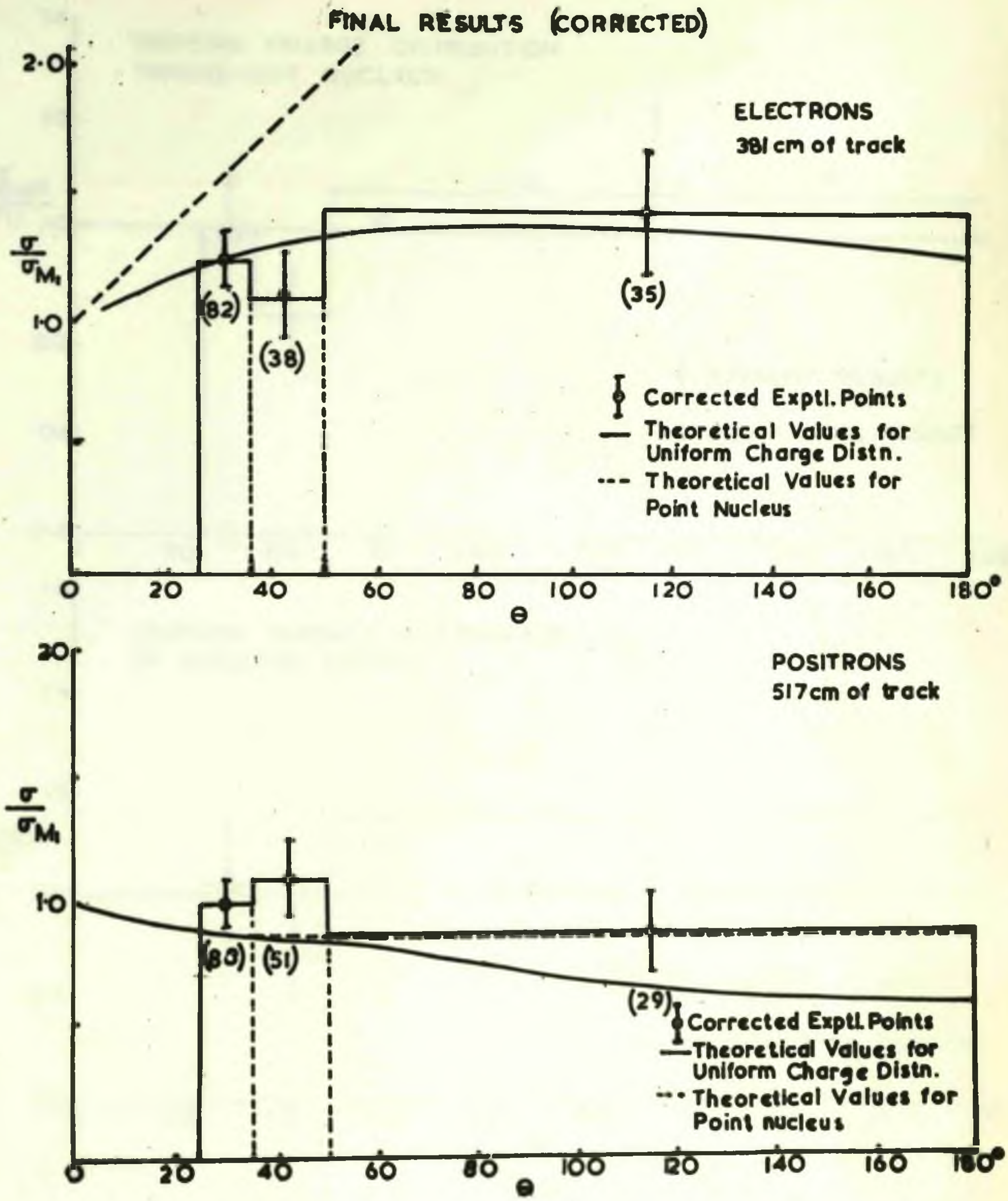

FINAL RESULTS (CORRECTED)
ELECTRONS
381 cm of track
2·0
1·0
(82)
(38)
(35)
Corrected Exptl. Points
Theoretical Values for Uniform Charge Distn.
Theoretical Values for Point Nucleus
0
20
40
60
80
100
120
140
160
180°
θ
POSITRONS
517 cm of track
2·0
1·0
(80)
(51)
(29)
Corrected Exptl. Points
Theoretical Values for Uniform Charge Distn.
Theoretical Values for Point nucleus
θ

Fig 67

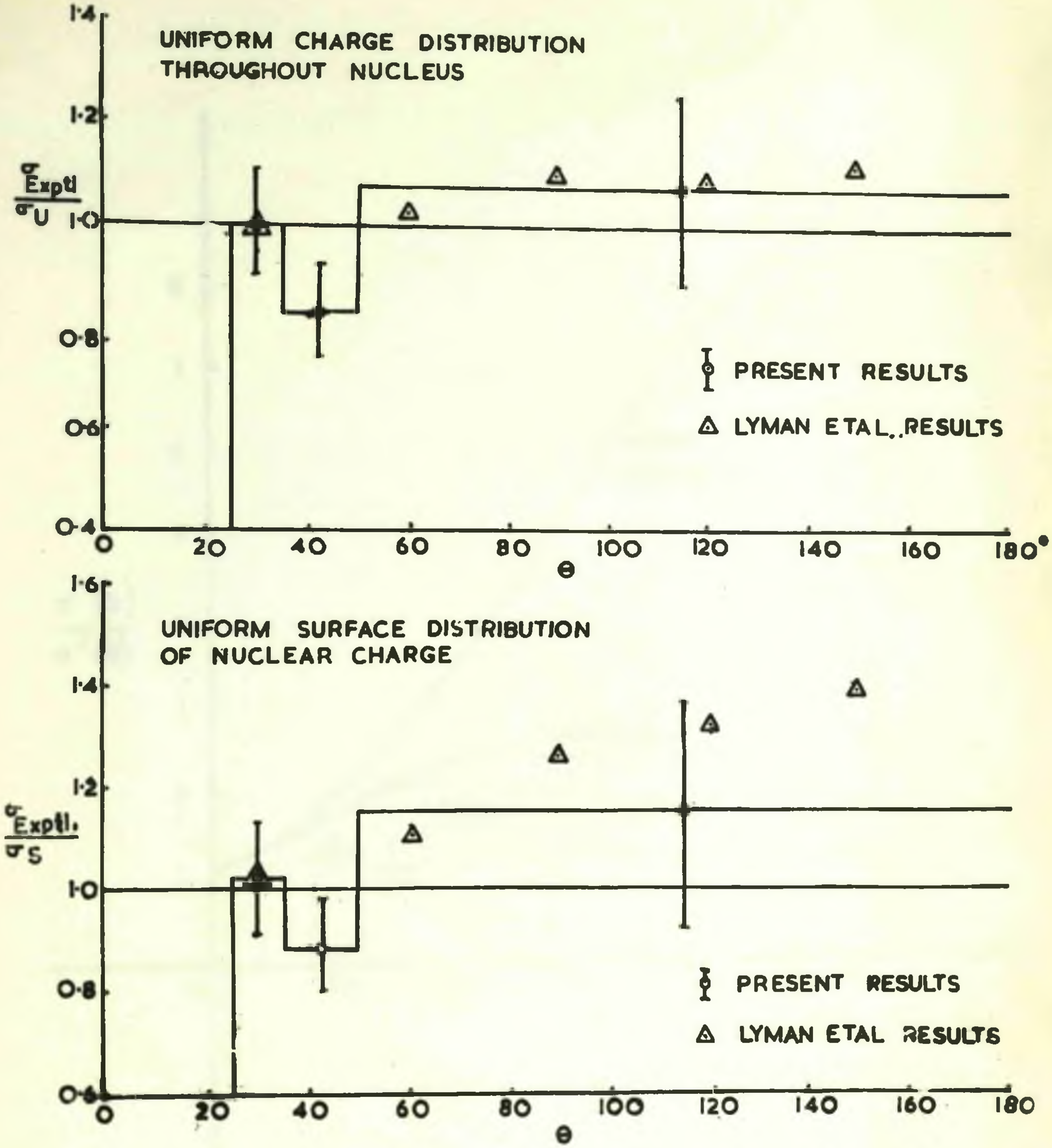
UNIFORM CHARGE DISTRIBUTION THROUGHOUT NUCLEUS
σ_{Exptl}/σ_U
PRESENT RESULTS
LYMAN ETAL. RESULTS
θ
UNIFORM SURFACE DISTRIBUTION OF NUCLEAR CHARGE
$\sigma_{Exptl.}/\sigma_S$
PRESENT RESULTS
LYMAN ETAL RESULTS
θ

Fig 68

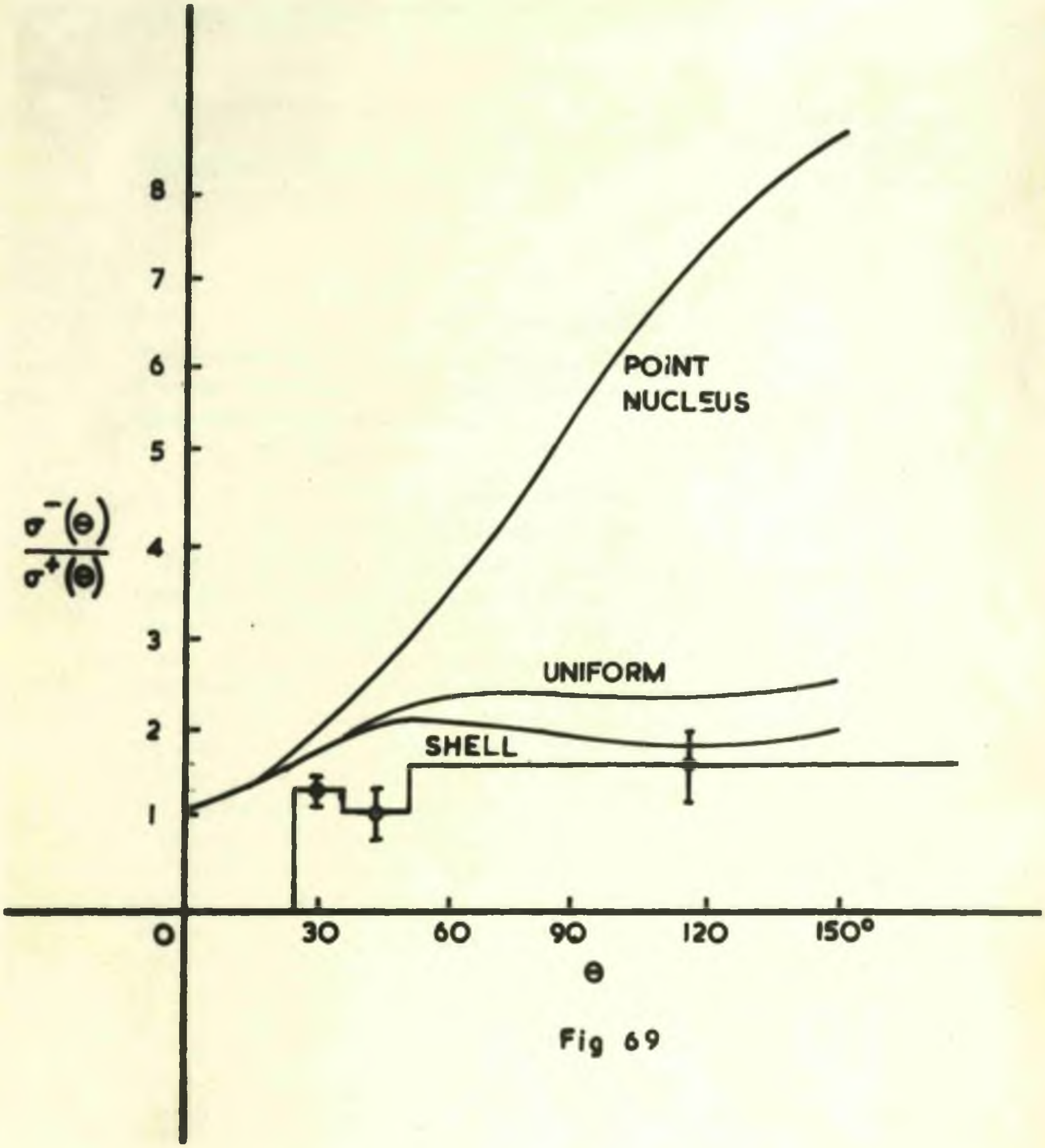

POINT
NUCLEUS
UNIFORM
SHELL
$\frac{\sigma^-(\theta)}{\sigma^+(\theta)}$
8
7
6
5
4
3
2
1
0
30
60
90
120
150°
θ

Fig 69